

Self-Assembled Peptides for Drug Delivery, Tissue Regeneration, and Biocatalytic Applications

A Thesis Submitted
In Partial Fulfillment of the Requirements
for the Degree of

DOCTOR OF PHILOSOPHY

by

“Moumita Halder”

(2018CYZ0011)



DEPARTMENT OF CHEMISTRY
INDIAN INSTITUTE OF TECHNOLOGY ROPAR
Rupnagar
July, 2023

**Copyright © 2023 by Indian Institute of Technology Ropar
All Rights Reserved**

Dedicated
to
Family & Friends

Declaration of Originality

I hereby declare that the work, which is being presented in the thesis, entitled “*Self-Assembled Peptides for Drug Delivery, Tissue Regeneration, and Biocatalytic Applications*”, has been solely authored by me. It presents the result of my own independent investigation/research conducted during the time period from July, 2018 to July, 2023 under the supervision of Dr. Yashveer Singh, Associate Professor, Department of Chemistry, IIT Ropar, Rupnagar. To the best of my knowledge, it is an original work, both in terms of research content and narrative, and has not been submitted or accepted elsewhere, in parts or in full, for the award of any degree, diploma, fellowship, associateship, or similar title of any university or institution. Further, due credit has been attributed to the relevant state-of-the-art and collaborations with appropriate citations and acknowledgments, in line with the established ethical norms and practices. I also declare that any idea/data/fact/source stated in my thesis has not been fabricated/ falsified/ misrepresented. All the principles of academic honesty and integrity have been followed. I fully understand that if the thesis is found to be unoriginal, fabricated, or plagiarized, the institute reserves the right to withdraw the thesis from its archive and revoke the associated degree conferred. Additionally, the institute also reserves the right to appraise all concerned sections of the society of the matter for their information and necessary action. If accepted, I hereby consent for my thesis to be available online in the Institute’s Open Access Repository, inter-library loan, and the title and abstract to be made available to outside organizations.



Signature

Name: Moumita Halder

Entry Number: 2018CYZ0011

Program: PhD

Department: Chemistry

Indian Institute of Technology Ropar

Rupnagar, Punjab 140001

Acknowledgments

A researcher would not have been able to complete this journey without the immense help and support of countless people who in one way or another contributed and extended their valuable assistance. First and foremost, I would like to thank God, the Almighty, for showering blessings throughout my research work and giving me strength to complete the research successfully.

I would like to express my deepest gratitude to my supervisor, **Dr. Yashveer Singh** for his constant guidance, support, and valuable insights throughout my doctoral research. His expertise, patience, and encouragement have been invaluable in shaping the direction of this thesis. Thank you, Sir, for having confidence in my potential and allowing me to work independently which boosted my self-confidence and enabled me to carry out multiple projects. I am also grateful for the numerous opportunities you have provided me to collaborate on various projects, present my research at conferences, and publish in reputable journals. Your insightful feedback, constructive criticism has been instrumental in refining my research methodology and enhancing the quality of my work. At this, I must admit that, I am truly fortunate to have you as my supervisor.

I am immensely grateful to the doctoral committee members, **Dr. C. M. Nagaraja, Dr. Indranil Chatterjee, Dr. Mukesh Kumar** and chairperson **Dr. T. J. Dhilip Kumar** for their time, thoughtful feedback, and valuable inputs during the presentation and other times. Their expertise and contributions have significantly enhanced the quality of this work. My sincere thanks to the present all the other faculty members of Department of Chemistry and Department of Biomedical Engineering for their sincere support and invaluable guidance. I am also thankful to all the staffs of Department of Chemistry and Department of Biomedical Engineering.

I would also like to acknowledge Department of Chemistry and Department of Biomedical Engineering for the infrastructure and research facilities. I should not forget to share my immense gratitude to **Dr. Durba Pal** and **Prof. Javed N Agrewala** for allowing me use their cell culture facilities. I am grateful to the funding agencies, DBT, SERB, and DST Indo-Taiwan for their financial support, which enabled me to conduct this research. I would also like to thank International Travel Support Grant, DST and IIT Ropar for providing me financial support to attend international conference at France.

I would also like to acknowledge the past and present members of the lab for their support and motivation throughout this journey and providing a friendly environment at the workplace. I would like to thank Dr. Kamal Malhotra, Dr. Peeyush Sharma and Dr. Neelam Chauhan for insightful discussions, and valuable feedback. I express my sincere gratitude to Nahida Rasool for being an integral part of my life, providing a comforting presence during both the highs and lows. Her unwavering belief in me, even when I doubted myself, has been a source of strength and inspiration. Her friendship and support have made this journey more enjoyable and fulfilling. I want to express my deepest appreciation to my present lab members Deepa, Vatan, Soumyajit, Yashika, Pruthvi, Gurpreet, Rupali, and Ankit for always supporting me and motivating me. I am grateful for the countless

moments we have shared, and the memories we have created together. I would also like to acknowledge my interns Yatin, Mukul, and Ananya for working with me. Their thoughtful questions, eagerness to learn, and active engagement in discussions has enriched the learning environment. I am also thankful to the other masters' students, Rajat, Priya, Shubham, Gunjan, Subhajt, Meghna, Sakshi, John, Ankur, Srijani for their assistance and generosity. I want to express my deepest appreciation to my friends and juniors, Sourav, Debarshi, Debarun, Diksha, Divyani, Gulshan, Dr. Gautam, Manisha, Majjid, Navpreet, Neelam, Prasoon, Rajesh, Sidhanta, Bhavya, Atul, Anwesha, Varun, Ganesh, Arijit, Manish and Gulshan for their constant support. A big thanks to Dr. Sandeep Singh Dhankar, Dr. Sheetanshu Saproo, Dr. Rekha Dhiman, Dr. Suman Dhingra, Dr. Leena Arora, Dr. Suman Pradhan, and Dr. Soumen Ghosh.

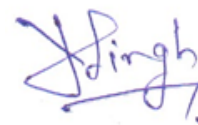
Lastly, I am deeply grateful to my family members, Dadu, Didu, Maa, Baba, and Bhai for their unwavering love, encouragement, and understanding throughout my academic pursuits. Their support and belief in me have been the driving force behind my accomplishments. In addition to emotional support, they have also been a pillar of encouragement in pursuing my dreams. They have celebrated my achievements, no matter how big or small, and their belief in my abilities has bolstered my confidence.

Thank you so much everyone for supporting me unconditionally. The work would not have been possible without these people and their countless blessings.

Certificate

This is to certify that the thesis, entitled **Self-Assembled Peptides for Drug Delivery, Tissue Regeneration, and Biocatalytic Applications**, submitted by **Moumita Halder (Entry # 2018CYZ0011)** for the award of the degree of **Doctor of Philosophy** of the Indian Institute of Technology Ropar, Rupnagar, is a record of original research work carried out under my guidance and supervision at the Department of Chemistry, IIT Ropar, Rupnagar. All other sources of information, material, and mentorship have been acknowledged at appropriate places in the thesis. To the best of my knowledge and belief, the work presented in this thesis is original and has not been submitted, either in part or full, for the award of any other degree, diploma, fellowship, associateship or similar title of any university or institution.

In my opinion, the thesis meets the requirements of the regulations relating to the award of PhD degree.



Signature of the Supervisor

Dr. Yashveer Singh

Department: Chemistry

Indian Institute of Technology Ropar

Rupnagar, Punjab 140001

Lay Summary

Self-assembling peptides are short chain of amino acids that have the ability to spontaneously organize themselves into higher-order structures or aggregates employing non-covalent interactions. These peptides contain specific sequences of amino acids to promote their self-assembly into well-defined nanostructures, like fibers, sheets, gels, or nanoparticles. The self-assembly process allows the peptide to form stable and ordered structures, often resembling natural protein structures and exhibit activities. The development of self-assembling peptide involves selecting or engineering a specific amino acid into the peptide sequence to influence its self-assembly behavior, resulting nanostructures, and biological activities. Self-assembling peptides have shown great potential in biomedical applications due to their properties, like safety towards living system, biological activities that can be tuned, and the ability to mimic extracellular matrix, which is a natural scaffold required for the cell proliferation and differentiation in regenerative medicine. In this thesis, we have developed self-assembled peptides for long-term drug delivery, chronic wound healing, and bone regeneration and to serve as enzyme-mimics. The introduction to the self-assembling peptide, survey of the prior work done, unmet needs, objectives of the thesis are presented in chapter 1. An antioxidant peptide gel loaded with an anti-diabetic drug glimepiride has been reported in chapter 2. It provides a long-term drug release, which is sensitive to the acidic pH present in the interstitial fluid of diabetic patients and protection against the oxidative damage of organ like liver. The development of peptide gels conjugated to anti-inflammatory drugs, naproxen and indomethacin, has been reported in chapter 3, which shows antioxidant, antibacterial, and antibiofilm activities and selective inhibition of cyclooxygenase-2 (COX-2) enzyme involved in stalled inflammation in difficult to treat chronic wounds. Tetrapeptides with different morphologies for the hydroxyapatite adsorption and ability to induce differentiation of stem cells to promote bone regeneration has been reported in chapter 4. The peptide immobilized on the surface of ceria nanoparticle to generate heterogenous, biocatalyst-mimic for enzymes, like esterase, phosphatase, and haloperoxidase has been discussed in chapter 5. The summary of this thesis, its contribution to the field of study and future perspectives have been provided in chapter 6.

Abstract

Molecular self-assembly is a process in which individual components interact via non-covalent interactions, like van der Waals, hydrogen bonding, electrostatic, hydrophobic, and π - π stacking in a well-defined manner to form hierarchical, supramolecular materials with desired function. Living organisms generate a wide range of biomolecules, such as polysaccharides, lipids, nucleic acids, and proteins, which spontaneously self-assemble into more complex and highly organized supramolecular nanostructures with clearly defined biological roles. Through rational design and engineering, peptides can adopt certain secondary, tertiary, and quaternary structures and, thus, provide new opportunities to design self-assembled, nanoscale materials with different size and morphology for various applications. The inherent biocompatibility, biodegradability, and flexible mechanical stability with diverse functionality have made peptides a promising entity to design biomaterials. This thesis deals with the design and development of self-assembled peptides for drug delivery, wound healing, tissue regeneration, and biocatalyst-mimic applications, and is organized into six chapters.

Chapter 1 of the thesis contains introduction to the self-assembly of peptides and their prospects in a wide range of biomedical applications along with the exhaustive literature survey, definition of problem, and specific objectives and outline of the thesis. In **chapter 2**, we have developed pH-responsive, antioxidant di- and tripeptide gels for the sustained release of an anti-diabetic drug glimepiride. The delivery system has the potential to reduce the side effects of drug, frequency of dosing, and improve the patient compliance and fluctuation in bioavailability, which is related to severe hypoglycemia and gastrointestinal disturbances. The antioxidant nature of peptides will provide protection against the oxidative stress caused by the production of hydrogen peroxide during the oxidation of glucose by glucose oxidase. The peptide gels were non-toxic to cell lines and promoted the glucose uptake at low pH. The gels developed in this work can perform as a multidimensional platform to minimize oxidative stress, hypoglycemia, and repetitive dosing of drugs in diabetes patients. Chronic wound is a major healthcare challenge around the world, which is characterized by the presence of bacterial infection, formation of biofilm, accumulation of reactive oxygen species (ROS), and persistent inflammation. Overexpression of cyclooxygenase 2 (COX-2) prolongs the inflammation phase and deteriorates the wound healing process. **Chapter 3** of the thesis deals with the synthesis of ultra-short peptides comprising of D- and L-amino acids with antioxidant and antibacterial properties and their conjugation to naproxen (Npx) and indomethacin (Ind) to provide better selectivity towards COX-2 enzyme, implicated in inflammation. The peptides were self-assembled into supramolecular gels and exhibited high proteolytic stability, potent antibacterial, and radical scavenging activities. These gels decreased the expression of proinflammatory cytokines and elevated the expression of anti-inflammatory cytokines. The gels show a strong potential as a topical agent for treating chronic wounds or as a coating material for medical devices to prevent implant-associated infections.

In chapter 4, we have investigated the self-assembled peptide gels to facilitate bone tissue regeneration because the conventional strategies to treat bone defects face challenges, like immunogenicity, lack of cell adhesion, and absence of osteogenic activity. We have developed collagen and non-collagen protein-inspired bioactive peptides with osteoinductive potential, which can play a role in biomineralization and promote bone formation. We have synthesized six amphiphilic tetra-peptides, out of which four were self-assembled into gels. The change in their nanostructured morphology was observed with the change of a single amino acid and have investigated their role in the adsorption of hydroxyapatite and differentiation of mesenchymal stem cells to accelerate bone tissue regeneration. Enzyme is a natural catalyst comprising of proteins, and their remarkable catalytic activity depends on the amino acids present at the active site. **Chapter 5** discusses the design and development of self-assembled peptides as enzyme mimetics. We have developed peptide-ceria nanoparticle conjugates and evaluated their potential to act as esterase, phosphatase and haloperoxidase-mimicking enzyme. The biocatalytic activity of the peptide immobilized on ceria nanoparticles can provide benefits in several therapeutic applications like bone tissue regeneration and anti-biofouling material preparation. **Chapter 6** provides a conclusion of the work done in this thesis along with the contribution of this work to the existing knowledge and its future perspectives.

Keywords: Biomaterials; Self-assembled peptides; Drug delivery; Chronic wound healing; Bone tissue regeneration; Biocatalyst-mimic

List of Publications

1. **Halder, M.;** Singh, A.; and Singh, Y.; Investigating the Role of Amino Acids in Ultrashort Peptide Based Biomaterials for Hydroxyapatite Binding and Osteogenic Differentiation of Mesenchymal Stem Cells to Aid Bone Tissue Regeneration (**chapter 4, manuscript submitted**)
2. Roy, S.; **Halder, M.;** Ramprasad, P.; Dasgupta, S.; Singh, Y.; and Pal, D.; Oxidized pullulan exhibits potent antibacterial activity against *S. aureus* by disrupting its membrane integrity. *Int. J. Biol. Macromol.* **2023**, *249*, 126049
3. **Halder, M.;** Narula, M.; and Singh, Y.; Supramolecular naproxen and indomethacin conjugated peptide gels with antioxidant, antibiofilm, and anti-inflammatory properties for chronic wounds. *Bioconjugate Chemistry*, **2023**, *34*, 645–663 (**chapter 3**)
4. **Halder, M.;** Bhatia, Y.; and Singh, Y.; Self-assembled di- and tripeptide gels for the passive entrapment and pH-responsive, sustained release of an antidiabetic drug, glimepiride. *Biomater. Sci.* **2022**, *10*, 2248-2262 (**chapter 2**)
5. Saini, S. K#.; **Halder, M#.;** Singh, Y.; Nair, R. V. Bactericidal Characteristics of Bioinspired Nontoxic and Chemically Stable Disordered Silicon Nanopyramids. *ACS Biomater. Sci. Eng.* **2020**, *6*(5), 2778–2786.
6. Sharma, P. K.; **Halder, M.;** Srivastava, U.; Singh, Y. Antibacterial PEG-Chitosan Hydrogels for Controlled Antibiotic/Protein Delivery. *ACS Appl. Bio Mater.* **2019**, *2* (12), 5313–5322 (invited research article)

Conferences

1. **Halder, M.**; Narula, M.; and Singh, Y., Naproxen and indomethacin-conjugated antioxidant and antimicrobial peptide gels for chronic wounds, *32nd Annual Conference of the European Society for Biomaterials (ESB 2022)*, Bordeaux, France, 4-8th September, 2022 (**poster, received International Travel Support grant from SERB, DST**).
2. **Halder, M.**; Bhatia, Y.; and Singh, Y, Sustained release of an antidiabetic drug, glimepiride, from self-assembled peptide gels, *ACS Spring 2022 Online*, 5-16th April, 2021 (**poster**).
3. **Halder, M.**; Bhatia, Y.; and Singh, Y, Dipeptide gels for the sustained release of an antidiabetic drug, glimepiride, *International Virtual Conference on Biomedical Materials Innovation-2020 (ICBMI-2020)*, Organized by SBAOI-STERMI, 6-9th December, 2020 (**poster, won the best poster award**).
4. *International Conference on Biomaterial Based Therapeutic Engineering and Regenerative Medicine (Bioterm 2019)*, IIT Kanpur, 28th Nov-1st Dec, 2019.

Table of Contents

Declaration	iv
Acknowledgement	v
Certificate	vii
Lay Summary	viii
Abstract	ix
List of Publications	xi
List of Conferences	xii
List of Figures	xvi
List of Tables	xviii
Notations and Abbreviations	xix
Chapter 1: Introduction	1-40
1.1. Self-assembled peptides	2
1.1.1. Secondary structures	3
1.1.2. Formation of nanostructures	4
1.1.3. Short/ultrashort peptides	5
1.2. Biomedical applications	7
1.2.1. Drug delivery	8
1.2.1.1. Stimulus for drug release	9
1.2.1.2. Routes of administration	9
1.2.1.3. Strategies for drug delivery	10
1.2.1.4. Antidiabetic drug delivery	12
1.2.2. Chronic wound healing	13
1.2.2.1. Types of wound healing	13
1.2.2.2. Treatment of chronic wounds	14
1.2.2.3. Rational design of peptide gels for wound healing	15
1.2.3. Bone tissue regeneration	19
1.2.3.1. Supramolecular peptide as a scaffold	20
1.2.3.2. Biochemical functions of self-assembled peptides	21
1.2.4. Biocatalysis	24
1.2.4.1. Design and fabrication of supramolecular biocatalysts	25
1.3. Knowledge gaps in the field	29
1.4. Objectives	30

1.5. Thesis outline	32
References	33-40
Chapter 2: Self-assembled peptide gels for drug delivery	41-64
2.1. Introduction	42
2.1.1. Diabetes mellitus (Type II)	42
2.1.2. Challenges	42
2.1.3. Research gap	43
2.2. Objectives	43
2.3. Experimental section	44
2.4. Results and discussions	49
2.5. Conclusions	59
References	60-64
Chapter 3: Self-assembled peptide gels for chronic wound healing	65-95
3.1. Introduction	66
3.1.1. Chronic wounds	66
3.1.2. Challenges	66
3.1.3. Research gap	67
3.1.4. Self-assembled peptide gel	67
3.2. Objectives	68
3.3. Experimental section	68
3.4. Results and discussions	76
3.5. Conclusions	81
References	93-95
Chapter 4: Self-assembled peptides for bone tissue regeneration	96-127
4.1. Introduction	97
4.1.1. Bone disorders/osteoporosis	97
4.1.2. Challenges	97
4.1.3. Biomaterials for bone tissue regeneration and research gap	98
4.1.4. Self-assembling peptides	99
4.2. Objectives	99
4.3. Experimental section	100
4.4. Results and discussions	107
4.5. Conclusions	122
References	124-127
Chapter 5: Immobilization of self-assembling peptide on ceria for biocatalysis	128-149
5.1. Introduction	129
5.1.1. Biocatalysis	129
5.1.2. Challenges	129
5.1.3. Self-assembling peptides as biocatalyst	130
5.1.4. Research gap	131
5.2. Objectives	131
5.3. Experimental sections	131
5.4. Results and discussions	137
5.5. Conclusions	146

References	147-149
Chapter 6: Conclusions and perspectives	150-156
6.1. Summary of the thesis	151
6.2. Contribution to the existing knowledge	154
6.3. Future perspectives	155
Appendix	157-232

List of Figures

S. No.	Figure Caption	Page No.
1.1.	The timeline of the development process and the various applications of designer chiral self-assembling peptides	2
1.2.	Secondary structures and nanostructures of self-assembled peptides	4
1.3.	Modification of peptides	6
1.4.	Applications of self-assembled peptides with various supramolecular nanostructures	7
1.5.	Release of drug from self-assembled peptide gels, factors affecting drug release from the scaffolds and strategies for drug delivery	8
1.6.	Four stages of wound healing, hemostasis, inflammation, proliferation, and remodelling	14
1.7.	Pathophysiology of chronic wound environment and properties of multifunctional wound dressings	16
1.8.	Stages of bone fracture healing	18
1.9.	Biochemical functionalization of peptides to achieve several properties for successful bone tissue regeneration	20
1.10.	Design of self-assembled peptide with the active catalytic site similar as the native enzyme to catalyze biochemical reaction	25
1.11.	Catalytic mechanism of serine protease involving catalytic triad (Ser-His-Asp)	26
1.12.	Catalytic mechanism of aldolase I involving catalytic site	27
1.13.	Proline-based aldolase mimicking catalysts to promote nitroaldol reaction	28
1.14.	Objectives of the thesis	31
2.1.	A pH-sensitive, self-assembled peptide gel for the delivery of glimepiride, an anti-diabetic drug	49
2.2.	Structures of peptides used to form self-assembled gels and glimepiride	51
2.3.	Scanning electron microscopy (SEM) images and secondary structures of peptides/gels by CD spectra and Thioflavin T assay	52
2.4.	Rheological properties of peptide gels with and without drug	54
2.5.	Percentage cumulative release of glimepiride from peptide gels at pH 5, 6, and 7.4	55
2.6.	Antioxidant activities of peptides and peptide gels by ABTS and DPPH assay	56
2.7.	Evaluation of cell viabilities by MTT assay	57
2.8.	Live/dead assay of cells treated with glimepiride-loaded peptide gel	57
2.9.	Effect of peptides and gels on reactive oxygen species in HepG2 cells	58
2.10.	Glucose uptake of HepG2 cells	59
3.1.	Naproxen (Npx)- and indomethacin (Ind)-conjugated with peptides forming supramolecular gels and their applications	77
3.2.	Structure of NSAID-peptide conjugates used to form supramolecular gels	78
3.3.	Secondary structures formed by peptide conjugate gels and their rheological properties	79
3.4.	Proteolytic stabilities and antioxidant activities	82
3.5.	Cyclooxygenase (COX) enzyme inhibition and antibacterial activities	84
3.6.	HR-TEM images of <i>S. aureus</i> bacteria	85
3.7.	Biofilm inhibition by gels using crystal violet staining assay	86
3.8.	Cell viability assay by MTT, CCK-8 assay, and live-dead staining	88
3.9.	Cytoskeletal staining and in vitro wound healing in cells	89

3.10.	Effects of conjugates and gels on reactive oxygen species and inflammation	91
4.1.	Self-assembling peptides and their application in bone tissue regeneration	107
4.2.	Structure of self-assembling tetrapeptides, zeta potential, and FESEM micrographs	109
4.3.	Secondary structure formed by peptides and their rheological analysis	110
4.4.	Binding of peptides on the surface of HAp	113
4.5.	Cell viability study by MTT assay and live-dead staining	115
4.6.	Cytoskeletal staining of MC3T3-E1 cells	116
4.7.	Antioxidant activity by ABTS and DCFDA assay	118
4.8.	Osteogenic differentiation study by ALP and Ca deposition assay	119
4.9.	Expression of osteogenesis related genes by qRT-PCR	122
5.1.	Fabrication of thiol-functionalized ceria nanoparticles and their conjugation to branched peptide amphiphile	137
5.2.	Characterization of self-assembled, branched amphiphilic peptide	138
5.3.	Characterization of Ceria nanoparticle (CeNPs), thiol-modified ceria nanoparticle (TC), and peptide-functionalized ceria nanoparticle (TCP)	140
5.4.	FESEM images and particle size distribution studies by DLS	141
5.5.	Catalytic activity	142
5.6.	Cytocompatibility, ALP mimicking and biomineralization study	144
5.7.	Anti-biofouling activity	145

List of Tables

S. No	Table Caption	Page No.
6.1	List of self-assembled peptide-based biomaterials developed	151
A1	The primer sequences used in the RT-PCR study	203
A2	Binding energy, interactions involved, and selectivity index of naproxen, indomethacin, and conjugates to COX-1 and COX-2	204
A3	Binding Affinities (K_{ads}) of HAp binding peptides	226
A4	The primer sequences used in RT-PCR study	227
A5	Ratio of Ce^{3+}/Ce^{4+} estimated using Ce 3d XPS spectrum of TCP	232

Notations and Abbreviations

Acronym	Name
2D/3D	Two/three dimensional
2-NBDG	2-[N-(7-nitrobenz-2-oxa-1,3-diazol-4-yl) amino]-2-deoxy-D-glucose
ABTS	2,2'-azino-bis(3-ethylbenzothiazoline-6-sulfonic acid) diammonium
ACN	Acetonitrile
ADHP	10-acetyl-3,7-dihydroxyphenoxazine
ALP	Alkaline Phosphatase
AMP	Antimicrobial Peptide
Asp	Aspartic acid
AUC	Area under curve
bFGF	basic Fibroblast Growth Factor
BMHP	Bone Marrow Homing Peptide
BMP	Bone Morphogenetic Protein
Boc	tert-Butyloxycarbonyl
CAP	Cell Adhesive Peptide
CCK	Cell counting kit
CD	Circular Dichroism
cDNA	Complementary deoxyribonucleic acid
CFU	Colony forming unit
CMCh	Carboxymethyl chitosan
COL 1	Collagen type I
COX	Cyclooxygenase
CPT	Camptothecin
DAPI	4',6-diamidino-2-phenylindole
DCFDA	2',7'-dichlorodihydrofluorescein diacetate
DCM	Dichloromethane
DEX	Dexamethasone
DFU	Diabetic foot ulcers
DI	Deionized
DIEA	N,N-diisopropylethylamine
DLS	Dynamic light scattering
DM	Diabetes Mellitus
DMEM	Dulbecco's Modified Eagle Medium
DMF	Dimethylformamide
DMP	Dimethoxyphenol
DMSO	Dimethyl Sulfoxide
DNA	Deoxyribonucleic acid
DOX	Doxorubicin
DPPH	1'-diphenyl-2-picrylhydrazyl
DTNB	5,5'-dithiobis-2-nitrobenzoic acid
ECM	Extracellular Matrix
EDT	1,2-ethanedithiol
EDTA	Ethylenediaminetetraacetic acid
EDX	Energy Dispersive X-ray
EGF	Epidermal Growth Factor
ELP	Elastin-Like Polypeptide
EPS	Extracellular polymeric substances
FAP- α	Fibroblast Activation Protein- α
FBS	Fetal Bovine Serum
FDA	Food and Drug Administration
FESEM	Field Emission Scanning Electron Microscopy

FGF	Fibroblast Growth Factor
FITC	Fluorescein isothiocyanate
FTIR	Fourier Transform Infrared
GAPDH	Glyceraldehyde-3-phosphate dehydrogenase
GBD	Global Burden of Disease
Glu	Glutamic acid
GSH	Glutathione
H ₂ O ₂	Hydrogen peroxide
HA	Hyaluronic Acid
HAp	Hydroxyapatite
HATU	1-[bis(dimethylamino)methylene]-1H-1,2,3-triazolo[4,5-b] pyridinium 3-oxide hexafluorophosphate
His	Histidine
HR-TEM	High resolution transmission electron microscope
Hyp	Hydroxyproline
IC ₅₀	Half-Maximal Inhibitory Concentration
IDF	International Diabetes Federation
IGF	Insulin-Like Growth Factor
IL-1/6/8/10	Interleukin-1/6/8/10
Ind	Indomethacin
iNOS	Inducible nitric oxide synthase
LB	Luria-Bertani
LPS	Lipopolysaccharide
LVR	Linear Viscoelastic Range
MCP-1	Monocyte Chemoattractant Protein-1
MEM α	Minimum essential medium alpha
MGC	Minimum Gelation Concentration
MMP-2	Matrix Metalloproteinase-2
MPTMS	3-mercaptopropyl trimethoxysilane
mRNA	Messenger ribonucleic acid
MSC	Mesenchymal Stem Cell
MTT	(3-(4,5-Dimethylthiazol-2-yl)-2,5-diphenyltetrazolium bromide
NaOH	Sodium hydroxide
NMR	Nuclear Magnetic Resonance
NO	Nitric Oxide
NP	Nanoparticle
Npx	Naproxen
NSAID	Nonsteroidal Anti-Inflammatory Drug
OA	Osteoarthritis
OB	Osteoblast
OC	Osteoclast
OCN	Osteocalcin
OD	Optical density
OM	Osteogenic media
OP	Organophosphate
OPN	Osteopontin
Pbf	2,2,4,6,7-pentamethyldihydrobenzofuran-5-sulfonyl
PBS	Phosphate Buffer Saline
PFD	Pirfenidone
PGA	Polyglycolic acid
PGE ₂	Prostaglandin E ₂
PI	Propidium iodide
PLA	Poly lactic acid
PLGA	Poly lactic-co-glycolic acid
pNPA	<i>para</i> -Nitrophenyl Acetate
pNPP	<i>para</i> -Nitrophenyl phosphate
Pro	Proline

pSer	Phosphoserine
PTX	Paclitaxel
RANKL	Receptor Activator of Nuclear Factor Kappa-B Ligand
ROS	Reactive oxygen species
RP-HPLC	Reverse-Phase High-Pressure Liquid Chromatography
RPM	Rotation per minute
RUNX 2	Runt-related transcription factor 2
SD	Standard deviation
SEM	Scanning Electron Microscopy
Ser	Serine
SPPS	Solid Phase Peptide Synthesis
tBu	Tertiary butyl
TCA	Tricarboxylic Acid
TCP	Tricalcium phosphate
TFA	Trifluoroacetic acid
TGA	Thermogravimetric analysis
TGase	Transglutaminase
ThT	Thioflavin-T
TIS	Triisopropyl Silane
TNF- α	Tumor Necrosis Factor alpha
TRAP	Tartrate-resistant acid phosphatase
Trp	Tryptophan
Trt	Trityl
Tyr	Tyrosine
UV	Ultra violet
VEGFA	Vascular Endothelial Growth Factor A
XPS	X-ray photoelectron spectroscopy
XRD	X-Ray diffraction

CHAPTER - 1

Introduction

1. Introduction

1.1. Self-assembled peptides

Molecular self-assembly refers to the spontaneous organization of molecules or building blocks into well-defined structures or patterns driven by inter-or intra-molecular non-covalent interactions, such as hydrogen bonding, van der Waals forces, hydrophobic interactions, electrostatic interactions, and π - π stacking.¹ It is a typical phenomenon observed in many biological processes that produce various supramolecular structures, such as nucleic acids, proteins, phospholipids, and even viral capsids.² The formation of the double helical DNA structure in biological systems is a classic example of molecular self-assembly driven by the identification of nucleobases on the complementary strands.³

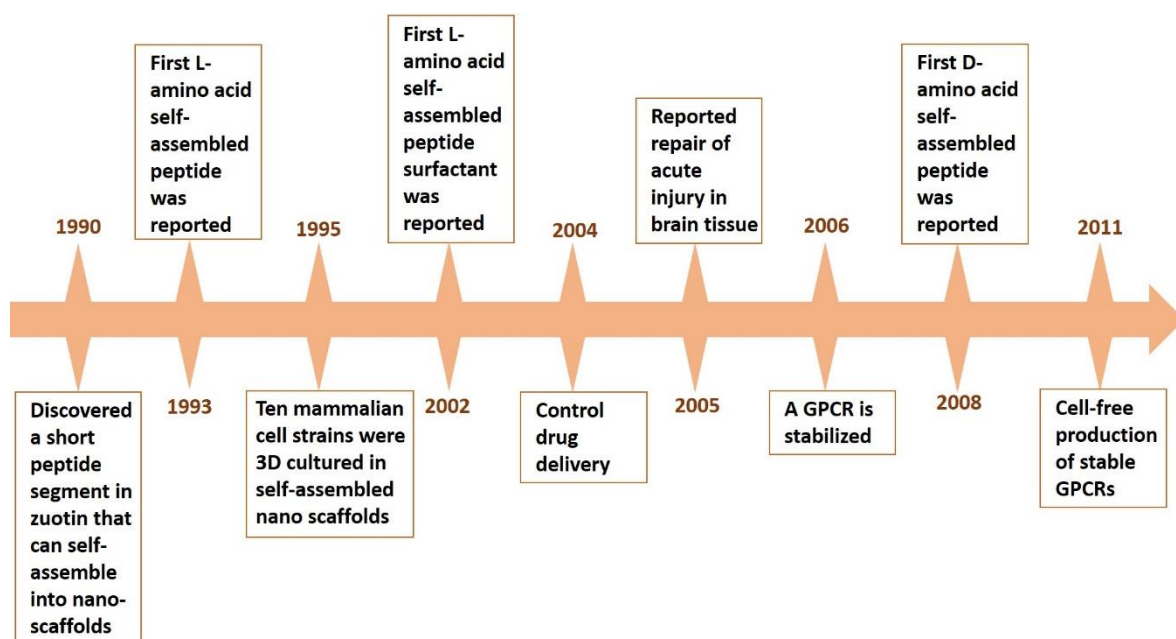


Figure 1.1. The timeline of the development process and various applications of designer chiral self-assembling peptides.

Another intriguing example is collagen protein, which produces the triple-helical structure regulated by the self-assembly process in the extracellular matrix (ECM).⁴ Natural and synthetic peptides (peptoids and peptidomimetics) can also generate stable and fascinating self-assembled structures, which have recently received a lot of attention in the disciplines of materials science, nanotechnology, medicine, and biomedical engineering.⁵ However, the concept of peptides as materials was not recognized until 1990, when a self-assembling peptide (EAK-16) was accidentally discovered by Prof. Zhang as a repeating sequence in a yeast protein (zuotin) (**Figure 1.1**).⁶ Peptides are interesting entities due to biological characteristics, such as biocompatibility, bioactivity, biodegradability, high water content, microporous structure, mechanical stability, elasticity, and potential injectability.

Therefore, it has gained enormous attention across the globe and several groups are currently pursuing research on diverse self-assembling peptides for a wide range of applications, including new biological materials, surface coating materials, and semi-conducting devices as well as a new class of antibiotics to fight drug resistance concerns.⁷ The field is still expanding. By controlling the interactions between molecules and the conditions of self-assembly, researchers can tailor the properties and functions of the resulting structures, opening up new possibilities for creating advanced materials and devices. The supramolecular self-assembly is regulated by the folding of individual peptides in aqueous solution, therefore, it is critical to understand, which secondary structures (α -helix, β -sheet, and random coils) exist and how they might be employed for self-assembly.⁸ Several ways for designing self-assembled peptides have been developed during the last several decades. Different supramolecular nanostructures, such as nanofibers, nanotubes, nanosphere, nanorod, nanotape have been developed after self-assembly with distinct features and functionalities.

1.1.1. Secondary structures

It is important to note that some self-assembling peptides can exhibit a mixture of secondary structures or undergo conformational changes during the self-assembly process.⁸ The specific secondary structure adopted by a self-assembling peptide depends on factors, such as the amino acid sequence, solvent conditions, temperature, pH, and the presence of external stimuli. The secondary structures influence the packing and arrangement of peptide molecules, ultimately determining the resulting nanostructures formed through self-assembly (**Figure 1.2A**).

α -Helices: α -Helices are characterized by a right-handed coil-like structure, where the peptide backbone forms a spiral shape stabilized by hydrogen bonding between the backbone amide and carbonyl groups. The α -helical conformation can facilitate the self-assembly of peptides into fibers or higher-order structures.

β -Sheets: Self-assembling peptides can also adopt β -sheet structures, where the peptide chains form extended, planar arrangements. β -Sheets are stabilized by hydrogen bonding between peptide strands running in parallel or antiparallel directions. These hydrogen bonds create a characteristic pleated-sheet structure.

Coiled-Coils: Coiled-coil structures are commonly observed in self-assembling peptides that contain heptad repeat sequences, such as the well-known leucine zipper motif. Coiled-coils consist of two or more α -helices winding around each other in a supercoiled manner. The hydrophobic interactions between the repeating amino acid residues in the coiled-coil motif contribute to the stability and self-assembly of the peptide.

Random Coils: Not all self-assembling peptides adopt well-defined secondary structures. Some peptides have regions that exist as random coils, lacking a specific secondary structure. Random coil regions can provide flexibility and conformational freedom, allowing self-assembling peptides to adapt to different environments or interact with other molecules.

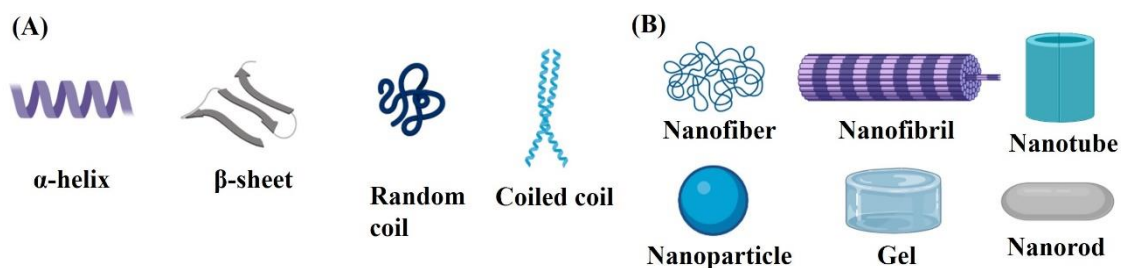


Figure 1.2. (A) Secondary structures of self-assembled peptides. (B) Nanostructures of self-assembled peptides.

1.1.2. Formation of nanostructures

Self-assembled peptides have gained significant interest in nanotechnology and biomedical applications due to their ability to form diverse nanostructures with various functionalities.⁹ Based on how they are designed, self-assembling peptide nanostructure can be divided into different categories, such as fibers, cylinders, or flat shapes.¹⁰ Micelles fall under the category of self-assembled nanostructures. These variations depend on the building block designs and result from the hydrophobic interaction of peptides in aqueous solutions. We have listed a few self-assembling peptide nanostructures here (**Figure 1.2B**).

Nanofibers. The self-assembling peptide EAK16 sequences with irregularly repeating positive and negative charges first construct conventional β -sheet structures before eventually forming a hydrogel network of nanofibers in a checkerboard-like pattern.⁶ Nanofibers typically have a diameter of less than 100 nm. In most cases, self-assembling peptide building blocks are employed to create nanofibers in aqueous solutions with ions of various pH levels. The most well-known self-assembling peptides that produce nanofibers are peptide amphiphiles with an alkyl group.¹¹

Nanotubes. Nanotubes have a structure that is comparable to that of the previously mentioned nanofibers. On the inside of the capillary, they are elongated nanostructures with a hole. Due to their benefits in self-organization and ease of control over nanotube sizes, recent research has concentrated on the production of non-covalent nanotubes. Cyclic peptides are the most utilized materials for nanotubes.¹² Cyclic peptide nanotubes are constructed by stacking peptides that are more stable than other peptide building blocks. Nanotube-based peptide assemblies have a wide range of uses in drug delivery since drugs can be put within these tubes and can be conjugated or attached to the outside of the tubes. A unique structure of nanotubes is created by the cyclic peptide cyclo[-(L-Gln-D-Ala-L-Glu-D-Ala)₂-] with an even number of alternate D- and L-amino acids.¹³

Nanoparticles. Nanoparticles come in a variety of shapes and are made up of many constituent parts. The structures include solid structures as well as hollow nanospheres. Poly(L-lysine)-b-poly(L-leucine) is a charged amphiphilic block co-polypeptide that self-assembles to form stable vesicles and micelles in aqueous solutions.¹⁴ Their hydrophobicity helps in maintaining their stability and stiffness. Additionally, arginine's guanidine residue boosts its cell-penetrating abilities, which helps in the

distribution of encapsulated elements, like medications. Elastin-like polypeptide (ELP), a temperature-responsive self-assembling peptide, is a linear di-block peptide that, upon drug loading, produces spherical micelles in response to a temperature change. By adding more ELP units, the sensitivity of ELP to temperature can be reduced. Nanostructures that form vesicles are also produced by cyclic peptides. Shirazi *et al.* showed that the [WR]₄ peptide, which has a circular vesicle-like shape and a size range of 25 to 60 nm, successfully served as a drug delivery vehicle for molecular cargo.¹⁵

Nanotapes. In order to create nanotapes, β -alanine-histidine dipeptide and lysine-threonine-threonine-lysine-serine pentapeptide are individually attached to C₁₆ palmitoyl hydrophobic lipid chains (C₁₆- β -AH and C₁₆-KTTS).¹⁶ Due to the hydrophobicity of the lipid tail, C₁₆-AH self-assemble into fibrils. pH or temperature can influence how C₁₆-KTTS self-assembles; if the pH drops to 4, tape morphology changes to fibrils but if it drops even lower to 3, the nanotape structure restores.¹⁷ Self-assembling peptide nanotape structures frequently interact with one another to generate double layers. These nanotapes have a tendency to create hydrogels when their concentration rises above a particular threshold.

Gels. Self-assembled peptides can form three-dimensional networks known as gels. Gels are water-swollen matrices that provide a hydrated and biocompatible environment.¹⁸ These peptide gels have unique mechanical properties and can be engineered to mimic the extracellular matrix, making them useful for tissue engineering, wound healing, and drug delivery applications.

1.1.3. Short/ultrashort peptides

Short/ultrashort peptides are incredibly promiscuous candidates that can provide a plethora of materials with fascinating features at low cost. Material properties can be easily modified by making changes to the sequence, backbone, and side-chains. These small alterations result in changes in the organization mode during the self-assembly process.

C-terminal modifications. Small peptide self-assembly involves a careful balance of solubility and hydrophobicity. Modification at C-terminal with glycosidic linkage (**Figure 1.3A**) enhance self-assembling tendency in water, thus increasing the biocompatibility.¹⁹ Modification with cationic pyridinium group enhances the antimicrobial properties (**Figure 1.3B**).²⁰

N-terminal modifications. Many researchers have been interested in ultrashort peptides with diverse aromatic and heteroaromatic groups at the N-terminus because these changes have a strong potential to lead to supramolecular assembly via aromatic interactions. Modification of N-terminus with diphenyl²¹ (**Figure 1.3C, D**) or Fmoc-group²²(**Figure 1.3C, E**) as a capping agent increases the aromatic interactions and propensity to form β -sheet structures. Protection of N-terminus by capping agent, like 4-(dihydroxyboryl)benzyloxycarbonyl (Bhcmoc)²³, was used for photo- and glucose-responsive insulin release (**Figure 1.3C, F**).

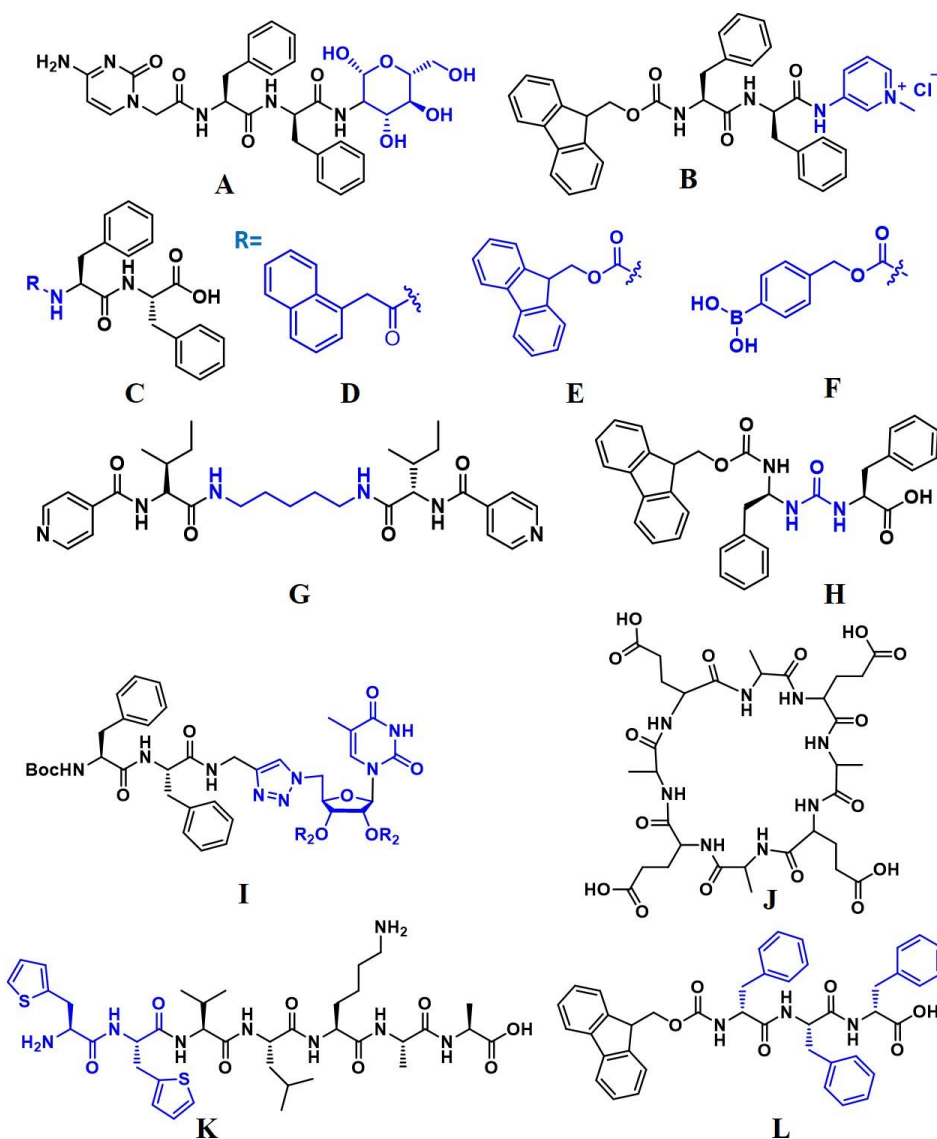


Figure 1.3. Modification of peptides. (A-B) C-terminal. (C-F) N-terminal. (G-H) Backbone. (I) Nucleic acid-based. (J) Cyclization. (K-L) Side chain.

Backbone modifications. Backbone alterations are aimed at controlling and manipulating the material characteristics and metabolic stability of the biomaterial. Insertion of hydrophobic aliphatic chain in the middle portion triggers the self-association and gelation potential of the peptide (**Figure 1.3G**)²⁴. Amide bond surrogate urea was also used to improve the mechanical strength of the self-assembled peptide gel (**Figure 1.3H**).²⁵

Nucleic acid-based modifications. Conjugation of nucleic acid at the C-terminus of the peptide via azide linker was reported to possess excellent stability towards external stimuli, such as pH and temperature (**Figure 1.3I**).²⁶

Modification through cyclization. Cyclization of linear peptide enhances their proteolytic stability and changes the nanostructure (nanovesicle) in its self-assembled form (**Figure 1.3J**).²⁷

Side chain modifications. Peptides contain a variety of functional groups, such as side chains from amino acids, ranging from hydroxyl groups to sulfur, aromatic, heteroaromatic, and carboxylic acid groups in addition to the amine at the N-terminus and the carboxylic group at the C-terminus. These side chains are widely investigated due to their reactivity. Modification of phenylalanine with thienylalanine increases the conductivity of the peptide (**Figure 1.3K**).²⁸ The incorporation of unnatural amino acids like D-amino acids results in extraordinary enzymatic stability (**Figure 1.3L**).²⁹

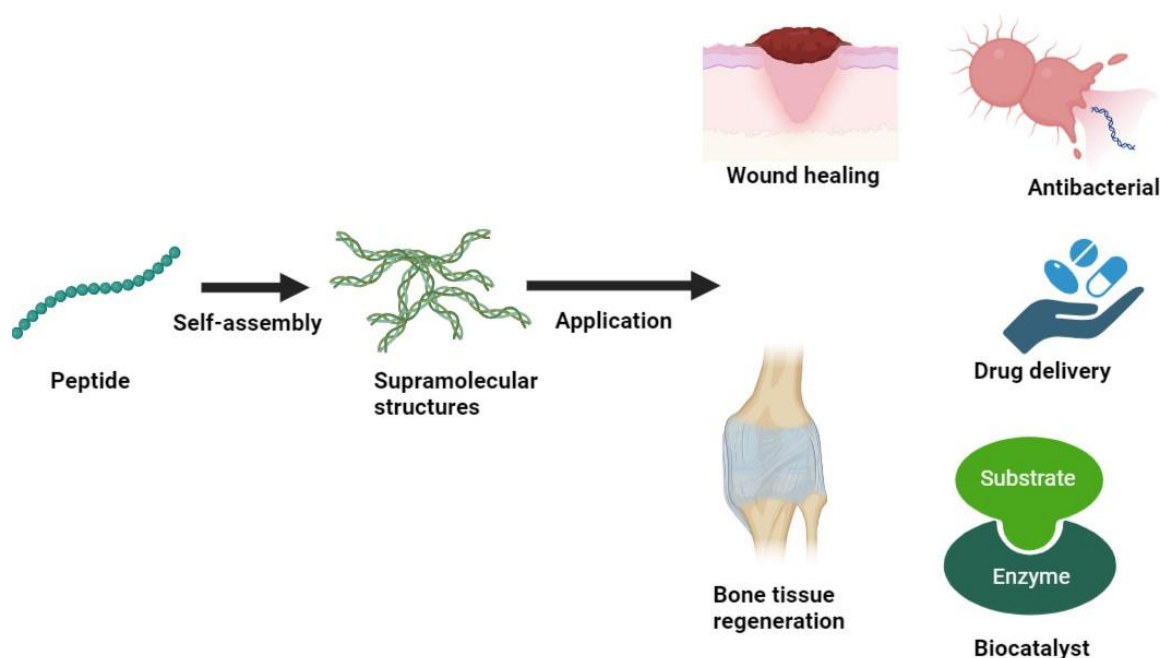


Figure 1.4. Applications of self-assembled peptides with various supramolecular nanostructures in biomedical field.

1.2. Biomedical applications

Peptide-based self-assembled materials have been involved in a variety of commercial goods and have genuinely moved from bench to market. Many dermatological treatments contain bioactive peptides, like Matrixyl.³⁰ C₁₆-GHK is a dermal collagen fragment utilized as an active ingredient to treat problems related to ageing skin, such as wrinkles, spots, and loss of suppleness. PuraMatrix is a commercially available self-assembled peptide used in 3D tissue culture that encourages tissue growth and vascularization, is biodegradable and nonimmunogenic, and may interact with cells.^{31,32} Thus, the importance of self-assembling peptide is growing at commercial level. Self-assembling peptide-based functional materials have been extensively researched for applications in a variety of domains but this thesis focuses mainly on drug delivery, antibacterial, tissue engineering, and biomimetic catalysis applications (**Figure 1.4**).^{33–35}

1.2.1. Drug delivery

Drug delivery refers to the process of administering pharmaceutical substances to the body in order to achieve a therapeutic effect.³⁶ It involves the transport of drugs from their site of administration to their target location within the body, where they can exert their desired pharmacological actions. Drug delivery systems are designed to enhance the effectiveness and safety of drugs by controlling their release rate, targeting specific tissues or organs, and improving their bioavailability. These systems can be classified into various categories based on the route of administration, such as oral, topical, transdermal, inhalation, intravenous, and implantable devices. The primary goals of drug delivery systems include sustained and/or controlled release, enhanced bioavailability, protection and stability, and targeted drug delivery. To achieve these goals, drug delivery systems employ various techniques, including encapsulation within nanoparticles, liposomes, or microspheres; incorporation into gels, patches, or implants; or utilizing specialized devices and carriers. Advancements in drug delivery systems have revolutionized the field of medicine, enabling more effective treatment of various diseases, such as cancer, diabetes, cardiovascular disorders, and neurological conditions. These systems offer better control over drug administration, improve patient compliance, and enhance therapeutic outcomes.

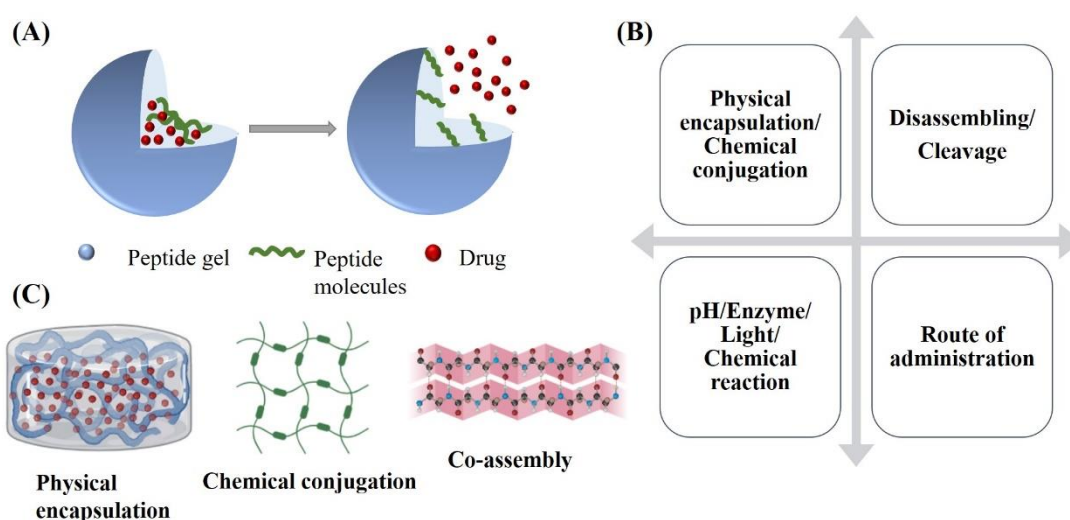


Figure 1.5. (A) Release of drug from self-assembled peptide gels. (B) Factors affecting the drug release from the scaffolds. (C) Strategies for drug delivery.

Self-assembling peptides offer several advantages in drug delivery, including their biocompatibility, ease of synthesis, and the ability to precisely control the release kinetics of drugs.³⁷ However, challenges still exist in terms of stability, scalability, and the fine-tuning of release profiles. Continued research and development are aimed at addressing these challenges to fully harness the potential of self-assembling peptides in drug delivery applications. Self-assembled peptide-based drug delivery systems typically transport pharmaceuticals via physical encapsulation or chemical conjugation, and drugs can be released via nanostructure disassembly or breaking of conjugated bonds. Following targeted delivery to tumor cells, nanomaterials can activate medication release in a specific region via

responsive factors.³⁸ The possible benefits, include reduced medication administration and spatiotemporal control of sustained drug release, which allows pharmaceuticals to be released at precise times and locations. In terms of the biological system, the internal responsive elements, such as pH, enzyme, and reducing conditions are employed to stimulate the release of medication. Several review articles published recently have discussed the diverse aspects of polymeric and peptide-based bioinspired materials in drug delivery.^{37,39–41}

1.2.1.1. Stimulus for drug release

By incorporating stimulus-responsive elements into the peptide gel structure, drug release can be triggered in a controlled manner, allowing for targeted and on-demand drug delivery (**Figure 1.5**). The choice of stimulus depends on the desired application and the specific requirements of the drug delivery system. Researchers continue to explore and develop novel peptide-based gel systems with tailored stimulus-responsive properties for effective drug delivery. The commonly used stimuli, which encourages the drug release from the scaffolds are described below.

pH. pH-responsive peptide scaffolds can be designed to respond to changes in pH. Peptides with pH-sensitive amino acids or pH-responsive motifs can undergo conformational changes or solubility alterations in response to specific pH conditions.⁴² By incorporating such peptides into the gel structure or designing peptide linkers with pH-sensitive properties, drug release from the peptide gel can be triggered in response to changes in pH levels.^{43,44}

Temperature. Temperature-responsive peptide gels can undergo phase transitions in response to temperature changes.^{45,46} Thermosensitive peptides can self-assemble into a gel at lower temperatures (sol-to-gel transition) and disassemble into a sol at higher temperatures (gel-to-sol transition). By tuning the gelation temperature, drug release can be triggered by simply adjusting the temperature of the gel. Thermosensitive polymer can also be integrated into the self-assembling peptide to make the system thermo-responsive.^{47,48}

Enzyme. Enzyme-responsive peptide gels can be designed to respond to specific enzymes present in the target tissue or cellular environment.^{49,50} Peptides can be engineered with enzyme-cleavable sequences that break down in the presence of specific enzymes. The enzymatic degradation of the peptide gel can lead to the release of the encapsulated drug.^{51,52}

Light. Light-responsive peptide gels can be constructed by incorporating light-sensitive molecules or photo responsive peptides. Light can trigger changes in the gel structure or properties, such as sol-gel phase transitions or disassembly, enabling drug release upon light exposure. Photo responsive peptides or molecules can undergo conformational changes or photochemical reactions upon light irradiation, resulting in gel dissolution and drug release.²³

1.2.1.2. Routes of administration

Peptide gels can be administered through various routes, depending on the intended application and target site. Here are some common routes of administration for peptide gels:

Topical application. Peptide gels can be applied directly to the skin or mucous membranes for local treatment. This route is commonly used for wound healing, dermatological conditions, or drug delivery to specific sites on the body surface.

Injectable. Peptide gels can be formulated as injectable formulations to be administered via injection. Depending on the gel's viscosity and the desired site of administration, the gel can be injected subcutaneously, intramuscularly, or intradermally. Injectable peptide gels are particularly useful for targeted drug delivery or tissue engineering applications.

Intraocular. Peptide gels can be administered directly into the eye for ophthalmic applications. They can be applied topically to the ocular surface or injected into the eye's anterior or posterior segment. Intraocular administration of peptide gels is employed for ocular drug delivery or to promote tissue repair in ophthalmic disorders.

Intranasal. Peptide gels can be formulated for intranasal administration. They can be applied as a gel formulation or as a gel-loaded device, such as a nasal spray or nasal gel. Intranasal administration is advantageous for delivering drugs to the nasal cavity, sinuses, or brain via the olfactory route.

Implantable. Peptide gels can be used as implantable devices or scaffolds. They can be surgically placed at the target site, such as in tissue engineering, regenerative medicine, or drug delivery applications. Implantable peptide gels provide sustained release of drugs and support tissue regeneration.

It is important to note that the route of administration for peptide gels may require appropriate formulation, sterilization, and safety considerations. The specific choice of administration route depends on the therapeutic goal, target tissue, and desired drug release profile.

1.2.1.3. Strategies for drug delivery

After comprehending the techniques of drug release followed by administration through different routes, this section offers flexible strategies to fabricate drug delivery systems and their relevant applications based on peptide-modulated self-assembly (**Figure 1.5C**).

Physical encapsulation of drug

Self-assembled peptide nanostructures can be developed to physically encapsulate the cargo in its hydrophobic spaces and release the drug upon degradation of the matrix.³⁷ The drug is released from the scaffold in response to various disease associated biochemical hallmarks/stimulus, such as pH, enzyme, temperature, and redox condition. Stupp and coworkers fabricated histidine-containing self-assembled peptide amphiphile and physically encapsulated anticancer drug, camptothecin (CPT) for acidic environment-sensitive release.⁵³ Histidine residues in the peptide amphiphile was protonated leading to electrostatic repulsion, which caused disassembling of the gel to release the drug. Another

responsive factor of tumor microenvironment is reducing condition. Yang *et al.* reported a gemcitabine supramolecular peptide gel, Nap-GFFYGD, which contain thiazolidinone as H₂O₂-responsive content at the C-terminal of the peptide.⁵⁴ At the tumor cell, the thiazolidinone moiety gets removed by H₂O₂ which triggers the gel-sol transition and release the drug. Matrix metalloproteinase-2 (MMP-2) responsive peptide-based scaffold was constructed by Nie and co-workers to specifically release pirfenidone (PFD) at the pancreatic tumor site where MMP-2 is overexpressed.⁵⁵

Different types of assemblies are formed by the peptides to deliver the bioactive substances. It can be in the form of gel or several nanoscale architectures.

Gels. Most of the time, nanogels were made of entangled nanofibers, which served as a reservoir for the delivery of bioactive substances. Drug release from nanogels is mostly influenced by nanofiber degradation or the diffusion effect, and the release profiles can be expertly tailored by making small adjustments to the constituent molecules or taking advantage of the synergistic interactions between the architecture and microenvironment. It is generally known that gels based on D-amino acids withstand enzymatic digestion better than those based on L-amino acids. In this instance, it was shown that gels containing D-amino acids had a superior potential as intelligent reservoirs for long-term controlled drug release, while gels containing L-amino acids were more ideal for short-term fast drug release.⁵⁶ It is advantageous to modulate the stiffness and porosity of the final supramolecular hydrogels by adding specific constituent amino acids to a peptide sequence, which might be used to create controlled drug release systems.

Nanoscale particles. The favored means of delivering bioactive substances into organisms have usually been nanoscale particles, like liposomes, micelles, and nanoparticles (NPs). The US Food and Drug Administration (FDA) has approved several delivery methods, including liposomal doxorubicin (Doxil), albumin-bound paclitaxel (PTX) NPs (Abraxane), micellar estradiol (Estrasorb), and others. Biocompatible peptides can be used as drug carriers in addition to polymers, phospholipids, and other typical excipients to release nonspecific physically encapsulated drug molecule. The peptide molecule might have characteristics, like controlled morphology, stimuli-responsiveness, and targeting. Researchers are also particularly interested in modifying delivery systems with peptide ligands because of their low immunogenicity and simplicity of manufacture. Zhang's group fabricated an amphiphilic chimeric peptide ((Fmoc)₂KH₇-TAT) that could self-assemble into micelles.⁵⁷ The micelles were able to achieve simultaneous co-delivery of the medication and gene by utilizing the hydrophobicity of the micelle core and the positive charge carried by TAT peptide (YGRKKRRQRRR).

Chemical conjugation of drug to the peptide

Covalently joining peptide and drug molecules results in peptide-drug conjugates, which serve as building blocks for the self-assembly of nanomaterials used in drug delivery systems. Drugs may be released by cleaving the linkers between them and peptides, either naturally or by inserting linkers

which are cleaved by the enzyme overexpressed at the disease site. Delehanty and co-workers⁵⁸ reported a drug delivery system, where three distinct linkages, ester, disulfide, and hydrazine, were used to conjugate the self-assembling peptide to the drug, doxorubicin (Dox), which were cleaved by cellular esterase, highly reductive cytosolic glutathione (GSH), and low pH environments to release Dox. Peptide dendrimer-doxorubicin (Dox) conjugate-based nanoparticles were developed by Gu and coworkers as an enzyme-responsive drug delivery system for the treatment of breast tumors. Dox is conjugated to the dendrimer through the enzyme-sensitive tetrapeptide (GFLG), which is a substrate of cathepsin B that is overexpressed in many tumor cells and tumor endothelial cells.⁵⁹

Co-assembly assisted drug delivery

The main distinction between co-assembly-based drug delivery and physically encapsulated drug delivery is that in the co-assembly drug delivery system, the drugs themselves act as one of the most essential building blocks for the carriers. In other words, the drugs are crucial to sustaining the morphologies of the formulations at the non-target site and exerting therapeutic impact at the target site from a co-assembled drug delivery system. Using in vitro co-assembly as a delivery method, small-molecule chemotherapeutic medicines were also administered. A fibroblast activation protein (FAP- α)-responsive peptide was used by Zhao *et al.* to functionalize DOX-loaded spherical NPs, where Dox caused the reassembly of fiber-like structures or co-assembly with peptides.⁶⁰ At the FAP- α overexpressed tumor locations, rapid and effective Dox release from this nano system was successfully demonstrated. This caused the breakdown of the tumor stroma and further increased drug penetration into the tumors.

1.2.1.4. Antidiabetic drug delivery

It has been observed from the literature that peptide gels are widely explored as a drug delivery vehicle for the release of chemotherapeutic agents to overcome their side effects due to non-specificity. However, antidiabetic drugs, like sulfonylurea derivatives also encounter certain limitations related to sudden drop of blood glucose (hypoglycemia) causing dysfunction of kidney and liver. Frequent administration of medication is also required to maintain an optimum level of glucose in blood. Peptides gels are very less exploited in this field to deliver a hydrophobic antidiabetic drug, which also suffers from low solubility in blood. Antidiabetic drug/insulin delivery has been achieved earlier by few scientists where biomaterials were developed to sense the glucose oxidase or low pH due to overproduction of gluconic acid. Some insightful reports from the literature include mesoporous silica nanoparticles, peptide scaffolds, peptide-polymer composites, and boronic acid grafted polymers for insulin delivery. Control release of lipopeptide (liraglutide)⁶¹ and polypeptide (lixisenatide)⁶² were also reported from polymeric hydrogel based drug delivery system, whereas metformin delivery was achieved from lauric acid coated microneedles.⁶³ All these biomaterials solely acted as drug delivery vehicle for short term use. Thus, it will be interesting to rationally design a peptide-based drug delivery system, which can act as a carrier of an antidiabetic drug, provide a sustained release profile, and also treat oxidative stress caused by the generation of reactive oxygen species.

1.2.2. Chronic wound healing

Many millions of individuals experience discomfort, suffering, and, in severe cases, impairment as a result of wounds brought on by trauma, burns, surgery, and chronic diseases.⁶⁴ As obesity and diabetes are becoming more common, the burden of chronic wounds is growing, leading to therapeutic issues, and rising medical expenses. As a result, the medical system continues to face significant difficulties in the treatment of wounds. The complex and well-organized process of wound healing begins as soon as an injury occurs.

1.2.2.1. Types of wound healing

Normal wound repair. Four overlapping but separate stages make up the normal mammalian dermal wound healing process⁶⁵: a) hemostasis and the early inflammatory response; b) the late inflammatory response (the removal of dead and devitalized tissues and the prevention of infection); c) angiogenesis and the proliferation of new tissue; and d) tissue remodeling (**Figure 1.5**). The entire process is strictly regulated by several cells and many growth factors, cytokines, and chemokines, which are produced in order to achieve barrier closure and functional recovery. When a cutaneous injury develops, the initial step in healing is to stop the bleeding and reduce hemorrhage. This quick process is accomplished by blood vessel constriction, platelet aggregation, and blood clot formation. In the following phase, inflammation starts right after the tissue injury. Infected and chronic wounds experience longer-lasting inflammation. Several inflammatory cytokines and cells are drawn in during homeostasis and activated. These cytokines also encourage fibroblast migration, which kick-starts the development of the subsequent step, tissue proliferation. In this stage, the wound develops new blood vessels (also known as neovascularization or angiogenesis), and ECM proteins (collagen fibers and granulation tissues) are produced and deposited, creating a fresh surface for keratinocyte migration in the following step. The regulation of angiogenesis depends heavily on vascular endothelial growth factor A (VEGFA).⁶⁶ The last stage is remodeling. During this stage, the majority of active inflammatory cells either exit the wound by programmed cell death or outflow, leaving mostly ECM proteins and collagen. The wound healing process is complete when collagen is remodeled and scarred. Pathogenic infection will impede the process of wound healing and, in severe circumstances, could be fatal. In order to ensure successful wound healing, it is crucial to prevent and treat infections.

Chronic wound repair. The pathophysiological manifestations of chronic wounds include prolonged or excessive inflammation, persistent infection, poor angiogenesis, challenging re-epithelialization, dysregulated levels of cytokines/growth factors, and enhanced protease activity (**Figure 1.7A**).⁶⁷ Vascular ulcers, diabetic ulcers, and pressure ulcers make up the bulk of chronic wound types. In contrast to acute wounds, chronic wounds have higher levels of pro-inflammatory cytokines (IL-1, IL-6, and TNF- α), as well as inflammatory chemokines (MCP-1 and IL-8). As a result, matrix metalloproteinases (MMPs) are produced more frequently and tissue inhibitors of MMPs are decreased, which prevents the formation of ECM and dermal reconstruction. A critical stage in the

healing of chronic wounds is the transition from the inflammatory to the proliferative stage; therefore, it is essential to develop methods to aid this transition efficiently.

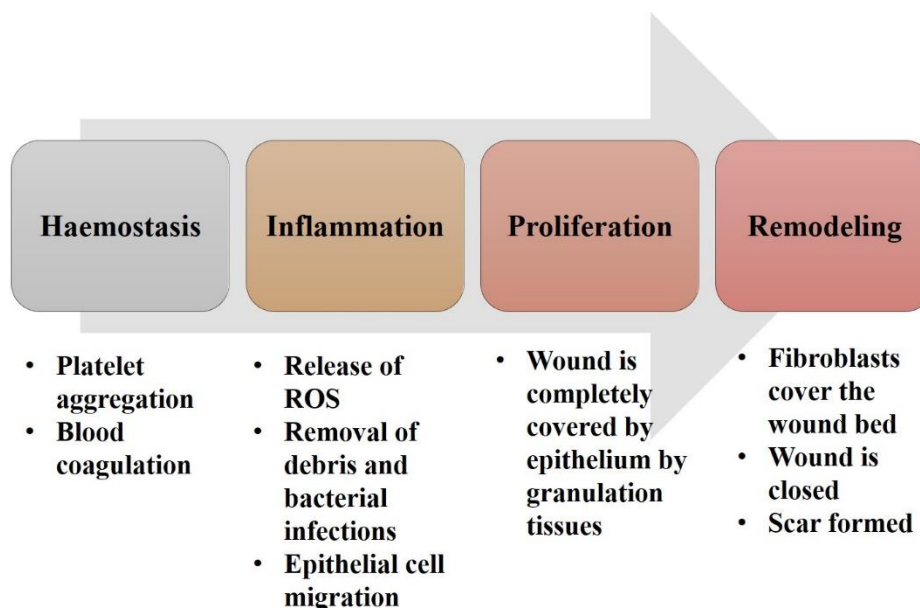


Figure 1.6. Four stages of wound healing- hemostasis, inflammation, proliferation, and remodeling.

1.2.2.2. Treatments of chronic wounds

Wounds can currently be treated with a variety of methods. Invasive surgical procedures (surgical debridement and skin grafting) include a risk of bleeding or tissue damage, necessitate bed rest, and are expensive to provide. Due to the following benefits, gel dressings have demonstrated considerable potential in non-invasive therapy: a soft tissue-like 3D structure, exceptional in situ solid gel formation following injection, and the capacity to act as specialized carriers of medicines, proteins, or cells. In order to promote wound healing, various types of biomaterial-based hydrogel dressings have been developed, including those made of peptides, chitosan, collagen, alginate, heparin, cellulose, and hyaluronic acid. Wound dressings made of peptides have drawn a lot of attention. Since peptides are widely distributed throughout the human body and have unique biological functionality, activity, and selectivity, both naturally occurring and synthetic peptide molecules can have a variety of biological impacts. For instance, several peptides, including OA-GL12, OA-GL21, RL-QN15, and Ot-WHP, found in the skin secretions of amphibians, have been shown to hasten the healing of wounds, both acute and chronic lesions caused by diabetes.⁶⁷ Furthermore, by playing crucial roles in wound proliferation and tissue remodeling, certain peptide growth factors, such as epidermal growth factor (EGF) and fibroblast growth factor (FGF), enhance wound healing.⁶⁸

Self-assembling peptides with rational design can mimic the extracellular matrix (ECM), activate humoral and cellular immunity, aid in drug transport, and target specific cells or organs. Additionally, compared to conventional polymer gels, low-molecular-weight peptide-based gels offer greater biocompatibility and biodegradability.⁶⁹ As a result, these gels rarely have serious negative effects and are suitable for the majority of tissue engineering applications. Self-assembling peptide-based gels

have numerous uses in nanotechnology and biomedicine, such as for the topical delivery of drugs, the treatment of tumors, and as an immunological adjuvant for 3D tissue cell culture, tissue healing, and tissue regeneration. Due to their capacity to adapt to changes throughout complex wound healing processes, self-assembling peptide-based molecules have demonstrated significant potential for multimodal treatment. By encoding peptide sequences, it is possible to produce self-assembling peptides with ordered structures, including spheres, vesicles, micelles, nanofibers, and nanotubes with new properties. For instance, it has been reported that nanospheres can contain and deliver medications and nanofibers that can entangle into gels under aqueous medium.⁷⁰ Additionally, the peptide-based fibrous network is similar to fibrin in the ECM in terms of structure and content, which makes it easier to repair injured tissues and restore their biological functions.

Applying cotton or gauze bandages or other natural or artificial bandages was the earliest form of wound care. This kept the wound dry and stopped bacteria from entering. Studies conducted afterwards proved that a warm, moist environment can promote quicker and more effective wound healing. Utilizing hydrogel formulations is seen to be a successful practice since it allows for spatiotemporal control of wound healing. In terms of their in vivo and environmental toxicity, hydrogels, and peptidyl gels in particular have several advantages over other materials. Hydrogels have a high-water content, adjustable mechanical stability, great injectability, and exceptional biocompatibility on a macroscopic level. Microscopically, appropriately created peptide sequences can respond to numerous in situ stimuli to self-assemble in addition to targeting particular receptors. Peptide-based self-assembling gels are capable of producing functionalized microscopic structures that serve as a temporary ECM to promote the migration and proliferation of different cells involved in wound healing and the microenvironmental remodeling of physiological tissues.

1.2.2.3. Rational design of peptide gels for wound healing

Self-assembling peptide-based hydrogels can deliver drugs, cytokines, or cells to the desired place before decomposing into bioactive peptide sequences or natural amino acids that can be used to repair the surrounding tissue (**Figure 1.7B**). Thus, these hydrogels have been widely used in several stages of wound healing, including hemostasis, infection and inflammation management, cell proliferation, and remodeling. Zhou *et al.* in his review article has provided insights on rational design of multifunctional dressings to promote acute and chronic wound healing.⁶⁴ In addition, Liang *et al.* had discussed the advanced functions that can be exerted by hydrogels to facilitate wound healing.⁷¹

Provoking hemostasis. Hydrogels have outstanding performance and therapeutic potential as hemostatic agents because they can halt bleeding both physically and chemically.⁷² In order to completely stop the bleeding from the wound, peptide-based nanofibers can cling to the area of the lesion and self-assemble into a hydrogel barrier. The formation of clots by peptide-based nanofibers during hemostasis may confine the blood's constituent parts and encourage platelet adhesion when it comes into contact with blood. The physical trapping of blood components in the nanofiber network resembles the behavior of a fibrin clot that has naturally coagulated. In comparison to conventional

hemostatic materials (such as gauze and chitosan), peptide-based gels have been shown to halt bleeding substantially faster (within 1 min). In a liver trauma model, quick and effective hemostasis was demonstrated coupled with low cytotoxicity and no nonspecific immunological reactions by a short self-assembling peptide (I₃QGK), which forms a gel under the control of transglutaminase (TGase).⁷³ EAK16 and (RADA)₄, which are longer ionic complementary self-assembling peptides, are also used for hemostasis and exhibit quick hemostasis in transverse liver studies.⁷⁴

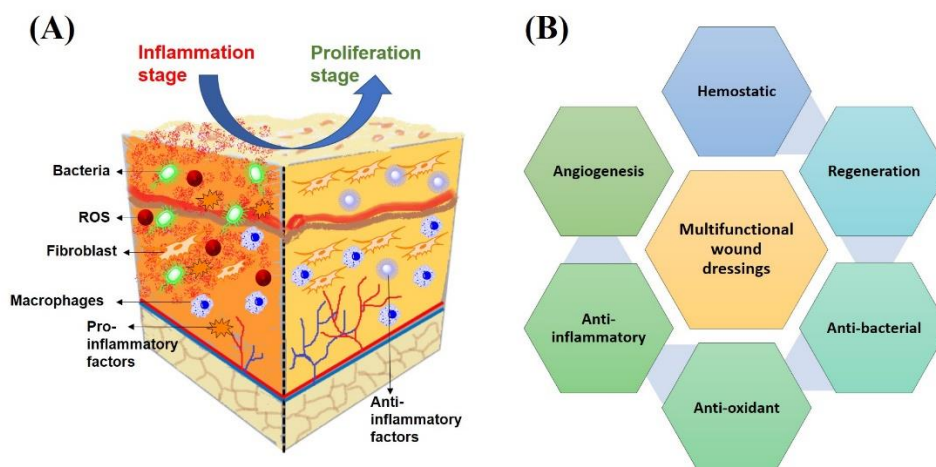


Figure 1.7. (A) Pathophysiology of chronic wound environment. (B) Properties of multifunctional wound dressings.

Prevention of microbial infection. Restricting infection brought on by the invasion of microorganisms is the most common challenge in wound healing, particularly in diabetic wounds. In burn and chronic wounds, antibiotic-resistant forms of bacteria like *Staphylococcus aureus* and *Pseudomonas aeruginosa* can induce postoperative infections, delaying wound healing, and raised mortality rates.⁷⁵ Peptide-based substances have been developed as powerful anti-infection scaffolds to address this problem. For instance, bacteria are less resistant to antimicrobial peptides (AMPs) than to antibiotics, which is advantageous for the healing of aseptic wounds. In order to heal infected wounds and prevent infection, current treatment methods mainly take advantage of the cationic characteristics and self-assembling structures of various peptide-based material systems. Lysine- and arginine-rich self-assembling peptides with polycationic surfaces exhibit antibacterial action against a variety of Gram-positive and Gram-negative bacteria. Bacterial cell death is caused by the interaction of cation-rich AMPs with bacterial cell membranes, which results in the destruction of membrane potential, changes to membrane permeability, and metabolite leakage. For instance, the cationic self-assembling gels MARG1 and MAX1 have inherent antibacterial properties.^{76,77} All of the lysine residues in MAX1 peptide fibers provide resistance to bacterial infection. Presence of arginine in MARG1 strengthened the antibacterial capabilities. Uncharged peptides have the ability to self-assemble into nanofibers that have antibacterial properties by rupturing bacterial cell membranes. FF is the most straightforward neutral, self-assembling antibacterial peptide. FF treatment causes the outer and inner membranes of

bacterial cells to permeate and depolarize.⁷⁸ It is important to note that the antibacterial activity of FF is a result of its ability to self-assemble. The formation of fibrous structures that break down the bacterial cell membrane can result in antibiotic actions when FF is modified with Fmoc, Nap, and other amino acids.

Anti-inflammatory activity. When a serious bacterial infection develops, the inflammatory response may worsen and cause long-lasting, systemic inflammation as the lesion heals. In this situation, effective methods of reducing inflammation are required. Inflammation in chronic wounds is frequently treated with anti-inflammatory medications (both steroids and non-steroids). However, local nanocarrier treatment leads in short retention duration and the unregulated release of anti-inflammatory medications in wounds, whereas oral drug administration can have negative effects in the gastrointestinal tract, kidneys, and cardiovascular systems. In order to achieve controlled drug release and improve the biological transmission and bioavailability of anti-inflammatory drugs, topical formulations of peptide-based self-assembling gels can encapsulate conventional anti-inflammatory drugs in peptide assemblies. This reduces implant-related inflammation and lessens toxic side effects during the anti-inflammatory process.⁶⁷

Co-assembly is a useful method for enhancing the anti-inflammatory medications' therapeutic effectiveness while minimizing their negative side effects. Dexamethasone (Dex), a steroid, is a potent immunosuppressant and anti-inflammatory drug. In order to increase Dex's ability to reduce inflammation, Liang *et al.* came up with a plan for peptides and Dex to assemble together intracellularly.⁷⁹ The peptide precursor (Nap-Phe-Phe-Tyr(H₂PO₃)-OH) and Dex sodium phosphate were co-assembled inside the cells as a result of the overexpressed ALP on the membranes of inflammatory macrophages acting as a catalyst to dephosphorylate them. The intracellular co-assembly caused by ALP significantly increased the anti-inflammation effectiveness of Dex in inflammatory cells. Anti-inflammatory medications can be chemically changed to offer more therapeutic characteristics through bio-conjugation. Chemical connections between peptides and medications that self-assemble well and have anti-inflammatory properties. Through an ester bond and a hydrolysable hydrazone connection, the peptide Nap-Phe-Phe-Lys-Tyr(H₂PO₃)-OH can be covalently conjugated to Dex.⁸⁰ Ibuprofen can spontaneously produce a hydrogel by conjugating with the peptide GFFY via a cleavable ester bond.⁸¹ Hydrogels can gently release anti-inflammatory medications and promote localized anti-inflammatory effect because of the improved tissue retention and enzyme activity at the site of the inflammation. It is important to note that the decrease in VEGF in the surrounding tissues slows angiogenesis and delays wound healing, which is an unfavorable side effect of Dex therapy.⁸² Nonsteroidal anti-inflammatory drugs (NSAIDs) may therefore be more effective at treating wound inflammation. The commonly used NSAIDs, such as naproxen and indomethacin encounter side effects associated with non-selective cyclooxygenase (COX) inhibition. Therefore, modification of these drug can be performed with self-assembling peptides without affecting their activity.

Proliferation and remodeling. The stage of skin and tissue proliferation that follows the management of wound infection is crucial for a good healing process. In this phase, collagen is deposited along with angiogenesis, fibroblast, and keratinocyte proliferation. Numerous 3D scaffolds for tissue engineering have been created using peptide-based gels with characteristics resembling those of the ECM.⁸³ In several research, vascular endothelial growth factor (VEGF) and its receptors have been used to control the angiogenic response because they help in the angiogenesis process in wounds. The angiogenesis-promoting abilities of VEGF-based peptide gels are superior to those of other peptide-based gels.⁸⁴ The peptide QK, which resembles the VEGF fragment and may act as an angiogenesis stimulant, can attach to the VEGF receptor.⁸⁵ As it has been demonstrated that NO helps with wound repair by encouraging endothelial cell development and migration and new blood vessel formation from existing vessels, it is a novel chemical of interest in wound healing. An effective method for creating self-assembling gels is to combine short peptide sequences with NO donors. An enzyme-controllable NO-releasing gel, for instance, has been fabricated by combining a sugar-caged NO donor with the peptide sequence Nap-FFGGG to augment angiogenesis in chronic wounds.⁸⁶ Two self-assembled peptide gels with nanofibrous structures were reported to enhance epithelial regeneration in burn wounds without exerting any inflammatory responses.

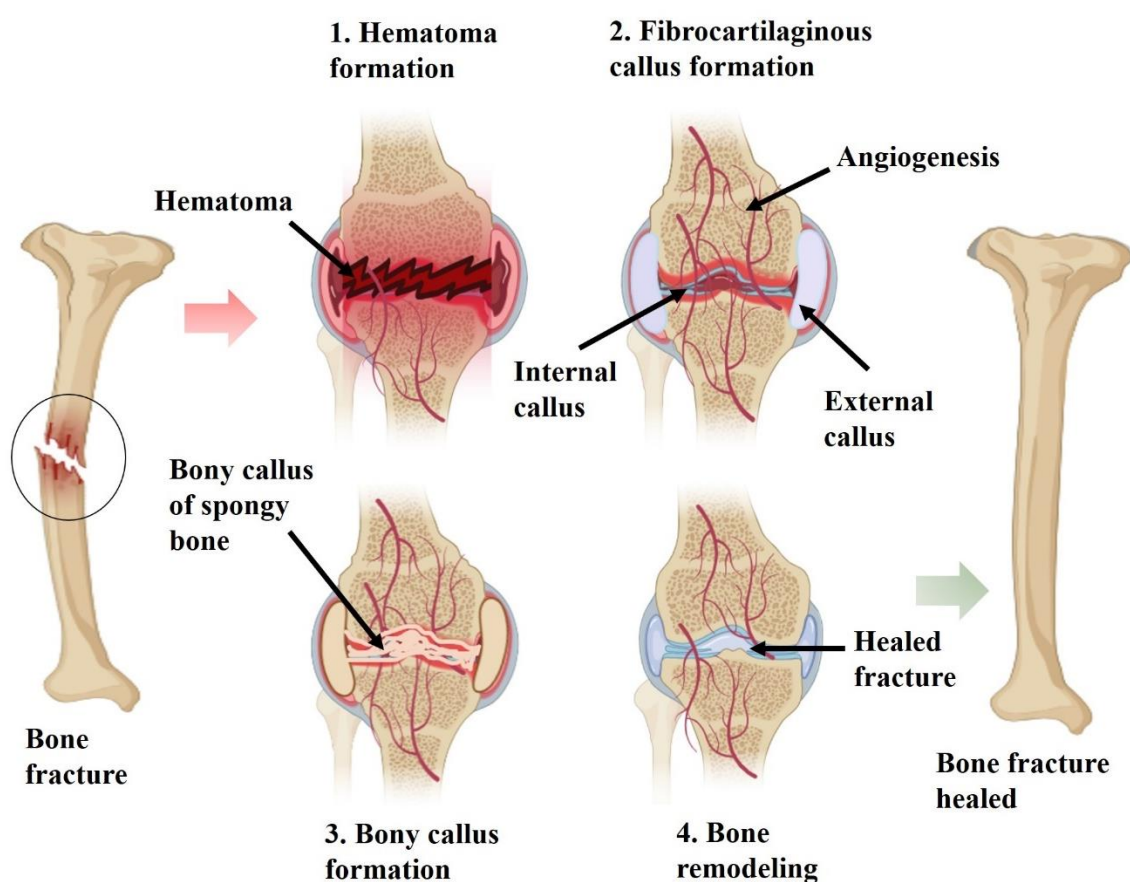


Figure 1.8. Stages of bone fracture healing.

In summary, several factors should be considered while designing self-assembling peptide-based gels for various applications. Future research should be directed towards the development of

multifunctional biomaterials to accelerate the chronic wound healing process. Overproduction of protease at the site of chronic wound cause proteolytic degradation of peptide-based scaffolds and, hence, proteolytically stable matrix is much needed. Reactive oxygen species (ROS) also deteriorate the process of healing. Self-assembling peptide with versatile activity can be conjugated with anti-inflammatory drugs to enhance selectivity towards COX-2 enzyme to provide a novel approach for facilitating the chronic wound healing process.

1.2.3. Bone tissue regeneration

Bones are complex organs composed of several different types of tissues. The primary components of bones include bone matrix, osteoblast, osteoclast, osteocytes, and osteoprogenitor cells. The matrix is the non-living, structural component of bone tissue consisting of organic (collagen and non-collagen proteins) and inorganic (hydroxyapatite) components.⁸⁷ Osteoblasts play a role in bone synthesis, osteoclasts in bone resorption, osteocytes in matrix mineral concentration maintenance, and osteoprogenitor or osteogenic cells in osteoblast development. Bone tissue regeneration is the process by which damaged or lost bone tissue is restored and replaced with new, healthy bone. This natural healing process occurs in the body through a complex series of cellular and molecular events. There are several factors that influence bone tissue regeneration including the severity of the injury, the location of the bone defect, and the individual's overall health. The basic steps involved in bone tissue regeneration typically include (**Figure 1.8**):

Inflammation. When a bone is injured, the body's natural response is to initiate an inflammatory process. Inflammatory cells, such as macrophages, release signaling molecules that attract other cells to the injury site and stimulate the subsequent healing process.

Formation of a hematoma. Following the initial inflammatory response, blood vessels in the injured area rupture, leading to the formation of a blood clot or hematoma. The hematoma serves as a scaffold for the subsequent steps of bone tissue regeneration.

Formation of a soft callus. Within a few days, specialized cells called fibroblasts invade the hematoma and start producing a soft callus. The soft callus consists of collagen and fibrous tissue that stabilizes the fracture site and bridges the gap between the broken bone ends.

Formation of a hard callus. Over time, the soft callus is gradually replaced by a hard callus, which is made up of cartilage and woven bone. Cartilage-forming cells called chondroblasts produce a temporary cartilage model, which is later replaced by bone-forming cells called osteoblasts.

Remodeling. The final step in bone tissue regeneration is remodeling, where the newly formed bone undergoes a remodeling process to restore its original shape, strength, and functionality. Osteoclasts, specialized cells that break down bone tissue, remove excess callus material, while osteoblasts deposit new bone in a process known as bone remodeling.

In addition to the body's natural healing process, bone defects due to injury, illness or ageing necessitate medical interventions to aid bone tissue regeneration. Osteoporosis falls into this category. It is a medical condition characterized by a decrease in bone mass and deterioration of bone tissue, leading to increased bone fragility and a higher risk of fractures. It occurs when the rate of bone resorption (breakdown) exceeds the rate of bone formation, resulting in a net loss of bone density. The approaches used to facilitate bone tissue regeneration includes the following:

Bone grafts. In cases where there is a significant bone loss or the body's natural healing process is insufficient, bone grafts may be used.⁸⁸ A bone graft involves transplanting bone tissue from one area of the body (autograft), a donor (allograft), or synthetic materials (alloplastic grafts) to the site of the bone defect to stimulate bone regeneration.

Growth factors and proteins. Certain growth factors and proteins, such as bone morphogenetic proteins (BMPs), can be used to enhance bone tissue regeneration. These substances are often applied directly to the site of the injury to stimulate the recruitment and differentiation of bone-forming cells.

Tissue engineering approaches. Tissue engineering techniques involve combining cells, scaffolds, and signaling molecules to create engineered bone tissue for transplantation. These approaches aim to create custom-made bone grafts that closely mimic the structure and properties of natural bone (Figure 1.9).

It is important to note that bone tissue regeneration is a complex process, and the success of the regeneration can vary depending on the individual and the specific circumstances of the injury. Close medical supervision and appropriate treatment plans are crucial to ensure optimal outcomes.

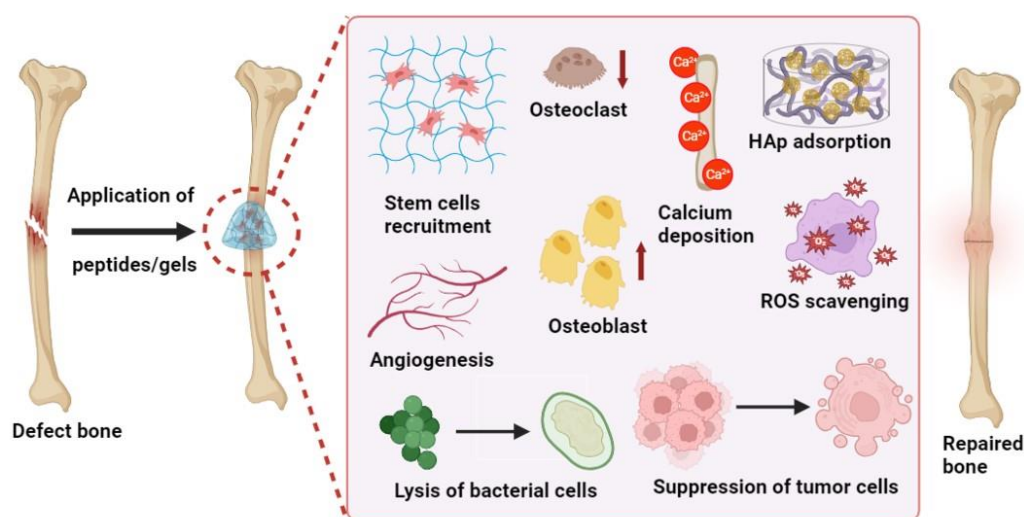


Figure 1.9. Biochemical functionalization of peptides to achieve successful bone tissue regeneration.

1.2.3.1. Supramolecular peptide as a scaffold

Peptides can be self-assembled into various scaffolds including gels and hydrogels. Due to their structural similarity to the extracellular matrix (ECM), which may facilitate cell behavior such as migration, adhesion, proliferation, and differentiation, hydrogels may be the best scaffolds for bone tissue engineering.⁸⁹ Bioactive motifs could be covalently attached to the peptide to control cell behavior, and bioactive factors could physically bind to the hydrogel matrix to be released over time. These possibilities depend on the crosslinking density, matrix affinities for the factors, and rate of biomaterial degradation. Biomaterials that are currently being tested as bone substitutes in clinical trials for bone tissue engineering include degradable bioceramics, like bioactive glass, polymers, like hyaluronic acid (HA), and undegradable metallic implants like printed titanium implants. In contrast to biomaterials now undergoing clinical trials, self-assembled peptide gels can be easily given diverse biochemical functionalities by conjugating bioactive motifs and absorbing bioactive agents. Other benefits of self-assembled peptide gels over existing bone substitutes include: 1) exhibit artificial microenvironment analogous to native ECM, which can modulate cells by ECM-cell interactions; 2) initiate almost no adverse immune response or tissue inflammation when implanted into the body; 3) no toxic substance formed during degeneration because they are primarily composed of amino acids; and 4) can be synthesized in high purity without batch-to-batch variations. They can be used to design bone grafts via bioprinting or bioreactors, in addition to being employed as injectable gels or composite nanoscaffolds. Recent reviews published by Koons *et al.*⁹⁰, Hao *et al.*⁸⁷, and Bahraminasab *et al.*⁹¹ describes the design of biomaterials for promoting bone tissue regeneration.

1.2.3.2. Biochemical functions of self-assembled peptides

Cell adhesion is the most fundamental process that enables exogenous or endogenous cells to survive, multiply, and differentiate when self-assembled peptides are transplanted into the body. Endogenous cells must be strongly recruited for newly developed cell-free scaffolds. Additionally, breakdown of self-assembled peptides must be controlled in order to support bone tissue regeneration during bone healing.⁹² We refer to these three processes- cell adhesions, cell recruitment, and matrix degradation as basic biochemical processes for bone tissue engineering. Matrix biomineralization and osteogenesis are required for the deposition of hydroxyapatite and collagen in order to regenerate bone tissue. Additionally, angiogenesis and neurogenesis are necessary because newly formed blood vessels may carry cells, nutrients, and oxygen, and newly formed nerve cells can stimulate osteogenesis by secreting neuropeptides. Immune cells also play important roles in the milieu of bone regeneration, and osteogenesis aided by the appropriate change of macrophage phenotype. Consequently, we categorize matrix biomineralization, osteogenesis, angiogenesis, neurogenesis, and immune modulation as enhanced biochemical processes for bone tissue engineering, and a suitable balance should be maintained among them. Furthermore, it is necessary to prevent postoperative infection and tumor recurrence since the milieu of bone defects brought on by the excision of an infection or tumor is not favorable for bone regeneration. Therefore, from the perspective of a therapeutic goal, sterilization and tumor suppression are considered to be supplementary roles. Each bioactive motif or

bioactive component exhibits many effects and they are mostly categorized as below according to their major function.

Cell adhesion. The most fundamental purpose of biomaterials is cell adhesion. It may be treated with cell adhesive peptides (CAPs), which may bind to related receptors on the cell membrane, including integrin, laminin binding proteins, and transmembrane proteoglycans.⁹³ RGD may bind to multiple integrins and thereby stimulate additional processes, including osteogenesis, angiogenesis, and neurogenesis. In order to generate useful nanofiber gels, the peptide and its derivatives, such as RGDS, PRGDSGYRGDS (PRG), and DGRGDSVAYG (DGR), have been covalently customized to a variety of supramolecular peptides.⁹⁴

Cell recruitment. In order to prevent the encapsulation of exogenous seed cells, endogenous repair cells from a core cell niche (such as bone marrow) or adjacent tissue are stimulated to move into biomaterials. This phenomenon is known as cell recruitment. The ability to recruit cells is supported by the porous, ECM-like milieu that self-assembled peptides offer. By using phage display screening, a group of polypeptides known as bone marrow homing peptides (BMHPs) rich in K, P, F, S, and T were discovered.⁹⁵ These peptides may help MSCs migrate or recruit, and BMHP1 (PFSSTKT) and BMHP2 (SKPPGTSS) have been employed extensively in bone tissue engineering.

Matrix degradation. The rate of degradation of matrix and tissue regeneration should remain in equilibrium. Some enzymes, including MMPs, may be produced when cells migrate into the gels, having indirect impacts on bone healing. Therefore, using MMP-clearable sequences is the best method for controlling the degradation of hydrogel matrix. GTAGLIGQ was the first type MMP-2 cleavable motif to fabricate cell-responsive peptide amphiphile. The self-assembled peptide gel was constructed by $\text{CH}_3(\text{CH}_2)_{14}\text{CONH-GTAGLIGQ-ERGDS}$, and Type IV collagenase was utilized to evaluate the gel's vulnerability to protease degradation.⁹⁶

Matrix biomineralization. The process of hydroxyapatite (HAp) being deposited on biomaterial substrates is known as matrix biomineralization, and it is advantageous for osteogenesis. For matrix biomineralization, acidic amino acids are typically utilized. The most common biomineralization motif at this moment is phosphoserine (J), which is enriched in dentin phosphoprotein and skeletal saliva protein. It can draw calcium ions and cause nucleation with alkaline phosphatase (ALP)-released phosphoric acids. Mineral crystals appeared on the 2D surface of peptide amphiphile nanofibers made by $\text{CH}_3(\text{CH}_2)_{14}\text{CONH-CCCCGGG-JRGD}$ after being exposed to a solution containing a mixture CaCl_2 and Na_2HPO_4 . The Ca/P ratio, as measured by energy dispersion X-ray spectroscopy, was 1.67 ± 0.08 , which is in agreement with HAp [$\text{Ca}_{10}(\text{PO}_4)_6(\text{OH})_2$].⁹⁷ Consecutive negative amino acids (EEE, EEEEE, and DDDDD) can direct mineralization similarly to J when conjugated to various self-assembled peptides.⁹⁸ Therefore, incorporating negative biomineralization segments as biomaterial scaffolds is still strongly advised for bone tissue engineering.

Osteogenesis. In addition to the osteogenic effects of mineralization, osteogenesis may be influenced by osteoinductive elements. The most often employed bioactive proteins are recombinant bone morphogenic proteins (BMPs), which exhibit osteoinductive capabilities. Hosseinkhani *et al.* reported a controlled release of BMP-2 and BMP-7 from self-assembled peptide gel for up to 25 days in vitro.⁹⁹ Another successful strategy is to attach a supramolecular peptides to a bioactive motif containing peptide. Literature report reveals that the incorporation of phosphorylated BMP-2-related peptide (SJVPT) to a functional gel efficiently controlled the proliferation and osteogenic differentiation of MSCs in vitro and induced bone regeneration.¹⁰⁰

Angiogenesis. Given that bone is a highly vascularized tissue and that the vasculature plays an important role in bone remodeling, regeneration, and maintenance, angiogenesis is an important factor to take into account when passive diffusion for oxygen and nutrient transfer is ineffective during bone repair. Angiogenic signals in biomaterials are therefore advantageous for bone regrowth. Vascular endothelial growth factor (VEGF), basic fibroblast growth factor (bFGF), insulin-like growth factors (IGFs), and many other bioactive proteins have angiogenic effects.¹⁰¹ VEGF has been utilized extensively as an angiogenic promoter. For instance, VEGF and BMP-2 were physically encapsulated into a self-assembled peptide gel and the results showed that the VEGF-incorporated scaffold promotes more new bone formation than the scaffolds containing BMP-2 only.¹⁰² Supramolecular peptides have also been designed using an IGF-1-derived motif (GYGSSRRAPQT) and a heparin-mimetic motif (K-pbs) to encourage angiogenesis.¹⁰³

Immune regulation. Immunoregulation plays a critical role in bone tissue regeneration by modulating the immune response and coordinating the interactions between immune cells and bone cells. The immune system is involved in the early stages of bone healing, including the inflammatory phase, and also contributes to the later stages of bone remodeling and regeneration. Numerous immune cells, including macrophages, neutrophils, and T cells, have an impact on bone remodeling, with macrophages playing a key role in this process.¹⁰⁴ Following trauma, circulating monocytes serve as the primary source of macrophages. Macrophages initially exhibit M1 morphologies, which can phagocytose dead cells and pathogens and cause inflammation, and subsequently they change into anti-inflammatory M2 phenotypes, which may promote osteogenesis. The major goals of the current research were to promote M2 macrophages and inhibit M1 macrophages. Immune regulators can be entrapped into peptide gels or the scaffold itself can demonstrate immunomodulation to promote bone formation.

Antibacterial. Acute and chronic bone infections are challenging to treat because of bacterial colonies in the grooves of the bone, different substances secreted by the bacteria, and an acidic microenvironment. Osteomyelitis, an infection-related inflammation of the bone or bone marrow, is frequently treated in clinics by thoroughly cleaning the lesion and then implanting an antibacterial substance. Due to the possibility that the residual bacteria can interfere with bone healing, antimicrobial elements should not be released quickly. The dual roles that self-assembled peptide gels

play as controlled release carriers and scaffolds may make them the optimal vehicle for the dual functions of antibacterial and osteogenesis. Yang *et al.* incorporated cationic antimicrobial peptides (AMPs) into RADA16 gel and tested it on a rabbit osteomyelitis model.¹⁰⁵ The gel allowed for the controlled release of AMPs to inhibit *Staphylococcus aureus* growth, and stimulated bone regeneration. In a different study, to reduce the risk of postoperative infection, ciprofloxacin was encapsulated inside a scaffold made of RADA16 and calcium phosphate cement.¹⁰⁶

Tumor suppression. Large-scale bone deformities brought on by tumor resection are extremely challenging to heal as leftover tumor cells can lead to tumor relapse. Scaffolds that inhibit tumor growth and stimulate bone formation are therefore very promising for treating bone deformities caused by tumors. Instead of chemotherapeutic treatments that harm MSCs, antitumor medications with osteogenic qualities are better suited for bone repair.¹⁰⁷ A controlled-release scaffold was developed by a group using metformin, a common diabetes medication with many effects that include encouraging osteogenesis and suppressing tumor growth. Although self-assembled peptide gels are frequently employed to remove tumors, few studies have used them as controlled-release scaffolds to repair bone defects caused by tumor excision. Adding anticancer compounds to the supramolecular peptides' backbone is another effective strategy to combat tumor relapse in bone defects.

While various injectable, 3D printed, self-assembled peptide-based scaffolds with rational design have been reported in literature, the effect of polar and charged building blocks (amino acids) in a peptide sequence have not been investigated thoroughly. The nanostructured morphology of the peptides can also provide biochemical cues, which can help in nanostructure guided differentiation of MSCs. A detailed understanding regarding the effect of individual amino acids on biomineralization, MSCs differentiation, and promoting osteogenesis would motivate the researchers to develop better peptide-based scaffolds for bone tissue regeneration.

1.2.4. Biocatalyst mimics

Enzymes have garnered a great deal of interest due to their exceptional selectivity and efficiency during catalysis. Intramolecular noncovalent interactions, such as van der Waals, electrostatic, hydrogen bonds, and stacking interactions, operate as the driving factors in the three-dimensional folding of enzymes.¹⁰⁸ They support the metabolic process and cellular processes of living creatures by catalyzing biochemical reactions under benign conditions. Although enzymes have received a lot of interest in the domains of food, textile, medical, petrochemical, biofuel, and other things due to their high catalytic efficiency and regio- and stereoselectivity, they face certain limitations on large scale, which includes: (i) the folded structure of the enzymes are due to the presence of non-covalent interactions, which are very prone to environmental changes, leading to the loss of activity; (ii) the complexity of enzyme structures makes it challenging to modify their structural characteristics and adjust their catalytic properties; (iii) the separation and purification of enzyme from cell is expensive and time consuming. The distinctive architectures of the active sites, which are in a three-dimensional cleft made up of residues from the primary sequences, are thought to be responsible for the catalytic

abilities of enzymes.¹⁰⁹ To selectively bind the substrates and catalyze the transformation, the functional groups in the active sites work with or support the organic or ionic cofactors. Supramolecular self-assembly, a bottom-up method of material manufacturing, has been extensively used to create enzyme-mimetic biocatalysts inspired by the structure-function relationship of enzymes.¹¹⁰

Supramolecular catalysts are produced by the spontaneous organization of the components of molecular catalytic system under thermodynamic equilibrium, which is fueled by numerous interactions. Unlike native enzymes, supramolecular catalysts can typically be made in a very quick and inexpensive manner, and they have tailorable architectures and functions because of the tunable building blocks. They also provide multiple reactive centers to enhance the rate of reaction. Additionally, the amphiphilicity of the structures can be adjusted by managing the polarity of the catalytic environment and functions.¹¹¹

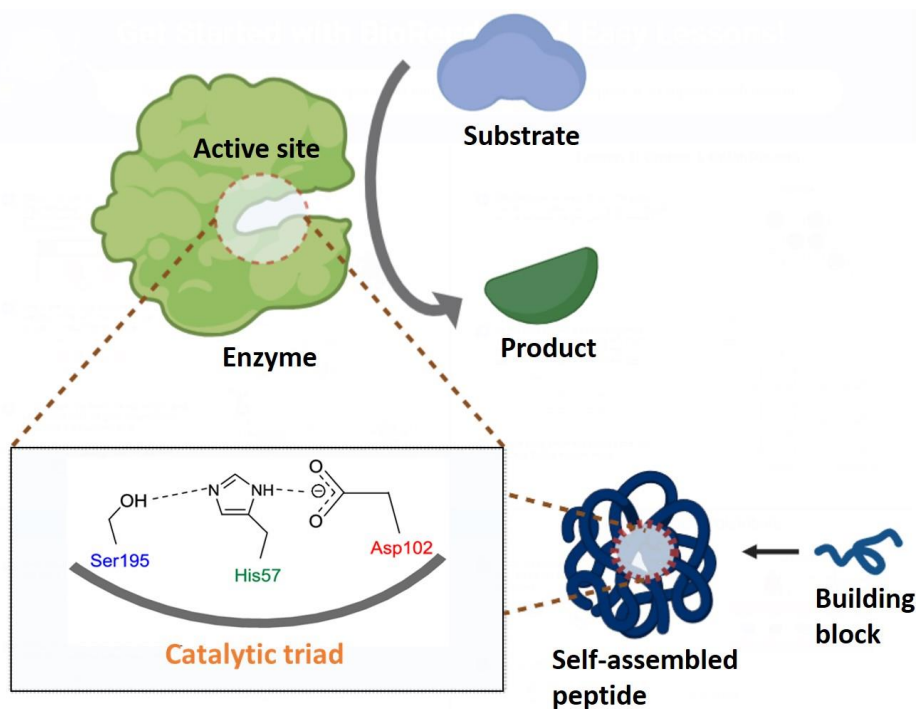


Figure 1.10. Design of self-assembled peptide with the active catalytic site similar to the native enzyme to catalyze biochemical reactions.

The purpose of generating supramolecular catalysts is to attain catalytic efficiency that can be comparable with that of natural enzymes, hence it is crucial to strategically construct the active sites of the biocatalysts-mimic. This is indeed difficult because the distribution of amino acid residues at the active site of enzyme is developed due to tertiary protein folding. There has been a lot of research on the fabrication of supramolecular catalysts with an arrangement of the catalytic groups to closely mimic an enzyme (**Figure 1.10**). The functional group present at the side chain of amino acids in the active sites cooperate to carry out enzymatic activities in the presence or absence of cofactors. In recent reviews, Hamley and coworkers have presented the scope of peptide and peptide conjugate

nanostructures as biocatalysts,¹¹² whereas Lou *et al.* have discussed the potential of de novo designed self-assembled peptides to mimic the active sites of various enzymes to catalyze different reactions.¹⁰⁸

1.2.4.1. Design and fabrication of supramolecular biocatalysts

Hydrolase mimic. Hydrolases are enzymes that catalyze hydrolysis reactions, which involve the breaking of chemical bonds by the addition of water molecules. Enzymes, like esterase, carbonic anhydrase, lipase, and phosphatase belong to this category. Hydrolase typically consists of at least one histidine (His, H) residue at its active site and the imidazole at its side chain can act as an acid-base catalyst to split water to generate proton. This leads to generation of a nucleophilic anion. A single histidine moiety can promote hydrolysis with low efficiency, whereas, cooperation of histidine with other amino acid residues forming catalytic dyad or triad can accelerate the reaction with a higher efficiency (**Figure 1.11**). Zn^{2+} sometime act as cofactor along with the catalytic triad. Therefore, hydrolase mimicking artificial enzymes can be of two types: metal free and metal containing.

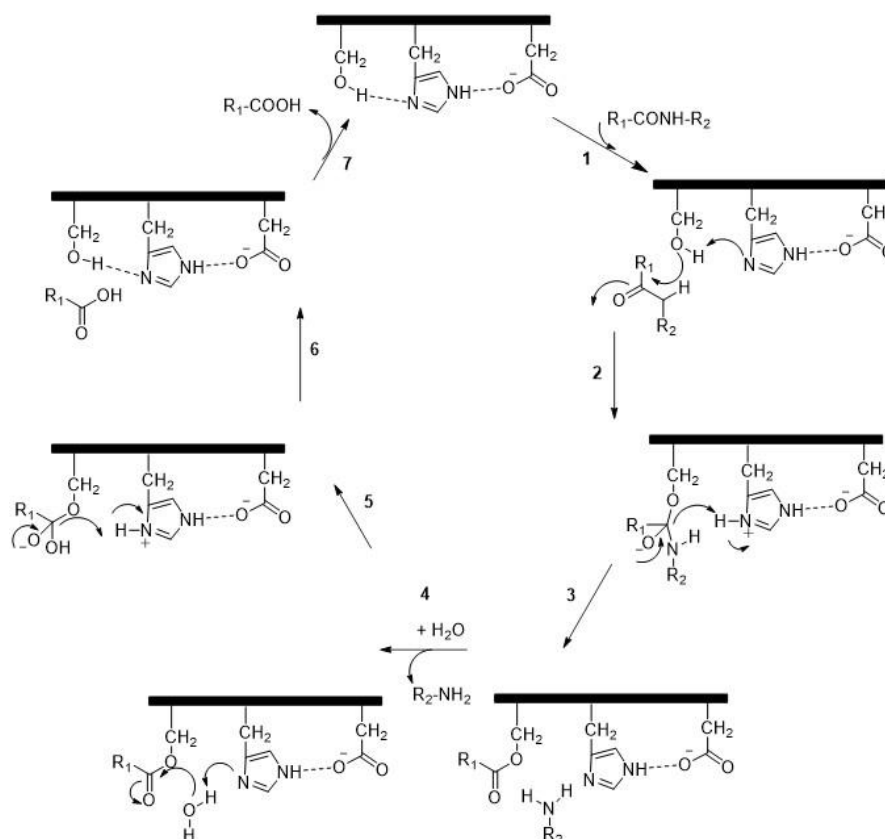


Figure 1.11. Catalytic mechanism of serine protease involving catalytic triad (Ser-His-Asp).

Metal free. For several hydrolytic enzymes, including serine proteases, serine esterases, and lipases from certain sources, the S (Ser)-H (His)-D (Asp) (or Glu, E) triad is a well-known structural characteristic.¹¹³ The serine hydroxyl group, which is typically protonated at the neutral pH, is hydrogen-bonded to the imidazole of histidine at the active site of serine proteinases (chymotrypsin or trypsin), which is then hydrogen-bonded to Asp to form a charge-relay network. Once the substrate (a peptide) has been bound, the oxygen on Ser's side chain attacks the carbonyl carbon of a peptide bond,

the hydrogen-bonded His acts as a general base to abstract the Ser proton, and the negatively charged Asp stabilizes the positive charge that forms on the His residue. As a result, the Ser hydroxyl's nucleophilicity is increased. The catalytic triad can be synthesized with minimal expense, which can be self-assembled to generate a supramolecular catalyst. Dejugnat and coworkers reported the His-based lipopeptide self-assembly to exhibit hydrolysis of p-nitrophenyl acetate (pNPA).¹¹⁴ Guler *et al.* employed a comparable strategy to produce the catalytic H/S/D triad by allowing the peptide amphiphile to self-assemble into the β -sheet configuration.¹¹⁵ The H/R (arginine) pair formed through peptide self-assembly also had shown synergistic catalytic activity towards the hydrolysis of pNPA in addition to the S/H/D triad. By acting as an oxanionic hole, the guanidyl group helps to stabilize the negative charge at the reaction's transition state. In addition to ester hydrolysis, the catalytic triad was reported to exhibit amidolytic activity through self-assembly of amyloid peptides containing H, S, and D residues.¹¹⁶ The transesterification of the p-nitrophenyl ester of N-carboxybenzylphenylalanine (Cbz-Phe-ONP) was catalyzed by using positively charged monolayer-capped gold nanoparticles as the multivalent scaffold instead of peptide self-assembly.¹¹⁷ The nanoparticles were used to bind peptides containing oligohistidine (1-3 His residues) and three Asp residues. Guler *et al.* reported the self-assembled nanofibrous scaffold, lauryl-VVAGHH CONH₂, which has the potential to mimic alkaline phosphatase, thus catalyzing phosphate hydrolysis.¹¹⁸ This property helped the scaffold to trigger the maturation of MSCs into bone forming cells (osteoblasts) and potentiate in vitro osteogenic differentiation.

Metal containing. Metal ions that function as enzyme cofactors can catalyze reaction with the help of the side chain groups of amino acid residues by making the substrates easier to access and bind. The residues alone cannot carry out the catalytic reaction. The interaction of the metal ions with ligating side chains affects the protein folding as well. Carbonic anhydrases and metalloproteases are two examples of hydrolases that frequently use Zn²⁺ ion as a cofactor. A bound water's pK_a is lowered by the Zn²⁺ ion, which helps in stabilizing and positioning hydroxide for nucleophilic attack on the substrate. In order to build a Zn²⁺ binding site, Korendovych and coworkers used a heptapeptide based on the β -sheet forming sequence, AcLKLKLL-CONH₂.¹¹⁹

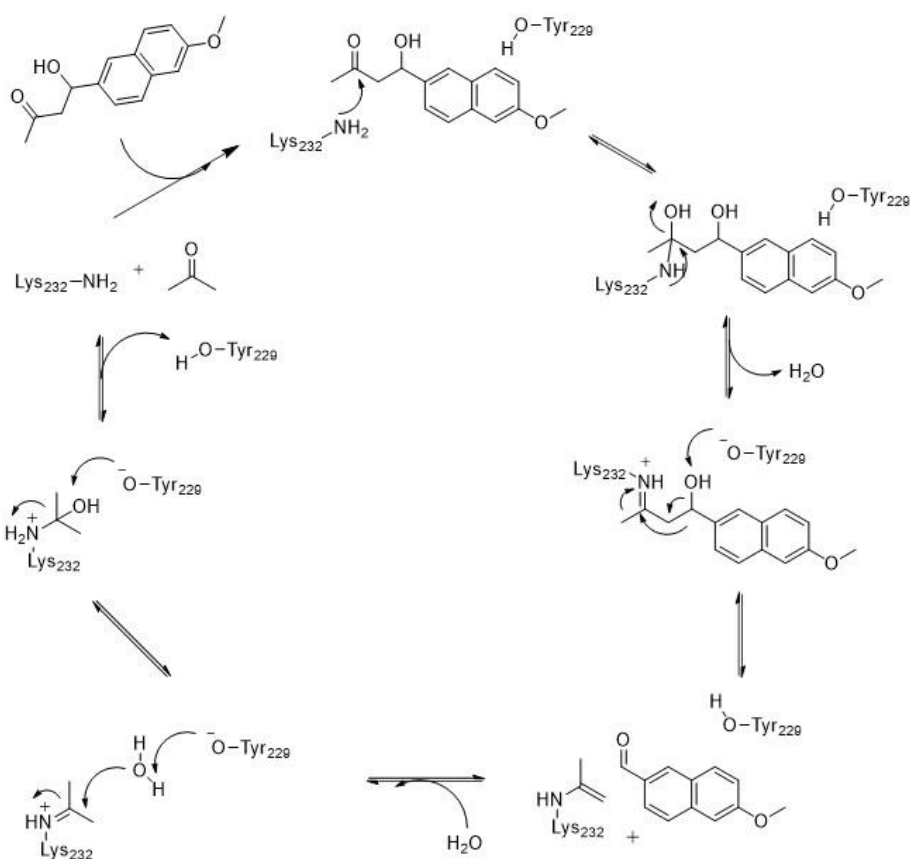


Figure 1.12. Catalytic mechanism of aldolase I involving catalytic site.

Aldolase mimic. Aldolases Class I, often known as aldolase I, is a broad family of enzymes that catalyzes the formation or cleavage of C-C bonds. It employs a multistep process where a covalent Schiff base imine adduct is formed between an active-site lysine and an intermediate. At the active site of native aldolases, lysine attacks a carbonyl group of the substrates to generate an imine intermediate, which continues to attack the electrophilic reagent. Prior to the formation of the imine, the phenolic OH of a proximal tyrosine serves as the hydrogen-bond donor to boost the electrophilicity of the carbonyl group of the substrate through proton transfer (**Figure 1.12**). Aldolases have found extensive use for asymmetric syntheses of biologically significant chemicals because the reversible cleavage of C-C bonds is a key transition in both chemistry and biology. Supramolecular peptide assembly offers an efficient method for producing synthetic aldolase.

Utilizing the nucleating core of the A β peptide (LVFF), which self-assembled into well-defined amyloid nanotubes, Lynn and coworkers synthesized peptide K1 (Ac-KLVFFAE-CONH₂) as artificial aldolase. In addition to lysine, proline had shown activity towards catalyzing the aldol C-C coupling process by generating an enamine intermediate with ketone and participating in the nucleophilic addition to the aldehyde.¹²⁰ Wennemers *et al.* designed self-assembled amphiphilic H-D-Pro-Pro-Glu-NH₂ to catalyze the addition of aldehydes to nitroolefins in water with high yield and stereoselectivity.¹²¹ Escuder and coworkers fabricated a L-proline based self-assembled gel to catalyze the Henry nitroaldol reactions between nitromethane or nitroethane and benzaldehyde derivative (**Figure 1.13**).¹²²

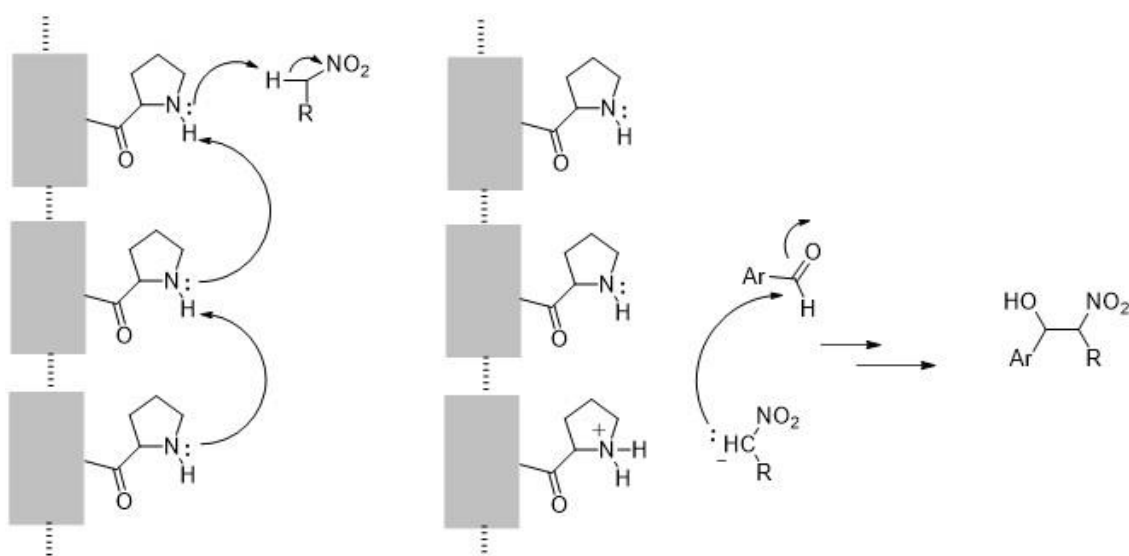


Figure 1.13. Proline-based aldolase-mimicking catalysts to promote nitroaldol reaction.

Oxidase mimic. With O_2 acting as the electron acceptor, oxidases catalyze oxidation and reduction reactions. A vast class of oxidases, such as laccase, ascorbate oxidase, tyrosinase oxidase, cytochrome c oxidase with Cu as a cofactor belongs to the class of catechol oxidase. A wide range of aromatic compounds, including aryl amines or phenols undergo one-electron oxidation by the 3D structure of catechol oxidase. Korendovych *et al.* developed peptide with seven residues to self-assemble with Cu^{2+} , which can further activate O_2 and 2,6-dimethoxyphenol (DMP) that acted as the reducing agent. Histidine residue in the peptide helped in forming co-ordination complex with Cu, thus facilitating the reaction.¹²³

Peroxidase mimic. Peroxidases are a common class proteins using hydrogen peroxide (H_2O_2) or other peroxides as oxidants to catalyze a range of oxidative reactions. Histidine is a crucial residue for the active site of native peroxidase but histidine being a part of the catalytic triad, is also essential for hydrolase. Das and coworkers designed a self-assembled peptide (Ac-HLVFFAL-CONH₂) with nanotube morphology, which can mimic the catalytic center of both peroxidase and hydrolase enzyme and perform a tandem catalysis reaction.¹²⁴ Xu *et al.* developed self-assembled molecular gel composed of Fmoc-Phe and Fmoc-His.¹²⁵ The phenylalanine residue provides the hydrophobic environment, whereas the imidazole ring in histidine residue is responsible for binding with heme to act like peroxidase active site.

In summary, inspired from the construction of the active site of native enzymes, self-assembled peptides are being developed to act as artificial biocatalysts and perform various catalytic reactions. Although these enzyme-mimicking supramolecular catalysts are used for several application but they encounter limitations associated with their reusability and aggregation. Therefore, immobilization of these supramolecular catalyst over nanoparticles can be used to develop heterogenous catalyst and reduce their tendency of aggregation. This technique can be further explored to enhance the stability of

the artificial enzyme and the inherent catalytic potential of certain metal nanoparticles can be exploited by conjugating them with the peptide catalysts in order to prepare multifunctional catalyst.

1.3. Knowledge gaps in the field

Researchers have developed self-assembled peptide-based scaffolds for various applications but their exploitation in the field of antidiabetic drug delivery is rarely reported. The inherent activities of the peptide building blocks can be used other than carrier to combat various issues related to diabetes. Development of multifunctional wound dressing is required to circumvent the problems associated with chronic wounds. Overexpression of cyclooxygenase-2 deteriorate the normal wound healing process by delaying the inflammation phase. Therefore, a selective COX-2 inhibitor is highly recommended to accelerate chronic wound healing. Although, self-assembled peptides are widely used as a biomaterial for bone tissue regeneration, but impact of polar and charged amino acids on adsorption of hydroxyapatite and differentiation of mesenchymal stem cells have not been thoroughly investigated earlier. Henceforth, there is a scope to study the potential role of few amino acids with different charges which can further help to construct better scaffold for bone tissue regeneration. Lastly, the enzyme mimicking nature of self-assembled peptides make them ideal candidate for the development of biocatalyst but their homogenous nature and non-recyclability hinder their use. This limitation can force the researchers to think of immobilization of peptides on solid nanoparticle surface to generate heterogenous biocatalyst which can be used for several cycles.

1.4. Objectives

The wide applications of self-assembling peptides particularly in the field of drug delivery, tissue regeneration, and biocatalyst-mimic are thoroughly discussed in the previous section. The thesis is intended to rationally design and develop a set of peptides with various properties to overcome the challenges associated with these fields and to generate more efficient scaffolds compared to the existing ones (**Figure 1.14**).

Self-assembled peptide gels are extensively used as a drug delivery vehicle for the release of cancer therapeutics. There is very less report where the inherent properties of the peptides are explored to circumvent the side effects associated with antidiabetic drugs. Therefore, the first object of my thesis was to fabricate self-assembled ultrashort peptide gels for the pH-sensitive, sustained release of glimepiride and scavenge the free radicals generated during oxidation of glucose and protect the organs from oxidative stress. Several self-assembled peptide-based scaffolds are reported in literature to combat the problems associated with chronic wounds. A major inflammatory factor of chronic wound is cyclooxygenase 2 (COX-2) but the NSAIDs used to treat inflammation cause non-selective COX inhibition, leading to side-effects associated with COX-1 inhibition. Therefore, there is a need to selectively inhibit COX-2 to protect the body from unwanted side effects. The second objective of my thesis was to conjugate antioxidant, antibacterial, and proteolytically stable peptides to anti-inflammatory drugs, naproxen and indomethacin (non-selective COX inhibitors) in order to develop nanostructured, self-assembled scaffold as a multifunctional wound dressing. The conjugate gel can

propagate the stalled inflammatory phase towards proliferative phase of wound healing and help in wound closure and skin tissue regeneration.

The requirement of bone tissue regeneration is high in case of several bone defects, especially osteoporosis, where the bone formation is extensively affected by bone resorption, resulting in the reduction of bone density. Therefore, there is a pressing need to develop scaffold for regenerating bone tissue. Self-assembled peptide gels are reported to exhibit various essential properties as an ideal scaffold for bone but the potential role of charged and polar amino acids in the peptide sequence has not thoroughly investigated. To surmount this knowledge gap, we planned the third objective of the thesis, which was to investigate the role of amino acids in self-assembled peptides for hydroxyapatite adsorption and differentiation of mesenchymal stem cells. The properties of amino acids can further help to generate various implant coating based on peptides for promoting bone tissue regeneration. Self-assembled peptides are also used for the development of artificial enzymes to conduct several catalytic reactions but they are associated with drawbacks, such as lower stability and non-recyclability. Keeping this in mind, we framed the fourth objective of the thesis, which was to develop a supramolecular peptide catalyst with the catalytic triad present in hydrolase enzyme and immobilize them on cerium nanoparticle with inherent haloperoxidase activity to make it a multifunctional heterogenous catalyst. Other than performing in vitro catalytic reactions, our objective was to use the catalyst in several applications for human welfare.

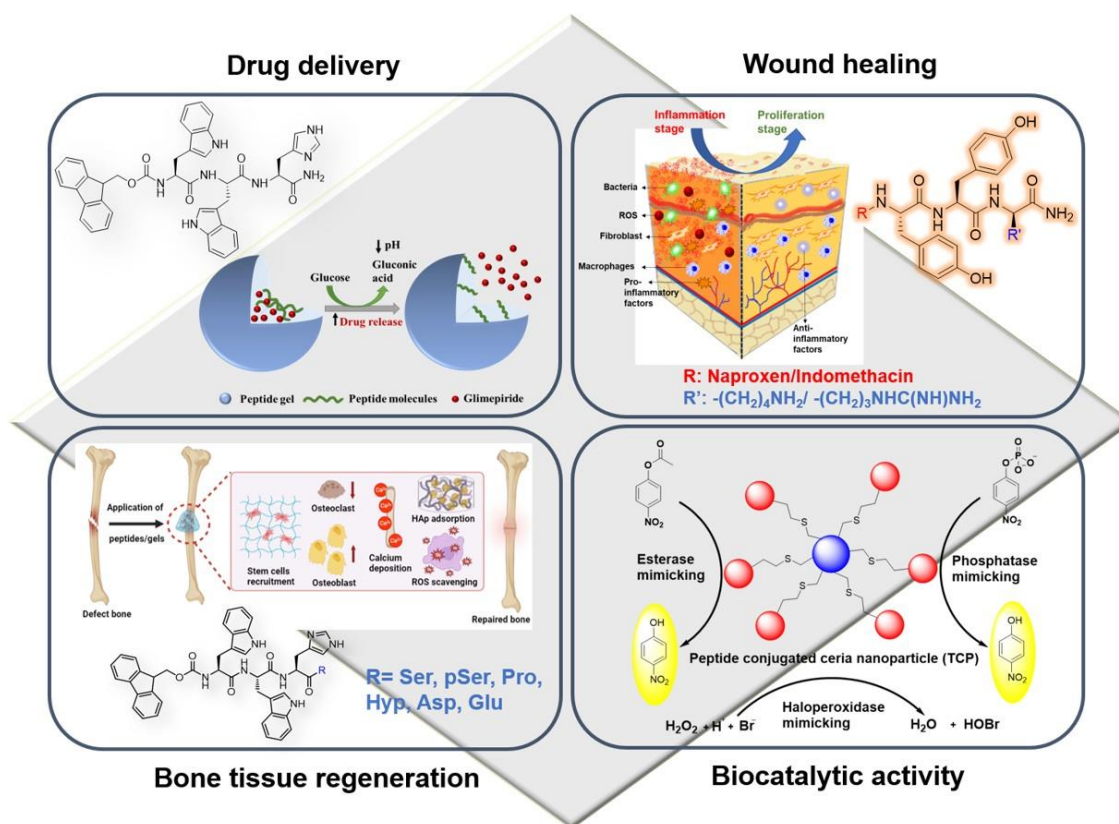


Figure 1.14. Objectives of the thesis. Development of self-assembled peptides for drug delivery, wound healing, bone tissue regeneration, and biocatalyst-mimic applications.

1.5. Thesis outline

The focus of this thesis was to develop self-assembled peptide-based biomaterials for drug delivery, wound healing, tissue regeneration, and biocatalytic applications. The first section of chapter one provides an overview on various secondary structures that the peptides can adapt to form distinct supramolecular assembly. The second part of this chapter discusses several examples of self-assembling peptides in biomedical applications, with emphasis on drug delivery, chronic wound management, bone regeneration, and biocatalyst-mimicking applications. Although the field of self-assembled peptide is very broad, this chapter presents an exhaustive literature survey, identifies knowledge gaps/challenges in the field, and presents well-defined objectives to address those challenges. In the second chapter, we have developed pH-responsive, di- and tripeptide gels (YY, WW, and WWH) for the sustained release of glimepiride and to scavenge the free radicals generated during the glucose oxidation, and in the third chapter, we have developed conjugate gels from ultra-short peptides (Npx-YYk, Npx-YYr, Ind-YYk, and Ind-YYr) comprising of D- and L- amino acids with antioxidant and antibacterial properties conjugated to Npx and Ind (NSAIDs), as a promising topical agent for treating chronic wounds or as a coating material for medical devices to prevent implant associated infections. The fourth chapter deals with the development of six amphiphilic, collagen and non-collagenous protein-inspired tetrapeptides (WWHS, WWHJ, WWHP, WWHO, WWHD and WWHE) for the adsorption of hydroxyapatite and differentiation of mesenchymal stem cells to accelerate bone tissue regeneration, whereas the fifth chapter deals with the development of self-assembled, nanofibrous catalytic peptide on ceria nanoparticles to mimic esterase, phosphatase, and haloperoxidase enzymes. Finally, the last chapter provides the conclusion of the work done along with the impact of this work in addressing the challenges in the field and future prospects.

References

- (1) Whitesides, G. M.; Grzybowski, B. Self-Assembly at All Scales. *Science* **2002**, 295 (5564), 2418–2421. <https://doi.org/10.1126/science.1070821>.
- (2) Lim, Y.; Lee, E.; Lee, M. Controlled Bioactive Nanostructures from Self-Assembly of Peptide Building Blocks. *Angewandte Chemie International Edition* **2007**, 46 (47), 9011–9014. <https://doi.org/10.1002/anie.200702732>.
- (3) Das, R.; Gayakwad, B.; Shinde, S. D.; Rani, J.; Jain, A.; Sahu, B. Ultrashort Peptides—A Glimpse into the Structural Modifications and Their Applications as Biomaterials. *ACS Appl. Bio Mater.* **2020**, 3 (9), 5474–5499. <https://doi.org/10.1021/acsabm.0c00544>.
- (4) Kisiday, J.; Jin, M.; Kurz, B.; Hung, H.; Semino, C.; Zhang, S.; Grodzinsky, A. J. Self-Assembling Peptide Hydrogel Fosters Chondrocyte Extracellular Matrix Production and Cell Division: Implications for Cartilage Tissue Repair. *Proceedings of the National Academy of Sciences* **2002**, 99 (15), 9996–10001. <https://doi.org/10.1073/pnas.142309999>.
- (5) Hamley, I. W. Self-Assembly, Bioactivity, and Nanomaterials Applications of Peptide Conjugates with Bulky Aromatic Terminal Groups. *ACS Appl. Bio Mater.* **2023**, acsabm.2c01041. <https://doi.org/10.1021/acsabm.2c01041>.
- (6) Zhang, S. Discovery and Design of Self-Assembling Peptides. *Interface Focus*. **2017**, 7 (6), 20170028. <https://doi.org/10.1098/rsfs.2017.0028>.
- (7) Huo, Y.; Hu, J.; Yin, Y.; Liu, P.; Cai, K.; Ji, W. Self-Assembling Peptide-Based Functional Biomaterials. *ChemBioChem* **2023**, 24 (2), e202200582. <https://doi.org/10.1002/cbic.202200582>.
- (8) Rad-Malekshahi, M.; Lempsink, L.; Amidi, M.; Hennink, W. E.; Mastrobattista, E. Biomedical Applications of Self-Assembling Peptides. *Bioconjugate Chem.* **2016**, 27 (1), 3–18. <https://doi.org/10.1021/acs.bioconjchem.5b00487>.
- (9) Mikhalevich, V.; Craciun, I.; Kyropoulou, M.; Palivan, C. G.; Meier, W. Amphiphilic Peptide Self-Assembly: Expansion to Hybrid Materials. *Biomacromolecules* **2017**, 18 (11), 3471–3480. <https://doi.org/10.1021/acs.biomac.7b00764>.
- (10) Lee, S.; Trinh, T. H. T.; Yoo, M.; Shin, J.; Lee, H.; Kim, J.; Hwang, E.; Lim, Y.; Ryou, C. Self-Assembling Peptides and Their Application in the Treatment of Diseases. *International Journal of Molecular Sciences* **2019**, 20 (23). <https://doi.org/10.3390/ijms20235850>.
- (11) Muraoka, T.; Cui, H.; Stupp, S. I. Quadruple Helix Formation of a Photoresponsive Peptide Amphiphile and Its Light-Triggered Dissociation into Single Fibers. *J. Am. Chem. Soc.* **2008**, 130 (10), 2946–2947. <https://doi.org/10.1021/ja711213s>.
- (12) Ghadiri, M. R.; Granja, J. R.; Milligan, R. A.; McRee, D. E.; Khazanovich, N. Self-Assembling Organic Nanotubes Based on a Cyclic Peptide Architecture. *Nature* **1993**, 366 (6453), 324–327. <https://doi.org/10.1038/366324a0>.
- (13) Hartgerink, J. D.; Clark, T. D.; Ghadiri, M. R. Peptide Nanotubes and Beyond. *Chemistry – A European Journal* **1998**, 4 (8), 1367–1372. [https://doi.org/10.1002/\(SICI\)1521-3765\(19980807\)4:8<1367::AID-CHEM1367>3.0.CO;2-B](https://doi.org/10.1002/(SICI)1521-3765(19980807)4:8<1367::AID-CHEM1367>3.0.CO;2-B).
- (14) Bellomo, E. G.; Wyrsta, M. D.; Pakstis, L.; Pochan, D. J.; Deming, T. J. Stimuli-Responsive Polypeptide Vesicles by Conformation-Specific Assembly. *Nature Materials* **2004**, 3 (4), 244–248. <https://doi.org/10.1038/nmat1093>.
- (15) Nasrolahi Shirazi, A.; Tiwari, R. K.; Oh, D.; Banerjee, A.; Yadav, A.; Parang, K. Efficient Delivery of Cell Impermeable Phosphopeptides by a Cyclic Peptide Amphiphile Containing Tryptophan and Arginine. *Mol. Pharmaceutics* **2013**, 10 (5), 2008–2020. <https://doi.org/10.1021/mp400046u>.
- (16) Aggeli, A.; Bell, M.; Boden, N.; N. Keen, J.; C. B. McLeish, T.; Nyrkova, I.; Radford, S. E.; Semenov, A. Engineering of Peptide β -Sheet Nanotapes. *J. Mater. Chem.* **1997**, 7 (7), 1135–1145. <https://doi.org/10.1039/A701088E>.
- (17) Dehsorkhi, A.; Castelletto, V.; Hamley, I. W.; Adamcik, J.; Mezzenga, R. The Effect of PH on the Self-Assembly of a Collagen Derived Peptide Amphiphile. *Soft Matter* **2013**, 9 (26), 6033–6036. <https://doi.org/10.1039/C3SM51029H>.
- (18) Kopeček, J.; Yang, J. Peptide-Directed Self-Assembly of Hydrogels. *Acta Biomaterialia* **2009**, 5 (3), 805–816. <https://doi.org/10.1016/j.actbio.2008.10.001>.
- (19) Li, X.; Yi, K.; Shi, J.; Gao, Y.; Lin, H.-C.; Xu, B. Multifunctional, Biocompatible Supramolecular Hydrogelators Consist Only of Nucleobase, Amino Acid, and Glycoside. *J. Am. Chem. Soc.* **2011**, 133 (43), 17513–17518. <https://doi.org/10.1021/ja208456k>.

- (20) Debnath, S.; Shome, A.; Das, D.; Das, P. K. Hydrogelation Through Self-Assembly of Fmoc-Peptide Functionalized Cationic Amphiphiles: Potent Antibacterial Agent. *J. Phys. Chem. B* **2010**, *114* (13), 4407–4415. <https://doi.org/10.1021/jp909520w>.
- (21) Martin, A. D.; Robinson, A. B.; Thordarson, P. Biocompatible Small Peptide Super-Hydrogelators Bearing Carbazole Functionalities. *J. Mater. Chem. B* **2015**, *3* (11), 2277–2280. <https://doi.org/10.1039/C5TB00067J>.
- (22) Wojciechowski, J. P.; Martin, A. D.; Mason, A. F.; Fife, C. M.; Sagnella, S. M.; Kavallaris, M.; Thordarson, P. Choice of Capping Group in Tripeptide Hydrogels Influences Viability in the Three-Dimensional Cell Culture of Tumor Spheroids. *ChemPlusChem* **2017**, *82* (3), 383–389. <https://doi.org/10.1002/cplu.201600464>.
- (23) Roth-Konforti, M. E.; Comune, M.; Halperin-Sternfeld, M.; Grigoriants, I.; Shabat, D.; Adler-Abramovich, L. UV Light-Responsive Peptide-Based Supramolecular Hydrogel for Controlled Drug Delivery. *Macromolecular Rapid Communications* **2018**, *39* (24), 1800588. <https://doi.org/10.1002/marc.201800588>.
- (24) Nebot, V. J.; Armengol, J.; Smets, J.; Prieto, S. F.; Escuder, B.; Miravet, J. F. Molecular Hydrogels from Bolaform Amino Acid Derivatives: A Structure-Properties Study Based on the Thermodynamics of Gel Solubilization. *Chemistry – A European Journal* **2012**, *18* (13), 4063–4072. <https://doi.org/10.1002/chem.201103193>.
- (25) Basavalingappa, V.; Guterman, T.; Tang, Y.; Nir, S.; Lei, J.; Chakraborty, P.; Schnaider, L.; Reches, M.; Wei, G.; Gazit, E. Expanding the Functional Scope of the Fmoc-Diphenylalanine Hydrogelator by Introducing a Rigidifying and Chemically Active Urea Backbone Modification. *Advanced Science* **2019**, *6* (12), 1900218. <https://doi.org/10.1002/advs.201900218>.
- (26) Datta, D.; Tiwari, O.; Ganesh, K. N. New Archetypes in Self-Assembled Phe-Phe Motif Induced Nanostructures from Nucleoside Conjugated-Diphenylalanines. *Nanoscale* **2018**, *10* (7), 3212–3224. <https://doi.org/10.1039/C7NR08436F>.
- (27) Sun, L.; Fan, Z.; Wang, Y.; Huang, Y.; Schmidt, M.; Zhang, M. Tunable Synthesis of Self-Assembled Cyclic Peptide Nanotubes and Nanoparticles. *Soft Matter* **2015**, *11* (19), 3822–3832. <https://doi.org/10.1039/C5SM00533G>.
- (28) Hamley, I. W.; Brown, G. D.; Castelletto, V.; Cheng, G.; Venanzi, M.; Caruso, M.; Placidi, E.; Aleman, C.; Revilla-López, G.; Zanuy, D. Self-Assembly of a Designed Amyloid Peptide Containing the Functional Thienylalanine Unit. *J. Phys. Chem. B* **2010**, *114* (32), 10674–10683. <https://doi.org/10.1021/jp105508g>.
- (29) Chronopoulou, L.; Sennato, S.; Bordi, F.; Giannella, D.; Di Nitto, A.; Barbetta, A.; Dentini, M.; Togna, A. R.; Togna, G. I.; Moschini, S.; Palocci, C. Designing Unconventional Fmoc-Peptide-Based Biomaterials: Structure and Related Properties. *Soft Matter* **2014**, *10* (12), 1944–1952. <https://doi.org/10.1039/C3SM52457D>.
- (30) Castelletto, V.; Hamley, I. W.; Whitehouse, C.; Matts, P. J.; Osborne, R.; Baker, E. S. Self-Assembly of Palmitoyl Lipopeptides Used in Skin Care Products. *Langmuir* **2013**, *29* (29), 9149–9155. <https://doi.org/10.1021/la401771j>.
- (31) Maquart, F.-X.; Pickart, L.; Laurent, M.; Gillery, P.; Monboisse, J.-C.; Borel, J.-P. Stimulation of Collagen Synthesis in Fibroblast Cultures by the Tripeptide-Copper Complex Glycyl-L-Histidyl-L-Lysine-Cu²⁺. *FEBS Letters* **1988**, *238* (2), 343–346. [https://doi.org/10.1016/0014-5793\(88\)80509-X](https://doi.org/10.1016/0014-5793(88)80509-X).
- (32) Allen, P.; Melero-Martin, J.; Bischoff, J. Type I Collagen, Fibrin and PuraMatrix Matrices Provide Permissive Environments for Human Endothelial and Mesenchymal Progenitor Cells to Form Neovascular Networks. *Journal of Tissue Engineering and Regenerative Medicine* **2011**, *5* (4), e74–e86. <https://doi.org/10.1002/term.389>.
- (33) Sedighi, M.; Shrestha, N.; Mahmoudi, Z.; Khademi, Z.; Ghasempour, A.; Dehghan, H.; Talebi, S. F.; Toolabi, M.; Pr  at, V.; Chen, B.; Guo, X.; Shahbazi, M.-A. Multifunctional Self-Assembled Peptide Hydrogels for Biomedical Applications. *Polymers* **2023**, *15* (5). <https://doi.org/10.3390/polym15051160>.
- (34) Mitrovic, J.; Richey, G.; Kim, S.; Guler, M. O. Peptide Hydrogels and Nanostructures Controlling Biological Machinery. *Langmuir* **2023**, *39* (34), 11935–11945. <https://doi.org/10.1021/acs.langmuir.3c01269>.
- (35) Kulkarni, N.; Rao, P.; Jadhav, G. S.; Kulkarni, B.; Kanakavalli, N.; Kirad, S.; Salunke, S.; Tanpure, V.; Sahu, B. Emerging Role of Injectable Dipeptide Hydrogels in Biomedical Applications. *ACS Omega* **2023**, *8* (4), 3551–3570. <https://doi.org/10.1021/acsomega.2c05601>.

- (36) Karavasili, C.; Fatouros, D. G. Self-Assembling Peptides as Vectors for Local Drug Delivery and Tissue Engineering Applications. *Advanced Drug Delivery Reviews* **2021**, *174*, 387–405. <https://doi.org/10.1016/j.addr.2021.04.024>.
- (37) Yang, J.; An, H.-W.; Wang, H. Self-Assembled Peptide Drug Delivery Systems. *ACS Appl. Bio Mater.* **2021**, *4* (1), 24–46. <https://doi.org/10.1021/acsabm.0c00707>.
- (38) Wang, Q.; Jiang, N.; Fu, B.; Huang, F.; Liu, J. Self-Assembling Peptide-Based Nanodrug Delivery Systems. *Biomater. Sci.* **2019**, *7* (12), 4888–4911. <https://doi.org/10.1039/C9BM01212E>.
- (39) Pandya, A. K.; Vora, L. K.; Umeyor, C.; Surve, D.; Patel, A.; Biswas, S.; Patel, K.; Patravale, V. B. Polymeric in Situ Forming Depots for Long-Acting Drug Delivery Systems. *Advanced Drug Delivery Reviews* **2023**, *200*, 115003. <https://doi.org/10.1016/j.addr.2023.115003>.
- (40) Cesaro, A.; Lin, S.; Pardi, N.; de la Fuente-Nunez, C. Advanced Delivery Systems for Peptide Antibiotics. *Advanced Drug Delivery Reviews* **2023**, *196*, 114733. <https://doi.org/10.1016/j.addr.2023.114733>.
- (41) Finbloom, J. A.; Huynh, C.; Huang, X.; Desai, T. A. Bioinspired Nanotopographical Design of Drug Delivery Systems. *Nature Reviews Bioengineering* **2023**, *1* (2), 139–152. <https://doi.org/10.1038/s44222-022-00010-8>.
- (42) Mei, L.; Xu, K.; Zhai, Z.; He, S.; Zhu, T.; Zhong, W. Doxorubicin-Reinforced Supramolecular Hydrogels of RGD-Derived Peptide Conjugates for PH-Responsive Drug Delivery. *Org. Biomol. Chem.* **2019**, *17* (15), 3853–3860. <https://doi.org/10.1039/C9OB00046A>.
- (43) Li, X.; Fu, M.; Wu, J.; Zhang, C.; Deng, X.; Dhinakar, A.; Huang, W.; Qian, H.; Ge, L. PH-Sensitive Peptide Hydrogel for Glucose-Responsive Insulin Delivery. *Acta Biomaterialia* **2017**, *51*, 294–303. <https://doi.org/10.1016/j.actbio.2017.01.016>.
- (44) Raza, F.; Zhu, Y.; Chen, L.; You, X.; Zhang, J.; Khan, A.; Khan, M. W.; Hasnat, M.; Zafar, H.; Wu, J.; Ge, L. Paclitaxel-Loaded PH Responsive Hydrogel Based on Self-Assembled Peptides for Tumor Targeting. *Biomater. Sci.* **2019**, *7* (5), 2023–2036. <https://doi.org/10.1039/C9BM00139E>.
- (45) Xun, W.; Wu, D.-Q.; Li, Z.-Y.; Wang, H.-Y.; Huang, F.-W.; Cheng, S.-X.; Zhang, X.-Z.; Zhuo, R.-X. Peptide-Functionalized Thermo-Sensitive Hydrogels for Sustained Drug Delivery. *Macromolecular Bioscience* **2009**, *9* (12), 1219–1226. <https://doi.org/10.1002/mabi.200900298>.
- (46) Cao, M.; Wang, Y.; Hu, X.; Gong, H.; Li, R.; Cox, H.; Zhang, J.; Waigh, T. A.; Xu, H.; Lu, J. R. Reversible Thermoresponsive Peptide–PNIPAM Hydrogels for Controlled Drug Delivery. *Biomacromolecules* **2019**, *20* (9), 3601–3610. <https://doi.org/10.1021/acs.biomac.9b01009>.
- (47) Zhang, Z.; Zhou, S.; Wang, X.; Liang, R.; Sheng, X.; Zhu, Y.; Huang, L.; Zhou, B.; Zhong, M. Synthesis of PH/ Temperature Sensitive Gelatin/Peptide Composite Hydrogels and Its Characterization for Potential Controlled Drug Release Applications. *Materials Today Communications* **2023**, *36*, 106425. <https://doi.org/10.1016/j.mtcomm.2023.106425>.
- (48) Almohammed, S.; Kanoun, M. B.; Goumri-Said, S.; Alam, M. W.; Fularz, A.; Alnaim, A.; Rice, J. H.; Rodriguez, B. J. Thermally-Controlled Spherical Peptide Gel Architectures Prepared Using the PH Switch Method. *Peptide Science* **2023**, *115* (3), e24304. <https://doi.org/10.1002/pep2.24304>.
- (49) Noddeland, H. K.; Lind, M.; Petersson, K.; Caruso, F.; Malmsten, M.; Heinz, A. Protease-Responsive Hydrogel Microparticles for Intradermal Drug Delivery. *Biomacromolecules* **2023**, *24* (7), 3203–3214. <https://doi.org/10.1021/acs.biomac.3c00265>.
- (50) Coulter, S. M.; Pentlavalli, S.; Vora, L. K.; An, Y.; Cross, E. R.; Peng, K.; McAulay, K.; Schweins, R.; Donnelly, R. F.; McCarthy, H. O.; Lavery, G. Enzyme-Triggered l- α /d-Peptide Hydrogels as a Long-Acting Injectable Platform for Systemic Delivery of HIV/AIDS Drugs. *Advanced Healthcare Materials* **2023**, *12* (18), 2203198. <https://doi.org/10.1002/adhm.202203198>.
- (51) Noddeland, H. K.; Lind, M.; Jensen, L. B.; Petersson, K.; Skak-Nielsen, T.; Larsen, F. H.; Malmsten, M.; Heinz, A. Design and Characterization of Matrix Metalloproteinase-Responsive Hydrogels for the Treatment of Inflammatory Skin Diseases. *Acta Biomaterialia* **2023**, *157*, 149–161. <https://doi.org/10.1016/j.actbio.2022.12.015>.
- (52) Zhou, Y.; Li, Q.; Wu, Y.; Li, X.; Zhou, Y.; Wang, Z.; Liang, H.; Ding, F.; Hong, S.; Steinmetz, N. F.; Cai, H. Molecularly Stimuli-Responsive Self-Assembled Peptide Nanoparticles for Targeted Imaging and Therapy. *ACS Nano* **2023**, *17* (9), 8004–8025. <https://doi.org/10.1021/acs.nano.3c01452>.

- (53) Soukasene, S.; Toft, D. J.; Moyer, T. J.; Lu, H.; Lee, H.-K.; Standley, S. M.; Cryns, V. L.; Stupp, S. I. Antitumor Activity of Peptide Amphiphile Nanofiber-Encapsulated Camptothecin. *ACS Nano* **2011**, *5* (11), 9113–9121. <https://doi.org/10.1021/nn203343z>.
- (54) Han, C.; Zhou, J.; Liang, C.; Liu, B.; Pan, X.; Zhang, Y.; Wang, Y.; Yan, B.; Xie, W.; Liu, F.; Yu, X.-Y.; Li, Y. Human Umbilical Cord Mesenchymal Stem Cell Derived Exosomes Encapsulated in Functional Peptide Hydrogels Promote Cardiac Repair. *Biomater. Sci.* **2019**, *7* (7), 2920–2933. <https://doi.org/10.1039/C9BM00101H>.
- (55) Ji, T.; Lang, J.; Wang, J.; Cai, R.; Zhang, Y.; Qi, F.; Zhang, L.; Zhao, X.; Wu, W.; Hao, J.; Qin, Z.; Zhao, Y.; Nie, G. Designing Liposomes To Suppress Extracellular Matrix Expression To Enhance Drug Penetration and Pancreatic Tumor Therapy. *ACS Nano* **2017**, *11* (9), 8668–8678. <https://doi.org/10.1021/acsnano.7b01026>.
- (56) Feng, Z.; Xu, B. Inspiration from the Mirror: D-Amino Acid Containing Peptides in Biomedical Approaches. **2016**, *7* (3), 179–187. <https://doi.org/10.1515/bmc-2015-0035>.
- (57) Albanese, A.; Tang, P. S.; Chan, W. C. W. The Effect of Nanoparticle Size, Shape, and Surface Chemistry on Biological Systems. *Annu. Rev. Biomed. Eng.* **2012**, *14* (1), 1–16. <https://doi.org/10.1146/annurev-bioeng-071811-150124>.
- (58) Sangtani, A.; Petryayeva, E.; Wu, M.; Susumu, K.; Oh, E.; Huston, A. L.; Lasarte-Aragones, G.; Medintz, I. L.; Algar, W. R.; Delehanty, J. B. Intracellularly Actuated Quantum Dot–Peptide–Doxorubicin Nanobioconjugates for Controlled Drug Delivery via the Endocytic Pathway. *Bioconjugate Chem.* **2018**, *29* (1), 136–148. <https://doi.org/10.1021/acs.bioconjchem.7b00658>.
- (59) Zhang, C.; Pan, D.; Luo, K.; She, W.; Guo, C.; Yang, Y.; Gu, Z. Peptide Dendrimer–Doxorubicin Conjugate-Based Nanoparticles as an Enzyme-Responsive Drug Delivery System for Cancer Therapy. *Advanced Healthcare Materials* **2014**, *3* (8), 1299–1308. <https://doi.org/10.1002/adhm.201300601>.
- (60) Ji, T.; Zhao, Y.; Ding, Y.; Wang, J.; Zhao, R.; Lang, J.; Qin, H.; Liu, X.; Shi, J.; Tao, N.; Qin, Z.; Nie, G.; Zhao, Y. Transformable Peptide Nanocarriers for Expeditious Drug Release and Effective Cancer Therapy via Cancer-Associated Fibroblast Activation. *Angewandte Chemie International Edition* **2016**, *55* (3), 1050–1055. <https://doi.org/10.1002/anie.201506262>.
- (61) Chen, Y.; Luan, J.; Shen, W.; Lei, K.; Yu, L.; Ding, J. Injectable and Thermosensitive Hydrogel Containing Liraglutide as a Long-Acting Antidiabetic System. *ACS Appl. Mater. Interfaces* **2016**, *8* (45), 30703–30713. <https://doi.org/10.1021/acsami.6b09415>.
- (62) Zhuang, Y.; Yang, X.; Li, Y.; Chen, Y.; Peng, X.; Yu, L.; Ding, J. Sustained Release Strategy Designed for Lixisenatide Delivery to Synchronously Treat Diabetes and Associated Complications. *ACS Appl. Mater. Interfaces* **2019**, *11* (33), 29604–29618. <https://doi.org/10.1021/acsami.9b10346>.
- (63) Liu, D.; Zhang, Y.; Jiang, G.; Yu, W.; Xu, B.; Zhu, J. Fabrication of Dissolving Microneedles with Thermal-Responsive Coating for NIR-Triggered Transdermal Delivery of Metformin on Diabetic Rats. *ACS Biomater. Sci. Eng.* **2018**, *4* (5), 1687–1695. <https://doi.org/10.1021/acsbiomaterials.8b00159>.
- (64) Zhou, L.; Min, T.; Bian, X.; Dong, Y.; Zhang, P.; Wen, Y. Rational Design of Intelligent and Multifunctional Dressing to Promote Acute/Chronic Wound Healing. *ACS Appl. Bio Mater.* **2022**, *5* (9), 4055–4085. <https://doi.org/10.1021/acsabm.2c00500>.
- (65) Qu, J.; Zhao, X.; Liang, Y.; Zhang, T.; Ma, P. X.; Guo, B. Antibacterial Adhesive Injectable Hydrogels with Rapid Self-Healing, Extensibility and Compressibility as Wound Dressing for Joints Skin Wound Healing. *Biomaterials* **2018**, *183*, 185–199. <https://doi.org/10.1016/j.biomaterials.2018.08.044>.
- (66) Wang, Z.; Hu, W.; You, W.; Huang, G.; Tian, W.; Huselstein, C.; Wu, C.-L.; Xiao, Y.; Chen, Y.; Wang, X. Antibacterial and Angiogenic Wound Dressings for Chronic Persistent Skin Injury. *Chemical Engineering Journal* **2021**, *404*, 126525. <https://doi.org/10.1016/j.cej.2020.126525>.
- (67) Guan, T.; Li, J.; Chen, C.; Liu, Y. Self-Assembling Peptide-Based Hydrogels for Wound Tissue Repair. *Advanced Science* **2022**, *9* (10), 2104165. <https://doi.org/10.1002/adv.202104165>.
- (68) Barrientos, S.; Stojadinovic, O.; Golinko, M. S.; Brem, H.; Tomic-Canic, M. PERSPECTIVE ARTICLE: Growth Factors and Cytokines in Wound Healing. *Wound Repair and Regeneration* **2008**, *16* (5), 585–601. <https://doi.org/10.1111/j.1524-475X.2008.00410.x>.
- (69) Kharaziha, M.; Baidya, A.; Annabi, N. Rational Design of Immunomodulatory Hydrogels for Chronic Wound Healing. *Advanced Materials* **2021**, *33* (39), 2100176. <https://doi.org/10.1002/adma.202100176>.

- (70) Silva, G. A.; Czeisler, C.; Niece, K. L.; Beniash, E.; Harrington, D. A.; Kessler, J. A.; Stupp, S. I. Selective Differentiation of Neural Progenitor Cells by High-Epitope Density Nanofibers. *Science* **2004**, *303* (5662), 1352–1355. <https://doi.org/10.1126/science.1093783>.
- (71) Liang, Y.; He, J.; Guo, B. Functional Hydrogels as Wound Dressing to Enhance Wound Healing. *ACS Nano* **2021**, *15* (8), 12687–12722. <https://doi.org/10.1021/acsnano.1c04206>.
- (72) Yuk, H.; Varela, C. E.; Nabzdyk, C. S.; Mao, X.; Padera, R. F.; Roche, E. T.; Zhao, X. Dry Double-Sided Tape for Adhesion of Wet Tissues and Devices. *Nature* **2019**, *575* (7781), 169–174. <https://doi.org/10.1038/s41586-019-1710-5>.
- (73) Chen, C.; Zhang, Y.; Fei, R.; Cao, C.; Wang, M.; Wang, J.; Bai, J.; Cox, H.; Waigh, T.; Lu, J. R.; Xu, H. Hydrogelation of the Short Self-Assembling Peptide I3QGK Regulated by Transglutaminase and Use for Rapid Hemostasis. *ACS Appl. Mater. Interfaces* **2016**, *8* (28), 17833–17841. <https://doi.org/10.1021/acsnano.1c04206>.
- (74) Luo, Z.; Wang, S.; Zhang, S. Fabrication of Self-Assembling d-Form Peptide Nanofiber Scaffold d-EAK16 for Rapid Hemostasis. *Biomaterials* **2011**, *32* (8), 2013–2020. <https://doi.org/10.1016/j.biomaterials.2010.11.049>.
- (75) Ali, A.; Liu, J.; Zhou, H.; Liu, T.; Ovais, M.; Liu, H.; Rui, Y.; Chen, C. Graphdiyne–Hemin-Mediated Catalytic System for Wound Disinfection and Accelerated Wound Healing. *Mater. Chem. Front.* **2021**, *5* (16), 6041–6051. <https://doi.org/10.1039/D1QM00490E>.
- (76) Salick, D. A.; Kretsinger, J. K.; Pochan, D. J.; Schneider, J. P. Inherent Antibacterial Activity of a Peptide-Based β -Hairpin Hydrogel. *J. Am. Chem. Soc.* **2007**, *129* (47), 14793–14799. <https://doi.org/10.1021/ja076300z>.
- (77) Martin, E. C.; May, P. D.; McMahon, W. A. Amino Acid Polymers for Biomedical Applications. I. Permeability Properties Of L-Leucine-DL-Methionine Copolymers. *J. Biomed. Mater. Res.* **1971**, *5* (1), 53–62. <https://doi.org/10.1002/jbm.820050105>.
- (78) Schnaider, L.; Brahmachari, S.; Schmidt, N. W.; Mensa, B.; Shaham-Niv, S.; Bychenko, D.; Adler-Abramovich, L.; Shimon, L. J. W.; Kolusheva, S.; DeGrado, W. F.; Gazit, E. Self-Assembling Dipeptide Antibacterial Nanostructures with Membrane Disrupting Activity. *Nature Communications* **2017**, *8* (1), 1365. <https://doi.org/10.1038/s41467-017-01447-x>.
- (79) Tang, W.; Yang, J.; Zhao, Z.; Lian, Z.; Liang, G. Intracellular Coassembly Boosts the Anti-Inflammation Capacity of Dexamethasone. *Nanoscale* **2017**, *9* (45), 17717–17721. <https://doi.org/10.1039/C7NR07197C>.
- (80) Tang, W.; Zhao, Z.; Chong, Y.; Wu, C.; Liu, Q.; Yang, J.; Zhou, R.; Lian, Z.-X.; Liang, G. Tandem Enzymatic Self-Assembly and Slow Release of Dexamethasone Enhances Its Antihepatic Fibrosis Effect. *ACS Nano* **2018**, *12* (10), 9966–9973. <https://doi.org/10.1021/acsnano.8b04143>.
- (81) Yu, X.; Zhang, Z.; Yu, J.; Chen, H.; Li, X. Self-Assembly of a Ibuprofen-Peptide Conjugate to Suppress Ocular Inflammation. *Nanomedicine: Nanotechnology, Biology and Medicine* **2018**, *14* (1), 185–193. <https://doi.org/10.1016/j.nano.2017.09.010>.
- (82) Franz, S.; Rammelt, S.; Scharnweber, D.; Simon, J. C. Immune Responses to Implants – A Review of the Implications for the Design of Immunomodulatory Biomaterials. *Biomaterials* **2011**, *32* (28), 6692–6709. <https://doi.org/10.1016/j.biomaterials.2011.05.078>.
- (83) Dou, X.-Q.; Feng, C.-L. Amino Acids and Peptide-Based Supramolecular Hydrogels for Three-Dimensional Cell Culture. *Advanced Materials* **2017**, *29* (16), 1604062. <https://doi.org/10.1002/adma.201604062>.
- (84) Webber, M. J.; Tongers, J.; Newcomb, C. J.; Marquardt, K.-T.; Bauersachs, J.; Losordo, D. W.; Stupp, S. I. Supramolecular Nanostructures That Mimic VEGF as a Strategy for Ischemic Tissue Repair. *Proceedings of the National Academy of Sciences* **2011**, *108* (33), 13438–13443. <https://doi.org/10.1073/pnas.1016546108>.
- (85) Kumar, V. A.; Taylor, N. L.; Shi, S.; Wang, B. K.; Jalan, A. A.; Kang, M. K.; Wickremasinghe, N. C.; Hartgerink, J. D. Highly Angiogenic Peptide Nanofibers. *ACS Nano* **2015**, *9* (1), 860–868. <https://doi.org/10.1021/nn506544b>.
- (86) Yao, X.; Liu, Y.; Gao, J.; Yang, L.; Mao, D.; Stefanitsch, C.; Li, Y.; Zhang, J.; Ou, L.; Kong, D.; Zhao, Q.; Li, Z. Nitric Oxide Releasing Hydrogel Enhances the Therapeutic Efficacy of Mesenchymal Stem Cells for Myocardial Infarction. *Biomaterials* **2015**, *60*, 130–140. <https://doi.org/10.1016/j.biomaterials.2015.04.046>.
- (87) Hao, Z.; Li, H.; Wang, Y.; Hu, Y.; Chen, T.; Zhang, S.; Guo, X.; Cai, L.; Li, J. Supramolecular Peptide Nanofiber Hydrogels for Bone Tissue Engineering: From Multihierarchical Fabrications

- to Comprehensive Applications. *Advanced Science* **2022**, *9* (11), 2103820. <https://doi.org/10.1002/advs.202103820>.
- (88) Chen, C. H.; Hsu, E. L.; Stupp, S. I. Supramolecular Self-Assembling Peptides to Deliver Bone Morphogenetic Proteins for Skeletal Regeneration. *Bone* **2020**, *141*, 115565. <https://doi.org/10.1016/j.bone.2020.115565>.
- (89) Das, A. K.; Gavel, P. K. Low Molecular Weight Self-Assembling Peptide-Based Materials for Cell Culture, Antimicrobial, Anti-Inflammatory, Wound Healing, Anticancer, Drug Delivery, Bioimaging and 3D Bioprinting Applications. *Soft Matter* **2020**, *16* (44), 10065–10095. <https://doi.org/10.1039/D0SM01136C>.
- (90) Koons, G. L.; Diba, M.; Mikos, A. G. Materials Design for Bone-Tissue Engineering. *Nature Reviews Materials* **2020**, *5* (8), 584–603. <https://doi.org/10.1038/s41578-020-0204-2>.
- (91) Bahraminasab, M.; Janmohammadi, M.; Arab, S.; Talebi, A.; Nooshabadi, V. T.; Koohsarian, P.; Nourbakhsh, M. S. Bone Scaffolds: An Incorporation of Biomaterials, Cells, and Biofactors. *ACS Biomater. Sci. Eng.* **2021**, *7* (12), 5397–5431. <https://doi.org/10.1021/acsbiomaterials.1c00920>.
- (92) Linder, H. R.; Glass, A. A.; Day, D. E.; Sell, S. A. Manipulating Air-Gap Electrospinning to Create Aligned Polymer Nanofiber-Wrapped Glass Microfibers for Cortical Bone Tissue Engineering. *Bioengineering* **2020**, *7* (4). <https://doi.org/10.3390/bioengineering7040165>.
- (93) Huettner, N.; Dargaville, T. R.; Forget, A. Discovering Cell-Adhesion Peptides in Tissue Engineering: Beyond RGD. *Trends in Biotechnology* **2018**, *36* (4), 372–383. <https://doi.org/10.1016/j.tibtech.2018.01.008>.
- (94) Luo, H.; Xu, C.; Liu, Z.; Yang, L.; Hong, Y.; Liu, G.; Zhong, H.; Cai, X.; Lin, X.; Chen, X.; Wang, C.; Nanwen, Z.; Xu, W. Neural Differentiation of Bone Marrow Mesenchymal Stem Cells with Human Brain-Derived Neurotrophic Factor Gene-Modified in Functionalized Self-Assembling Peptide Hydrogel in Vitro. *Journal of Cellular Biochemistry* **2019**, *120* (3), 2828–2835. <https://doi.org/10.1002/jcb.26408>.
- (95) Nowakowski, G. S.; Dooner, M. S.; Valinski, H. M.; Mihaliak, A. M.; Quesenberry, P. J.; Becker, P. S. A Specific Heptapeptide from a Phage Display Peptide Library Homes to Bone Marrow and Binds to Primitive Hematopoietic Stem Cells. *Stem Cells* **2004**, *22* (6), 1030–1038. <https://doi.org/10.1634/stemcells.22-6-1030>.
- (96) Jun, H.-W.; Yuwono, V.; Paramonov, S. E.; Hartgerink, J. D. Enzyme-Mediated Degradation of Peptide-Amphiphile Nanofiber Networks. *Advanced Materials* **2005**, *17* (21), 2612–2617. <https://doi.org/10.1002/adma.200500855>.
- (97) Hartgerink, J. D.; Beniash, E.; Stupp, S. I. Self-Assembly and Mineralization of Peptide-Amphiphile Nanofibers. *Science* **2001**, *294* (5547), 1684–1688. <https://doi.org/10.1126/science.1063187>.
- (98) Onak, G.; Gökmen, O.; Yaralı, Z. B.; Karaman, O. Enhanced Osteogenesis of Human Mesenchymal Stem Cells by Self-Assembled Peptide Hydrogel Functionalized with Glutamic Acid Templated Peptides. *Journal of Tissue Engineering and Regenerative Medicine* **2020**, *14* (9), 1236–1249. <https://doi.org/10.1002/term.3095>.
- (99) Hosseinkhani, H.; Hosseinkhani, M.; Khademhosseini, A.; Kobayashi, H. RETRACTED: Bone Regeneration through Controlled Release of Bone Morphogenetic Protein-2 from 3-D Tissue Engineered Nano-Scaffold. *Journal of Controlled Release* **2007**, *117* (3), 380–386. <https://doi.org/10.1016/j.jconrel.2006.11.018>.
- (100) Liang, P.; Zheng, J.; Zhang, Z.; Hou, Y.; Wang, J.; Zhang, C.; Quan, C. Bioactive 3D Scaffolds Self-Assembled from Phosphorylated Mimicking Peptide Amphiphiles to Enhance Osteogenesis. *Journal of Biomaterials Science, Polymer Edition* **2019**, *30* (1), 34–48. <https://doi.org/10.1080/09205063.2018.1505264>.
- (101) Wang, B.; Wu, B.; Jia, Y.; Jiang, Y.; Yuan, Y.; Man, Y.; Xiang, L. Neural Peptide Promotes the Angiogenesis and Osteogenesis around Oral Implants. *Cellular Signalling* **2021**, *79*, 109873. <https://doi.org/10.1016/j.cellsig.2020.109873>.
- (102) Bakshi, R.; Hokugo, A.; Khalil, D.; Wang, L.; Shibuya, Y.; Zhou, S.; Zhang, Z.; Rezzadeh, K.; McClendon, M.; Stupp, S. I.; Jarrahy, R. A Chemotactic Functional Scaffold with VEGF-Releasing Peptide Amphiphiles Facilitates Bone Regeneration by BMP-2 in a Large-Scale Rodent Cranial Defect Model. *Plastic and Reconstructive Surgery* **2021**, *147* (2).
- (103) Wang, H.; Shang, Y.; Chen, X.; Wang, Z.; Zhu, D.; Liu, Y.; Zhang, C.; Chen, P.; Wu, J.; Wu, L.; Kong, D.; Yang, Z.; Li, Z.; Chen, X. Delivery of MSCs with a Hybrid β -Sheet Peptide Hydrogel Consisting IGF-1C Domain and D-Form Peptide for Acute Kidney Injury Therapy.

- International Journal of Nanomedicine* **2020**, *15*, 4311–4324. <https://doi.org/10.2147/IJN.S254635>.
- (104) Wu, Z.; Bai, J.; Ge, G.; Wang, T.; Feng, S.; Ma, Q.; Liang, X.; Li, W.; Zhang, W.; Xu, Y.; Guo, K.; Cui, W.; Zha, G.; Geng, D. Regulating Macrophage Polarization in High Glucose Microenvironment Using Lithium-Modified Bioglass-Hydrogel for Diabetic Bone Regeneration. *Advanced Healthcare Materials* **2022**, *11* (13), 2200298. <https://doi.org/10.1002/adhm.202200298>.
 - (105) Yang, G.; Huang, T.; Wang, Y.; Wang, H.; Li, Y.; Yu, K.; Dong, L. Sustained Release of Antimicrobial Peptide from Self-Assembling Hydrogel Enhanced Osteogenesis. *Journal of Biomaterials Science, Polymer Edition* **2018**, *29* (15), 1812–1824. <https://doi.org/10.1080/09205063.2018.1504191>.
 - (106) Li, K.; Guo, A.; Ran, Q.; Tian, H.; Du, X.; Chen, S.; Wen, Y.; Tang, Y.; Jiang, D. A Novel Biocomposite Scaffold with Antibacterial Potential and the Ability to Promote Bone Repair. *J Biomater Appl* **2021**, *36* (3), 474–480. <https://doi.org/10.1177/0885328221994448>.
 - (107) Long, J.; Zhang, W.; Chen, Y.; Teng, B.; Liu, B.; Li, H.; Yao, Z.; Wang, D.; Li, L.; Yu, X.-F.; Qin, L.; Lai, Y. Multifunctional Magnesium Incorporated Scaffolds by 3D-Printing for Comprehensive Postsurgical Management of Osteosarcoma. *Biomaterials* **2021**, *275*, 120950. <https://doi.org/10.1016/j.biomaterials.2021.120950>.
 - (108) Lou, Y.; Zhang, B.; Ye, X.; Wang, Z.-G. Self-Assembly of the de Novo Designed Peptides to Produce Supramolecular Catalysts with Built-in Enzyme-like Active Sites: A Review of Structure–Activity Relationship. *Materials Today Nano* **2023**, *21*, 100302. <https://doi.org/10.1016/j.mtnano.2023.100302>.
 - (109) Friedle, S.; Reisner, E.; Lippard, S. J. Current Challenges of Modeling Diiron Enzyme Active Sites for Dioxygen Activation by Biomimetic Synthetic Complexes. *Chem. Soc. Rev.* **2010**, *39* (8), 2768–2779. <https://doi.org/10.1039/C003079C>.
 - (110) Vaissier Welborn, V.; Head-Gordon, T. Computational Design of Synthetic Enzymes. *Chem. Rev.* **2019**, *119* (11), 6613–6630. <https://doi.org/10.1021/acs.chemrev.8b00399>.
 - (111) Zozulia, O.; Dolan, M. A.; Korendovych, I. V. Catalytic Peptide Assemblies. *Chem. Soc. Rev.* **2018**, *47* (10), 3621–3639. <https://doi.org/10.1039/C8CS00080H>.
 - (112) Hamley, I. W. Biocatalysts Based on Peptide and Peptide Conjugate Nanostructures. *Biomacromolecules* **2021**, *22* (5), 1835–1855. <https://doi.org/10.1021/acs.biomac.1c00240>.
 - (113) Hedstrom, L. Serine Protease Mechanism and Specificity. *Chem. Rev.* **2002**, *102* (12), 4501–4524. <https://doi.org/10.1021/cr000033x>.
 - (114) Bélières, M.; Chouini-Lalanne, N.; Déjugnat, C. Synthesis, Self-Assembly, and Catalytic Activity of Histidine-Based Structured Lipopeptides for Hydrolysis Reactions in Water. *RSC Adv.* **2015**, *5* (45), 35830–35842. <https://doi.org/10.1039/C5RA02853A>.
 - (115) Gulseren, G.; Khalily, M. A.; Tekinay, A. B.; Guler, M. O. Catalytic Supramolecular Self-Assembled Peptide Nanostructures for Ester Hydrolysis. *J. Mater. Chem. B* **2016**, *4* (26), 4605–4611. <https://doi.org/10.1039/C6TB00795C>.
 - (116) Wong, Y.-M.; Masunaga, H.; Chuah, J.-A.; Sudesh, K.; Numata, K. Enzyme-Mimic Peptide Assembly To Achieve Amidolytic Activity. *Biomacromolecules* **2016**, *17* (10), 3375–3385. <https://doi.org/10.1021/acs.biomac.6b01169>.
 - (117) Zaramella, D.; Scrimin, P.; Prins, L. J. Self-Assembly of a Catalytic Multivalent Peptide–Nanoparticle Complex. *J. Am. Chem. Soc.* **2012**, *134* (20), 8396–8399. <https://doi.org/10.1021/ja302754h>.
 - (118) Gulseren, G.; Yasa, I. C.; Ustahuseyin, O.; Tekin, E. D.; Tekinay, A. B.; Guler, M. O. Alkaline Phosphatase-Mimicking Peptide Nanofibers for Osteogenic Differentiation. *Biomacromolecules* **2015**, *16* (7), 2198–2208. <https://doi.org/10.1021/acs.biomac.5b00593>.
 - (119) Rufo, C. M.; Moroz, Y. S.; Moroz, O. V.; Stöhr, J.; Smith, T. A.; Hu, X.; DeGrado, W. F.; Korendovych, I. V. Short Peptides Self-Assemble to Produce Catalytic Amyloids. *Nature Chem* **2014**, *6* (4), 303–309. <https://doi.org/10.1038/nchem.1894>.
 - (120) Omosun, T. O.; Hsieh, M.-C.; Childers, W. S.; Das, D.; Mehta, A. K.; Anthony, N. R.; Pan, T.; Grover, M. A.; Berland, K. M.; Lynn, D. G. Catalytic Diversity in Self-Propagating Peptide Assemblies. *Nature Chemistry* **2017**, *9* (8), 805–809. <https://doi.org/10.1038/nchem.2738>.
 - (121) Duschmalé, J.; Kohrt, S.; Wennemers, H. Peptide Catalysis in Aqueous Emulsions. *Chem. Commun.* **2014**, *50* (60), 8109–8112. <https://doi.org/10.1039/C4CC01759E>.

- (122) Tena-Solsona, M.; Nanda, J.; Díaz-Oltra, S.; Chotera, A.; Ashkenasy, G.; Escuder, B. Emergent Catalytic Behavior of Self-Assembled Low Molecular Weight Peptide-Based Aggregates and Hydrogels. *Chemistry – A European Journal* **2016**, 22 (19), 6687–6694. <https://doi.org/10.1002/chem.201600344>.
- (123) Makhlynets, O. V.; Gosavi, P. M.; Korendovych, I. V. Short Self-Assembling Peptides Are Able to Bind to Copper and Activate Oxygen. *Angewandte Chemie International Edition* **2016**, 55 (31), 9017–9020. <https://doi.org/10.1002/anie.201602480>.
- (124) Chatterjee, A.; Afrose, S. P.; Ahmed, S.; Venugopal, A.; Das, D. Cross- β Amyloid Nanotubes for Hydrolase–Peroxidase Cascade Reactions. *Chem. Commun.* **2020**, 56 (57), 7869–7872. <https://doi.org/10.1039/D0CC00279H>.
- (125) Wang, Q.; Yang, Z.; Zhang, X.; Xiao, X.; Chang, C. K.; Xu, B. A Supramolecular-Hydrogel-Encapsulated Hemin as an Artificial Enzyme to Mimic Peroxidase. *Angewandte Chemie International Edition* **2007**, 46 (23), 4285–4289. <https://doi.org/10.1002/anie.200700404>.

CHAPTER - 2

Self-assembled peptide gels for the pH-responsive, sustained release of an antidiabetic drug, glimepiride

Self-assembled peptide gels for drug delivery

2.1. Introduction**2.1.1. Diabetes mellitus (Type II)**

Diabetes mellitus (DM) is a long-term metabolic disorder characterized by the elevated blood glucose levels (hyperglycemia), which can have negative effects on the kidneys and heart.^{1,2} Due to ageing, obesity, poor diet, and sedentary lifestyle of global population, the incidence and prevalence of Type 2 diabetes is rising rapidly.³ According to the International Diabetes Federation (IDF) Diabetes Atlas 2021, there are approximately 537 million people living with diabetes globally, making it a disease with fastest-growing population in the twenty-first century. Between the ages of 20 and 64, diabetes affects 352 million people, or three out of every four individuals. By 2030, there will be about 643 million adults with diabetes, and by 2045, there will be nearly 783 million. People suffering from type 2 diabetes confront specific challenges. Through the processes of glycolysis and tricarboxylic acid cycle (TCA) cycle, elevated glucose levels are produced and it causes the synthesis of organic acids, such as gluconic acid. Diabetic individuals can produce more H^+ than is necessary for proper physiological activity, which impairs mitochondrial function. High quantities of ketone bodies, therefore, manifest in peripheral tissues, leading to ketoacidosis and an acidic pH.⁴⁻⁶ The overproduction of superoxide in mitochondria, which is triggered by high blood glucose levels, is another consequence of this disease that can cause organ damage from oxidative stress.⁷ Free radicals produced by the self-oxidation reaction of sugars, sugar adducts, proteins, and unsaturated lipids in plasma and membrane proteins are potential causes of oxidative stress and protein degradation in diabetes.⁸

2.1.2. Challenges

Most of the anti-diabetic drugs are designed to lower blood sugar levels, promote insulin secretion, and repair pancreatic beta-cell damage. However, many of them have negative side effects, such as a fast reduction in blood sugar that could result in liver and renal malfunction as well as an increased risk of cardiovascular issues.⁹ In order to maintain the optimum blood glucose level, patients require frequent administration of medicine. One of the top three most often given oral antidiabetic drugs, glimepiride is a third-generation sulfonylurea derivative used to treat type 2 diabetes in people, who are not reliant on insulin. Glimepiride lowers blood glucose levels by activating pancreatic beta cells, while simultaneously raising insulin levels.¹⁰ It also increases the sensitivity of intracellular insulin receptors to the action of insulin but glimepiride's solubility is pH-dependent, which results in fluctuating bioavailability and severe side-effects, such as hypoglycemia and gastrointestinal problems.¹¹ The medication is associated with limited physiological stability, non-specific targeting, and poor membrane permeability, which are traits of small molecule medications. Therefore, it is crucial to develop an effective drug delivery system that can detect pH changes brought on by variations in glucose

concentration and release a suitable amount of drug for a sustained period of time to address these issues and improve patient satisfaction and compliance in type II diabetes therapy.^{12–14}

2.1.3. Research gap

Glucose and pH-responsive biomaterials are being investigated for treating diabetes. Researchers have developed several formulations, including self-assembled peptide gels,^{4,15} polymeric hydrogels,¹³ glycopolymeric nanoparticles,¹⁶ polymerosomes,¹² and microneedle array patches,¹⁷ but these formulations are limited to the delivery of insulin. There are very limited publications on nanoparticulate antidiabetic drug delivery methods for glipizide¹⁸ and repaglinide.¹⁹ However, these formulations did not exhibit a long-term, controlled release profile. The fabrication of sustained release formulations containing glimepiride can control diabetes effectively. Several glimepiride-loaded formulations have been reported by Ahmed and coworkers, such as self-nanoemulsifying delivery systems with chitosan and hydroxypropyl methyl cellulose, zein-based glimepiride nanoparticles encapsulated into a gel comprising of thermoresponsive triblock copolymers poly(lactide-co-glycolide)-block-poly(ethylene glycol)-block-poly(lactide-co-glycolide) but they encountered issues, like early burst release and use of plasticizers and permeation enhancers.^{10,20,21} The glimepiride encapsulated delivery systems (glimepiride loaded into niosomes-containing nonionic surfactants) prepared by Mohsen *et al.*²² and Abdallah *et al.*²³ (transdermal delivery of glimepiride from proniosomal gel) showed a sustained release for only 24 h. To the best of our knowledge, peptide gels have not been investigated for the sustained, long-term administration of glimepiride.

2.1.4. Self-assembled peptide gel

Peptides can be utilized to design self-assembled biomaterials (gels, nano-assemblies) that can be used to increase the effectiveness of drug delivery and decrease drug toxicity because of their diversified design, dynamic self-assembly property, and biocompatibility.^{24–26} Since the side chain at the α -carbon atom in peptides can vary, different biomaterials can be developed by non-covalent interactions between amino acids, such as hydrogen bonding, ionic, hydrophobic, and stacking interactions.²⁷ Peptide gels produced by molecular self-assembly have become one of the most intriguing biomaterials with applications in many areas of biomedicine.^{28,29} One can control the properties of peptide gels by changing the structure and length of the building blocks. Given that peptide self-assembly is primarily fueled by hydrophobicity and aromatic groups, peptide gels are the optimum vehicle for glimepiride administration. Peptides are also more appropriate as a drug delivery scaffold with less cytotoxicity due to their biodegradable and biocompatible nature.³⁰ To the best of our knowledge, delivery of glimepiride for a sustained period of time has not been achieved earlier with self-assembled peptide gel as a carrier.

2.2. Objectives

To surmount the limitations described above, we aimed to develop ultra-short, self-assembled peptide gels from peptides with inherent antioxidant properties. Tyrosine (Y) and tryptophan (W) were chosen in the current study to build the peptide backbone due to their outstanding antioxidant capacity, and

histidine was added since it can make the gel pH-sensitive.^{31,32} Two dipeptides, Fmoc-Tyr-Tyr-NH₂ (YY) and Fmoc-Trp-Trp-NH₂ (WW), and a tripeptide Fmoc-Trp-Trp-His-NH₂ (WWH), were synthesized by solid-phase peptide synthesis (SPPS) and characterized by mass spectrometry, NMR, and RP-HPLC. Peptides were self-assembled into gels in DMSO/water and glimepiride was encapsulated. Investigations were done on the secondary structures, surface morphology, viscoelastic characteristics, self-healing capacity, swelling and degradation behavior, pH-dependent release, and antioxidant activities. The MTT assay was used to investigate the cytotoxicity of gels on L929, Min6, and HepG2 cell lines as well as glucose uptake experiment on HepG2 cell lines.

2.3. Experimental Section

2.3.1. Materials

Analytical grade reagents were purchased and used without any further purification. Rink amide AM resin (200-400 mesh, 0.8 mmol/g loadings) was bought from Novabiochem. Fmoc-Tyr(tBu)-OH, Fmoc-Trp-OH, Fmoc-His(Trt)-OH, anhydrous N,N'-dimethylformamide (DMF), trifluoroacetic acid (TFA), 2,2'-azino-bis(3-ethylbenzothiazoline-6-sulfonic acid) diammonium salt (ABTS), 2',7'-dichlorodihydrofluorescein diacetate (DCFDA), and (\pm)-6-hydroxy-2,5,7,8-tetramethylchromane-2-carboxylic acid (Trolox) were procured from Sigma-Aldrich. The 1-[bis(dimethylamino)methylene]-1H-1,2,3-triazolo[4,5-b] pyridinium 3-oxide hexafluorophosphate (HATU), N,N-diisopropylethylamine (DIEA), 1,2-ethanedithiol (EDT), triisopropyl silane (TIS), glimepiride, 1,1-diphenyl-2-picrylhydrazyl free radical (DPPH) were purchased from TCI Chemicals, India. Dichloromethane (DCM), dimethyl sulfoxide (DMSO), and HPLC grade acetonitrile, methanol, and isopropyl alcohol were procured from Merck. Diethyl ether and piperidine were bought from Rankem and Spectrochem. Bio-Rad PolyPrep chromatography columns were used for the solid-phase peptide synthesis (SPPS). HPLC grade solvents were utilized for reverse-phase high-pressure liquid chromatography (RP-HPLC). Deionized water (DI, 18.2 M Ω .cm) was obtained from a Milli-Q system and used in all experiments. For cell culture studies, L929, Min6, HepG2 cells were used. L929 cell line was a generous gift from Dr. Durba Pal, Assistant Professor, DBME, IIT Ropar. Min6 and HepG2 cell lines were purchased from NCCS, Pune. RPMI 1640, DMEM, fetal bovine serum (FBS), 0.25% trypsin/EDTA, Penstrep, MTT reagent, 2-[N-(7-nitrobenz-2-oxa-1,3-diazol-4-yl) amino]-2-deoxy-D-glucose (2-NBDG) used in cell culture studies were procured from Thermo Fisher Scientific.

2.3.2. Synthesis of peptides

Fmoc-Tyr-Tyr-NH₂ (YY), Fmoc-Trp-Trp-NH₂ (WW), and Fmoc-Trp-Trp-His-NH₂ (WWH) were synthesized following the protocol reported by our group earlier.³³ Standard 9-fluorenylmethoxycarbonyl (Fmoc)-based SPPS method was employed using the Rink amide AM resin as a solid support. Fmoc-protected amino acids (3 equiv.) were coupled to the resin using a mixture of HATU (2.85 equiv.) and DIEA (5.7 equiv.) in anhydrous DMF for 4 h. After each coupling reaction, the Fmoc group was deprotected by mixing the resin with 20% piperidine in DMF for 50 min at room temperature. Each step was followed by washing the resin with DMF and DCM for 3 times to remove

the unreacted reagents. Finally, the deprotection of side chains and cleavage of peptides from the solid support was performed by using a mixture of TFA:TIS/EDT:water (95:2.5:2.5) for 3.5 h at room temperature. The peptides were precipitated from cold diethyl ether, washed several times, and dried in a vacuum. The purity of crude peptides was determined by RP-HPLC (XBridge BEH C₁₈ column, 250 × 4.6 mm, 5 μm) using acetonitrile/water (50:50) with 0.1% TFA as a mobile phase at a flow rate of 1 mL/min. The peptides were characterized by mass (XEVO G2-XS QTOF) and ¹H NMR (JEOL JNM-ECS NMR, 400 MHz).

2.3.3. Gelation

Self-assembled YY, WW, and WWH (2% w/v) gels were fabricated in DMSO/H₂O in a ratio of 50:50 (v/v) for YY and WW gels, and 30:70 (v/v) for WWH gels. The peptides (2 mg) were dissolved in DMSO and DI water was added to it dropwise. The solution was allowed to stand at 37 °C for 0.5-6 h to form gels. The glimepiride-loaded gels were prepared by adding glimepiride solution (2 mg/mL for dipeptides and 3.33 mg/mL for tripeptide in DMSO) to the peptide solution, followed by the dropwise addition of water. Each gel contained 100 μg of the drug. Minimum gelation concentration (MGC) of peptides was also determined using different quantity of peptides (0.5, 1, 1.5, and 2 mg).

2.3.4. Morphology of gels

The morphologies of all gels (YY, WW, and WWH) were investigated by scanning electron microscopy (SEM). The gels (without and with drug) were prepared on metal stubs, dried for 24 h under vacuum, and coated with platinum by sputtering. Micrographs were recorded using a JEOL JSM-6610LV microscope with a tungsten filament at an accelerating voltage of 10 kV.

2.3.5. Spectroscopic studies

The following spectroscopic studies were performed.

Circular dichroism (CD). Peptide solutions (0.1 mM) were prepared in acetonitrile/water and CD spectra were acquired using JASCO J-1500 circular dichroism spectrophotometer in the range of 200-300 nm at a continuous scanning rate of 200 nm/min.

Fourier transform infrared (FTIR). FTIR spectra of peptides were recorded in the ATR mode (Bruker Tensor 27) between 400-4000 cm⁻¹.

Thioflavin-T (ThT) binding assay. ThT assay was performed as reported earlier, with slight modifications.³⁴ A stock solution was prepared by dissolving ThT (8 mg) in DI water (10 mL) and filtering through a 0.2 μm syringe filter. A 1 mL of this stock solution was taken and diluted to 50 mL with water to prepare the working solution. To 100 μL of each sample (gels and drug-loaded gels), 900 μL of the working solution of ThT was added and incubated for 6 h at room temperature. Tecan multimode microplate reader was used to record the fluorescence spectra from 450 to 600 nm at an excitation wavelength of 440 nm to measure the binding of ThT to the secondary structure of peptides. ThT solution without peptide was considered as a blank.

2.3.6. Zeta potential

Zeta potential of the peptide solutions (1 mM) of pH 5, 6 and 7.4 were measured using a Particle-Matrix zeta sizer. The effect of pH on the ionization of peptides was also determined.

2.3.7. Rheology

Viscoelastic properties of the peptide gels were investigated by rheometer (Anton Paar MCR 102) with a 25 mm parallel-plate configuration. The gels with and without the drug (2% w/v, 200 μ L) were prepared and kept at 37 °C for overnight. All measurements were carried out at room temperature with a shear gap of 0.3 mm. Liquid paraffin was added around the plate to restrict the evaporation of water during measurements. An amplitude sweep test was conducted at a constant frequency of 10 rad/s with a varying strain of 0.01 to 100% to determine the linear viscoelastic range (LVR) of gels. Frequency sweep study was carried out at a constant amplitude of 1% and angular frequency was varied from 0.1 to 100 rad/s. Self-healing properties of gels were determined by applying six alternative cycles of extreme (30%) and mild strain (0.1%) at a constant angular frequency of 10 rad/s.

2.3.8. Swelling and degradation

The peptide gels (2% w/v, 100 μ L, free and drug-loaded) were formed using the method mentioned earlier and immersed in a buffer solution (1 mL) of pH 5 (acetate), 6, and 7.4 (phosphate). Next, the gels were incubated at 37 °C with constant shaking at 100 rpm and media was withdrawn after each time interval, blotted carefully, and weighed. The amounts of media absorbed by the gel was calculated gravimetrically and expressed in terms of swelling percentage using **Equation 2.1** below:

$$\% \text{ Swelling/Degradation} = \frac{W_t - W_i}{W_i} \times 100 \quad \text{Equation 2.1}$$

where, W_t is the weight of swollen gel at time t and W_i is the initial weight.

2.3.9. Drug release

The drug-loaded (glimepiride) peptide gels (2% w/v) were used to measure the in vitro drug release at acidic (pH 5 and 6) and neutral (pH 7.4) pH. Peptide gels were washed initially with buffer to remove any loosely bound drug. The release media (1 mL, acetate buffer of pH 5, and phosphate buffers of pH 6 and 7.4) was added to gels and incubated at 37 °C with a constant shaking rate of 100 rpm. The release media was completely aspirated and replenished with the same amount of fresh buffer at each time interval for 28 days. The amount of released drug in the media was quantified by HPLC against a standard curve of glimepiride, and the drug was detected by measuring the absorbance at 231 nm.

2.3.10. Antioxidant properties

The antioxidant properties of the peptides and gels were assessed by ABTS and DPPH assays.

ABTS assay. The experiment was carried out using a method reported earlier with few modifications.³⁵ ABTS (7 mM) was dissolved in water and mixed with an equal volume of potassium persulfate (2.45 mM). The mixture was kept at room temperature for 12 h in the dark to generate ABTS^{•+}. Next, the radical solution was diluted with PBS of pH 7.4 and the absorbance was adjusted to 0.8 at 734 nm. A

200 μL of this diluted ABTS^{•+} solution was added to 100 μL of samples (peptides and gels) and incubated at 37 °C in dark for 1 h. Thereafter, 100 μL of the solution was removed and absorbance was measured at 734 nm using a plate reader. An equivalent volume of PBS without sample was taken as a blank and ABTS radical without sample was considered as a control. Ascorbic acid (1 mg/mL) was used as a standard antioxidant for comparison. The ABTS radical scavenging potential of the materials was calculated using the **Equation 2.2**:

$$\% \text{ Radical Scavenging Effect} = \frac{A_c - A_s}{A_c} \times 100 \quad \text{Equation 2.2}$$

where, A_c is the absorbance of the control and A_s is the absorbance of the sample.

DPPH assay. The scavenging capability of peptides and gels against 1'-diphenyl-2-picrylhydrazyl (DPPH) radicals were investigated.³⁶ The sample (100 μL) was immersed in the solution of DPPH (200 μL , 0.1 mM) in methanol and incubated at 37 °C for 2 h in dark. The absorbance of the solution was measured at 517 nm and DPPH radical scavenging activity was calculated using **Equation 2.2**. DPPH solution without sample was taken as a control and Trolox (25 μM) was used as a standard antioxidant for comparison. IC₅₀ values of all peptides were evaluated to estimate the DPPH scavenging capacity. Different quantity of peptides, ranging from 0.05-2 mg, were used and they were incubated with DPPH solution as mentioned earlier.

2.3.11. Cell viability

The viabilities of murine fibroblast (L929), mouse pancreatic beta (Min6), and human liver carcinoma (HepG2) cell lines in the presence of peptides and gels were evaluated by MTT assay with slight modifications.^{33,37} L929 was cultured in RPMI medium, supplemented with 10% fetal bovine serum (FBS) and 1% antibiotic. Min6 was cultured in high glucose Dulbecco's Modified Eagle Medium (DMEM) containing 15% fetal bovine serum, 1% antibiotic, and 50 μM of β -mercaptoethanol, and HepG2 in DMEM with 10% FBS and 1% antibiotic solution. All cell lines were incubated at 37 °C in a humidified environment containing 5% CO₂. Cells were maintained by passaging at regular intervals till they reached 75-80% confluency. Peptides and gels (2% w/v, freeze-dried) were fabricated as described earlier and sterilized by exposing under UV for 30 min. They were immersed in complete media (RPMI/DMEM) for 24 h at 37 °C, and the media were filtered using a 0.2 μm syringe filter to remove particles. Meanwhile, cells were seeded in treated 96 well plates with a seeding density of 10⁴ cells/well. After 24 h of incubation, the medium was replenished with sample extracts (200 μL /well) and the cells were again incubated at 37 °C in a humidified environment containing 5% CO₂. The sample was incubated for 24 and 48 h. The cells incubated with the complete medium without sample extracts were considered as a positive control. Following incubation, MTT solution (20 μL , 5 mg/mL in PBS) was added to each well and incubated for 3.5 h. After that, the medium with MTT solution was carefully withdrawn and 100 μL of DMSO was added into each well followed by gentle shaking of plate for 15 min at room temperature to dissolve the formazan crystals. The absorbance was measured at 570 nm

using a plate reader. Cell viability was measured by the ratio of absolute absorbance of cells incubated with the extracts of peptide gels to that of the cells incubated with the culture medium only.

2.3.12. Live-dead staining

The cytotoxicity of peptide gels was observed using live/dead staining (LIVE/DEAD Cell Imaging Kit, Molecular Probes) according to the manufacturer's protocol. After sterilization of samples, extracts were collected as mentioned earlier. L929 and Min6 cells were seeded in a 48 well plate at an initial density of 2×10^4 cells/well and incubated at 37 °C in a humidified environment containing 5% CO₂ for 24 h. Following incubation, culture media was replaced with extracts from peptides and gels and incubated again for 24 h. A 150 µL solution containing calcein AM and ethidium bromide dissolved in PBS (pH 7.4) was added, followed by 30 min of incubation. A fluorescence microscope was used to image the live and dead cells.

2.3.13. ROS scavenging assay

The oxidant-sensitive fluorescent probe, H₂-DCFDA, was used to determine the intracellular reactive oxygen species (ROS) level in living cells.³⁸ HepG2 (1×10^4) cells were incubated in Nunc-coated 96 well black plates at 37 °C in a humidified environment containing 5% CO₂. Following 24 h of incubation, media was removed and 100 µL of sample extracts (samples with incomplete media for 24 h and syringe filtered) were added to each well and incubated for 24 h. The cells were exposed to 0.5 mM of H₂O₂ to induce ROS production and then incubated with 2',7'-dichlorofluorescein diacetate (DCFDA) at a concentration of 25 µM in dark for 45 min. Media was withdrawn and PBS was added. Finally, fluorescence intensities were determined at an emission wavelength of 530 nm using an excitation wavelength of 485 nm, on a plate reader. Cells without sample extract were taken as a control. Ascorbic acid (1mg/mL) was treated as a positive control.

2.3.14. Glucose uptake assay

Glucose-stimulated insulin secretion from pancreatic β-cells (Min6) was determined by treating the cells with the drug release media (pH 5, 6, and 7.4) and the free drug.^{39,40} The supernatant released by the cells was collected and added to HepG2 cells for the glucose uptake study in the presence of insulin secreted by pancreatic β-cells. Min6 cells were seeded in 24-well plates at a density of 5×10^4 cells/well. After 48 h, media was aspirated and cells were incubated with the drug release media of pH 5, 6 and 7.4 along with the incomplete DMEM containing 4.5 g/L of D-glucose for 12 h to initiate the glucose-stimulated insulin secretion. Uptake of fluorescently labelled glucose, 2-NBDG, by HepG2 cells was performed as described earlier in literature.⁴¹ The HepG2 cells were seeded at a density of 10^4 cells/well in Nunc-coated 96 well black plates at 37 °C in a humidified environment containing 5% CO₂. Following 24 h of incubation, media was removed and cells were washed with DPBS and starved with glucose-free DMEM for 4 h. The supernatant collected from Min6 cells was added to each well and incubated for 40 min. A 100 nM insulin solution was considered as a positive control and cells without external insulin or secretory media were considered as a negative control. The 2-NBDG (50 µM in incomplete

glucose-free DMEM) was added to each well followed by the incubation for 20 min at 37 °C. The cells were washed and the fluorescence intensity of cells containing 2-NBDG was measured immediately at 535 nm using a microplate reader and an excitation wavelength of 485 nm.^{41–43} The cells were also imaged under a fluorescence microscope to confirm the 2-NBDG uptake using the FITC channel.

2.3.15. Statistical analysis

All experiments were performed in triplicates. Comparisons between two groups were carried out using Student's t-test. The results were presented as mean \pm SD. $p < 0.05$ was considered statistically significant.

2.4. Results and discussion

The objective of this work was to develop pH-sensitive, self-assembled, injectable peptide gels with potent antioxidant properties, which can physically encapsulate glimepiride, an antidiabetic drug, and subsequently release it in a sustained manner in diabetic patients to overcome the side effects of this drug, such as hypoglycemia (**Figure 2.1**). We have focused on short peptide sequences where the N-terminus is capped with an aromatic moiety, Fmoc, which is expected to reinforce intermolecular interactions through π - π stacking and promote self-assembly and gelation in the peptide sequence.



Figure 2.1. A pH-sensitive, self-assembled peptide gel for the delivery of glimepiride, an anti-diabetic drug.

We have focused our attention on the selection of hydrophobic amino acids, such as tyrosine and tryptophan, which are expected to produce intermolecular as well as intramolecular hydrophobic interactions with the Fmoc group, resulting in self-assembling of the ultra-short peptide sequence into supramolecular gels. We also included histidine, as it is expected to make the gel pH- sensitive.^{44,45} The charged state of the amino acids is expected to be controlled by the pH of the medium and affect the

molecular interactions, thus directing the formation or breaking of self-assembly.⁴⁶ Based on these considerations, we developed gels from the following peptides: Fmoc-Tyr-Tyr-NH₂ (YY), Fmoc-Trp-Trp-NH₂ (WW), and Fmoc-Trp-Trp-His-NH₂ (WWH).

2.4.1. Peptides

Using the Fmoc-based SPPS procedures, we synthesized and characterized two dipeptides, YY and WW, and a tripeptide, WWH, to increase drug release from gels at acidic pH (**Figure 2.2A-C**). RP-HPLC analysis of all peptides revealed greater than 95% purity (**Figure A1, Appendix**). Retention times were determined to be 6.1, 15.7, and 5.7 min for YY, WW, and WWH, respectively. Due to the inclusion of the polar amino acid histidine in WWH, the hydrophobicity of WW was reduced compared to YY. Inferred from mass spectrometry, the observed molecular weights of peptides matched the calculated molecular weights (**Figure A2-A4, Appendix**). The ¹H NMR spectra of the peptides with the assigned peaks are provided in **Figure A5-A7, Appendix**.

2.4.2. Self-assembled gel

The peptides (2% w/v) were self-assembled into gels using aq. DMSO and glimepiride was encapsulated into it (**Figure 2.2D**). In 50% aq. DMSO at 37 °C, the YY and WW formed opaque gels in 30 min but the WWH formed transparent gel in 6 h under comparable conditions (**Figure 2.2E-G**). For each peptide, the minimal gelation concentrations (MGC) were calculated. At 1% (w/v), no gels were formed. When the concentration was raised to 1.5% (w/v), the self-assembly process began, and gels began to form, although they were unstable (**Figure A8, Appendix**).

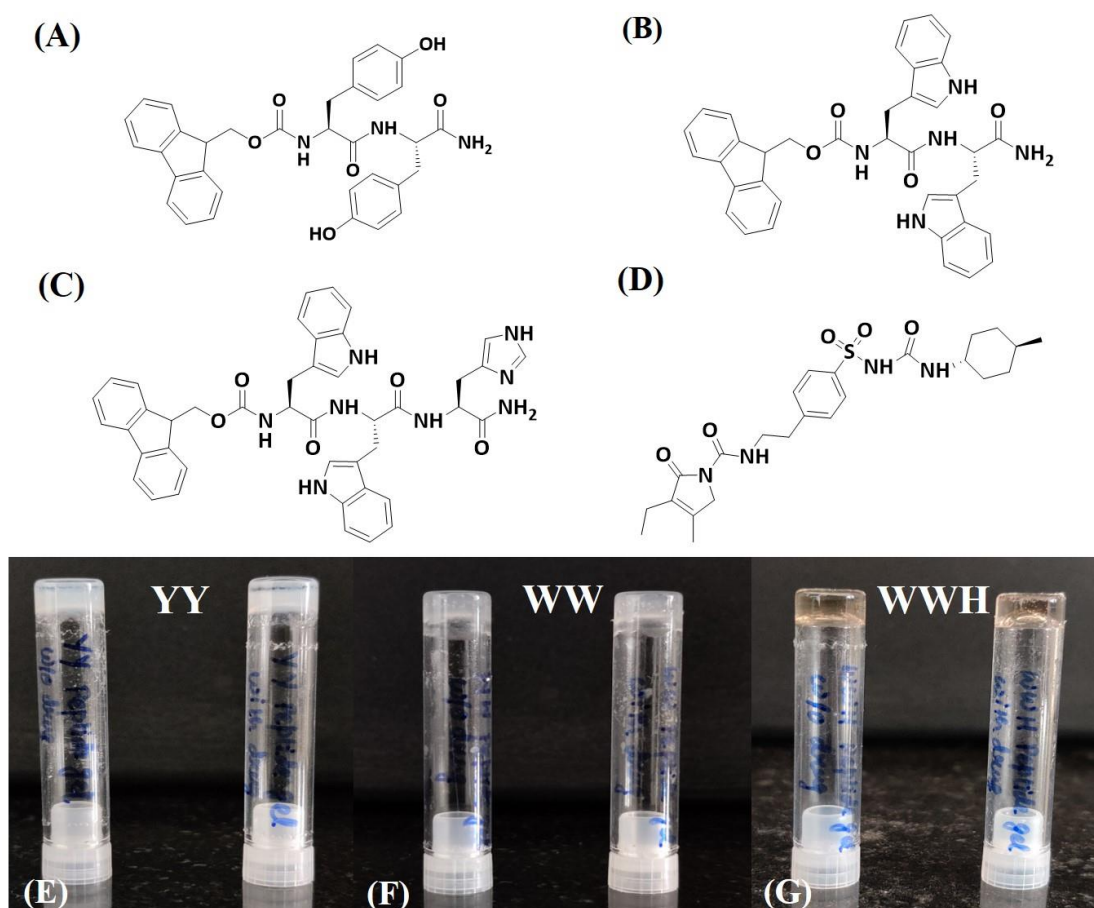


Figure 2.2. Structures of peptides used to form self-assembled gels and glimepiride. (A) Fmoc-Tyr-Tyr-NH₂ (YY). (B) Fmoc-Trp-Trp-NH₂ (WW). (C) Fmoc-Trp-Trp-His-NH₂ (WWH). (D) Glimepiride. (E-G) Images of free and drug-loaded peptide gels (2% w/v).

Scanning electron microscope (SEM) was used to study the morphology of gels, and the results showed that they had a porous matrix-like morphology (**Figure 2.3A-C**). Pores were seen in the WW and WWH gels, whereas the YY gel showed entangled networks with tiny pores. The porous and entangled network morphology of gels was not disrupted after encapsulation of drug, which confirms no interference exerted by the drug on their morphological characteristics (**Figure A9, Appendix**).

2.4.3. Secondary structures of peptides

Intermolecular interactions that provide information regarding the formation of secondary structure were investigated to better understand the mechanism of peptide self-assembly. The primary use of circular dichroism (CD) is the analysis of peptide secondary structures. Signals from the π - π system primarily affect the CD spectrum because of their high extinction coefficient and associated π - π coupling. A large negative peak at 200–220 nm, which corresponds to an anti-parallel β -sheet structure, was present in the dipeptides (YY and WW), whereas, WWH exhibited random coil like structure.²⁷ Local peaks at 235 nm demonstrated amino acid side chain stacking (**Figure 2.3D**).

To identify the H-bonding connections that peptides form, FTIR spectroscopy was employed. The amide I peak is mainly used for the identification of stretching vibrations attributable to C=O, which can quickly identify the formation of a sheet-like structure via hydrogen bonding (**Figure A10, Appendix**). The amide I area corresponds to peaks at 1620-1690 cm^{-1} , indicating the presence of sheet-like structures.^{47,48} The characteristic β -sheet structure was confirmed by assigning the amide II (1480-1575 cm^{-1}) and III (1229-1301 cm^{-1}) peaks due to the bending motion of the N-H coupled to C-N stretching.⁴⁹ It is very difficult to conclusively state the secondary structure of such extremely short peptides since the peaks representing amide I are not so prominent and the π -stacking effects can possibly obscure the underlying beta-sheet secondary structure.

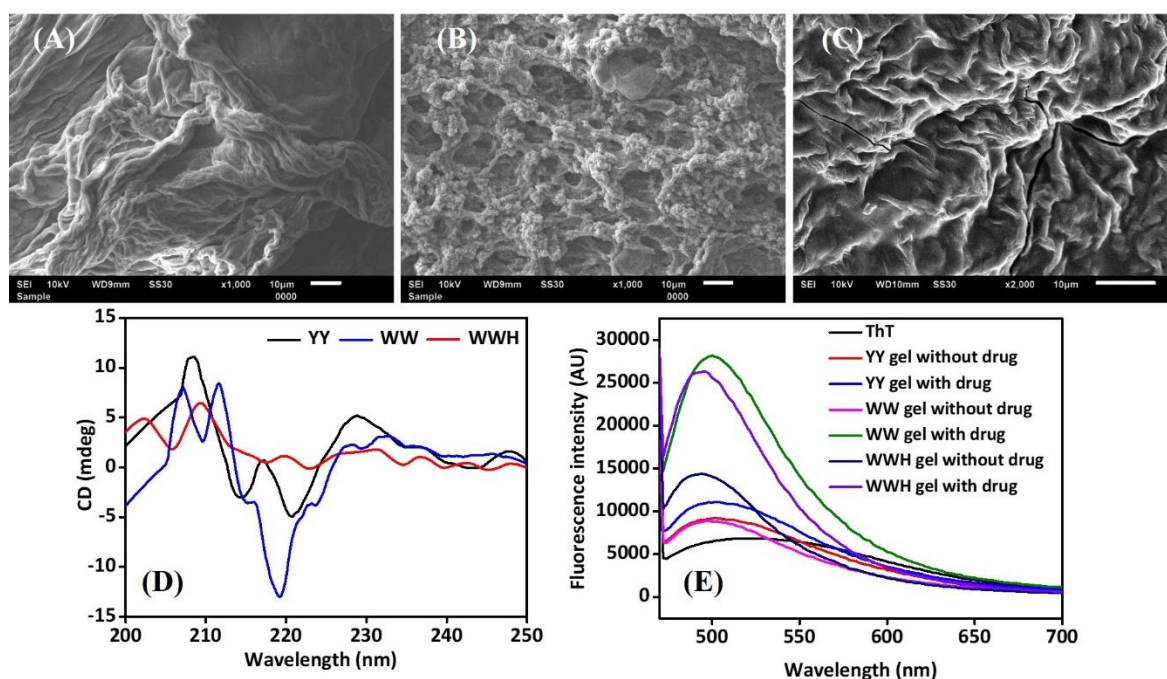


Figure 2.3. (A-C) Scanning electron microscopy (SEM) images of dried peptide gels (2% w/v). (A) YY. (B) WW. (C) WWH. Scale bar 10 μm . (D, E) Secondary structures formed by peptides/gels. (D) CD spectra. (E) Thioflavin T assay.

The sheet-like structures were further confirmed using the thioflavin-T (ThT) assay. ThT binds to the hydrophobic areas of the peptide, increasing its fluorescence intensity compared to unbound ThT.^{34,50,51} In our case, the presence of β -sheet like structures considerably boosted the fluorescence intensity of ThT in drug-loaded gels compared to unloaded gels (**Figure 2.3E**). In case of drug-loaded WW gel, the β -sheet structure is more prominent as it exhibited the highest fluorescence intensity in ThT assay.

2.4.4. Viscoelastic properties

Another aspect of the gel that is impacted by the peptide-based self-assembled structure is its mechanical strength. Using a parallel plate geometry and a rheometer at 37 $^{\circ}\text{C}$, the rheological behavior of gels made from YY, WW, and WWH was investigated. To measure the storage modulus (G') and loss modulus (G'') of gels as a function of strain, angular frequency, and time, dynamic oscillatory

experiments were carried out. The storage modulus was greater than the loss modulus, indicating that all gels exhibited a mostly elastic behavior. Due to the greater hydrophobic contacts induced by the aromatic amino acids, tyrosine, and tryptophan, the YY and WW gels were relatively stiff, with the storage modulus ranging from 4-5 kPa at a frequency of 10 rad/s (**Figure 2.4A-F**). High mechanical rigidity gives biomaterials strength but it also slows down their rate of degradation, which is partially necessary for drug delivery.⁵² To reduce stiffness and increase disintegration at acidic pH, we added a third hydrophilic amino acid, histidine, to the WW sequence at the C terminus. The storage modulus (92.93 Pa) of the WWH gel significantly decreased over time with constant frequency, which can be attributed to the fact that the peptide became amphiphilic in nature and the hydrophobic interactions were hindered by the presence of histidine residue. The pH of the gel was found to be around 6.2, which can protonate the imidazole ring of the histidine residue, causing the ionic repulsion during the self-assembly process. It can reduce the strength of the gel, thus lowering the storage modulus as compared to the other two gels (YY and WW). The storage modulus of this gel (WWH) was roughly equivalent to the storage modulus of $K_2(SL)_3SA(SL)_2K_2$ and $K_2(SL)_2(SA)_2(SL)_2K_2$ gels reported by Li *et al.*⁵³ The data is also comparable with the storage modulus of short peptide gels (WLVEFFK)²⁶ used for the sustained release of antitumor, antimicrobial, and protein molecules, and two-component co-assembled peptide gels reported by Rosa *et al.*⁵⁴ This gel is better than the supramolecular hydrogel of RGD-derived peptide conjugate used for the pH-responsive drug delivery.⁵⁵ After glimepiride was encapsulated in gels, the storage and loss modulus of the gels increased, providing further evidence that the drug participates in the self-assembly process by taking part in hydrophobic and hydrogen bonding interactions.

Self-healing feature is advantageous for injectable gels, which are used to encapsulate cargoes like biomolecules, cells, or medications and delivering them to the systemic circulation.⁵⁶ The self-healing properties of gels was also evaluated by subjecting the gels to alternating cycles of high (30%) and mild strain (1%) at a constant frequency. After the high strain was removed, gels were able to regain their storage modulus (**Figure 2.4G-I**). We loaded and extruded the gel into syringes in order to assess its injectability. The WWH gel's thixotropic feature was demonstrated by its ability to extrude out of the syringe while maintaining its gel-like state (**Figure A11, Appendix**).

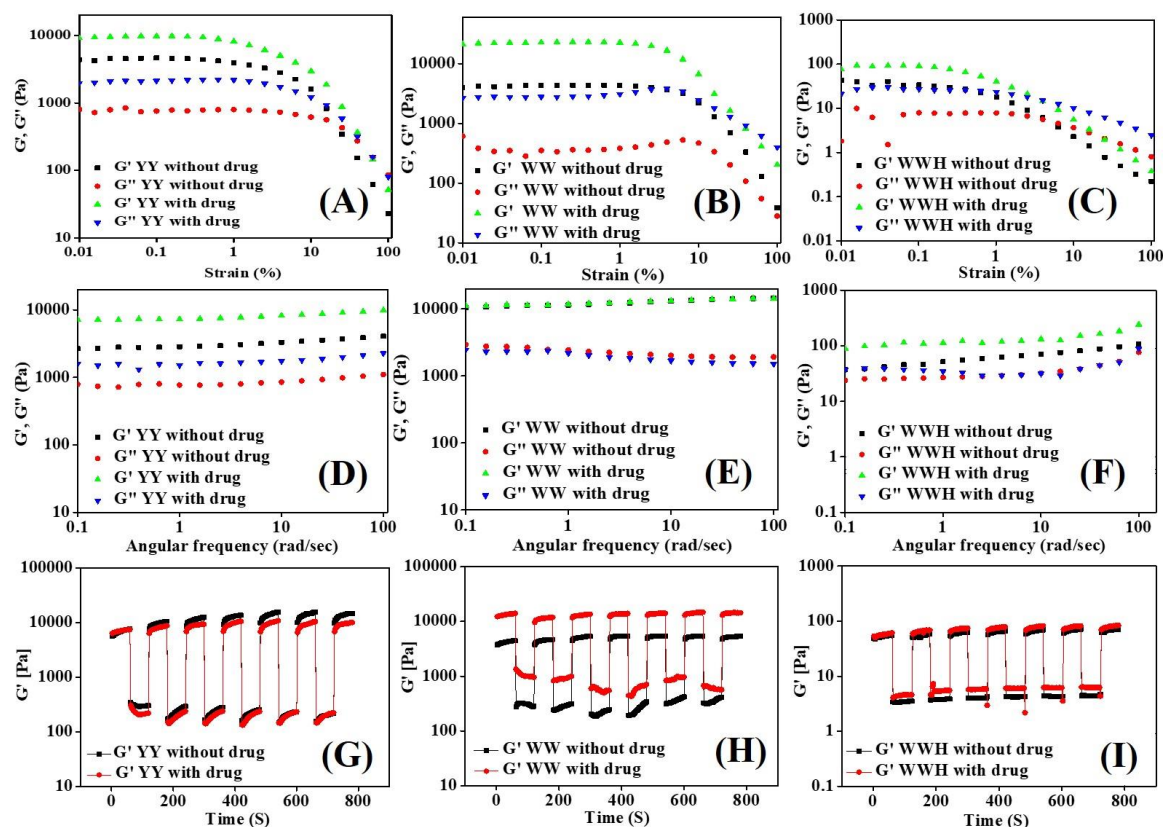


Figure 2.4. Rheological properties of peptide gels, YY, WW, and WWH (2% w/v) with and without drug. (A-C) Amplitude sweep studies exhibiting storage and loss modulus of gels and corresponding crossover values at a constant angular frequency of 10 rad/s. (D-F) Frequency sweep of peptide gels at a constant strain of 1%. (G-I) The storage modulus of gels at alternating strains of 30% and 1% for 6 cycles.

2.4.5. In-vitro drug release

In order to evaluate the acid sensitivity of peptide gels, they were exposed to a wide range of pH (5, 6, and 7.4). The pH value decreased to roughly 5 in hyperglycemic situations as a result of accumulating gluconic acid produced by the enzymatic conversion of glucose, according to Fu et al.'s^{4,15} findings on the relationship between pH and glucose concentration. The pH-dependent swelling and degradation patterns of gels were examined to assess the impact of pH on the dissociation of peptide gels (**Figure A12, Appendix**). The degradation rates of YY and WW gels were higher at pH 7.4 than pH 5 and 6, and the WWH gel exhibited higher degradation at acidic pH 5. This phenomenon could be attributed to the protonation of the imidazole ring of histidine residue in mildly acidic condition, which interrupts the self-assembling process and disintegrate the gels.^{55,57}

We have investigated the release of glimepiride in the drug delivery experiment using release media with three distinct pH values: 5, 6, and 7.4 to simulate healthy tissues and glucose concentrations in diabetic circumstances, respectively. The gels were fully submerged in one of the buffers (1 mL) and incubated at 37 °C while being constantly shaken. At certain intervals, the release media was removed and replaced with new media. RP-HPLC was used to measure the drug content in the release media

using the standard curve of glimepiride (**Figure A13, Appendix**). The WWH gel provided a higher drug release at acidic pH, which is far better than the previously reported materials used for glimepiride delivery in terms of pH-responsiveness and sustained release profiles, as shown by the plotting of cumulative release against time. Only 30% of the drug from the YY gel was released at pH 5, 70% at pH 6, and 95% at pH 7.4 over the course of 7 days (**Figure 2.5A**). In contrast, 36% of the drug in the WW gel was released at pH 5, and 56% and 75% were simultaneously released at pH 6 and 7.4 (**Figure 2.5B**). The WWH gel provided 96.9, 77.4 and 62.37% of the medication at pH 5, 6, and 7.4 in 28 days and showed a stronger pH-responsive release (**Figure 2.5C**). The slower disintegration of gels may be the cause of the lower release rates. The initial burst release of the drug is influenced by its presence at or near the gel-solvent interface and the subsequent slower release of the drug is caused by the drug being embedded in the gel matrix and having to diffuse out to the gel surface through the mesh. The pK_a values of the side chains, which are 10.6 and 16.9 for Y and W, can be used to explain the distinctive releasing behavior of peptide gels.⁵⁸ We propose that tyrosine and tryptophan are uncharged below the pK_a value, specifically at acidic pH but start to get charged when the pH rises. Zeta potential measurements of YY and WW, which were -13.9 and -34.93 mV at pH 7.4, served as the confirmation. On the other hand, the pK_a of histidine being 6.0 and the zeta potential of WWH was found to be 32.03, 12.98, and 7.5 mV at pH 5, 6, and 7.4, respectively, indicating that at low pH, the imidazole ring of histidine gets protonated, generating electrostatic repulsion that causes the self-assembly to breakdown and release the medication.

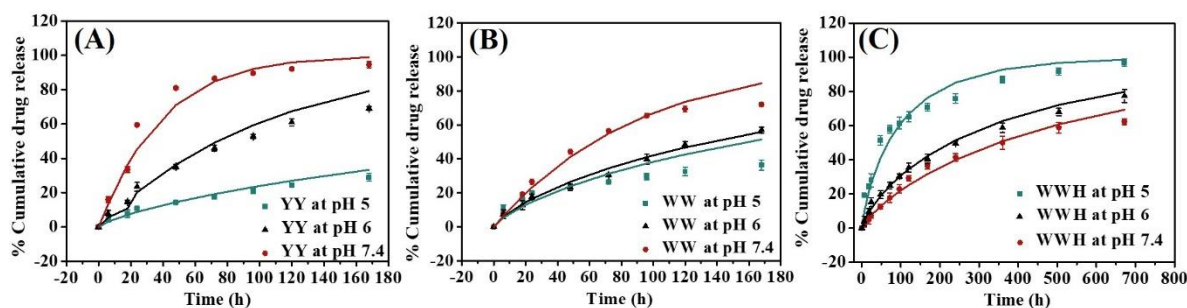


Figure 2.5. Percentage cumulative release of glimepiride (0.1 mg) from peptide gels (2% w/v) at pH 5, 6, and 7.4. (A) YY. (B) WW. (C) WWH.

In order to better understand the process of release, many kinetic models were used to match the release data. It was found that the Weibull model, which is regarded as one of the most suited models for protracted drug release matrices, best fits the release data.⁵⁹ It has been determined that the exponent b in the Weibull equation has a value in the range of 0.75 to 0.88, which shows that both a Fickian diffusion and the case II transport technique are involved in the mechanism of glimepiride release from the gel matrix. Additionally, the swelling and degradation of the gel matrix regulate drug release.

2.4.6. Antioxidant properties

Even at a concentration of 2%, all peptides, and free and drug-loaded gels displayed strong antioxidant activities (>90%) within 1 hour of incubation with ABTS^{•+} solution (**Figure 2.6A**).

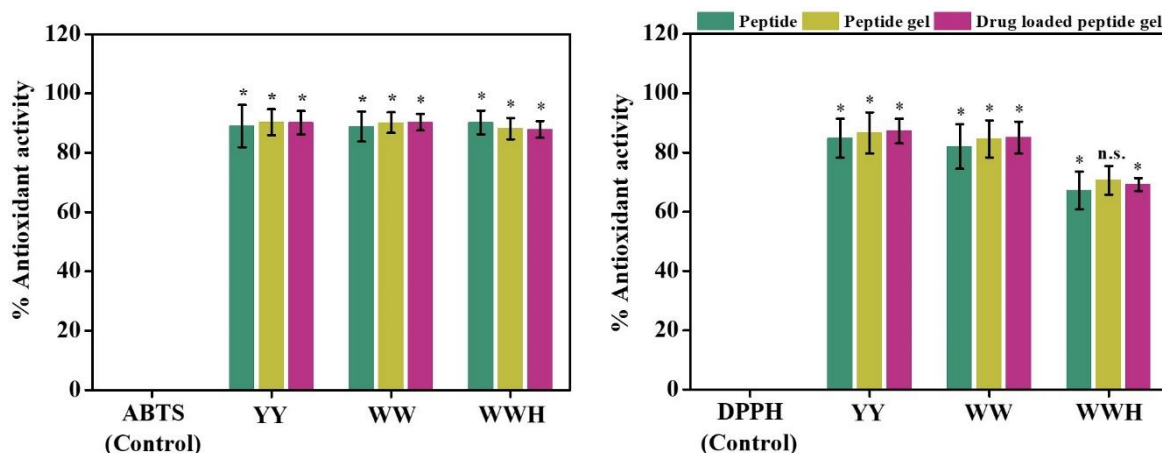


Figure 2.6. Antioxidant activities of peptides and peptide gels (unloaded and drug-loaded). (A) ABTS assay. (B) DPPH assay. ABTS and DPPH refers to negative control (radicals without sample) and Ascorbic acid and Trolox are used as positive control. Data reported are mean \pm SE (n = 3). Comparisons between two groups (samples to control) were carried out using Student's t-test. *p < 0.05 indicates statistically significant data.

The presence of histidine and the glimepiride had no negative impact on the antioxidant qualities. The activities were equivalent to or superior to ascorbic acid (1 mg/mL), which was considered as a positive control, whereas ABTS^{•+} was the negative control, where no sample was used. A DPPH assay was also performed and the results showed that, in comparison to the ABTS assay, the scavenging capabilities of gels against DPPH were a bit lower. After 2 h of incubation, the YY and WW gels showed 85% DPPH· scavenging capacity but the WWH gel only displayed about 70% activity (**Figure 2.6B**). The radical scavenging capacities were equivalent to the positive control, and Trolox (25 M) and DPPH· were regarded as negative controls. The antioxidant potential of peptide gels is significantly higher than the antioxidant activities of peptides and peptide gels reported by Wei *et al.*, Samaei *et al.*, and Hussain *et al.*, which were respectively 80%, 85%, and 71%.^{60–62}

2.4.7. Cell viabilities

The cell viabilities of the peptides and gels (both free and drug-loaded) were analyzed by MTT assay on different cell lines, such as mouse fibroblast (L929), mouse pancreatic beta (Min6), and human liver cancer (HepG2). The cell viability of L929 cells was between 90% and 120%, as can be seen in **Figure 2.7**. The metabolic activity of Min6 and HepG2 cells could be maintained, and they displayed viabilities of 95–116% and 110–140%, respectively. Images of L929 and Min6 cells after being exposed to peptides and gels (both free and drug-loaded) revealed that the cells were alive and widely distributed. No discernible alterations in cellular morphology were seen following the treatment for 24 h (**Figure A14, Appendix**). The live/dead experiment has further confirmed the cytocompatibility of peptides and gels (both free and drug-loaded) (**Figure A15, Appendix**). L929 and Min6 cells were cultivated in extract

media made from samples for 24 and 48 h. Cell viability was then examined under a fluorescence microscope. The morphology of the cells was always retained, and the presence of live cells was shown by the dominance of green color in both the control and test samples (**Figure 2.8**). The viability of all cell lines was unaffected by drug encapsulation in peptide gels.

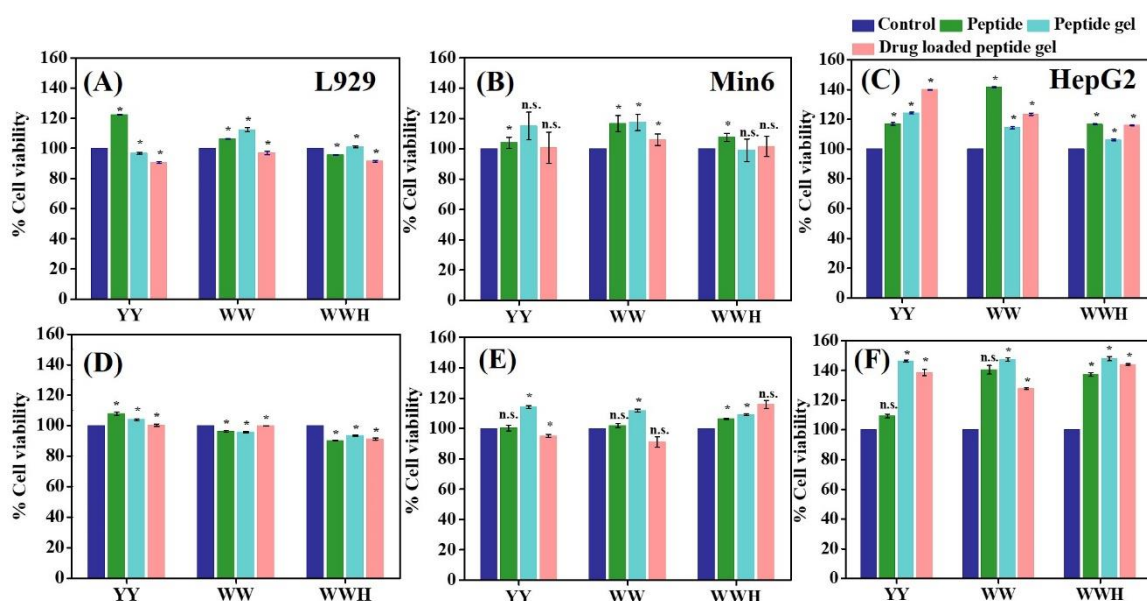


Figure 2.7. Evaluation of cell viabilities by MTT assay after exposure to peptides and gel extracts for 24 and 48 h. (A, D) L929. (B, E) Min6. (C, F) HepG2. Data reported are mean \pm SE ($n = 3$). Comparisons between two groups (samples to control) were carried out using Student's t-test. * $p < 0.05$ indicates statistically significant data.

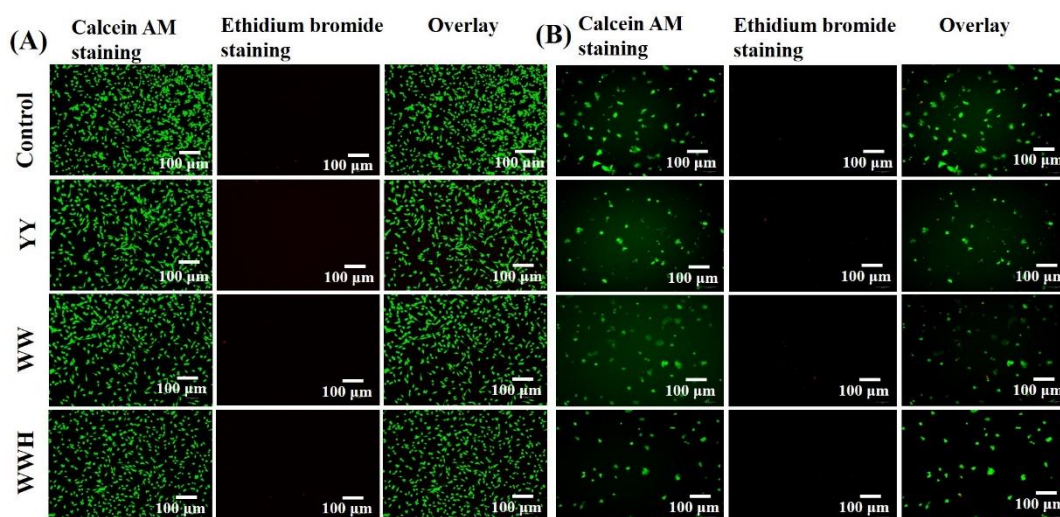


Figure 2.8. Live/dead assay of cells treated with glimepiride-loaded peptide gel (YY, YYW, and WWH, 2% w/v) releasates. (A) L929. (B) Min6. Scale bar: 100 μm . Fluorescence images of live and dead cells stained with calcein AM and ethidium bromide were acquired after 24 h of treatment. Cells without gels were considered as a control.

2.4.8. Reactive oxygen species (ROS) scavenging

To reduce intracellular ROS activity, we fabricated gels using naturally antioxidant amino acids. H_2O_2 (0.5 mM) was used in this work to cause oxidative stress in HepG2 cells and 2',7'-dichlorofluorescein diacetate (DCFDA) was used to evaluate the ROS scavenging capacity of the peptide gels. The 2',7'-dichlorofluorescein was generated upon oxidation by ROS and the intracellular level of ROS was visualized by fluorescence microscopy.³⁸ The formation of intracellular ROS was successfully inhibited by the addition of antioxidant peptides and peptide gels, resulting in a low fluorescence intensity (**Figure 2.9A**). When compared to controls, the fluorescence intensity of samples with cells exposed to only H_2O_2 was practically halved. Drug incorporation had no effect on fluorescence intensity, demonstrating that it lacks an innate capacity to scavenge free radicals.

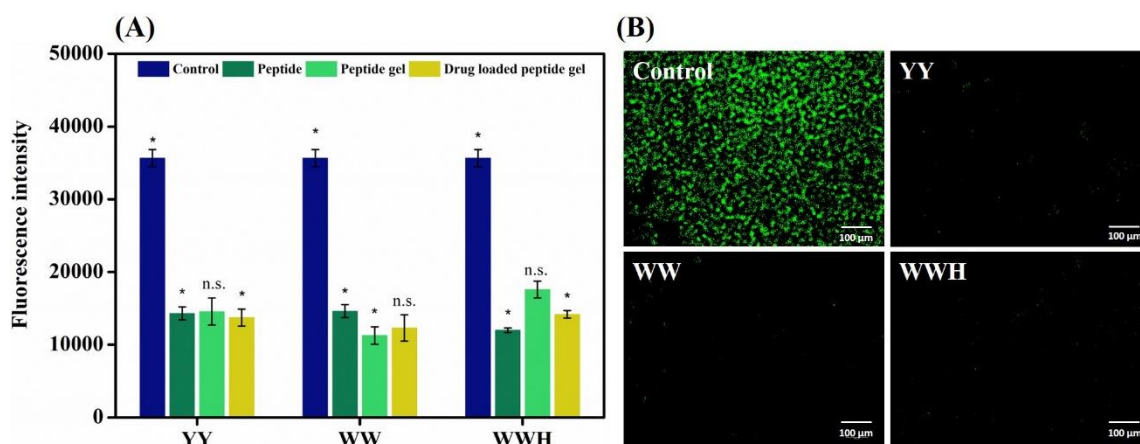


Figure 2.9. Effect of releasates of peptides and peptide gels (free and drug-loaded) on reactive oxygen species (ROS) in HepG2 cells. (A) Fluorescence intensity of cells incubated with DCFDA. (B) Images of cells treated with drug-loaded peptide gels, YY, WW, WWH, and then DCFDA. Control is cells treated with H_2O_2 only. Data reported are mean \pm SE ($n = 3$). Comparisons between two groups (samples with control) were carried out using Student's t-test. * $p < 0.05$ indicates statistically significant data.

Fluorescence microscopy images were acquired and a lot of green fluorescence in the control group denoted higher levels of ROS formation in the cells (**Figure 2.9B**). HepG2 cells displayed very little green signal after being treated with peptide gel releasates, confirming the ability of peptides and gels to scavenge intracellular free radicals. The cytotoxicity of the samples in the presence of H_2O_2 was assessed using the MTT assay, which revealed that peptide gels reduced the effects of oxidative stress, lowered cell mortality, and improved the ability of HepG2 cells to survive in the presence of H_2O_2 (**Figure A16, Appendix**). Therefore, peptide gels reduced the ROS levels in diabetes patients in addition to releasing the drug in a pH-sensitive manner.

2.4.9. Glucose uptake study

Glucose uptake studies were conducted on HepG2 cells to assess the efficacy of the drug delivery vehicle to release the cargo in its active form. We chose Min6 cell line for glucose-stimulated insulin secretion by glimepiride and HepG2 cells to study the uptake of fluorescent labelled analog of glucose (2-

NBDG).⁴¹ HepG2 cells tend to absorb glucose in the presence of insulin (100 nM, positive control), which accounts for the greater fluorescence intensity compared to the negative control, where insulin is absent. Additionally, glimepiride (0.1 mg/mL) stimulated the insulin secretion in Min6 cells, thus, increasing the fluorescence intensity (**Figure A17, Appendix**).⁴⁰ Since the drug release profile at acidic media was enhanced compared to neutral pH, which was maintained for up to 28 days, the drug release media also showed increased uptake of glucose in acidic media (pH 5 and 6) (**Figure 2.10A**). The efficacy of drug release media to stimulate glucose uptake was further confirmed using fluorescence microscopy images by visualizing the intracellular localization of fluorescent probe, 2-NBDG. Strong green signals validated the pH-responsive increased absorption of 2-NBDG in cells treated with pH 5 and 6 extracts, showing a better release profile of gels in a slightly acidic media (**Figure 2.10B-E**).

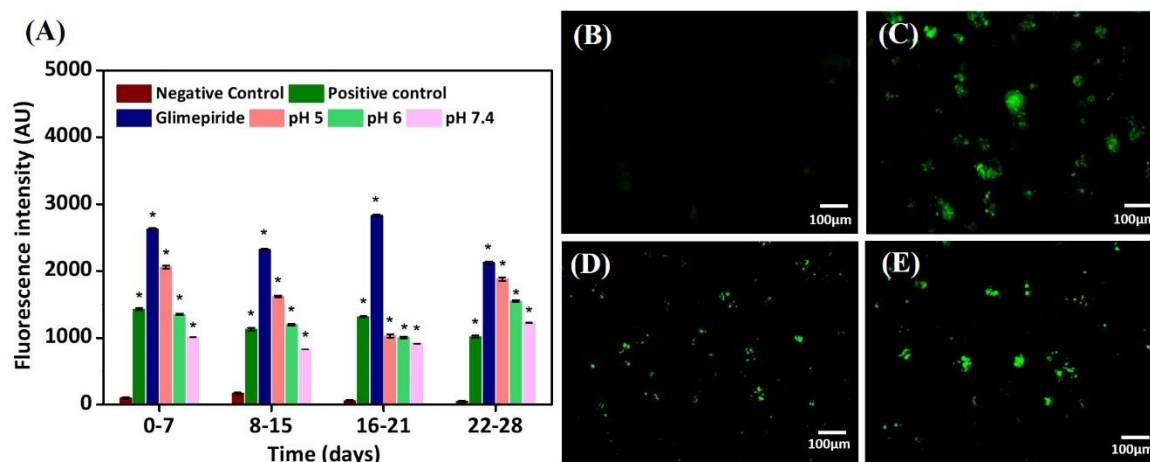


Figure 2.10. Glucose uptake of HepG2 cells treated with releasates of glimepiride-loaded WWH gels. (A) Uptake of 2-NBDG on incubation with drug release media of pH 5, 6, and 7.4. (B-E) Fluorescence microscopy images of HepG2 cells incubated with 2-NBDG for 5 days in presence of: (B) Culture media (negative control), (C) Drug release media (pH 5), (D) Drug release media (pH 6), and (E) Drug release media (pH 7.4). Scale bar: 100 μm . Data reported are mean \pm SE ($n = 3$). Comparisons between two groups (samples with negative control) were carried out using Student's t-test. * $p < 0.05$ indicates statistically significant data.

2.5. Conclusions

In conclusion, we have effectively designed and constructed drug delivery platforms from ultra-short peptide gels that can be utilized for the sustained release of a hydrophobic, anti-diabetic drug, glimepiride. These gels can serve as effective injectable drug depots because of their excellent viscoelastic, self-healing, and thixotropic properties. It is interesting that adding histidine to the dipeptide backbone has helped to fabricate an acidic media-sensitive gel that can help diabetic patients by avoiding the issue of nonspecific medication release from scaffolds. A long-acting, sustained release profile of glimepiride is made possible by the tripeptide gel's slow rate of disintegration. All gels also have good antioxidant properties, which is helpful in removing the significant amount of reactive oxygen species (ROS) produced by the oxidation of glucose in diabetes patients. Additionally, all gels show pH-

dependent glucose uptake in human liver cancer cell line and great biocompatibility with a variety of cell lines. The adverse effect of glimepiride such as hypoglycemia can be resolved and the shortcomings like the initial burst release and short-time release profile of glimepiride associated with the earlier drug delivery vehicle can also be overcome. Therefore, the self-assembled tripeptide gel developed in this work can be employed as an injectable device for the pH-sensitive, long-term controlled/sustained release of glimepiride to reduce its adverse effects and frequency of dose in diabetic patients.

References

- (1) Zhang, K.; Liu, X.; Xu, J.; Yuan, J.; Cai, W.; Chen, T.; Wang, K.; Gao, Y.; Nie, S.; Xu, X.; Qin, X.; Su, Y.; Xu, W.; Olvera, A.; Xue, K.; Li, Z.; Zhang, M.; Zeng, X.; Zhang, C. L.; Li, O.; Zhang, E. E.; Zhu, J.; Xu, Y.; Kermany, D.; Zhou, K.; Pan, Y.; Li, S.; Lai, I. F.; Chi, Y.; Wang, C.; Pei, M.; Zang, G.; Zhang, Q.; Lau, J.; Lam, D.; Zou, X.; Wumaier, A.; Wang, J.; Shen, Y.; Hou, F. F.; Zhang, P.; Xu, T.; Zhou, Y.; Wang, G. Deep-Learning Models for the Detection and Incidence Prediction of Chronic Kidney Disease and Type 2 Diabetes from Retinal Fundus Images. *Nature Biomedical Engineering* **2021**, 5 (6), 533–545. <https://doi.org/10.1038/s41551-021-00745-6>.
- (2) Chen, Y.; Luan, J.; Shen, W.; Lei, K.; Yu, L.; Ding, J. Injectable and Thermosensitive Hydrogel Containing Liraglutide as a Long-Acting Antidiabetic System. *ACS Appl. Mater. Interfaces* **2016**, 8 (45), 30703–30713. <https://doi.org/10.1021/acsami.6b09415>.
- (3) Fu, Y.; Liu, W.; Wang, L.; Zhu, B.; Qu, M.; Yang, L.; Sun, X.; Gong, T.; Zhang, Z.; Lin, Q.; Zhang, L. Erythrocyte-Membrane-Camouflaged Nanoplatforam for Intravenous Glucose-Responsive Insulin Delivery. *Advanced Functional Materials* **2018**, 28 (41), 1802250. <https://doi.org/10.1002/adfm.201802250>.
- (4) Fu, M.; Zhang, C.; Dai, Y.; Li, X.; Pan, M.; Huang, W.; Qian, H.; Ge, L. Injectable Self-Assembled Peptide Hydrogels for Glucose-Mediated Insulin Delivery. *Biomater. Sci.* **2018**, 6 (6), 1480–1491. <https://doi.org/10.1039/C8BM00006A>.
- (5) Zhang, L.; Qin, H.; Li, J.; Qiu, J.-N.; Huang, J.-M.; Li, M.-C.; Guan, Y.-Q. Preparation and Characterization of Layer-by-Layer Hypoglycemic Nanoparticles with PH-Sensitivity for Oral Insulin Delivery. *J. Mater. Chem. B* **2018**, 6 (45), 7451–7461. <https://doi.org/10.1039/C8TB02113A>.
- (6) Tao, N.; Li, G.; Liu, M.; Gao, W.; Wu, H. Preparation of Dual Responsive Low-Molecular-Weight Hydrogel for Long-Lasting Drug Delivery. *Tetrahedron* **2017**, 73 (22), 3173–3180. <https://doi.org/10.1016/j.tet.2017.04.051>.
- (7) Green, K.; Brand, M. D.; Murphy, M. P. Prevention of Mitochondrial Oxidative Damage as a Therapeutic Strategy in Diabetes. *Diabetes* **2004**, 53 (suppl 1), S110. <https://doi.org/10.2337/diabetes.53.2007.S110>.
- (8) Coughlan, M. T.; Sharma, K. Challenging the Dogma of Mitochondrial Reactive Oxygen Species Overproduction in Diabetic Kidney Disease. *Kidney International* **2016**, 90 (2), 272–279. <https://doi.org/10.1016/j.kint.2016.02.043>.
- (9) Jana, B. A.; Shinde, U.; Wadhwani, A. Synthetic Enzyme-Based Nanoparticles Act as Smart Catalyst for Glucose Responsive Release of Insulin. *Journal of Biotechnology* **2020**, 324, 1–6. <https://doi.org/10.1016/j.jbiotec.2020.09.023>.
- (10) Ahmed, O. A.; Afouna, M. I.; El-Say, K. M.; Abdel-Naim, A. B.; Khedr, A.; Banjar, Z. M. Optimization of Self-Nanoemulsifying Systems for the Enhancement of *in Vivo* Hypoglycemic Efficacy of Glimepiride Transdermal Patches. *Expert Opinion on Drug Delivery* **2014**, 11 (7), 1005–1013. <https://doi.org/10.1517/17425247.2014.906402>.
- (11) Ahmed, O. A. A.; El-Say, K. M.; Alahdal, A. M. A PLGA-Reinforced PEG in Situ Gel Formulation for Improved Sustainability of Hypoglycaemic Activity of Glimepiride in Streptozotocin-Induced Diabetic Rats. *Sci Rep* **2017**, 7 (1), 16384. <https://doi.org/10.1038/s41598-017-16728-0>.
- (12) Zhou, D.; Li, S.; Fei, Z.; Zhou, P.; Zhao, Y.; Zhi, L.; Li, C.; Peng, X.; Liu, X.; Zhao, C. Glucose and PH Dual-Responsive Polymersomes with Multilevel Self-Regulation of Blood Glucose for Insulin Delivery. *Biomacromolecules* **2021**, 22 (9), 3971–3979. <https://doi.org/10.1021/acs.biomac.1c00772>.
- (13) Zhao, L.; Niu, L.; Liang, H.; Tan, H.; Liu, C.; Zhu, F. PH and Glucose Dual-Responsive Injectable Hydrogels with Insulin and Fibroblasts as Bioactive Dressings for Diabetic Wound Healing. *ACS Appl. Mater. Interfaces* **2017**, 9 (43), 37563–37574. <https://doi.org/10.1021/acsami.7b09395>.
- (14) Xu, W.; Hong, Y.; Song, A.; Hao, J. Peptide-Assembled Hydrogels for PH-Controllable Drug Release. *Colloids and Surfaces B: Biointerfaces* **2020**, 185, 110567. <https://doi.org/10.1016/j.colsurfb.2019.110567>.
- (15) Li, X.; Fu, M.; Wu, J.; Zhang, C.; Deng, X.; Dhinakar, A.; Huang, W.; Qian, H.; Ge, L. PH-Sensitive Peptide Hydrogel for Glucose-Responsive Insulin Delivery. *Acta Biomaterialia* **2017**, 51, 294–303. <https://doi.org/10.1016/j.actbio.2017.01.016>.
- (16) Fu, Y.; Sun, Y.; Chen, M.; Xing, W.; Xu, Y.; Qian, X.; Zhu, W. Glycopolymer Nanoparticles with On-Demand Glucose-Responsive Insulin Delivery and Low-Hypoglycemia Risks for Type 1

- Diabetic Treatment. *Biomacromolecules* **2022**, acs.biomac.1c01496. <https://doi.org/10.1021/acs.biomac.1c01496>.
- (17) Sun, X.; Ji, W.; Zhang, B.; Ma, L.; Fu, W.; Qian, W.; Zhang, X.; Li, J.; Sheng, E.; Tao, Y.; Zhu, D. A Theranostic Microneedle Array Patch for Integrated Glycemia Sensing and Self-Regulated Release of Insulin. *Biomater. Sci.* **2022**, 10.1039.D1BM01834E. <https://doi.org/10.1039/D1BM01834E>.
- (18) Jain, S.; Saraf, S. Influence of Processing Variables and in Vitro Characterization of Glipizide Loaded Biodegradable Nanoparticles. *Diabetes & Metabolic Syndrome: Clinical Research & Reviews* **2009**, 3 (2), 113–117. <https://doi.org/10.1016/j.dsx.2009.04.003>.
- (19) Jain, S. K.; Awasthi, A. M.; Jain, N. K.; Agrawal, G. P. Calcium Silicate Based Microspheres of Repaglinide for Gastroretentive Floating Drug Delivery: Preparation and in Vitro Characterization. *Journal of Controlled Release* **2005**, 107 (2), 300–309. <https://doi.org/10.1016/j.jconrel.2005.06.007>.
- (20) Ahmed, T. A.; El-Say, K. M.; Aljaeid, B. M.; Fahmy, U. A.; Abd-Allah, F. I. Transdermal Glimepiride Delivery System Based on Optimized Ethosomal Nano-Vesicles: Preparation, Characterization, in Vitro, Ex Vivo and Clinical Evaluation. *International Journal of Pharmaceutics* **2016**, 500 (1–2), 245–254. <https://doi.org/10.1016/j.ijpharm.2016.01.017>.
- (21) Ahmed, O. A. A.; Kurakula, M.; Banjar, Z. M.; Afouna, M. I.; Zidan, A. S. Quality by Design Coupled with Near Infrared in Formulation of Transdermal Glimepiride Liposomal Films. *Journal of Pharmaceutical Sciences* **2015**, 104 (6), 2062–2075. <https://doi.org/10.1002/jps.24448>.
- (22) Mohsen, A. M.; AbouSamra, M. M.; ElShebiney, S. A. Enhanced Oral Bioavailability and Sustained Delivery of Glimepiride via Niosomal Encapsulation: *In-Vitro* Characterization and *in-Vivo* Evaluation. *Drug Development and Industrial Pharmacy* **2017**, 43 (8), 1254–1264. <https://doi.org/10.1080/03639045.2017.1310224>.
- (23) Abdallah, M. H.; Sabry, S. A.; Hasan, A. A. Enhancing Transdermal Delivery of Glimepiride Via Entrapment in Proniosomal Gel. *JYP* **2016**, 8 (4), 335–340. <https://doi.org/10.5530/jyp.2016.4.8>.
- (24) Sheehan, F.; Sementa, D.; Jain, A.; Kumar, M.; Tayarani-Najjaran, M.; Kroiss, D.; Ulijn, R. V. Peptide-Based Supramolecular Systems Chemistry. *Chem. Rev.* **2021**, 121 (22), 13869–13914. <https://doi.org/10.1021/acs.chemrev.1c00089>.
- (25) Yang, J.; An, H.-W.; Wang, H. Self-Assembled Peptide Drug Delivery Systems. *ACS Appl. Bio Mater.* **2021**, 4 (1), 24–46. <https://doi.org/10.1021/acsabm.0c00707>.
- (26) Roy, K.; Pandit, G.; Chetia, M.; Sarkar, A. K.; Chowdhuri, S.; Bidkar, A. P.; Chatterjee, S. Peptide Hydrogels as Platforms for Sustained Release of Antimicrobial and Antitumor Drugs and Proteins. *ACS Appl. Bio Mater.* **2020**, 3 (9), 6251–6262. <https://doi.org/10.1021/acsabm.0c00314>.
- (27) Pal, V. K.; Jain, R.; Roy, S. Tuning the Supramolecular Structure and Function of Collagen Mimetic Ionic Complementary Peptides via Electrostatic Interactions. *Langmuir* **2020**, 36 (4), 1003–1013. <https://doi.org/10.1021/acs.langmuir.9b02941>.
- (28) Wang, Y.; Zhan, J.; Huang, J.; Wang, X.; Chen, Z.; Yang, Z.; Li, J. Dynamic Responsiveness of Self-Assembling Peptide-Based Nano-Drug Systems. *Interdisciplinary Medicine* **2023**, 1 (1), e20220005. <https://doi.org/10.1002/INMD.20220005>.
- (29) Zhang, Q.; Liu, N.; Wang, J.; Liu, Y.; Wang, K.; Zhang, J.; Pan, X. The Recent Advance of Cell-Penetrating and Tumor-Targeting Peptides as Drug Delivery Systems Based on Tumor Microenvironment. *Mol. Pharmaceutics* **2023**, 20 (2), 789–809. <https://doi.org/10.1021/acs.molpharmaceut.2c00629>.
- (30) Eskandari, S.; Guerin, T.; Toth, I.; Stephenson, R. J. Recent Advances in Self-Assembled Peptides: Implications for Targeted Drug Delivery and Vaccine Engineering. *Advanced Drug Delivery Reviews* **2017**, 110–111, 169–187. <https://doi.org/10.1016/j.addr.2016.06.013>.
- (31) MARCUSE, R. Antioxidative Effect of Amino-Acids. *Nature* **1960**, 186 (4728), 886–887. <https://doi.org/10.1038/186886a0>.
- (32) Sharma, P.; Kaur, H.; Roy, S. Inducing Differential Self-Assembling Behavior in Ultrashort Peptide Hydrogelators Using Simple Metal Salts. *Biomacromolecules* **2019**, 20 (7), 2610–2624. <https://doi.org/10.1021/acs.biomac.9b00416>.
- (33) Chauhan, N.; Singh, Y. Self-Assembled Fmoc-Arg-Phe-Phe Peptide Gels with Highly Potent Bactericidal Activities. *ACS Biomater. Sci. Eng.* **2020**, 6 (10), 5507–5518. <https://doi.org/10.1021/acsbiomaterials.0c00660>.
- (34) Wang, S.-T.; Lin, Y.; Spencer, R. K.; Thomas, M. R.; Nguyen, A. I.; Amdursky, N.; Pashuck, E. T.; Skaalure, S. C.; Song, C. Y.; Parmar, P. A.; Morgan, R. M.; Ercius, P.; Aloni, S.; Zuckermann,

- R. N.; Stevens, M. M. Sequence-Dependent Self-Assembly and Structural Diversity of Islet Amyloid Polypeptide-Derived β -Sheet Fibrils. *ACS Nano* **2017**, *11* (9), 8579–8589. <https://doi.org/10.1021/acsnano.7b02325>.
- (35) Zheng, L.; Zhao, M.; Xiao, C.; Zhao, Q.; Su, G. Practical Problems When Using ABTS Assay to Assess the Radical-Scavenging Activity of Peptides: Importance of Controlling Reaction PH and Time. *Food Chemistry* **2016**, *192*, 288–294. <https://doi.org/10.1016/j.foodchem.2015.07.015>.
- (36) Hao, T.; Li, J.; Yao, F.; Dong, D.; Wang, Y.; Yang, B.; Wang, C. Injectable Fullerenol/Alginate Hydrogel for Suppression of Oxidative Stress Damage in Brown Adipose-Derived Stem Cells and Cardiac Repair. *ACS Nano* **2017**, *11* (6), 5474–5488. <https://doi.org/10.1021/acsnano.7b00221>.
- (37) Diaferia, C.; Netti, F.; Ghosh, M.; Sibillano, T.; Giannini, C.; Morelli, G.; Adler-Abramovich, L.; Accardo, A. Bi-Functional Peptide-Based 3D Hydrogel-Scaffolds. *Soft Matter* **2020**, *16* (30), 7006–7017. <https://doi.org/10.1039/D0SM00825G>.
- (38) Li, Y.; Sun, M.; Liu, Y.; Liang, J.; Wang, T.; Zhang, Z. Gymnemic Acid Alleviates Type 2 Diabetes Mellitus and Suppresses Endoplasmic Reticulum Stress *in Vivo* and *in Vitro*. *J. Agric. Food Chem.* **2019**, *67* (13), 3662–3669. <https://doi.org/10.1021/acs.jafc.9b00431>.
- (39) Luo, Y.; Zhang, X.; Li, Y.; Deng, J.; Li, X.; Qu, Y.; Lu, Y.; Liu, T.; Gao, Z.; Lin, B. High-Glucose 3D INS-1 Cell Model Combined with a Microfluidic Circular Concentration Gradient Generator for High Throughput Screening of Drugs against Type 2 Diabetes. *RSC Adv.* **2018**, *8* (45), 25409–25416. <https://doi.org/10.1039/C8RA04040K>.
- (40) Zhang, M.; Yan, S.; Xu, X.; Yu, T.; Guo, Z.; Ma, M.; Zhang, Y.; Gu, Z.; Feng, Y.; Du, C.; Wan, M.; Hu, K.; Han, X.; Gu, N. Three-Dimensional Cell-Culture Platform Based on Hydrogel with Tunable Microenvironmental Properties to Improve Insulin-Secreting Function of MIN6 Cells. *Biomaterials* **2021**, *270*, 120687. <https://doi.org/10.1016/j.biomaterials.2021.120687>.
- (41) Zhang, W.-Y.; Lee, J.-J.; Kim, Y.; Kim, I.-S.; Han, J.-H.; Lee, S.-G.; Ahn, M.-J.; Jung, S.-H.; Myung, C.-S. Effect of Eriodictyol on Glucose Uptake and Insulin Resistance *in Vitro*. *J. Agric. Food Chem.* **2012**, *60* (31), 7652–7658. <https://doi.org/10.1021/jf300601z>.
- (42) Zou, C.; Wang, Y.; Shen, Z. 2-NBDG as a Fluorescent Indicator for Direct Glucose Uptake Measurement. *Journal of Biochemical and Biophysical Methods* **2005**, *64* (3), 207–215. <https://doi.org/10.1016/j.jbbm.2005.08.001>.
- (43) Baptistella, G. B.; Manica, G. C. M.; de Souza, S. W.; Santana, F. S.; Fachini, L. G.; Hughes, D. L.; de Sá, E. L.; Picheth, G.; Soares, J. F.; Rego, F. G. M.; Nunes, G. G. An Oxalate-Bridged Oxidovanadium(IV) Binuclear Complex That Improves the *in Vitro* Cell Uptake of a Fluorescent Glucose Analog. *Polyhedron* **2021**, *198*, 115071. <https://doi.org/10.1016/j.poly.2021.115071>.
- (44) Diaferia, C.; Ghosh, M.; Sibillano, T.; Gallo, E.; Stornaiuolo, M.; Giannini, C.; Morelli, G.; Adler-Abramovich, L.; Accardo, A. Fmoc-FF and Hexapeptide-Based Multicomponent Hydrogels as Scaffold Materials. *Soft Matter* **2019**, *15* (3), 487–496. <https://doi.org/10.1039/C8SM02366B>.
- (45) McCloskey, A. P.; Draper, E. R.; Gilmore, B. F.; Lavery, G. Ultrashort Self-Assembling Fmoc-Peptide Gelators for Anti-Infective Biomaterial Applications: Fmoc-Peptides Demonstrate Selective Activity Against Biofilms. *J. Pept. Sci.* **2017**, *23* (2), 131–140. <https://doi.org/10.1002/psc.2951>.
- (46) Wang, Y.; Li, P.; Chen, F.; Jia, L.; Xu, Q.; Gai, X.; Yu, Y.; Di, Y.; Zhu, Z.; Liang, Y.; Liu, M.; Pan, W.; Yang, X. A Novel PH-Sensitive Carrier for the Delivery of Antitumor Drugs: Histidine-Modified Auricularia Auricular Polysaccharide Nano-Micelles. *Scientific Reports* **2017**, *7* (1), 4751. <https://doi.org/10.1038/s41598-017-04428-8>.
- (47) Morris, K. L.; Chen, L.; Rodger, A.; Adams, D. J.; Serpell, L. C. Structural Determinants in a Library of Low Molecular Weight Gelators. *Soft Matter* **2015**, *11* (6), 1174–1181. <https://doi.org/10.1039/C4SM02532F>.
- (48) Panda, J. J.; Mishra, A.; Basu, A.; Chauhan, V. S. Stimuli Responsive Self-Assembled Hydrogel of a Low Molecular Weight Free Dipeptide with Potential for Tunable Drug Delivery. *Biomacromolecules* **2008**, *9* (8), 2244–2250. <https://doi.org/10.1021/bm800404z>.
- (49) Byler, D. M.; Susi, H. Examination of the Secondary Structure of Proteins by Deconvolved FTIR Spectra. *Biopolymers* **1986**, *25* (3), 469–487. <https://doi.org/10.1002/bip.360250307>.
- (50) Kumaraswamy, P.; Lakshmanan, R.; Sethuraman, S.; Krishnan, U. M. Self-Assembly of Peptides: Influence of Substrate, PH and Medium on the Formation of Supramolecular Assemblies. *Soft Matter* **2011**, *7* (6), 2744–2754. <https://doi.org/10.1039/C0SM00897D>.

- (51)Qin, Z.; Sun, Y.; Jia, B.; Wang, D.; Ma, Y.; Ma, G. Kinetic Mechanism of Thioflavin T Binding onto the Amyloid Fibril of Hen Egg White Lysozyme. *Langmuir* **2017**, *33* (22), 5398–5405. <https://doi.org/10.1021/acs.langmuir.7b00221>.
- (52)Sun, J. E. P.; Stewart, B.; Litan, A.; Lee, S. J.; Schneider, J. P.; Langhans, S. A.; Pochan, D. J. Sustained Release of Active Chemotherapeutics from Injectable-Solid β -Hairpin Peptide Hydrogel. *Biomater. Sci.* **2016**, *4* (5), 839–848. <https://doi.org/10.1039/C5BM00538H>.
- (53)Li, I.-C.; Moore, A. N.; Hartgerink, J. D. “Missing Tooth” Multidomain Peptide Nanofibers for Delivery of Small Molecule Drugs. *Biomacromolecules* **2016**, *17* (6), 2087–2095. <https://doi.org/10.1021/acs.biomac.6b00309>.
- (54)Martí-Centelles, R.; Dolz-Pérez, I.; De la O, J.; Ontoria-Oviedo, I.; Sepúlveda, P.; Nebot, V. J.; Vicent, M. J.; Escuder, B. Two-Component Peptidic Molecular Gels for Topical Drug Delivery of Naproxen. *ACS Appl. Bio Mater.* **2021**, *4* (1), 935–944. <https://doi.org/10.1021/acsabm.0c01422>.
- (55)Mei, L.; Xu, K.; Zhai, Z.; He, S.; Zhu, T.; Zhong, W. Doxorubicin-Reinforced Supramolecular Hydrogels of RGD-Derived Peptide Conjugates for PH-Responsive Drug Delivery. *Org. Biomol. Chem.* **2019**, *17* (15), 3853–3860. <https://doi.org/10.1039/C9OB00046A>.
- (56)Lindsey, S.; Piatt, J. H.; Worthington, P.; Sönmez, C.; Satheye, S.; Schneider, J. P.; Pochan, D. J.; Langhans, S. A. Beta Hairpin Peptide Hydrogels as an Injectable Solid Vehicle for Neurotrophic Growth Factor Delivery. *Biomacromolecules* **2015**, *16* (9), 2672–2683. <https://doi.org/10.1021/acs.biomac.5b00541>.
- (57)Zhang, L.; Xu, J.; Wang, F.; Ding, Y.; Wang, T.; Jin, G.; Martz, M.; Gui, Z.; Ouyang, P.; Chen, P. Histidine-Rich Cell-Penetrating Peptide for Cancer Drug Delivery and Its Uptake Mechanism. *Langmuir* **2019**, *35* (9), 3513–3523. <https://doi.org/10.1021/acs.langmuir.8b03175>.
- (58)Yagil, G. The Proton Dissociation Constant of Pyrrole, Indole and Related Compounds. *Tetrahedron* **1967**, *23* (6), 2855–2861. [https://doi.org/10.1016/0040-4020\(67\)85151-2](https://doi.org/10.1016/0040-4020(67)85151-2).
- (59)Papadopoulou, V.; Kosmidis, K.; Vlachou, M.; Macheras, P. On the Use of the Weibull Function for the Discernment of Drug Release Mechanisms. *International Journal of Pharmaceutics* **2006**, *309* (1), 44–50. <https://doi.org/10.1016/j.ijpharm.2005.10.044>.
- (60)Wei, Q.; Duan, J.; Ma, G.; Zhang, W.; Wang, Q.; Hu, Z. Enzymatic Crosslinking to Fabricate Antioxidant Peptide-Based Supramolecular Hydrogel for Improving Cutaneous Wound Healing. *J. Mater. Chem. B* **2019**, *7* (13), 2220–2225. <https://doi.org/10.1039/C8TB03147A>.
- (61)Samaei, S. P.; Martini, S.; Tagliazucchi, D.; Gianotti, A.; Babini, E. Antioxidant and Angiotensin I-Converting Enzyme (ACE) Inhibitory Peptides Obtained from Alcalase Protein Hydrolysate Fractions of Hemp (*Cannabis Sativa* L.) Bran. *J. Agric. Food Chem.* **2021**, *69* (32), 9220–9228. <https://doi.org/10.1021/acs.jafc.1c01487>.
- (62)Hussain, M.; Suo, H.; Xie, Y.; Wang, K.; Wang, H.; Hou, Z.; Gao, Y.; Zhang, L.; Tao, J.; Jiang, H.; Zhu, J. Dopamine-Substituted Multidomain Peptide Hydrogel with Inherent Antimicrobial Activity and Antioxidant Capability for Infected Wound Healing. *ACS Appl. Mater. Interfaces* **2021**, *13* (25), 29380–29391. <https://doi.org/10.1021/acsami.1c07656>.

CHAPTER - 3

Supramolecular, nanostructured peptide-NSAID conjugates for the selective inhibition of COX-2, biofilm, and inflammation in chronic wounds

Self-assembled peptide gels for chronic wound healing

3.1. Introduction

3.1.1. Chronic wound

Hemostasis, inflammation, proliferation, and remodelling are the four steps that make up the intricate but well-structured process of wound healing.^{1,2} The constant interplay of numerous enzymes, cells, chemokines, cytokines, and growth factors is essential for the tissue repair process, and a breakdown in these intricate relationships results in non-healing chronic wounds. According to the literature, 4–10% of diabetes patients experience chronic lesions, such as diabetic foot ulcers (DFU), which have a negative impact on the quality of life of nearly 2.5% populations of the United States.³ More than 80% of DFU cases are removed surgically, and over the past five years, the mortality rate has stayed between 40 and 45%. More than 2% of the world's population currently has chronic wounds, and the annual cost of treating them is \$19 billion.⁴ Bacterial infection, biofilm development, excessive production of pro-inflammatory cytokines, reactive oxygen species (ROS), and secretion of numerous proteases are all characteristics features of chronic wounds.⁵ Although inflammation is necessary for the wound healing process in order to destroy bacteria, excessive and chronic inflammation slows down the healing process and produces discomfort. In chronic wounds, the stalled inflammatory phase is more severe, difficult to resolve, and hinders the healing process from advancing to the proliferation and remodelling phase.⁶ Despite attempts, it is difficult to successfully reverse the stopped healing associated with chronic wounds.

3.1.2. Challenges

Reactive oxygen species (ROS) are necessary for cellular function but oxidative stress develops when there is an imbalance in oxidative activity due to the ROS level exceeding the cellular antioxidant defense.⁷ It can cause harm to macromolecules, such as proteins, lipids, and DNA, which is strongly tied to the emergence of chronic wounds associated with inflammation and the weakening of immune defenses, thus, increasing susceptibility to infections. Additionally, it promotes bacterial colonization near the wound. *Staphylococcus aureus* is known to worsen the healing of wounds in particular and the tissue damage is associated with the release of inflammatory cytokines, which are invaded by bacteria during wound infection.⁶ *S. aureus* and other Gram-positive bacteria respond to this harsh environment by forming a biofilm that shields them from the host's immune system. Early elimination of bacterial adhesion and settling at the wound site is essential for successful wound healing. Antibiotics are used to control, treat, and prevent bacterial infections but due to their extensive usage, multidrug-resistant bacteria have emerged, posing a serious threat to human health.⁸ Inside the biofilm, bacteria function as multicellular organisms and generate defenses against drug penetration.⁹ Inside the biofilm, they are in a distinct metabolic state (the stationary phase), which causes a 100-1000-fold increase in their antibiotic

resistance. Often, infection caused by biofilms cannot be treated with antibiotics that are effective against planktonic bacteria.

3.1.3. Research gap

For the resolution of the inflammatory phase and to start the proliferative phase, it is required to scavenge excessive ROS, limit bacterial infection, and remove biofilm to speed up the overall wound healing and improve the quality of the repair.^{10,11} Non-steroidal anti-inflammatory drugs (NSAIDs), naproxen (Npx), and indomethacin (Ind) are examples of anti-inflammatory treatments that can reduce the levels of inflammatory mediators (prostaglandins) and normalize chronic wounds that are associated with significant inflammation and pain.¹² Inhibition of the COX-2 enzyme causes a significant drop in the amount of ROS, which in turn prevents the production of proinflammatory cytokines, like prostaglandin E₂ (PGE₂), nitric oxide (NO), tumor necrosis factor-alpha (TNF- α), and interleukin-6 (IL-6). However, Npx and Ind do not specifically inhibit COX-2, and instead, they also inhibit COX-1, which has unfavorable side effects, such increased risks for gastrointestinal and renal problems. Chronic wounds necessitate a multipurpose wound dressing. The dressings must be able to preserve moisture, absorb excess exudate, reduce pain, exert antioxidant, antibacterial, and anti-inflammatory effects, and tolerate protease enzyme-induced proteolytic destruction at the wound site. Biomaterials have been developed to enhance the wound-healing processes, including smart hydrogels, antimicrobial foams,¹³ metal nanoparticles,¹⁴ injectable cryogels,¹⁵ bactericidal films,¹⁶ and extracellular matrix (ECM)-based scaffolds. To treat skin injuries, multi-responsive polymeric hydrogels with a high-water content, porous structure, and exceptional biocompatibility have been developed.¹⁷ These biomaterials will need two to three components or electrospinning technologies to generate nanofibrous structures in order to function well.^{18,19} Hydrogels also frequently exhibit poor mechanical performance, insufficient antibacterial activity, and involve multistep production.²⁰

3.1.4. Self-assembled peptide gel

Self-assembled antimicrobial peptide (AMP) gels have become a promising candidate in this situation because of their capacity to mimic extracellular matrix, provide a moist wound environment, dynamic transience, improve biocompatibility, and increase chemical functionality and adaptability.²¹ The cationic and hydrophobic residues²² of AMPs can help them to integrate into the bacterial membrane's anionic phospholipid layers, which causes the membrane to rupture, release cytoplasmic material, and lead to bacterial apoptosis. Bacteria find it difficult to modify or repair the elements of their membranes through metabolic processes, which significantly reduces the emergence of drug resistance.²³ Based on the supramolecular self-assembly of AMPs, several wound repair gels have been reported. Some of these gels additionally contain antibiotics²⁴ and growth hormones.²⁵ These gels can only destroy planktonic microorganisms but cannot completely remove biofilms that have been already formed, which restricts their usage in chronic wounds.²⁶ Most of these AMP gels have a single function, such as to promote cell growth or have antibacterial properties. In order to treat chronic wounds, Hussain *et al.*,⁸ Chen *et al.*,²⁷ Cui *et al.*,²⁸ and Wang *et al.*⁶ have created supramolecular AMP gels that either have

antibacterial, biofilm suppression, and antioxidant capabilities, or they have anti-inflammatory effects. Literature report reveals a complete absence of versatile peptide-based scaffolds that may address various elements of chronic wounds. Proteolytic stability also continues to be a significant issue with antimicrobial peptides.

3.2. Objectives

To address the problem of poor selectivity of NSAIDs, Npx and Ind, towards COX-2 enzyme and the inability of AMPs to target diverse aspect of chronic wounds, we decided to conjugate the anti-inflammatory drugs to peptides with inherent antibacterial, antibiofilm, antioxidant characteristics, and higher selectivity towards COX-2 enzyme. We have developed drug peptide conjugates, naproxen-^LTyr-^LTyr-^DLys-NH₂ (Npx-YYk), naproxen-^LTyr-^LTyr-^DArg-NH₂ (Npx-YYr), indomethacin-^LTyr-^LTyr-^DLys-NH₂ (Ind-YYk), and indomethacin-^LTyr-^LTyr-^DArg-NH₂ (Npx-YYr), and self-assembled them into nanostructured, supramolecular gels to obtain multifunctional wound healing scaffolds for chronic wounds. In order to design the peptides, the cationic amino acid k or r was used for their antibacterial characteristics and the amino acid Y for its capacity to form gels and antioxidant capabilities. Since it is well known that the inclusion of D-amino acids in a sequence boosts the proteolytic stability and selectivity towards COX-2 enzyme, the cationic amino acids were integrated into the peptide sequence in D-form. The scaffolds' ability to aid in wound healing was thoroughly characterized and examined in cell culture. The Npx- and Ind-conjugated peptides have shown good antibacterial, antibiofilm, ROS scavenging, anti-inflammatory, and wound healing capabilities, and as a result, they have a significant potential as chronic wound healing scaffold.

3.3. Experimental Section

3.3.1. Materials

Reagents of analytical grade were purchased and used without purification. Rink amide AM resin (200-400 mesh with a loading of 0.8 mmol/g) was purchased from Novabiochem. Fmoc-Tyr(tBu)-OH, 2,2'-azino-bis(3-ethylbenzothiazoline-6-sulfonic acid) diammonium salt (ABTS), 2',7'-dichlorodihydrofluorescein diacetate (DCFDA), and (±)-6-hydroxy-2,5,7,8-tetramethylchromane-2-carboxylic acid (Trolox) were procured from Sigma-Aldrich. Fmoc-^LLys(Boc)-OH, naproxen, indomethacin, trifluoroacetic acid (TFA), 1-bis(dimethylamino)methylene]-1H-1,2,3-triazolo[4,5-b]pyridinium 3-oxide hexafluorophosphate (HATU), N,N-diisopropylethylamine (DIEA), 1,2-ethanedithiol (EDT), triisopropyl silane (TIS), 1,1-diphenyl-2-picrylhydrazyl free radical (DPPH) were purchased from TCI Chemicals, India. Fmoc-^DLys(Boc)-OH, Fmoc-^LArg(Pbf)-OH, Fmoc-^DArg(Pbf)-OH were procured from BLD Pharmaceuticals. Dichloromethane (DCM), anhydrous N, N'-dimethylformamide (DMF), and diethyl ether were bought from Rankem Laboratories. Dimethyl sulfoxide (DMSO) and HPLC grade solvents, acetonitrile, methanol, and isopropyl alcohol were purchased from Merck and used for reverse phase high-pressure liquid chromatography (RP-HPLC). Piperidine was bought from Spectrochem. PolyPrep chromatography columns from Bio-Rad were used

for solid-phase peptide synthesis (SPPS). Deionized water (DI, 18.2 MΩ cm) was obtained from a Milli-Q system and used in all experiments. L929 and RAW 264.7 cells used in the study were a generous gift from Dr. Durba Pal, Assistant Professor, DBME, IIT Ropar. RPMI 1640, DMEM, 0.25% trypsin/EDTA, penstrep, lipopolysaccharide from *E. coli* were purchased from Thermo Fisher Scientific. MTT reagent, ascorbic acid, DAPI (4',6-diamidino-2-phenylindole, dihydrochloride) and fetal bovine serum (FBS) were procured from Himedia. COX fluorescent inhibitor screening assay kit was obtained from Cayman chemicals. LIVE/DEAD™ BacLight™ Bacterial Viability Kit and LIVE/DEAD™ Viability/Cytotoxicity Kit for mammalian cells, and Alexa Fluor™ 488, Phalloidin were purchased from Invitrogen.

3.3.2. Synthesis of drug-peptide conjugates

The peptides were synthesized and conjugated with NSAIDs (naproxen and indomethacin) employing standard 9-fluorenylmethoxycarbonyl (Fmoc)-based SPPS method using a Rink amide AM resin as a solid support. After coupling of all the amino acids on the solid support, the drugs, Npx and Ind, were incorporated at the N-terminus of peptides, followed by cleavage from support using a mixture of TFA:TIS:water (90:5:5) for 3.5 h at room temperature to produce amide-terminated peptide conjugates. Npx-YYK-NH₂, Npx-YYk-NH₂, Npx-YYR-NH₂, Npx-YYr-NH₂, Ind-YYK-NH₂, Ind-YYk-NH₂, Ind-YYR-NH₂, and Ind-YYr-NH₂ conjugates obtained were precipitated from cold diethyl ether, washed several times, and dried in a vacuum. The purity of the drug-peptide conjugates was determined by RP-HPLC using Xbridge BEH C₁₈ column (250 × 4.6 mm, 5 μm) and acetonitrile/water (50:50) with 0.1% TFA as a mobile phase at a flow rate of 0.8 mL/min for Npx-YYR and Npx-YYr, and 1 mL/min for other conjugates. The conjugates were further characterized by mass (XEVO G2-XS QTOF) and ¹H NMR (JEOL JNM-ECS, 400 MHz) analysis.

3.3.3. Preparation of supramolecular gels

All conjugates were self-assembled into gels by pH-triggered induction and solvent-switch methods. Npx-YYK-NH₂, Npx-YYk-NH₂, Npx-YYR-NH₂, and Npx-YYr-NH₂ were fabricated using a pH-switch method. The conjugates (2 mg) were completely solubilized in 150 μL DI water at pH 9 and 5 μL of 1M NaOH was added to form homogeneous gels within 0.5 h at a concentration of 1.33% (w/v). Ind-YYK-NH₂, Ind-YYk-NH₂, Ind-YYR-NH₂, and Ind-YYr-NH₂ were self-assembled into gels by solvent-switch method using DMSO/H₂O (30:70 v/v). In this case, 2 mg of conjugates were solubilized in 30 μL of DMSO, followed by dropwise addition of 70 μL DI water with gentle tapping to form gels (2% w/v) in 2 h.

3.3.4. Morphological analysis of gels

The morphologies of Npx-YYk-NH₂, Npx-YYr-NH₂, Ind-YYk-NH₂, and Ind-YYr-NH₂ were observed under scanning electron microscope (SEM) and high-resolution transmission electron microscope (HR-TEM). For SEM studies, gels were prepared on metal stubs, air dried for 48 h, and the surface was sputter-coated with platinum for few seconds under vacuum. Micrographs were acquired using JEOL

JSM-6610LV microscope with a tungsten filament at an accelerating voltage of 10 kV. For HR-TEM experiments, gels (2% w/v) were diluted and 10 μ L of gel solution was placed on the copper grid and left for drying. Micrographs were acquired using HR-TEM JEM-2100 Plus instrument operating at 200 kV.

3.3.5. Spectroscopic studies

The following spectroscopic studies were performed to understand the secondary structures of Npx-YYk-NH₂, Npx-YYr-NH₂, Ind-YYk-NH₂, and Ind-YYr-NH₂.

Circular dichroism (CD). CD analysis was carried on a CD spectrometer (JASCO J-1500) using a 0.1 cm path length quartz cuvette. The measurements were performed at 37 °C and spectra of conjugates were acquired at a concentration of 0.5 mM in the range of 195-350 nm at a continuous scanning rate of 200 nm/min. Solutions were prepared in DI water and incubated at room temperature for 5 days before the study.

Fourier transform infrared (FT-IR). FTIR spectra of all the drug-peptide conjugates were recorded in the ATR mode using Bruker Tensor 27 spectrometer between 400-4000 cm⁻¹.

Thioflavin-T (ThT) binding assay. Binding of conjugates with ThT were measured by fluorescence spectra, using a reported method.²⁹ The fluorescence spectra were recorded in a range of 430-700 nm using a Tecan multimode microplate reader at an excitation wavelength of 440 nm to quantify the binding of thioflavin T with the secondary structures of conjugates. ThT solution without any peptides were considered as a blank.

Zeta potential. The zeta potential of conjugate solutions (1 mM) was measured using the Malvern Zetasizer Nano ZS instrument at room temperature. Sample solutions were equilibrated overnight in alkaline borate buffer of pH 8.5, before the measurement.

3.3.6. Rheology experiments

All rheological studies were carried out on an Anton Paar MCR 102 rheometer with 25 mm parallel plate configuration and a shear gap of 0.3 mm to determine the viscoelastic properties of gels. The conjugate gels were prepared at a concentration of 1.33 or 2% w/v and kept at 37 °C for overnight. A 200 μ L of gel was sandwiched between the plates at room temperature and liquid paraffin was added around the plate to limit the evaporation of water during measurements. The storage modulus (G') and loss modulus (G'') were obtained as function of strain (0.01-100%) for amplitude sweep studies. The linear viscoelastic range (LVR) of gels were determined from amplitude sweep study by keeping angular frequency constant at 10 rad/s. Dynamic oscillatory frequency sweep measurements were conducted at a constant amplitude of 1%, with angular frequency varying from 0.1-100 rad/s. The self-healing properties of gels were investigated by applying six alternative cycles of extreme (30%) and mild strain (0.1%) at a constant angular frequency of 10 rad/s.

3.3.7. Swelling and degradation

The gels (1.33 w/v or 2% w/v, 100 μ L) were prepared as mentioned earlier and immersed in a 1 mL buffer solution of pH 7.4 (phosphate) and 8.5 (borate). The gels were incubated at 37 °C with constant shaking of 100 rpm and media was removed after each time interval (6, 12, and 24 h), blotted carefully to remove any trace of buffer solution, and weighed. The amounts of media absorbed by the gels gravimetrically were calculated and expressed in terms of swelling/degradation percentage using the following equation:

$$\% \text{ Swelling/Degradation} = \frac{W_t - W_i}{W_i} \times 100 \quad \text{Equation 3.1}$$

where, W_t is the weight of swollen gel at time t and W_i is the initial weight.

3.3.8. Proteolytic stability

A proteolytic mixture containing a mocktail of proteolytic enzymes was used to assess the proteolytic stability of gels (both D- and L). A stock solution was prepared using 1.87, 1.49 and 1.45 U of enzymes, proteinase K, chymotrypsin, and pepsin, in PBS and 1 mL of this mocktail was added to gels (100 μ L), and incubated at 37 °C under 100 rpm in an orbital shaker. After specified time intervals (0, 6, 12 and 24 h), the samples were centrifuged (10000 rpm, 4 °C, 10 min), washed with DI water for three times, and freeze-dried. The freeze-dried samples were dissolved in 500 μ L of methanol, syringe filtered (0.2 μ), and degradation was monitored by RP-HPLC using ACN:water (50:50) with 0.1% TFA as a mobile phase. To compare the proteolytic stability of D- and L-amino acid containing conjugate gels, percent of peptide remaining undegraded was determined by calculating the area under the curve in chromatogram. The following formula was used to determine the percent of remaining peptide:

$$\% \text{ Remaining Peptide} = \frac{\text{Area under the peak at time } t}{\text{Area under the peak at time } 0 \text{ h}} \times 100 \quad \text{Equation 3.2}$$

where, t = 0, 6, 12 and 24 h.

3.3.9. Antioxidant properties

Two different in vitro antioxidant assays (ABTS and DPPH) were carried out to evaluate the antioxidant capacity of gels.

ABTS assay. The scavenging capacity against the ABTS radicals was assessed according to the method mentioned earlier.²⁹ An equivalent volume of PBS without sample was taken as a blank and ABTS radical without sample was taken as a control. Ascorbic acid (1 mg/mL) was used as a standard antioxidant for comparison. The ABTS radical scavenging activity of materials was calculated using the following equation:

$$\% \text{ Radical Scavenging Effect} = \frac{A_c - A_s}{A_c} \times 100 \quad \text{Equation 3.3}$$

where, A_c is the absorbance of the control and A_s is the absorbance of the sample.

DPPH assay. The 1,1'-diphenyl-2-picrylhydrazyl (DPPH) radical scavenging activity of conjugates and gels were evaluated according to the method as mentioned earlier. The reduction of DPPH free radicals was determined by measuring the absorbance of the solution at 517 nm using a plate reader. The ability to scavenge the DPPH radicals was calculated using **Equation 3.3**.

3.3.10. Cyclooxygenase (COX) enzyme inhibition assay

Conjugates with both D- and L-amino acids were evaluated for their COX inhibition potential against COX-1 and COX-2 enzymes using a COX Fluorescent Inhibitor Screening Assay kit. All reagents were prepared according to the protocol mentioned in the kit. COX-1 (SC-560) and COX-2 (DuP-697) inhibitors, potassium hydroxide (KOH), and DMSO were used as supplied. The assay buffer, hemin, and arachidonic acid were prepared as per the instructions mentioned in kit. The supplied inhibitors and conjugates were incubated with both enzymes at room temperature. A 10 µL of 10-acetyl-3,7-dihydroxyphenoxazine (ADHP) was added followed by 10 µL of arachidonic acid (reaction initiator). The black plates were incubated for 2 min at room temperature and fluorescence spectra was recorded at an excitation wavelength of 530 nm and emission wavelength of 585 nm using a plate reader. The percentage of COX-1 and COX-2 inhibition was calculated using the following equation:

$$\% \text{ COX Inhibition} = \frac{(\text{COX activity no inhibitor} - \text{NSAID/peptide activity})}{\text{COX activity no inhibitor}} \times 100 \quad \text{Equation 3.4}$$

Selectivity index, S (% COX-2 inhibition/% COX-1 inhibition), of all conjugates towards both enzymes was also measured, and the fluorescence of the background was subtracted from fluorescence obtained for samples. The percentage inhibition of conjugates was compared with the provided test inhibitors and NSAIDS (Npx and Ind) alone to determine whether the conjugation of NSAID to peptides altered their selectivity towards COX-2 enzyme. The assay was done in triplicates. The in silico molecular modelling studies were also carried out, and the details are provided in the **Appendix**.

3.3.11. In vitro antibacterial activity

The antibacterial activities of conjugates and gels were evaluated against Gram-positive bacterial strain, *Staphylococcus aureus*, by optical density (OD) and colony counting method. *S. aureus* was cultured in Luria-Bertani (LB) culture medium (37 °C and 100 rpm) for overnight to reach the mid-log phase. The resulting bacterial suspensions were diluted to adjust the OD₆₀₀ value to 0.1 AU (1 × 10⁷ cfu/mL) using the fresh LB medium. A 100 µL of gel was prepared in 96 well plate, dried under vacuum for 72 h, followed by UV sterilization for 30 min. The dried gels were equilibrated with 50 µL of fresh LB media for 2 h, and 100 µL of bacterial suspension was added to it and kept inside a constant temperature shaker (37 °C, 100 rpm) for incubation. OD₆₀₀ values of supernatants were recorded at 0, 2, 4, 6, 12, and 24 h, using a multimode plate reader. The percentage bacterial inhibition was calculated using the following equation:

$$\% \text{ Antibacterial Activity} = \frac{\text{OD of negative control} - \text{OD of sample}}{\text{OD of negative control}} \times 100 \quad \text{Equation 3.5}$$

Fresh LB was considered as a blank, whereas bacterial strain in LB was taken as a negative control and gentamycin sulfate (0.1 mg/mL) was taken as a positive control. After 12 h, the bacterial solution in both controls and samples were serially diluted for 10^4 times and 100 μ L solution was plated on Luria-agar plates. These plates were incubated at 37 °C until the colonies were properly visible. The number of colonies grown in sample plates were compared with that of negative control.

Bacterial viability by live-dead staining. To investigate the viability of *S. aureus* in presence of conjugates and gels, the live/dead assay was done. After incubating bacterial solution with samples for 12 h, as described earlier, 100 μ L of bacteria was withdrawn from each well and treated with a 50 μ L of SYTO 9 (Ex/Em = 483/503) and PI (Ex/Em = 535/617) mixture (1:1 in DI water) followed by an incubation of 15 min in dark at RT. A 10 μ L of stained bacterial cells were mounted on glass slides and images were acquired using a Leica microscope.

Morphology of bacteria. The change in morphology of bacteria before and after contact with gels was investigated by high resolution transmission electron microscope (HR-TEM). Gels (1.33 or 2% w/v) were treated with bacterial suspension for 12 h, and the suspension was collected and centrifuged (10000 rpm, 4 °C, 10 min) to obtain bacteria in pellet. Multiple batches of samples were treated with bacterial suspension to collect enough number of bacteria for HR-TEM study. The pellet was resuspended in 500 μ L of PBS (pH 7.4) and centrifuged three times for washing. A 3.5% v/v glutaraldehyde solution was added for fixation and kept at 4 °C for overnight. The samples were washed again with PBS and stained with 1% osmium tetroxide solution for 30 min, followed by dehydration using the graded ethanol (30, 50, 70 and 90%). The pellet was finally suspended in 100% ethanol and about 5 μ L of sample was placed on a carbon-coated copper grid (mess size: 300), air dried, and imaged using HRTEM.

3.3.12. Inhibition of biofilm formation

Gels (1.33 or 2% w/v) were formed in a 48-well plate, dried under vacuum for 72 h, UV sterilized, and 200 μ L of *S. aureus* suspension ($OD_{600} = 0.1$) and 50 μ L of LB media was added to each well and kept at 37 °C inside an incubator under static condition to allow the biofilm formation. In case of conjugates, a suspension was prepared in 50 μ L of LB followed by the addition of 200 μ L of bacterial suspension. After 48 h of incubation, the wells were gently washed with PBS for three times to remove the samples and planktonic cells, and 200 μ L of 0.1% (w/v) crystal violet solution in ethanol was added to each well and incubated again for 15 min in dark. The excess crystal violet was aspirated and wells were washed with PBS and air dried. The cell bound crystal violet was dissolved in 30% acetic acid and the growth of biofilm was observed by measuring the absorbance at 570 nm using a plate reader. Biofilm without any sample was considered as a negative control.

3.3.13. Biofilm eradication

The conjugates and gels were UV sterilized. A 200 μ L of *S. aureus* suspension ($OD_{600} = 0.1$) was added to a 48 well plate and incubated at 37 °C for 48 h under static condition to allow the formation of integrated SA biofilm. The same method as described earlier was used for this study. In addition, the

effect of these materials on the viability of biofilm was also determined by LIVE/DEAD (SYTO 9/propidium iodide) staining.³⁰ After 24 h of treatment of matured biofilm with samples, the wells were gently washed with PBS. Staining solution was prepared in DI water at a concentration of 5 $\mu\text{L}/\text{mL}$ for each dye from a stock solution of 3.34 mM of SYTO 9 and 20 mM of PI. A 10 μL of this solution was added to each well with 190 μL of DI water and incubated in dark for 30 min. The wells were rinsed with DI water to remove the excess dye and biofilm was analyzed using a fluorescence microscope.

3.3.14. Cell viability

The cytocompatibility of conjugates and gels were evaluated on mouse fibroblast (L929) and macrophage-like (RAW 264.7) cell line by MTT, CCK-8, and live/dead assays.

MTT and CCK-8 Assay: L929 was cultured in RPMI medium and RAW was cultured in DMEM medium. Complete media was prepared by supplementing 10% fetal bovine serum (FBS) and 1% antibiotic. Both cell lines were incubated at 37 °C in a humidified environment containing 5% CO₂. Cells were passaged at regular interval until they reached 80% confluency. Conjugates and gels were prepared (1.33 or 2% w/v, 100 μL , freeze dried) and sterilized, as described earlier. Samples were immersed in 1 mL of complete media (RPMI/DMEM), extracted for 24 h at 37 °C, and passed through a syringe filter to remove particulates. Cells (L929/RAW) were seeded in a 96 well plate with a seeding density of 10⁴ cells/well, and the original cell culture media were replaced by sample extracts (200 μL) after 24 h of incubation, and cells were incubated with sample extracts for another 24 h. MTT solution (20 μL , 5 mg/mL in PBS) was added into each well and incubated for 4 h in dark. The media with MTT solution was aspirated without disturbing the formazan crystals formed in wells. A 100 μL DMSO was added to each well, and the plate was shaken gently at room temperature for 15 min to dissolve the crystals, which led to the development of purple color. The absorption was measured by a plate reader at 570 nm. Cell without any sample extract was considered as control. The cell viability was calculated using the following equation:

$$\% \text{ Cell Viability} = \frac{\text{Absorbance of sample}}{\text{Absorbance of control}} \times 100 \quad \text{Equation 3.6}$$

Cell proliferation properties were also determined by cell counting kit-8 assay. Cells (L929) were seeded in a 96 well plate and treated with sample extracts. After 24 h of incubation, 10 μL of CCK-8 solution was added to each well followed by another incubation of 3.5 h. A 100 μL of medium from each well was transferred to another 96 well plate and optical density of the orange color solution present in each well was measured at 450 nm. The cell viability was calculated using the **equation 3.6**.

Live-Dead Staining. Live/dead staining was done using manufacturer's protocol. Conjugates and gels were sterilized and extracts were collected as mentioned earlier. Cells (L929/RAW) were seeded at a density of 2 \times 10⁴ cells/well in a 48 well plate at 37 °C in a humidified environment containing 5% CO₂ for 24 h. Media was aspirated and 200 μL of sample extract was added to each well and further incubated for 24 h. Samples were withdrawn and 150 μL of dye solution containing a mixture of calcein AM and

ethidium bromide in PBS was added and incubated for another 30 min avoiding any exposure to light. A fluorescence microscope was used to image cells.

3.3.15. Cytoskeletal staining

Immunostaining was performed on L929 cells to investigate the shape and structure of cells after treatment with gel extracts. To image F-actin filaments in live cells, Alexa Fluor 588 phalloidin was used. Cells were seeded on a coverslip and incubated for 24 h at 37 °C in a humidified environment containing 5% CO₂. The media was replaced with gel extracts and incubated for 24 h. The sample extract was aspirated, washed with PBS, and cells were fixed with 4% solution of paraformaldehyde for 30 min. Next, cells were washed with PBS, and 0.1% triton X-100 was used to permeabilize cells for 15 min. A working solution of Alexa Fluor 488 phalloidin was prepared by diluting the stock solution (66 µM) 40 times with DPBS to stain F-actin and 300 nM DAPI solution was prepared in DPBS to stain the cell nuclei. After cell permeabilization, 200 µL of dye was added and kept under dark for 30 min, followed by washing with PBS and incubation with 200 µL of DAPI for 10 min. The coverslip was fixed on to the glass slide with the help of mounting solution and imaged under a fluorescent microscope.

3.3.16. In vitro wound healing

The in vitro wound healing potential of the drug-peptide conjugate gel was confirmed by scratch assay following a reported protocol.¹⁴ L929 cells were seeded into a 6 well plate with a density of 10⁵ cells/well and incubated until the cells reached 100% confluency. A cell monolayer was scraped in a straight line with a sterile 200 µL tip to develop a distinct scratch. The cell debris was removed by gently washing every well with 1 mL of PBS, and the extract media was added and incubated at 37 °C. After 12 and 24 h, images were acquired by an inverted microscope (Evos XL core, Invitrogen) to monitor healing, and compared to a control well (cells without treatment with extract media). The percentage wound healing was calculated in terms of the percentage of initial scratch area using ImageJ software and following equation:

$$\% \text{ of Initial Scratch Area} = \frac{\text{Area at time } t}{\text{Area at 0 h}} \times 100 \quad \text{Equation 3.7}$$

where, t = 12 and 24 h.

3.3.17. ROS scavenging assay

The impact of gels on the level of intracellular reactive oxygen species (ROS) in living cells was evaluated in H₂O₂ stressed RAW 264.7 macrophages using the oxidant-sensitive fluorescent probe H₂-DCFDA. Cells (1 × 10⁴) were incubated in Nunc-coated 96 well black plates at 37 °C in a humidified environment containing 5% CO₂. After 24 h of incubation, the media was aspirated, and 100 µL of sample extracts (samples incubated for 24 h with incomplete media and syringe-filtered) were added to each well and again incubated for 24 h. Next, cells were exposed to 0.5 mM of H₂O₂ solution to induce the production of ROS, and the media was aspirated, washed with PBS, and finally treated with 25 µM of DCFDA solution. After 1 h of exposure in dark, incomplete media containing DCFDA was

withdrawn, PBS was added, and fluorescence intensity was measured on a plate reader at an excitation and emission wavelengths of 485 and 530 nm. Cells without any sample extracts were considered as a negative control and ascorbic acid (1 mg/mL) was taken as a positive control. The radical scavenging was quantitatively estimated. For qualitative analysis of ROS production inside cells, same protocol was followed as mentioned earlier. Instead of Nunc-coated black 96 well plate, 48 well plate was used and 2×10^4 cells/well were seeded. FITC channel in the fluorescence microscope was used to visualize the intracellular DCFDA in cells. The protective effect of conjugates and gels on the viability of oxidative stress induced macrophages was evaluated by MTT assay. A 100 ng/mL of lipopolysaccharide (LPS) was used to inculcate oxidative stress into macrophages.

3.3.18. In vitro anti-inflammatory effect

The effect of gels on inflammatory (TNF- α and IL-6) and anti-inflammatory (IL-10) gene expressions in RAW 264.7 was analyzed using Q-RT PCR methods. RAW 264.7 were cultured in 6 well plate and exposed to LPS (100 ng/mL) in DMEM for 12 h before incubation with 1 mL of sample extracts. After 24 h, total cellular mRNA from each well was isolated using Trizol reagent (Invitrogen), and 1 μ g of this mRNA was converted to cDNA using BioRad cDNA synthesis kit, according to the manufacturer's instructions. Quantitative RT-PCR was performed using SYBR green to detect inflammatory and anti-inflammatory markers. Glyceraldehyde-3-phosphate dehydrogenase (GAPDH) served as a house keeping gene for internal control. The primer sequences used for amplification are mentioned in **Table A1, Appendix**. The results are presented as a fold-change relative to control cells (without any treatment of LPS or sample extracts).

3.3.19. Statistical analysis

All experiments were performed in triplicates and data are presented as mean \pm standard deviation (SD). Comparisons between two groups were performed using Student's t-test, and $p < 0.05$ (*) was considered as statistically significant.

3.4. Results and discussion

The objective of this work was to develop an antimicrobial supramolecular peptide gel to eradicate biofilms and rescue stalled inflammation associated with chronic wounds. We have developed supramolecular gels from naproxen (Npx)- and indomethacin (Ind)-conjugated peptides, Npx-^LTyr-^LTyr-^DLys-NH₂ (Npx-YYk), Npx-^LTyr-^LTyr-^DArg-NH₂ (Npx-YYr), Ind-^LTyr-^LTyr-^DLys-NH₂ (Ind-YYk), and Ind-^LTyr-^LTyr-^DArg-NH₂ (Ind-YYr), and evaluated their antibacterial, antibiofilm, radical scavenging, anti-inflammatory, and wound healing potential in cell culture (**Figure 3.1**). The two Ys in the sequence were used for their antioxidant properties and ability to form gels, and cationic K and R were used for their antibacterial and antibiofilm properties. The Npx and Ind conjugated to the peptide are NSAIDs that exert anti-inflammatory effect by nonselective inhibition of COX-1 and COX-2 enzymes, which leads to side effects. K and R were used in the D-form to enhance the proteolytic

stability of peptides and improve its selectivity for COX-2 enzyme. The nanofibers can mimic the extracellular matrix structures, which can facilitate cell adhesion, migration, and proliferation.

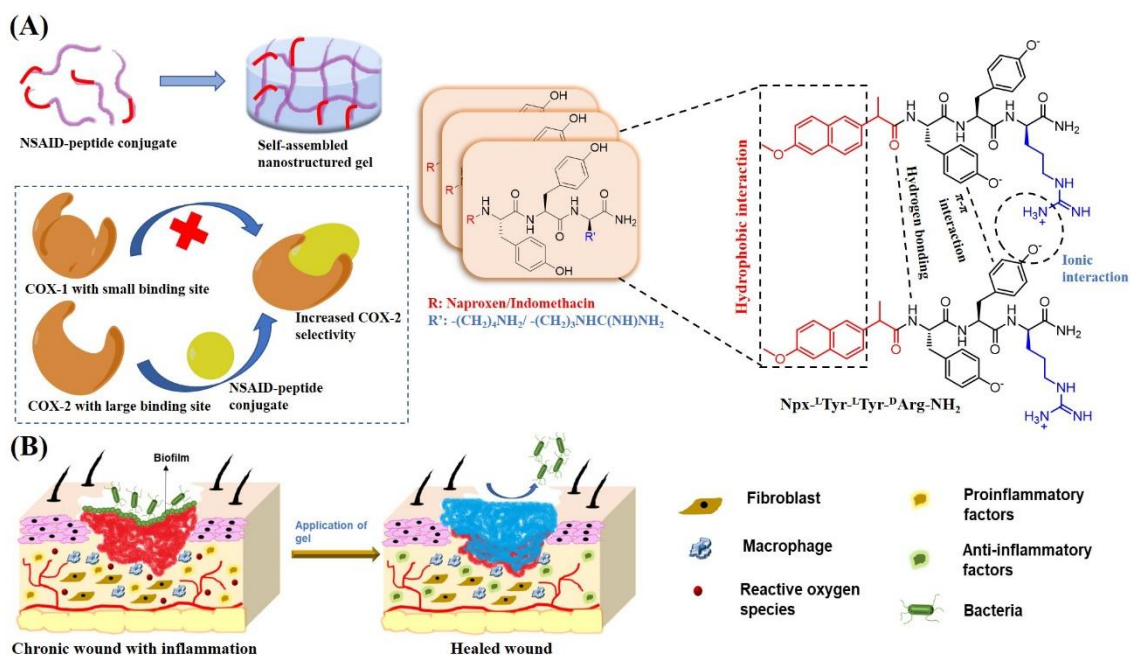


Figure 3.1. (A) Naproxen (Npx)- and indomethacin (Ind)-conjugated with peptides forming supramolecular gels by non-covalent interactions for selective COX-2 inhibition (anti-inflammatory). (B) Application of gel at the site of wound to promote healing by exerting antibacterial, antibiofilm, antioxidant, and selective COX-2 inhibition (anti-inflammatory) activities.

3.4.1. Synthesis and characterization of drug-peptide conjugates

Peptides were synthesized utilizing a Fmoc-based solid-phase peptide synthesis technique. Non-steroidal anti-inflammatory drugs (NSAIDs), naproxen (Npx) and indomethacin (Ind), were conjugated to peptides at the N-terminus to produce the following conjugates: naproxen- L -Tyr- L -Tyr- L -Lys- NH_2 (Npx-YYK), naproxen- L -Tyr- L -Tyr- D -Lys- NH_2 (Npx-YYk), naproxen- L -Tyr- L -Tyr- L -Arg- NH_2 (Npx-YYR), naproxen- L -Tyr- L -Tyr- D -Arg- NH_2 (Npx-YYr), indomethacin- L -Tyr- L -Tyr- L -Lys- NH_2 (Ind-YYK), indomethacin- L -Tyr- L -Tyr- D -Lys- NH_2 (Ind-YYk), indomethacin- L -Tyr- L -Tyr- L -Arg- NH_2 (Ind-YYR), and indomethacin- L -Tyr- L -Tyr- D -Arg- NH_2 (Ind-YYr) (**Figure 3.2A-D** and **Figure A18, Appendix**). Therefore, the peptide sequences were made up of positively charged K/k or R/r in L- or D- form for increased antibacterial action and selective inhibition of COX-2 enzyme, and hydrophobic Y residues as the center component to impart self-assembling property. The conjugates were characterized by RP-HPLC, 1H NMR, and mass spectrometry. RP-HPLC analysis showed 90-95% purity and retention times were found as 2.6 (Npx-YYK), 2.5 (Npx-YYk), 3.9 (Npx-YYR), 3.9 (Npx-YYr), 4.6 (Ind-YYK), 4.6 (Ind-YYk), 4.4 (Ind-YYR), and 4.4 min (Ind-YYr) (**Figure A19, Appendix**). Due to its increased hydrophobicity, indomethacin increased the retention period. The molecular weights of conjugates determined by mass spectrometry matched those predicted by theory (**Figure A20-27, Appendix**). The

¹H NMR spectra of conjugates along with their peak assignments are included in the **Appendix (Figure A28-35)**.

3.4.2. Preparation and characterization of gels

The amphiphilic peptide-conjugates were self-assembled into supramolecular gels. The Npx-conjugated gels were formed by using a pH-trigger approach and Ind-conjugated gels by a solvent-switch method (**Figure 3.2E, A36, Appendix**). At pH 9 or higher, the Npx-conjugates produced clear solutions, and gelation was induced by adding a drop of NaOH solution. At pH 9, Ind-conjugates were precipitated out because it was slightly more hydrophobic than Npx and did not produce clear solutions. We employed the solvent switch approach to gel these conjugates since they could be dissolved in DMSO. Within a few hours, the gel formed after water was gradually added to the DMSO solution. A crucial balance between the molecule hydrophilicity and hydrophobicity of the surrounding media, particularly water, which creates hydrogen bonding connections, is needed for conjugates to self-assemble. Drugs' aromatic rings and the amino acids in the peptide sequence induce hydrophobic π - π stacking, which promotes intermolecular interactions and aids in the formation of supramolecular gels.

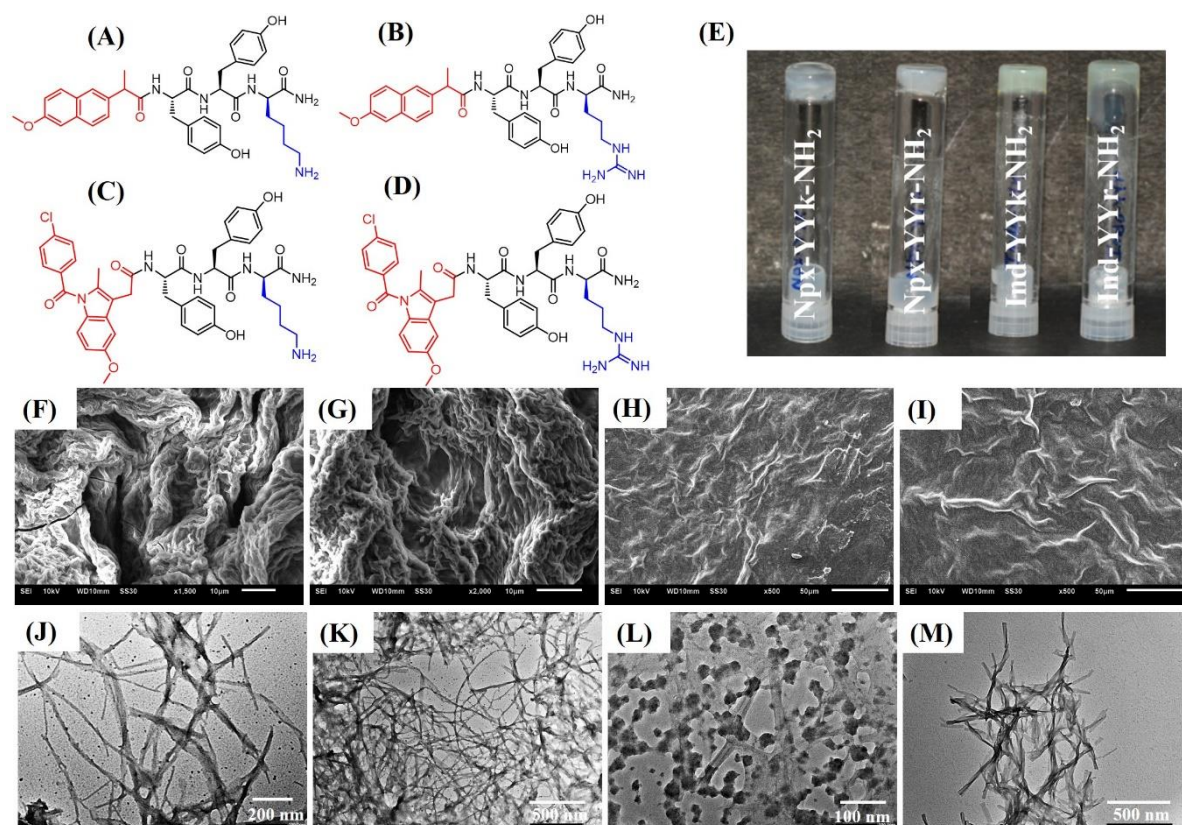


Figure 3.2. Structure of NSAID-peptide conjugates used to form supramolecular gels. (A) Npx-YYk. (B) Npx-YYr. (C) Ind-YYk. (D) Ind-YYr. (E) Images of 2% (w/v) gels in inverted vials. (F-I) SEM images. Scale bar: 10 μ m. (J-M) HR-TEM images of dried gels (2% w/v). (F, J) Npx-YYk. (G, K) Npx-YYr. (H, L) Ind-YYk. (I, M) Ind-YYr.

To better understand the nanoscale architecture of molecular assemblies, images were obtained using SEM (**Figure 3.2F-I**) and HR-TEM (**Figure 3.2J-M**). The SEM images of Npx-YYk and Npx-YYr showed entangled, twisted networks, whereas the HR-TEM images demonstrated that the peptide gelators self-assembled into thin, long, flexile nanofibers. These nanofibers ranged in width from 10 to 20 nm and were made to reach lengths of several micrometers. In order to create a nanofibrillar network of gels, the self-assembling gelator molecules engage in non-covalent interactions, such as hydrogen bonding and hydrophobic contact. A self-supporting gel is formed when water is trapped in the large amount of space that the nanofiber network provides. In case of 2% Ind-conjugated gels, the hydrophobic segments were packed densely away from the aqueous interface, generating non-homogeneous, nanotape-like structure. The immobilization of surrounding solvent molecules inside these networks lead to gel formation.

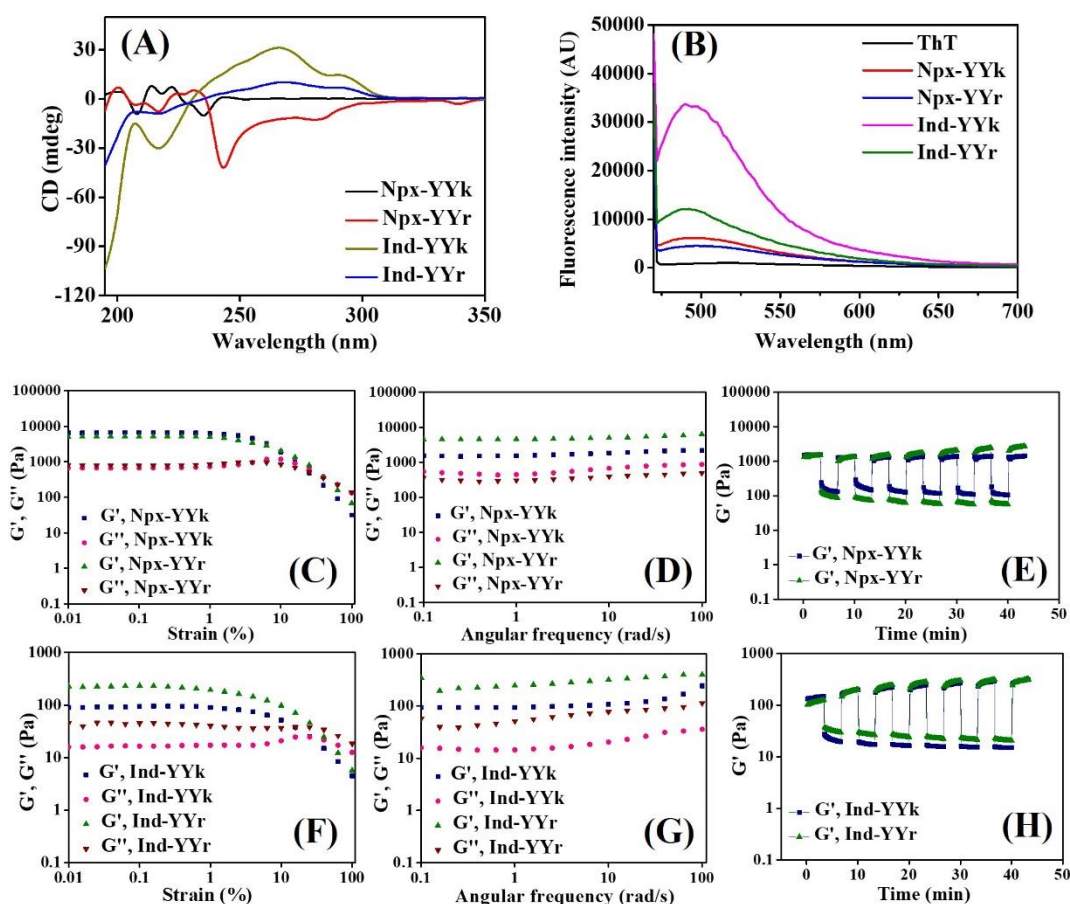


Figure 3.3. (A-B) Secondary structures formed by peptide conjugate gels. (A) CD spectra. (B) Thioflavin-T (ThT) binding assay. (C-H) Rheological analysis of gels (2% w/v). (C, F) Amplitude sweep demonstrating storage and loss modulus, and crossover values at a constant angular frequency of 10 rad s⁻¹. (D, G) Frequency sweep at a constant strain of 1%. (E, H) Storage modulus at alternating strains of 30% and 0.1% for 6 cycles.

To comprehend the mechanism of self-assembly, intermolecular interactions that reveal the formation of secondary structure were examined. The primary function of circular dichroism (CD) is to investigate

the secondary structures found in peptide conjugates. The signals in CD spectra were dominated by the high extinction coefficient connected to collateral coupling of π - π systems. Indomethacin conjugates showed characteristic peaks for β -sheet conformations along with random coil. A large negative peak around 200-220 nm and a positive peak close to 195 nm (**Figure 3.3A**). The formation of a β -sheet structure by stacking phenyl rings found in the side chains of amino acids was indicated by a local-maxima at about 235 nm. Naproxen conjugates exhibited random coil or disordered conformation. FT-IR spectroscopy was used to study the hydrogen bonding interactions between the peptide backbones, another factor that promotes self-assembly.³¹ Characteristics peaks of amide I at 1620-1690 cm^{-1} , amide II at 480-1575 cm^{-1} , and amide III at 1229-1390 cm^{-1} suggests the possibility of β -sheet like structures in the peptide conjugates (**Figure A37, Appendix**). Owing to the less intense peak of amide I, one cannot claim the presence of β -sheets only. The thioflavin-T (ThT) assay was also used to verify β -sheet like structures. The presence of β -sheet conformation in self-assembled structures, arising from π - π interactions, is suggested by the fact that ThT's fluorescence intensity was greatly increased when treated with gels (**Figure 3.3B**). At pH 8.5, all conjugates were found to have positive zeta potentials, however those containing arg, such as Npx-YYr (30.9 mV) and Ind-YYr (28.46 mV), showed more positive charge due to the presence of guanidinium group than those containing lys, such as Npx-YYk (24.2 mV) and Ind-YYk (14.33 mV).

3.4.3. Rheological studies

Rheological investigations were used to determine the stability and mechanical strength of gels. The 2% (w/v) gels were used in this study and kept overnight at 37 °C before the experiment. In case of amplitude sweep study, the storage modulus (G') was higher than the loss modulus (G'') suggested that gels have an elastic quality. The maximal storage modulus of the Npx-conjugated gels, Npx-YYk and Npx-YYr, which was roughly seven to ten times higher than the maximal loss modulus (600-800 Pa), demonstrating that these gels have the characteristics of a solid-like material (**Figure 3.3C**). G' and G'' were almost independent of angular frequency for the frequency sweep experiment, demonstrating a good tolerance to external shear force (**Figure 3.3D**). As a result of the presence of Npx and aromatic group in tyrosine, there were greater π - π and van der Waals' intermolecular interactions, which caused the fibers to grow longer and become entangled. According to McCloskey *et al.*,²³ gels made from Npx-FFKK exhibited less storage and loss modulus compared to what we presented here. It might be caused by the replacement of phe with tyr. Gels can become more robust by hydrogen bonding, which is induced by the -OH in the side chain of tyr. The storage modulus of these gels is nearly identical to the Nap-GFFKH gel, reported by Cui *et al.*,²⁸ and the viscoelastic properties are comparable to the dopamine substituted multidomain hydrogel reported for wound healing applications earlier.⁸ When compared to Npx-conjugated gels, the Ind-YYk and Ind-YYr gels showed a lower storage and loss modulus, which can be explained by the creation of shorter nanotape structures rather than the longer, entangled nanofibers seen in Npx-containing gels (**Figure 3.3F, G**). Higher storage modulus was found in arg-containing gels, indicating that it is preferable to build intermolecular hydrogen bonds and start the self-assembling of gels.

A significant high strain (30%) reduced the storage modulus but after the strain was relieved (0.1%), the gels recovered their storage modulus, demonstrating their self-healing abilities (**Figure 3.3E, H**). In order to make a direct comparison, the viscoelastic properties of gels containing only L-amino acids were also assessed. These gels displayed significantly higher storage moduli than gels containing a D-amino acid, which could be explained by the stronger non-covalent interactions in the L- conformation that promotes a stronger self-assembly and higher storage modulus (**Figure A38, Appendix**).

As previously described, a chronic inflammatory wound's pH changes to an alkaline pH of 8.5 or higher.³² The cause of this elevated pH is the bacteria's synthesis of the enzyme urease, which catalyzes the generation of ammonia from urea and raises pH levels that encourage bacterial adhesion and development at the wound surface. In comparison to 30-40% degradation at neutral pH, gels degraded by about 20% at pH 8.5 (**Figure A39, Appendix**). K, R, and Y have pK_a values of 10.53, 12.48, and 10.07 for their amino acid side chains, respectively. Peptides continue to be more protonated at pH 7.4 compared to 8.5, which results in the dissociation of self-assembly in supramolecular gels at neutral pH.

3.4.4. Proteolytic stability

After being exposed to a simulated cocktail of proteolytic enzymes, proteinase K, chymotrypsin, and pepsin in PBS (pH 7.4) at 37 °C for up to 24 h, all four D-amino acid gels showed extraordinary resistance to proteolysis. RP-HPLC analysis was performed at various time points to assess the peptide breakdown and digestion by enzymes, and the RP-HPLC profiles of digested conjugates are presented in the **Appendix (Figure A40-43)**. The percentage of conjugate that is still undegraded or remaining was calculated using the area under the curve. Only 15-25% of the conjugates with peptides including a D-amino acid was degraded, while 40%-50% was degraded for control conjugates with all L-amino acids (**Figure 3.4A, B**). The outcomes are equivalent to those of peptide gels made of D/L(FKFE)₂-NH₂, as reported by Swanekampet *et al.*,³³ and those of Baral *et al.*,³⁴ who used a combination of natural and synthetic amino acids. These gels are also equivalent to the $\alpha\gamma$ -peptide gels that our group previously reported in terms of proteolytic stability.

3.4.5. Radical scavenging activity

Antioxidant material insertion has proven to be a successful method for accelerating the healing of chronic wounds. By using ABTS and DPPH assays, the free radical scavenging capacity of conjugates and gels was assessed. All conjugates and gels exhibited more than 90% ABTS⁺ radical scavenging activities, and 70-75% of DPPH⁺ scavenging activity (**Figure 3.4C, D**). The results for both assays were compared with ascorbic acid (1 mg/mL), which was considered as a positive control and ABTS and DPPH radical without samples were taken as a negative control. Conjugation of antioxidant peptides with NSAIDs like Npx and Ind can decrease the chance of ulcers developed by NSAIDs. The gels mentioned here have antioxidant capabilities that are superior to those of peptide gels published by Wei *et al.*,³⁵ Araujo *et al.*,⁵ and comparable with the scaffold reported by Csire *et al.*³⁶

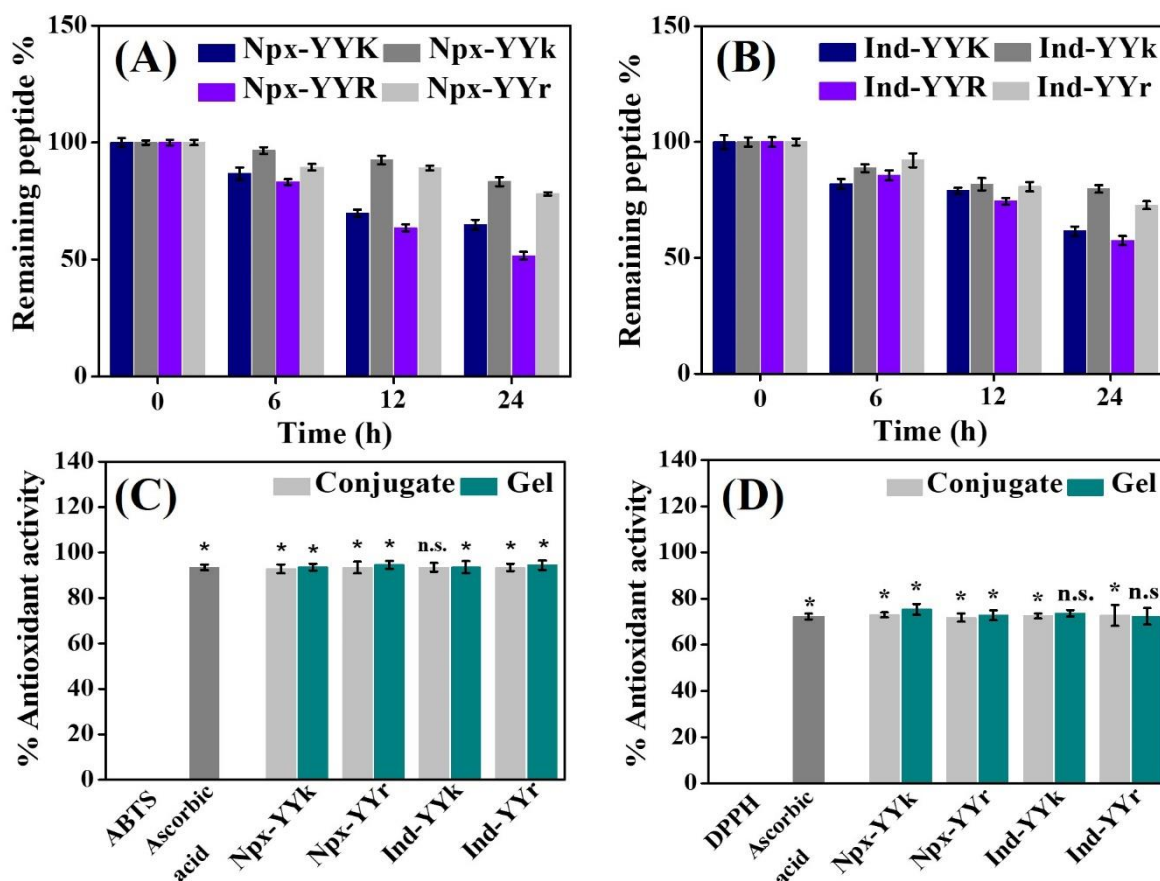


Figure 3.4. Proteolytic stabilities and antioxidant activities. (A, B) Proteolytic stabilities of gels (2% w/v) treated with a mocktail of proteolytic enzymes at pH 7.4. (C, D) Antioxidant activities of peptide conjugates and gels. (C) ABTS assay. (D) DPPH assay. ABTS and DPPH were used as negative controls (radicals without sample) and ascorbic acid (1 mg/mL) as a positive control. Data are presented as mean \pm SE (n = 3). Comparisons between two groups (samples to control) were performed using Student's t-test. *p < 0.05 indicates statistically significant data.

3.4.6. Cyclooxygenase enzyme inhibition

COX-2 suppression is advantageous since its activity is linked to the erroneous formation of scar tissues during the later stages of wound healing. The structural distinction between COX-1 and COX-2 binding sites has a significant impact on the development of selective COX-2 inhibitors. The second pocket in the cyclooxygenase binding site, which is easier to access in COX-2 due to the replacement of ile523 (found in COX-1) with val523, a smaller side chain residue, is the main difference. Small peptides were conjugated to the carboxylate group present in Npx and Ind in order to specifically bind to the large open region of COX-2 isoform. The selectivity towards COX-2 was found to be enhanced by amino acids in the D-isofom.

To assess the effectiveness of NSAID-peptide conjugates for selective COX-2 inhibition, we carried out in vitro inhibition assays for both COX-1 and COX-2 (**Figure 4A**). With selectivity indices of 0.74 and 0.87 ($S = \% \text{ COX-2 inhibition} / \% \text{ COX-1 inhibition}$), Npx and Ind inhibited COX-1 more effectively than COX-2. In comparison to NSAIDs alone, NSAID-peptide conjugates showed improved selectivity

for COX-2. In contrast to their L-isoforms, Npx and Ind conjugated to peptides containing D-amino acids improved their selectivity towards COX-2 (**Figure 3.5A**). COX-1 and COX-2 were not significantly inhibited by peptides without NSAID conjugation (**Figure A44, Appendix**). With a S value of 2.47, Npx-YYk had the maximum selectivity, while its L-isoform (Npx-YYK) only displayed a S value of 1.07. The conjugates containing arg showed a more profound cyclooxygenase inhibition property than the lys-containing analogs, which can be attributed to the better H-bonding property of R with amino acids present inside the active binding pocket of COX-2 enzyme. As compared to NSAID-peptide conjugates previously reported, the selectivity towards COX-2 inhibition is nearly equal.^{23,37}

In silico molecular docking investigations were also carried out to comprehend the selective COX-2 inhibition displayed by conjugates. The ligand binding sites of the COX-1 (6Y3C) and COX-2 (1PXX) enzymes were docked with Npx, Ind, and their conjugates using AutoDock (**Figure A45, Appendix**). In appendix (**Table A2**), all ligands for both enzymes have been listed together with their binding energies, interactions, and selectivity indices. This work further demonstrated that conjugates have stronger selectivity for COX-2 than free drugs, and that the selectivity is enhanced by the inclusion of a D-amino acid in the peptide sequence.

3.4.7. In vitro antibacterial study

The antibacterial activity of these gels was examined against Gram-positive bacteria, *S. aureus*, which is the primary pathogenic organism linked to chronic wound infection, in order to study the possibility that the NSAID-peptide conjugate gels can be employed as an antibacterial scaffold. As a positive control, gentamycin sulphate (0.1 mg/mL) was utilized. The optical density (OD) and colony counting methods were used to evaluate the antibacterial property. According to the OD experiments, the 2% w/v gels Npx-YYk, Npx-YYr, Ind-YYk, and Ind-YYr exhibited 60-65% antimicrobial activity after just 3 h and more than 95% activity in just 12 h. All conjugates and gels had antibacterial characteristics that lasted for 24 h, and the findings were comparable to those obtained with 0.1 mg/mL of gentamycin sulphate (**Figure 3.5B**). The two NSAIDs had very little inhibitory efficacy (15-20%) against *S. aureus*,³⁸ but >90% antibacterial activity was shown by peptides without NSAID conjugation (**Figure A46, A47 Appendix**). The positive charge of the cationic amino acid residues, k and r, which aids in penetrating the negatively charged bacterial cell membrane, may be the cause of the superior antibacterial activity of gels and peptides. The interaction with thick bacterial lipid layers can also be facilitated by hydrophobic tyr residues and drugs, Npx and Ind. Gels with arg residue demonstrated greater antibacterial action than peptides with lys, suggesting that the guanidinium group in arg has a higher positive charge than the amine group in lys.²²

The antibacterial activity was further confirmed by colony count method on agar plate (**Figure 3.5C**). After being treated with Npx-YYr and Ind-YYr, the agar plate containing the bacterial solution showed no visible colonies, indicating the outstanding antibacterial action of these gels, whereas, a significant reduction of colonies was observed for Npx-YYk and Ind-YYk. The activity against *S. aureus* is like the activity reported by Cao *et al.*,³⁹ Hou *et al.*,⁴⁰ Gahane *et al.*,⁴¹ Wang *et al.*,⁴² and Bai *et al.*⁴³

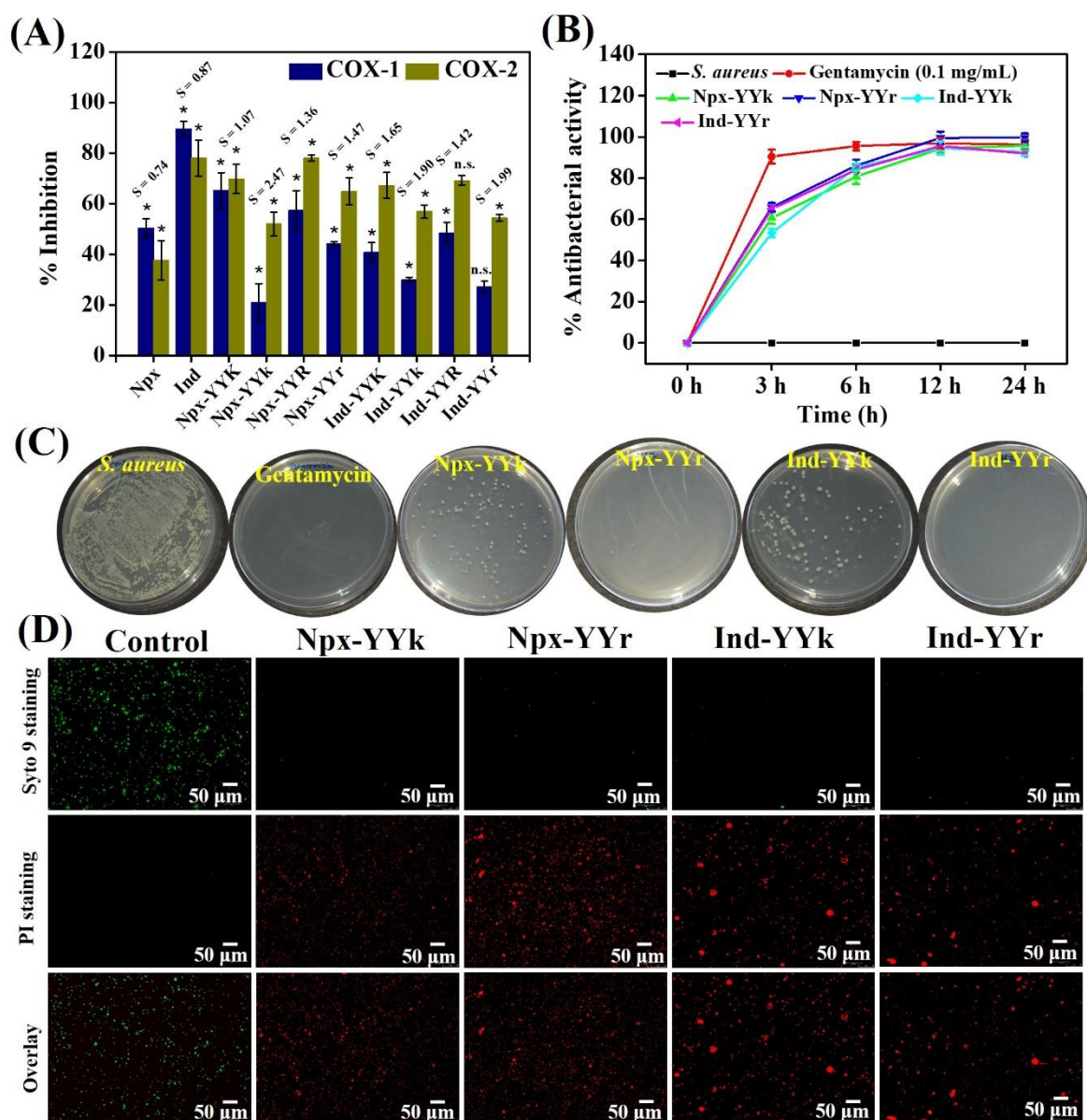


Figure 3.5. Cyclooxygenase (COX) enzyme inhibition and antibacterial activities. (A) Percentage inhibition of COX-1 and COX-2 enzymes by NSAID-peptide conjugates. S is the selectivity index, and it is defined as the ratio of COX-2 to COX-1 inhibition. (B) Evaluation of antibacterial activities of gels against *S. aureus*. Data are presented as mean \pm SD, n = 3, and *p < 0.05 indicates statistically significant data. (C) Images of bacterial colonies after treatment with gels. (D) Live/dead staining of bacteria after treatment with gels. Scale bar: 50 μ m.

Live/Dead cell staining of *S. aureus* treated with gels were performed with SYTO 9 and PI (**Figure 3.5D**) and fluorescence image of untreated *S. aureus* showed mostly green emission with very little red emission, which indicates that the cells were still alive. In bacteria treated with 2% gels, red color was frequently seen, signifying the presence of dead cells. This proved conclusively that the gel treatment significantly damaged the bacterial membrane.

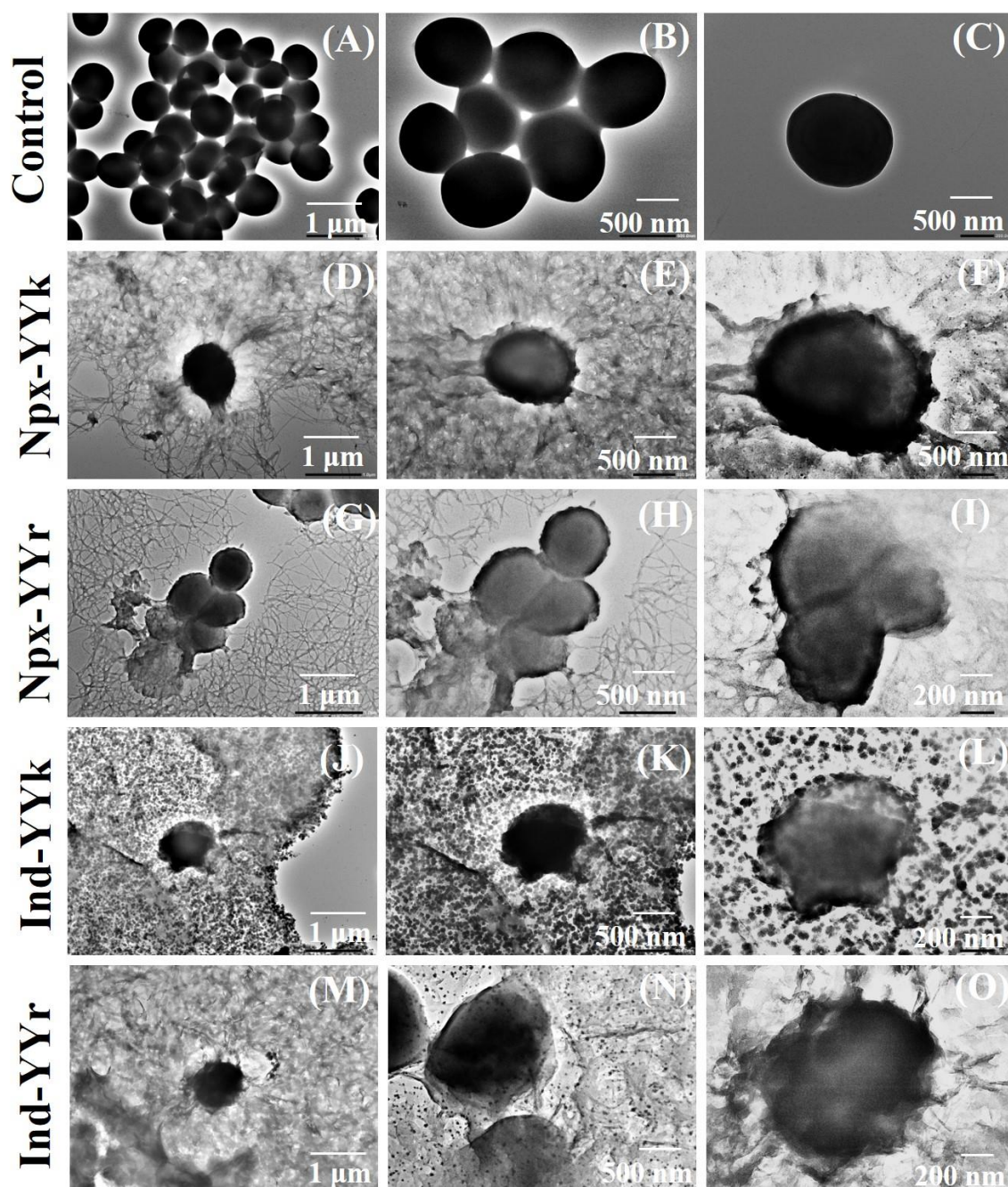


Figure 3.6. HR-TEM images of *S. aureus* bacteria. (A-C) Untreated. (D-O) Treated with 2% w/v gels: (D-F) Npx-YYk, (G-I) Npx-YYr, (J-L) Ind-YYk, and (M-O) Ind-YYr.

HR-TEM studies were carried out to investigate the mechanism of antibacterial effect of gels (**Figure 3.6**). It is evident from HR-TEM images that there are significant changes in bacterial cell wall morphology after treatment with gels. Micrographs of untreated *S. aureus* shows smooth and intact surface but upon interaction with gels, bacteria lose the structural integrity and surface intactness, which triggers the leakage of metabolites from bacterial cells. Adsorption of peptide on the bacterial surface is mainly driven by electrostatic interaction between cationic amino acids (lys and arg) in peptide and lipoteichoic acids in Gram-positive bacterial cell wall, leading to the formation of a transmembrane pore

in the peptidoglycan layer.^{44,45} Also, the hydrophobic amino acid, tyr can augment the diffusion through the lipid layer of bacteria.

3.4.8. Biofilm inhibition

The capability of gels for eradication of biofilm and disruption of preformed biofilm developed by *S. aureus* was examined using the crystal violet staining method. Around 80-90% of biofilm formation was inhibited by conjugates and gels (**Figure 3.7A**). Short peptides with hydrophobic and cationic residues typically have the strength to pierce and rupture bacterial membranes, resulting in the biocidal qualities that aid in the prevention of biofilm development.

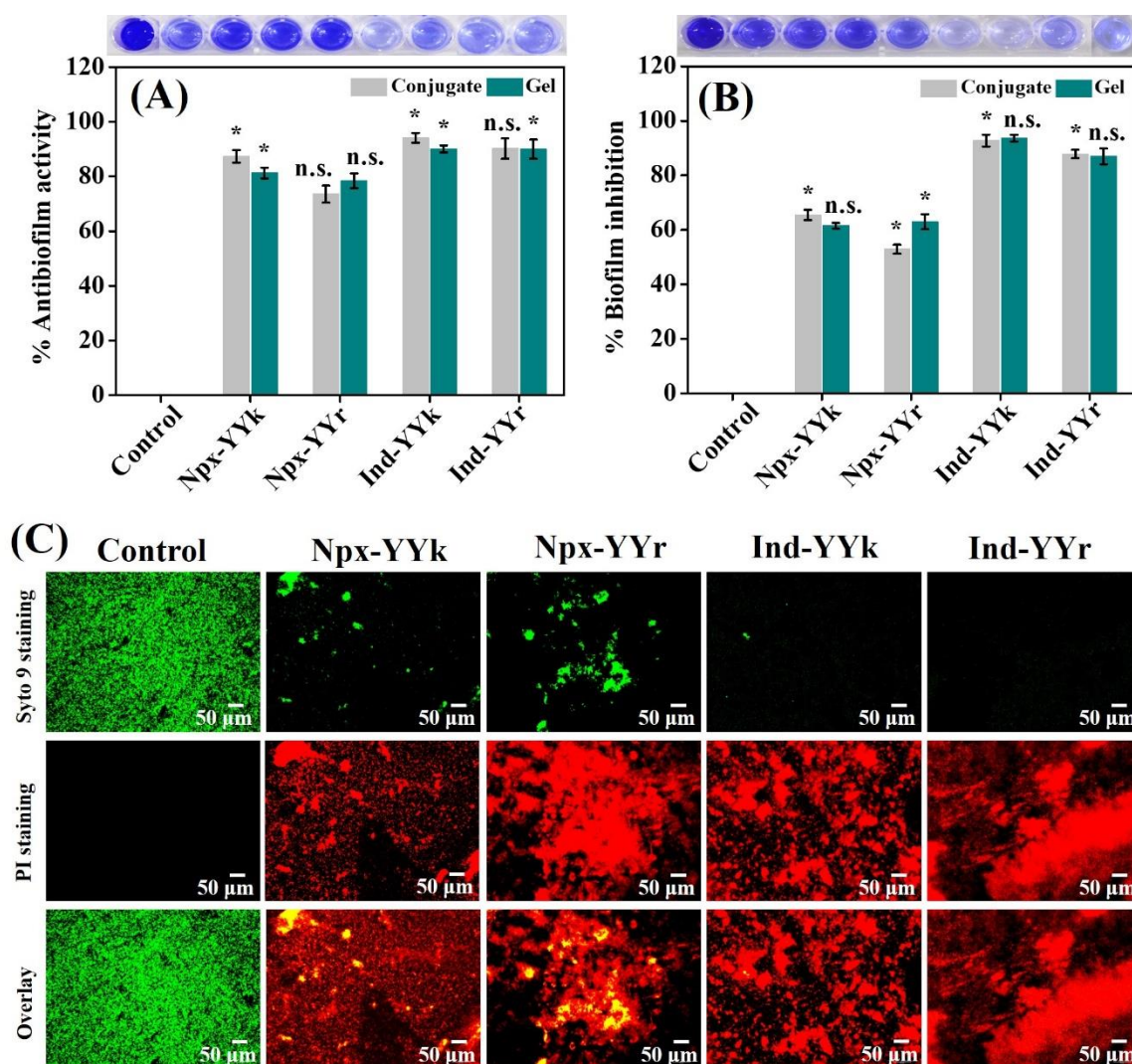


Figure 3.7. Biofilm inhibition by gels using crystal violet staining assay. (A) Biofilm formation. (B) Established biofilm. Data are presented as mean \pm SD, $n = 3$, and * $p < 0.05$ indicates statistically significant data. (C) Representative fluorescence microscopy images of biofilm formed by *S. aureus*. Control denotes the biofilm formed without any treatment with gels. Scale bar: 50 μ m.

The potential of antibacterial conjugates and gels in the destruction of preformed biofilms is illustrated in **Figure 3.7B**. Npx-conjugates and gels exhibited about 60% biofilm eradication activity, while Ind-

conjugates and gels had 85-90% activity. Bacteria secrete extracellular polymeric substances (EPS) while developing an integrated biofilm, and it is difficult to remove, which may be the reason for the reduced biofilm eradication efficacy. The ability of indole rings to prevent bacterial quorum sensing-based signal transmission could be the reason behind the destruction of the biofilm by Ind-conjugates. We hypothesize that incorporating positive charge and hydrogen bonding forming units to the peptide backbone will increase the hydrogen bonds and electrostatic interactions with the extracellular matrix components of the biofilm, like exopolysaccharides and extracellular DNA. Additionally, the lipophilic component of conjugates improves the contact with the bacterial membrane even more.

Staining of the biofilm was carried out to assess the effectiveness of gels in eradicating the stationary phase (metabolically inactive) cells and rupturing the produced biofilms of *S. aureus* (**Figure 3.7C**). Green fluorescence indicates an even, non-destructive coating of biofilm on the untreated bacteria, while red fluorescence indicates that the biofilm has been disrupted and bacterial cells have been killed on the gel treatment. Very few antimicrobial peptides with remarkable biofilm suppression properties have been reported till now and these gels are among those potential antibiofilm peptides that have been reported so far.⁴⁶

3.4.9. Cytocompatibility study

The cell viability of conjugates and gels were measured on murine fibroblast cells (L929), which is the most important cell in wound healing process and murine macrophage-like cells (RAW 264.7), which is involved in the inflammation stages of wound healing and gene regulation by MTT assay (**Figure 3.8A, B**). After 24 h of incubation, the compounds promoted proliferation in both the cell lines (up to 120% cell viabilities). CCK-8 assay also exhibited that gels are proliferative to L929 cells, when compared to control (**Figure 3.8C**).

These findings were further confirmed by performing live-dead staining on both cell lines and the fluorescence microscopic observation suggested that L929 cells grew well and showed spindle-like healthy morphologies and RAW 264.7 cells retained its round-shape morphology upon being in contact with the peptide-drug conjugates (**Figure A48, Appendix**) and gels (**Figure 3.8D, E**). Prevalence of green colored cells suggests that both conjugates and gel extracts did not affect the viability of these cell lines. Staining the F-actin and cell nucleus with Alexa Fluor 488 phalloidin and DAPI further confirmed the morphology of L929 cells (**Figure 3.9A**). After being treated with gel extracts, L929 cells still had a fibrous, spindle-shaped morphology that is equivalent to that of the untreated control group.

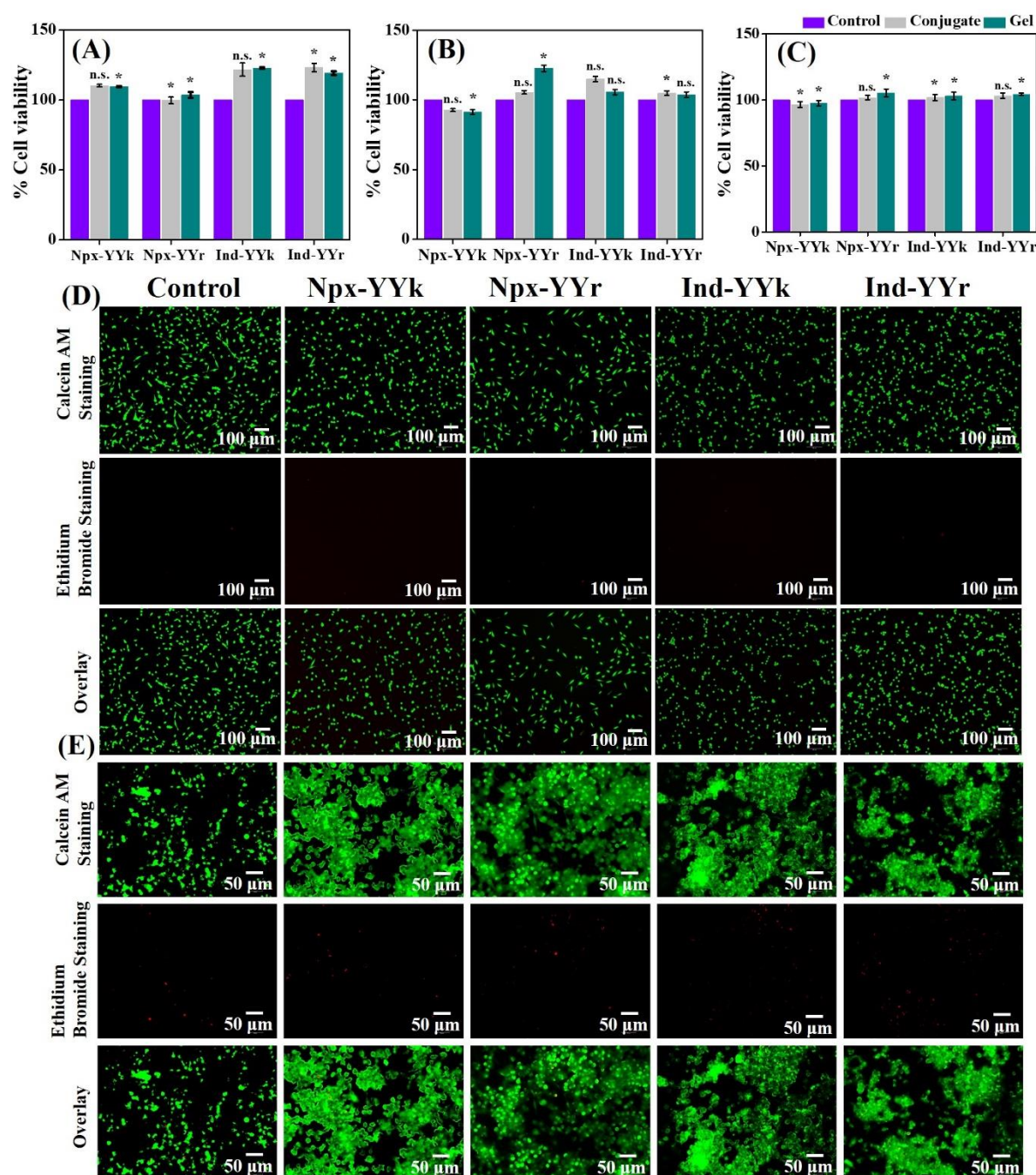


Figure 3.8. Cell viability assay of conjugates and gel extracts at 24 h. (A-B) MTT assay with L929 and RAW 264.7 cell lines. (C) CCK-8 assay with L929 cell line. Data are presented as mean \pm SD, $n = 3$, and $*p < 0.05$ indicates statistically significant data. (D, E) Live/Dead staining of mammalian cells after treatment with gel extracts for 24 h. (D) L929. (E) RAW 264.7. Cells were stained with calcein AM and ethidium bromide. Cells without any treatment were taken as a control. Scale bar: (D) 100 μm , and (E) 50 μm .

3.4.10. In vitro wound healing study

We further investigated the effect of these gels on two crucial factors of wound healing, cell migration and proliferation using the scratch assay with L929 cells (**Figure 3.9B**). The monolayer of cells was scratched, and then they were treated with gel extracts. Images of the scratch were taken at various time

intervals, and it was clear that the extract-treated cells migrated more quickly and filled the gap in 24 h. For Npx-conjugates, the scratch has healed to around 85-90% of its original extent, and for Ind-conjugates, the wound has completely closed (**Figure A49, Appendix**). Ind-conjugates has the greatest effect on cell migration and proliferation among the four gel groups when compared to the control group. The reduction of the anti-proliferative effects of transforming growth factor- β isoforms on fibroblast cells by Ind-conjugates is most likely the mechanism behind this increased wound healing response. These gels' ability to promote cell migration and wound healing in vitro is comparable to those of materials described by Wang *et al.*,⁶ Lee *et al.*,⁴⁷ and Wang *et al.*⁴⁸

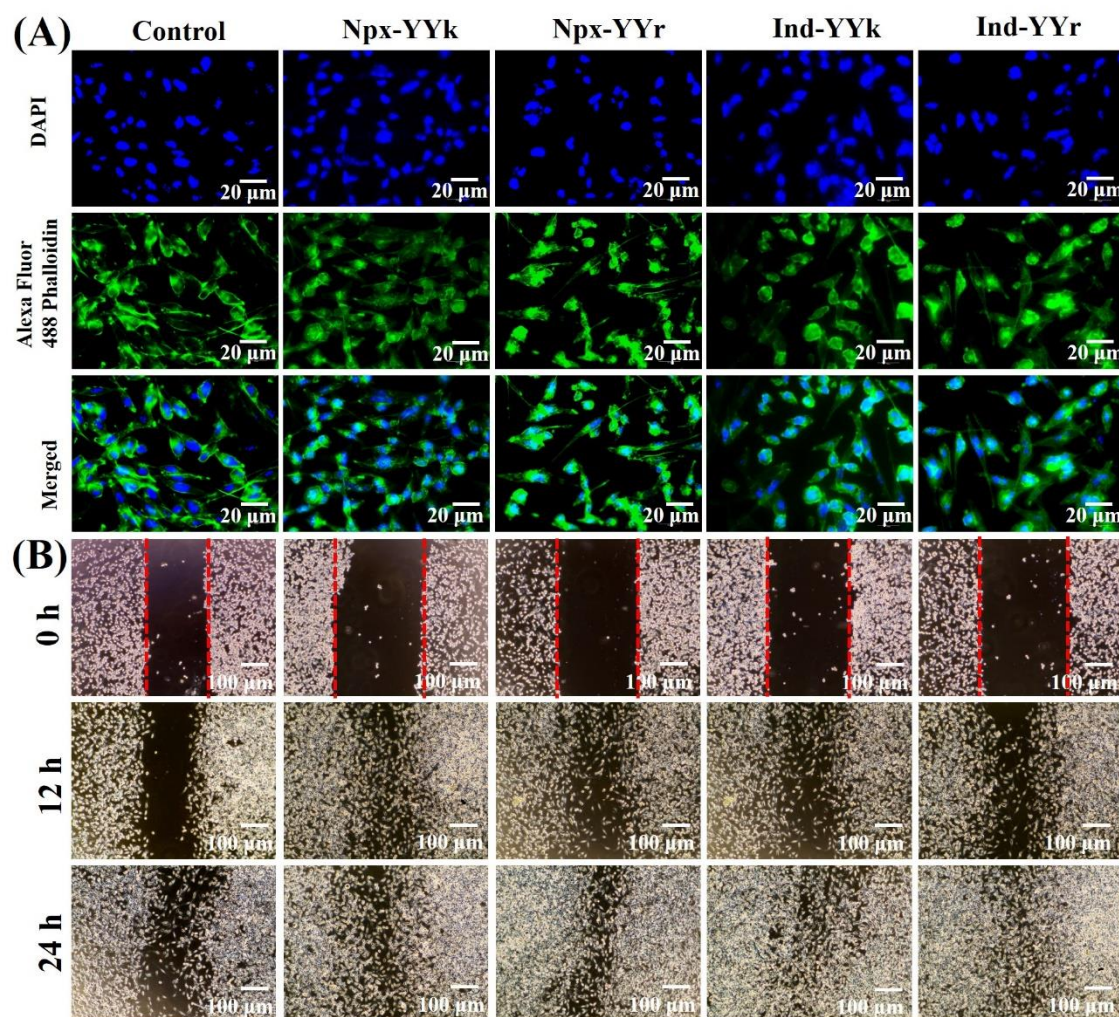


Figure 3.9. Cytoskeletal staining and in vitro wound healing in cells treated with gel extracts. (A) Cytoskeletal staining of L929. Cell nuclei was stained with DAPI (blue) and F-actin stained with Alexa Fluor 488 phalloidin (green). (B) Images of migration of L929 cells and healing of scratch at different time intervals. Cells without any treatment were considered as a control. Scale bar: (A) 20 μ m, and (B) 100 μ m.

3.4.11. In vitro ROS scavenging capability

Reactive oxygen species (ROS) and oxidative stress were induced in RAW 264.7 using H_2O_2 or LPS, and the effect of gels on the level of cellular ROS in H_2O_2 stressed RAW 264.7 macrophages was

assessed by DCFDA assay to determine whether conjugates and gels protect against cellular damage by preventing ROS formation. RAW 264.7 macrophages were examined under a fluorescent microscope to evaluate the intracellular ROS localization for qualitative analysis (**Figure 3.10A**). In contrast to control cells, which has very little green fluorescence, H₂O₂-treated cells displayed striking green fluorescence, which indicated an increase in intracellular ROS levels. The macrophages treated with gels reduced the green fluorescence, which indicated that all gels are efficient at scavenging free radicals. Quantitative analysis revealed that the fluorescence intensity of cells after exposure to conjugates and gels almost subsided by half when compared with H₂O₂-treated cells (**Figure 3.10B**). This supports the previous data related to the potential role of this conjugate gels in scavenging of intracellular ROS. Comparing the ROS scavenging potential of our compounds with the existing literature, we discovered that the outcomes are consistent with the information previously reported.^{8,49}

3.4.12. In vitro anti-inflammatory effect

In our investigation, LPS was used to preactivate macrophages (RAW 264.7) in order to simulate an inflammatory microenvironment before they were incubated with gel extracts. By using the MTT assay, the impact of these substances on the survival of LPS-induced inflamed RAW 264.7 cells were examined. When compared to the control (without LPS treatment), the viability after LPS treatment was significantly reduced to 40% after 24 h and the conjugates and their gels were able to significantly increase survival rates in the region of 85-90%, suggesting their potential role in reducing macrophage inflammatory responses (**Figure 3.10C**). On lipopolysaccharide (LPS)-induced RAW 264.7 macrophages, the gels' ability to modulate inflammation was investigated (**Figure 9D–F**).

Using non-activated macrophages as a reference, we verified the expression of pro-inflammatory (TNF- α and IL-6) and anti-inflammatory (IL-10) cytokines using real-time reverse transcriptase polymerase chain reaction (RT-PCR). The production of pro-inflammatory cytokines increased significantly after LPS activation, and the expression of anti-inflammatory cytokines decreased. TNF- α causes necrosis and IL-6 is elevated in bacterial infection, whereas IL-10 plays important role in ECM remodeling after injury. TNF- α expression was decreased in cells treated with gel extracts, while Npx-YYk gels showed a more pronounced downregulation (almost 40 folds compared to that of the LPS-treated group) (**Figure 3.10D**). In LPS-induced highly inflamed macrophages, Npx-YYk extracts likewise showed the strongest downregulation (31-folds) of IL-6, whereas other gel extracts only showed a mild reduction of IL-6 production (**Figure 3.10E**). In addition, Npx-YYk extracts significantly increased the production of IL-10 by almost 150 times compared to the stress-induced cells (**Figure 3.10F**). The expression of IL-10 was increased in the other gel extracts, albeit only to a mild extent (12–25 folds). These findings confirm conjugate gels' potent anti-inflammatory effects, which is the ideal characteristic for scaffolds for chronic wound healing. These conjugates' and gels' anti-inflammatory properties are likewise analogous to prior described scaffolds that were used to circumvent stalled inflammation phases and advance the healing process.^{1,50,51}

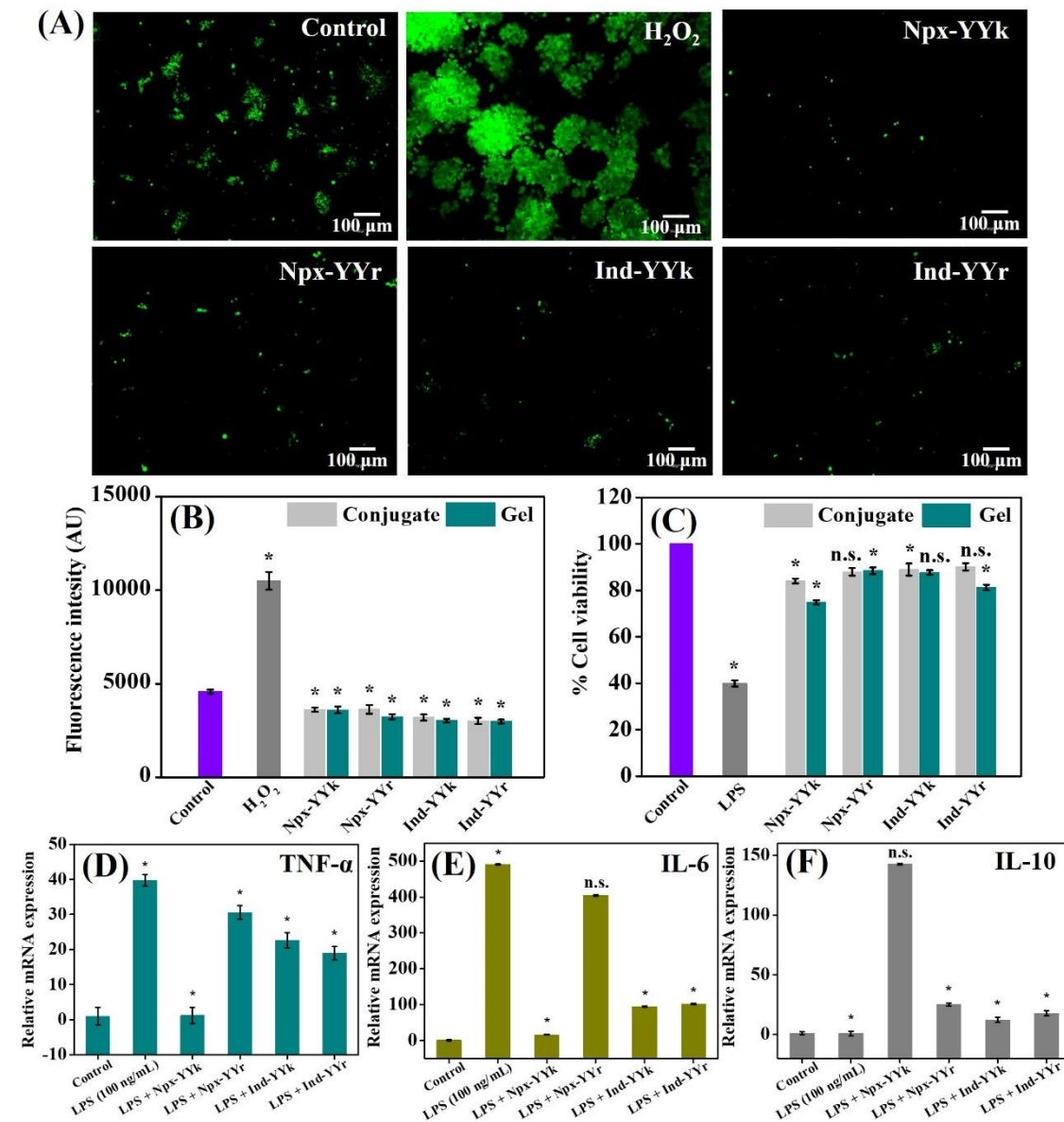


Figure 3.10. Effects of conjugates and gel extracts on reactive oxygen species (ROS) and inflammation. (A) Fluorescence microscopy images of RAW 264.7 cells treated with gel extracts, followed by DCFDA. Scale bar: 100 μm . (B) Fluorescence intensity of RAW 264.7 cells after treatment with extracts and DCFDA. Cells without exposure to H_2O_2 were considered as a control. (C) Viability of LPS-induced RAW 264.7 cells after treatment with extracts for 24 h, using MTT assay. (D-F) Anti-inflammatory properties of gel extracts in terms of $\text{TNF-}\alpha$, IL-6, and IL-10 expressions by RT-PCR analysis. Control denotes the gene expression of cells without LPS induction. All experiments were performed in triplicates (mean \pm SD, $n = 3$), and * $p < 0.05$ indicates statistically significant data. ns indicates non significance.

3.5. Conclusions

In this work, our goal was to develop a multifunctional wound healing scaffold for chronic wounds that possessed antibacterial, antibiofilm, antioxidant, radical scavenging, and anti-inflammatory

characteristics. It was accomplished by synthesizing peptides with two tyrosine, which are antioxidants and have the capacity to create supramolecular gels, and a cationic amino acid, lysine or arginine, in the appropriate order for antibacterial and antibiofilm capabilities. The cationic amino acids of the sequence were chosen in the D-form to increase its resistance to proteolytic enzyme breakdown and its selectivity for the cyclooxygenase-2 enzyme, which is crucial for inflammation. Two non-steroidal anti-inflammatory drugs, naproxen and indomethacin were covalently conjugated to the tripeptides to synthesize peptide-drug conjugates. The self-assembled supramolecular gels made from the peptide-drug conjugates were investigated for their surface morphology, stability, viscoelastic properties, swelling, and degradation profile. In cell culture, these potential of the gels as a scaffold for persistent wound healing was also evaluated. As anticipated, naproxen- and indomethacin-conjugated peptide gels showed high proteolytic stability and selective cyclooxygenase-2 enzyme inhibition, which will be beneficial in scar-free wound repair. The gels demonstrated strong antibacterial activity against *S. aureus*, the primary pathogen responsible for chronic wounds, through a mechanism including rupture of cell wall and membrane as well as inhibition of biofilm development and disruption of established biofilms. They displayed anti-inflammatory properties, provided protection against reactive oxygen species, and oxidative stress, and promoted cell proliferation in mouse fibroblast and macrophage cells. Overall, this work offers a promising method for creating multifunctional peptide-based scaffolds for chronic wound healing that have the ability to reduce bacterial infections, the growth of biofilms, and heightened inflammatory responses, to speed up the healing process.

References

- (1) Wang, Y.; Wu, Y.; Long, L.; Yang, L.; Fu, D.; Hu, C.; Kong, Q.; Wang, Y. Inflammation-Responsive Drug-Loaded Hydrogels with Sequential Hemostasis, Antibacterial, and Anti-Inflammatory Behavior for Chronically Infected Diabetic Wound Treatment. *ACS Appl. Mater. Interfaces* **2021**, *13* (28), 33584–33599. <https://doi.org/10.1021/acsami.1c09889>.
- (2) Zhou, L.; Min, T.; Bian, X.; Dong, Y.; Zhang, P.; Wen, Y. Rational Design of Intelligent and Multifunctional Dressing to Promote Acute/Chronic Wound Healing. *ACS Appl. Bio Mater.* **2022**, *5* (9), 4055–4085. <https://doi.org/10.1021/acsabm.2c00500>.
- (3) Sen, C. K. Human Wound and Its Burden: Updated 2020 Compendium of Estimates. *Advances in Wound Care* **2021**, *10* (5), 281–292. <https://doi.org/10.1089/wound.2021.0026>.
- (4) Lo, Z. J.; Lim, X.; Eng, D.; Car, J.; Hong, Q.; Yong, E.; Zhang, L.; Chandrasekar, S.; Tan, G. W. L.; Chan, Y. M.; Sim, S. C.; Oei, C. W.; Zhang, X.; Dharmawan, A.; Ng, Y. Z.; Harding, K.; Upton, Z.; Yap, C. W.; Heng, B. H. Clinical and Economic Burden of Wound Care in the Tropics: A 5-Year Institutional Population Health Review. *International Wound Journal* **2020**, *17* (3), 790–803. <https://doi.org/10.1111/iwj.13333>.
- (5) Araújo, M.; Silveira, J.; Sousa, A.; Bessa-Gonçalves, M.; Santos, S. G.; Barrias, C. C. A Bioinspired Multifunctional Hydrogel Patch Targeting Inflammation and Regeneration in Chronic Intestinal Wounds. *Biomater. Sci.* **2021**, *9* (19), 6510–6527. <https://doi.org/10.1039/D1BM00118C>.
- (6) Wang, J.; Chen, X.-Y.; Zhao, Y.; Yang, Y.; Wang, W.; Wu, C.; Yang, B.; Zhang, Z.; Zhang, L.; Liu, Y.; Du, X.; Li, W.; Qiu, L.; Jiang, P.; Mou, X.-Z.; Li, Y.-Q. PH-Switchable Antimicrobial Nanofiber Networks of Hydrogel Eradicate Biofilm and Rescue Stalled Healing in Chronic Wounds. *ACS Nano* **2019**, *13* (10), 11686–11697. <https://doi.org/10.1021/acs.nano.9b05608>.
- (7) Xu, Z.; Han, S.; Gu, Z.; Wu, J. Advances and Impact of Antioxidant Hydrogel in Chronic Wound Healing. *Adv. Healthcare Mater.* **2020**, *9* (5), 1901502. <https://doi.org/10.1002/adhm.201901502>.
- (8) Hussain, M.; Suo, H.; Xie, Y.; Wang, K.; Wang, H.; Hou, Z.; Gao, Y.; Zhang, L.; Tao, J.; Jiang, H.; Zhu, J. Dopamine-Substituted Multidomain Peptide Hydrogel with Inherent Antimicrobial Activity and Antioxidant Capability for Infected Wound Healing. *ACS Appl. Mater. Interfaces* **2021**, *13* (25), 29380–29391. <https://doi.org/10.1021/acsami.1c07656>.
- (9) Høiby, N.; Ciofu, O.; Johansen, H. K.; Song, Z.; Moser, C.; Jensen, P. Ø.; Molin, S.; Givskov, M.; Tolker-Nielsen, T.; Bjarnsholt, T. The Clinical Impact of Bacterial Biofilms. *Int J Oral Sci* **2011**, *3* (2), 55–65. <https://doi.org/10.4248/IJOS11026>.
- (10) Kim, Y. E.; Kim, J. ROS-Scavenging Therapeutic Hydrogels for Modulation of the Inflammatory Response. *ACS Appl. Mater. Interfaces* **2022**, *14* (20), 23002–23021. <https://doi.org/10.1021/acsami.1c18261>.
- (11) Feng, Z.; Zhang, Y.; Yang, C.; Liu, X.; Huangfu, Y.; Zhang, C.; Huang, P.; Dong, A.; Liu, J.; Liu, J.; Kong, D.; Wang, W. Bioinspired and Inflammation-Modulatory Glycopeptide Hydrogels for Radiation-Induced Chronic Skin Injury Repair. *Advanced Healthcare Materials* **2023**, *12* (1), 2201671. <https://doi.org/10.1002/adhm.202201671>.
- (12) Romana-Souza, B.; Santos, J. S. dos; Bandeira, L. G.; Monte-Alto-Costa, A. Selective Inhibition of COX-2 Improves Cutaneous Wound Healing of Pressure Ulcers in Mice through Reduction of iNOS Expression. *Life Sciences* **2016**, *153*, 82–92. <https://doi.org/10.1016/j.lfs.2016.04.017>.
- (13) Li, S.; Zhang, Y.; Ma, X.; Qiu, S.; Chen, J.; Lu, G.; Jia, Z.; Zhu, J.; Yang, Q.; Chen, J.; Wei, Y. Antimicrobial Lignin-Based Polyurethane/Ag Composite Foams for Improving Wound Healing. *Biomacromolecules* **2022**, *23* (4), 1622–1632. <https://doi.org/10.1021/acs.biomac.1c01465>.
- (14) Rasool, N.; Srivastava, R.; Singh, Y. Cationized Silica Ceria Nanocomposites to Target Biofilms in Chronic Wounds. *Biomaterials Advances* **2022**, *138*, 212939. <https://doi.org/10.1016/j.bioadv.2022.212939>.
- (15) Zhao, X.; Liang, Y.; Guo, B.; Yin, Z.; Zhu, D.; Han, Y. Injectable Dry Cryogels with Excellent Blood-Sucking Expansion and Blood Clotting to Cease Hemorrhage for Lethal Deep-Wounds, Coagulopathy and Tissue Regeneration. *Chemical Engineering Journal* **2021**, *403*, 126329. <https://doi.org/10.1016/j.cej.2020.126329>.
- (16) Ahmadian, Z.; Correia, A.; Hasany, M.; Figueiredo, P.; Dobakhti, F.; Eskandari, M. R.; Hosseini, S. H.; Abiri, R.; Khorshid, S.; Hirvonen, J.; Santos, H. A.; Shahbazi, M.-A. A Hydrogen-Bonded Extracellular Matrix-Mimicking Bactericidal Hydrogel with Radical Scavenging and Hemostatic Function for PH-Responsive Wound Healing Acceleration. *Advanced Healthcare Materials* **2021**, *10* (3), 2001122. <https://doi.org/10.1002/adhm.202001122>.

- (17) Kaur, G.; Narayanan, G.; Garg, D.; Sachdev, A.; Matai, I. Biomaterials-Based Regenerative Strategies for Skin Tissue Wound Healing. *ACS Appl. Bio Mater.* **2022**, *5* (5), 2069–2106. <https://doi.org/10.1021/acsabm.2c00035>.
- (18) Lau, H. K.; Kiick, K. L. Opportunities for Multicomponent Hybrid Hydrogels in Biomedical Applications. *Biomacromolecules* **2015**, *16* (1), 28–42. <https://doi.org/10.1021/bm501361c>.
- (19) Xi, Y.; Ge, J.; Wang, M.; Chen, M.; Niu, W.; Cheng, W.; Xue, Y.; Lin, C.; Lei, B. Bioactive Anti-Inflammatory, Antibacterial, Antioxidative Silicon-Based Nanofibrous Dressing Enables Cutaneous Tumor Photothermo-Chemo Therapy and Infection-Induced Wound Healing. *ACS Nano* **2020**, *14* (3), 2904–2916. <https://doi.org/10.1021/acs.nano.9b07173>.
- (20) Koehler, J.; Brandl, F. P.; Goepferich, A. M. Hydrogel Wound Dressings for Bioactive Treatment of Acute and Chronic Wounds. *European Polymer Journal* **2018**, *100*, 1–11. <https://doi.org/10.1016/j.eurpolymj.2017.12.046>.
- (21) Chu, B.; He, J.-M.; Liu, L.-L.; Wu, C.-X.; You, L.-L.; Li, X.-L.; Wang, S.; Chen, C.-S.; Tu, M. Proangiogenic Peptide Nanofiber Hydrogels for Wound Healing. *ACS Biomater. Sci. Eng.* **2021**, *7* (3), 1100–1110. <https://doi.org/10.1021/acsbmaterials.0c01264>.
- (22) Konai, M. M.; Haldar, J. Lysine-Based Small Molecules That Disrupt Biofilms and Kill Both Actively Growing Planktonic and Nondividing Stationary Phase Bacteria. *ACS Infect. Dis.* **2015**, *1* (10), 469–478. <https://doi.org/10.1021/acsinfecdis.5b00056>.
- (23) McCloskey, A. P.; Draper, E. R.; Gilmore, B. F.; Laverty, G. Ultrashort Self-Assembling Fmoc-Peptide Gelators for Anti-Infective Biomaterial Applications: Fmoc-Peptides Demonstrate Selective Activity Against Biofilms. *J. Pept. Sci.* **2017**, *23* (2), 131–140. <https://doi.org/10.1002/psc.2951>.
- (24) Shi, Y.; Wareham, D. W.; Yuan, Y.; Deng, X.; Mata, A.; Azevedo, H. S. Polymyxin B-Triggered Assembly of Peptide Hydrogels for Localized and Sustained Release of Combined Antimicrobial Therapy. *Advanced Healthcare Materials* **2021**, *10* (22), 2101465. <https://doi.org/10.1002/adhm.202101465>.
- (25) Tian, R.; Qiu, X.; Yuan, P.; Lei, K.; Wang, L.; Bai, Y.; Liu, S.; Chen, X. Fabrication of Self-Healing Hydrogels with On-Demand Antimicrobial Activity and Sustained Biomolecule Release for Infected Skin Regeneration. *ACS Appl. Mater. Interfaces* **2018**, *10* (20), 17018–17027. <https://doi.org/10.1021/acsami.8b01740>.
- (26) Mi, L.; Xue, H.; Li, Y.; Jiang, S. A Thermoresponsive Antimicrobial Wound Dressing Hydrogel Based on a Cationic Betaine Ester. *Advanced Functional Materials* **2011**, *21* (21), 4028–4034. <https://doi.org/10.1002/adfm.201100871>.
- (27) Chen, H.; Cheng, J.; Cai, X.; Han, J.; Chen, X.; You, L.; Xiong, C.; Wang, S. PH-Switchable Antimicrobial Supramolecular Hydrogels for Synergistically Eliminating Biofilm and Promoting Wound Healing. *ACS Appl. Mater. Interfaces* **2022**, *13*.
- (28) Cui, T.; Li, X.; He, S.; Xu, D.; Yin, L.; Huang, X.; Deng, S.; Yue, W.; Zhong, W. Instant Self-Assembly Peptide Hydrogel Encapsulation with Fibrous Alginate by Microfluidics for Infected Wound Healing. *ACS Biomater. Sci. Eng.* **2020**, *6* (9), 5001–5011. <https://doi.org/10.1021/acsbmaterials.0c00581>.
- (29) Halder, M.; Bhatia, Y.; Singh, Y. Self-Assembled Di- and Tripeptide Gels for the Passive Entrapment and PH-Responsive, Sustained Release of an Antidiabetic Drug, Glimepiride. *Biomater. Sci.* **2022**, *10* (9), 2248–2262. <https://doi.org/10.1039/D2BM00344A>.
- (30) Vishwakarma, A.; Dang, F.; Ferrell, A.; Barton, H. A.; Joy, A. Peptidomimetic Polyurethanes Inhibit Bacterial Biofilm Formation and Disrupt Surface Established Biofilms. *J. Am. Chem. Soc.* **2021**, *143* (25), 9440–9449. <https://doi.org/10.1021/jacs.1c02324>.
- (31) Morris, K. L.; Chen, L.; Rodger, A.; Adams, D. J.; Serpell, L. C. Structural Determinants in a Library of Low Molecular Weight Gelators. *Soft Matter* **2015**, *11* (6), 1174–1181. <https://doi.org/10.1039/C4SM02532F>.
- (32) Rumbaugh, K.; Watters, C.; Yuan, T. Beneficial and Deleterious Bacterial–Host Interactions in Chronic Wound Pathophysiology. *CWCMR* **2015**, *53*. <https://doi.org/10.2147/CWCMR.S60317>.
- (33) Swanekamp, R. J.; Welch, J. J.; Nilsson, B. L. Proteolytic Stability of Amphipathic Peptide Hydrogels Composed of Self-Assembled Pleated β -Sheet or Coassembled Rippled β -Sheet Fibrils. *Chem. Commun.* **2014**, *50* (70), 10133–10136. <https://doi.org/10.1039/C4CC04644G>.
- (34) Baral, A.; Roy, S.; Ghosh, S.; Hermida-Merino, D.; Hamley, I. W.; Banerjee, A. A Peptide-Based Mechano-Sensitive, Proteolytically Stable Hydrogel with Remarkable Antibacterial Properties. *Langmuir* **2016**, *32* (7), 1836–1845. <https://doi.org/10.1021/acs.langmuir.5b03789>.

- (35) Wei, Q.; Duan, J.; Ma, G.; Zhang, W.; Wang, Q.; Hu, Z. Enzymatic Crosslinking to Fabricate Antioxidant Peptide-Based Supramolecular Hydrogel for Improving Cutaneous Wound Healing. *J. Mater. Chem. B* **2019**, 7 (13), 2220–2225. <https://doi.org/10.1039/C8TB03147A>.
- (36) Csire, G.; Dupire, F.; Canabady-Rochelle, L.; Selmeczi, K.; Stefan, L. Bio-Inspired Casein-Derived Antioxidant Peptides Exhibiting a Dual Direct/Indirect Mode of Action. *Inorg. Chem.* **2022**, 61 (4), 1941–1948. <https://doi.org/10.1021/acs.inorgchem.1c03085>.
- (37) Li, J.; Kuang, Y.; Gao, Y.; Du, X.; Shi, J.; Xu, B. D-Amino Acids Boost the Selectivity and Confer Supramolecular Hydrogels of a Nonsteroidal Anti-Inflammatory Drug (NSAID). *J. Am. Chem. Soc.* **2013**, 135 (2), 542–545. <https://doi.org/10.1021/ja310019x>.
- (38) Paes Leme, R. C.; da Silva, R. B. Antimicrobial Activity of Non-Steroidal Anti-Inflammatory Drugs on Biofilm: Current Evidence and Potential for Drug Repurposing. *Front. Microbiol.* **2021**, 12, 707629. <https://doi.org/10.3389/fmicb.2021.707629>.
- (39) Cao, F.; Mei, L.; Zhu, G.; Song, M.; Zhang, X. An Injectable Molecular Hydrogel Assembled by Antimicrobial Peptide PAF26 for Antimicrobial Application. *RSC Adv.* **2019**, 9 (53), 30803–30808. <https://doi.org/10.1039/C9RA06130D>.
- (40) Hou, Y.; Tan, T.; Guo, Z.; Ji, Y.; Hu, J.; Zhang, Y. Gram-Selective Antibacterial Peptide Hydrogels. *Biomater. Sci.* **2022**, 10 (14), 3831–3844. <https://doi.org/10.1039/D2BM00558A>.
- (41) Gahane, A. Y.; Ranjan, P.; Singh, V.; Sharma, R. K.; Sinha, N.; Sharma, M.; Chaudhry, R.; Thakur, A. K. Fmoc-Phenylalanine Displays Antibacterial Activity against Gram-Positive Bacteria in Gel and Solution Phases. *Soft Matter* **2018**, 14 (12), 2234–2244. <https://doi.org/10.1039/C7SM02317K>.
- (42) Wang, X.; Zhao, D.; Li, Y.; Zhou, X.; Hui, Z.; Lei, X.; Qiu, L.; Bai, Y.; Wang, C.; Xia, J.; Xuan, Y.; Jiang, P.; Wang, J. Collagen Hydrogel with Multiple Antimicrobial Mechanisms as Anti-Bacterial Wound Dressing. *International Journal of Biological Macromolecules* **2023**, 232, 123413. <https://doi.org/10.1016/j.ijbiomac.2023.123413>.
- (43) Bai, J.; Gong, Z.; Wang, J.; Wang, C. Enzymatic Hydrogelation of Self-Assembling Peptide I4K2 and Its Antibacterial and Drug Sustained-Release Activities. *RSC Adv.* **2017**, 7 (77), 48631–48638. <https://doi.org/10.1039/C7RA09743C>.
- (44) Gan, B. H.; Gaynord, J.; Rowe, S. M.; Deingruber, T.; Spring, D. R. The Multifaceted Nature of Antimicrobial Peptides: Current Synthetic Chemistry Approaches and Future Directions. *Chem. Soc. Rev.* **2021**, 50 (13), 7820–7880. <https://doi.org/10.1039/D0CS00729C>.
- (45) Hansda, B.; Majumder, J.; Mondal, B.; Chatterjee, A.; Das, S.; Kumar, S.; Gachhui, R.; Castelletto, V.; Hamley, I. W.; Sen, P.; Banerjee, A. Histidine-Containing Amphiphilic Peptide-Based Non-Cytotoxic Hydrogelator with Antibacterial Activity and Sustainable Drug Release. *Langmuir* **2023**, 39 (21), 7307–7316. <https://doi.org/10.1021/acs.langmuir.3c00235>.
- (46) Guo, Z.; Wang, Y.; Tan, T.; Ji, Y.; Hu, J.; Zhang, Y. Antimicrobial D-Peptide Hydrogels. *ACS Biomater. Sci. Eng.* **2021**, 7 (4), 1703–1712. <https://doi.org/10.1021/acsbiomaterials.1c00187>.
- (47) Lee, S.; Kim, M. S.; Jung, S.-J.; Kim, D.; Park, H. J.; Cho, D. ERK Activating Peptide, AES16-2M Promotes Wound Healing through Accelerating Migration of Keratinocytes. *Scientific Reports* **2018**, 8 (1), 14398. <https://doi.org/10.1038/s41598-018-32851-y>.
- (48) Wang, S. Y.; Kim, H.; Kwak, G.; Yoon, H. Y.; Jo, S. D.; Lee, J. E.; Cho, D.; Kwon, I. C.; Kim, S. H. Development of Biocompatible HA Hydrogels Embedded with a New Synthetic Peptide Promoting Cellular Migration for Advanced Wound Care Management. *Advanced Science* **2018**, 5 (11), 1800852. <https://doi.org/10.1002/advs.201800852>.
- (49) Cheng, X.; Gao, D.-X.; Song, J.-J.; Ren, F.-Z.; Mao, X.-Y. Casein Glycomacropeptide Hydrolysate Exerts Cytoprotection against H₂O₂-Induced Oxidative Stress in RAW 264.7 Macrophages via ROS-Dependent Heme Oxygenase-1 Expression. *RSC Adv.* **2015**, 5 (6), 4511–4523. <https://doi.org/10.1039/C4RA10034D>.
- (50) Mizuno, Y.; Taguchi, T. Anti-Inflammatory and Tissue Adhesion Properties of an α -Linolenic Acid-Modified Gelatin-Based In Situ Hydrogel. *ACS Appl. Bio Mater.* **2020**, 3 (9), 6204–6213. <https://doi.org/10.1021/acsabm.0c00737>.
- (51) Gao, W.; Wang, L.; Wang, K.; Sun, L.; Rao, Y.; Ma, A.; Zhang, M.; Li, Q.; Yang, H. Enhanced Anti-Inflammatory Activity of Peptide–Gold Nanoparticle Hybrids upon Cigarette Smoke Extract Modification through TLR Inhibition and Autophagy Induction. *ACS Appl. Mater. Interfaces* **2019**, 11 (36), 32706–32719. <https://doi.org/10.1021/acsami.9b10536>.

CHAPTER - 4

Ultrashort Peptide-Based Biomaterials for
Hydroxyapatite Binding and Osteogenic
Differentiation of Mesenchymal Stem Cells to Aid
Bone Tissue Regeneration

Self-assembled peptides for bone tissue regeneration

4.1. Introduction**4.1.1. Bone disorders/osteoporosis**

Bone is composed of four types of cells- osteoblast, osteoclast, osteocyte, and osteoprogenitor cells, and the extracellular matrix (ECM), which has both organic and inorganic substances.¹ Each type of cell in bones is present in various places and has a specific function. Osteoblasts help in bone formation, osteoclasts are responsible for bone resorption, osteocytes maintain the mineral concentration in the matrix, and osteoprogenitor or osteogenic cells help in the development of osteoblasts. Bone is a highly neurovascularized, calcified tissue that can undergo self-healing and regeneration after injury. A wide range of bone deformities caused by injury, illness, and ageing require clinical interventions, which leads to long-term defects and persistent pain, thus, lowering the patient's quality of life.² According to the Global Burden of Disease (GBD) study 2019, 178 million new cases of bone fractures were reported globally in 2019. The risk of fractures is exacerbated by osteoporosis, which results in the loss of bone mass and renders the bone brittle. An osteoporotic fracture happens every 3 seconds and accounts for more than 8.9 million fractures worldwide.³ Osteoblast (OB) activity is outweighed by that of osteoclasts (OCs) activity and the homeostasis between bone resorption and bone formation is lost in case of osteoporosis, leading to reduction of bone mass and mineral density. One of the main causes of osteoporosis is reactive oxygen species (ROS), which plays a significant role in osteoclastogenesis because under normal physiological circumstances they can encourage the resorption of bone tissues, which is necessary for the regular process of bone rejuvenation.⁴ However, under stress conditions, such as those caused by intestinal chronic illness and estrogen deprivation during menopause, ROS can overcome natural antioxidant defense systems, leading to the death of OBs and osteocytes and the promotion of OC formation (osteoclastogenesis) and activity.

4.1.2. Challenges

The use of an autologous bone transplant is currently regarded as the gold-standard treatment for most of the bone abnormalities but this procedure is associated with numerous drawbacks, such as limited availability, variable resorption, higher morbidity, and the need for subsequent surgery.⁵ Allogeneic bone grafts, a different option, however, carry the danger of transmission of disease and potential immune rejection.⁶ Tissue engineering techniques have been used to cure tissue defects in order to overcome these difficulties. Bone tissue engineering entails using cells, biomaterials, and appropriate growth factors to construct an environment that fosters the formation and regeneration of bone tissues.^{1,7} The basic element of bone tissue engineering includes a scaffold material that should mimic the traits and properties of the extracellular matrix (ECM) found in natural bone to offer the proper biomechanical support and metabolic environment for cell adhesion, migration, proliferation, and osteogenic differentiation without fear of an immunological rejection.^{8,9}

4.1.3. Biomaterials for bone tissue regeneration and research gap

Type I collagen is the most abundant protein, which forms 90% of the matrix.¹⁰ Other than this, noncollagenous proteins and hydroxyapatite are the other constituents of bone matrix. Therefore, scaffolds inspired from collagen and noncollagenous proteins with a binding affinity towards hydroxyapatite (HAp) can mimic the biomineralization process and induce regeneration of bone and increase its rigidity.^{11,12} The multipotent nature of mesenchymal stem cells has emerged as important participants in tissue engineering and regenerative medicine.^{13,14} They easily generate progenitors for a variety of cell types, including myocytes, chondrocytes, adipocytes, and osteocytes. In the context of bone tissue engineering, MSCs have been reported to differentiate into osteoblast-like cells in vitro upon culturing with appropriate materials, capable of differentiating.¹⁵

There are a variety of scaffolds tested to promote the regeneration of bone tissue and that includes, natural biomaterials, like collagen,¹⁶ gelatin,¹⁷ chitosan¹⁸ or silk fibroin,¹⁹ ceramics, such as, hydroxyapatite (HAp)²⁰ or tricalcium phosphate (TCP), synthetic polymeric materials, like poly lactic-co-glycolic acid (PLGA)²¹, polylactic acid (PLA) or polyglycolic acid (PGA), and composite scaffolds.²² Gilarska *et al.* have fabricated hybrids composed of collagen/chitosan/hyaluronic acid and amine-functionalized silica nanoparticles decorated with apatite to encapsulate alendronate for the repair of small osteoporotic bone defects.²³ Zhao *et al.* have developed a composite nanoparticle hydrogel by combining carboxymethyl chitosan (CMCh) and amorphous calcium phosphate, which supports adhesion and proliferation of MSCs and induce osteogenic differentiation.²⁴ In a study by Liang *et al.*, the immunomodulatory capability of gold nanoparticle-loaded mesoporous silica nanoparticles was evaluated along with their osteogenic properties.²⁵ Ullah *et al.* reported the preparation of Sr/Fe co-substituted HAp bioceramics for applications in developing bone implant.²⁶ Titanium and their alloys are also reported by Attar *et al.* for their osteogenic potential due to their porous structure.²⁷ Raja *et al.* fabricated unique coiled-structure bioceramics encapsulated in alginate hydrogel beads as a new bone substitute for simultaneous release of drug, quercetin and stem cells.²⁸

Majority of these kinds of materials suffer from disadvantages, like low mechanical properties (i.e., stiffness), immunogenicity, brittleness, limited biodegradability, drug-associated side effects, and potential cytotoxicity. Growth factors, like bone morphogenic proteins (BMP) also play a leading role in this field because of their propensity to promote the proliferation and differentiation of osteoprogenitor cells.²⁹ Nevertheless, the use of growth factors, like BMPs suffer from serious drawbacks, such as high costs and adverse effects, like heterotopic bone formation, pseudo arthritis, problematic immune response, and local inflammation.³⁰ As a result, alternative methods are required to either completely eliminate or greatly minimize the amount of BMPs required in bone tissue engineering procedures in order to promote tissue regeneration with high efficacy and minimal side effects.

4.1.4. Self-assembling peptides

The biomaterial-based methods may benefit from the use of novel, small-scale osteoinductive compounds that are cheaper to produce, safe towards immune system, and physiologically stable. Another appealing and thoroughly investigated substitutes are ultrashort peptides, which can be evolved from ECM proteins, soluble factors, engineered or naturally occurring.³¹ Peptides can be easily synthesized by using cost-effective liquid- or solid-phase synthesis techniques and are less likely to trigger immunological reactions due to their small size. In addition, more peptides can be grafted onto a biomaterial per unit of surface area due to their small size, exposing target cells to higher densities of active sites. Peptides are extremely adaptable tools, as they can be designed to stimulate cell adherence to the implanted biomaterial, proliferation, differentiation, angiogenesis, or a combination of actions.³² These ultrashort peptides have very less chance to initiate adverse immune response or tissue inflammation when introduced into the body and no toxic substances are generated during degradation since they are mainly composed of amino acids.⁷ Therefore, peptides with various nanostructures are emerging as biomaterials for bone tissue regeneration. Compared to other biomaterials, gels can be an ideal choice for this because of their porous, nanostructured morphology like ECM, soft texture, which can reduce the inflammatory response of neighboring cells and tissues, and they can also serve as a carrier for cells and growth factors.³³ Alshehri *et al.* rationally designed self-assembling tetrapeptide (IVFK) for 3D cell culture, osteogenesis, and angiogenesis applications.³⁴ Immobilization of osteoblast targeting peptide (SDSSD) on chitosan surface has been exploited by Tang *et al.* for macrophage polarization and promoting the healing of bone defects.³⁵ One of the pioneer works in this field is reported by Pal *et al.*, where they employed collagen-inspired peptide (NapFFGDO) with negative charge for the mineralization of HAp to develop a bone-filling material.³⁶

4.2. Objectives

Although several self-assembled, amphiphilic peptides have been reported in the literature with significant osteogenic properties but the effect of charged amino acids in developing nanostructured scaffolds to offer a closer structural support to native bone architecture is overlooked. Herein, our objective was to develop injectable, self-assembled, nano-structured peptides, which can emerge as a promising scaffold with an excellent mechanical and antioxidant properties, resemble ECM, and stimulate cell growth as well as guide bone tissue regeneration. The defined structure of biomaterial scaffolds can provide a sort of mechanical cue, which can modify the local microenvironment, affect cell activity, and regulate crucial molecular and cellular characteristics.

Therefore, we have designed six amphiphilic tetrapeptides, where the first three amino acids (Trp, Trp and His) are same in all the sequences and the fourth amino acid with different surface charges have been used (Ser, pSer, Pro, Hyp, Asp, or Glu) to investigate their impact on the adsorption of HAp and differentiation of MSCs for promoting bone tissue regeneration. Serine (Ser, S), phosphoserine (pSer, J), aspartic acid (Asp, D) and glutamic acid (Glu, E) are the component of noncollagenous protein, whereas proline (Pro, P) and hydroxyproline (Hyp, O) are the part of collagenous protein present in bone

ECM. Out of these six peptides Fmoc-Trp-Trp-His-Ser-NH₂ (WWHS), Fmoc-Trp-Trp-His-pSer-NH₂ (WWHJ), Fmoc-Trp-Trp-His-Pro-NH₂ (WWHP), Fmoc-Trp-Trp-His-Hyp-NH₂ (WWHO), Fmoc-Trp-Trp-His-Asp-NH₂ (WWHD), and Fmoc-Trp-Trp-His-Glu-NH₂ (WWHE), four peptides (WWHS, WWHO, WWHD and WWHE) were able to form hydrogels. The other two peptides (WWHJ and WWHP) were self-assembled into various nanostructures with different morphologies. Interestingly, the addition of charged amino acids allowed them to be adsorbed on the surface of HAp due to electrostatic and hydrogen-bonding interactions. The osteogenic differentiation of MSCs by these peptides was evaluated by ALP production, calcium deposition, and expression of various osteogenic markers. In addition, the immunogenic response of these peptides was observed on macrophages by analyzing the expression of M1 and M2 phase markers. The osteogenic and anti-osteoclastogenic activity of the peptides were demonstrated in a co-culture model of osteoblast and macrophages. Therefore, our strategy provides a rational design of bioinspired, ultrashort peptides for the construction of nanostructured scaffolds to promote bone tissue regeneration.

4.3. Experimental Section

4.3.1. Materials

All solvents and chemicals were of high analytical grade and utilized without additional purification unless otherwise specified. Rink amide AM resins (0.80 mmol/g loading) was purchased from Novabiochem. Fmoc protected amino acids, Fmoc-Trp-OH, Fmoc-His(trt)-OH, Fmoc-Glu(OtBu)-OH, Fmoc-Ser(trt)-OH, Fmoc-Pro-OH, Fmoc-Asp(OtBu)-OH, anhydrous N, N-dimethylformamide (DMF), 2,2'-azino-bis (3-ethylbenzothiazoline-6-sulfonic acid) diammonium salt (ABTS), and 2',7'-dichlorodihydrofluorescein diacetate (DCFDA) were acquired from Sigma Aldrich. Fmoc-O-phospho-L-serine and Fmoc-Hyp(tBu)-OH were purchased from BLD Pharmaceuticals. 1-bis(dimethylamino)methylene]-1H-1,2,3-triazolo[4,5-b] pyridinium 3-oxide hexafluorophosphate (HATU), trifluoroacetic acid (TFA), N, N-diisopropylethylamine (DIEA), triisopropyl silane (TIS), 1,1-diphenyl-2-picrylhydrazyl free radical (DPPH), and 4-nitrophenylphosphate (pNPP) were purchased from TCI Chemicals, India. Dimethyl sulfoxide (DMSO) and HPLC grade solvents, acetonitrile, methanol, and isopropyl alcohol were purchased from Merck and used for reverse phase high-pressure liquid chromatography (RP-HPLC). Piperidine and dichloromethane (DCM) were bought from Spectrochem and Rankem Laboratories. PolyPrep chromatography columns from Bio-Rad were used for solid-phase peptide synthesis (SPPS). Deionized water (DI, 18.2 MΩ cm) was obtained from a Milli-Q system and used in all experiments. MC3T3-E1 cells (CRL-2593, Subclone-4) were purchased from ATCC. Minimum Essential Medium alpha (MEM-α), 0.25% trypsin/EDTA, penstrep, SYBR™ Green Master Mix, and trizol were purchased from Thermo Fisher Scientific. MTT reagent (3-(4,5-dimethylthiazol)-2,5-diphenyltetrazolium bromide), ascorbic acid, DAPI (4',6-diamidino-2-phenylindole, dihydrochloride) and fetal bovine serum (FBS) were procured from Himedia. LIVE/DEAD™ Viability/Cytotoxicity Kit for mammalian cells, and Alexa Fluor™ 488, and Phalloidin were bought from Invitrogen. The iScript™ cDNA synthesis kit was procured from Bio-Rad.

4.3.2. Peptide synthesis and characterization

The peptides were synthesized using standard 9-fluorenylmethoxycarbonyl (Fmoc)-based SPPS method. Rink amide AM resin was employed as a solid support. A mixture of HATU (2.85 equiv.) and DIEA (5.7 equiv.) was utilized for coupling amino acids, and 3 mL of 20% piperidine in DMF was used to deprotect Fmoc group. A cleavage cocktail comprising 95% v/v TFA, 2.5% v/v TIS, and 2.5% v/v water was utilized (3.5 h) to cleave the peptides from the resin. Subsequently, the amide terminated peptides, Fmoc-Trp-Trp-His-Ser-NH₂ (WWHS), Fmoc-Trp-Trp-His-pSer-NH₂ (WWHJ), Fmoc-Trp-Trp-His-Pro-NH₂ (WWHP), Fmoc-Trp-Trp-His-Hyp-NH₂ (WWHO), Fmoc-Trp-Trp-His-Asp-NH₂ (WWHD), and Fmoc-Trp-Trp-His-Glu-NH₂ (WWHE) were precipitated in cold diethyl ether, which was followed by centrifugation and drying under vacuum. The purity of these peptides was determined by using a RP-HPLC equipped with Xbridge BEH C₁₈ column (250 × 4.6 mm, 5 μm), and acetonitrile/water (50:50) with 0.1% TFA was used as a mobile phase at a flow rate of 1 mL/min. The peptides were further characterized by mass (XEVO G2-XS QTOF) and ¹H NMR (JEOL JNM-ECS, 400 MHz) analysis.

4.3.3. Supramolecular gel formation and characterization

A solution of NaOH (150 μL, pH = 9) was added to 2 mg of peptides to make a clear solution upon heating. Out of six peptides, only WWHS, WWHO, WWHD, and WWHE were soluble. Next, 5 μL of 1M NaOH was added to the peptide solution with constant tapping. Self-assembled gels (1.33% w/v) were formed from WWHS, WWHO, WWHD, and WWHE after vortexing the mixture for 5 min. The vial inversion test was performed to confirm the gelation. The morphology of gels was analyzed by field emission scanning electron microscopy (FESEM). The gels (1.33% w/v) were diluted with water and 10 μL of gel solution was drop casted on silicon wafer and air dried. The surface was sputter-coated with platinum for few seconds under vacuum. Micrographs were acquired using JEOL JSM-6610LV microscope with a tungsten filament at an accelerating voltage of 10 kV.

4.3.4. Spectroscopic studies

The following spectroscopic studies were carried out to determine the secondary structures of WWHS, WWHJ, WWHP, WWHO, WWHD, and WWHE.

Circular dichroism (CD). CD analysis was performed on a CD spectrometer (JASCO J-1500) using a 0.1 cm path length quartz cuvette. Peptide solutions were prepared in DI water and incubated at room temperature for five days before the study to facilitate the formation of secondary structures. The measurements were carried out at 37 °C and spectra of peptides were recorded at of concentration of 0.5 mM in the range of 195-350 nm at a continuous scanning rate of 200 nm/min.

Fourier transform infrared (FT-IR). FT-IR spectra of all peptides were recorded in the ATR mode using Bruker Tensor 27 spectrometer between 400-4000 cm⁻¹.

Thioflavin-T (ThT) binding assay. Binding of peptides with ThT were determined by fluorescence spectra, using a method reported earlier.³⁷ A solution of ThT was incubated with peptides for 6 h and the fluorescence spectra were acquired in a range of 430-700 nm using a Tecan multimode microplate reader at an excitation wavelength of 440 nm to estimate the binding of thioflavin T with the secondary structures of peptides. ThT solution without any peptides was treated as a blank.

4.3.5. Zeta potential

The zeta potential of peptide solutions (1 mM) was measured using the Malvern Zetasizer Nano ZS instrument at room temperature. Peptides were dissolved in phosphate buffer saline and equilibrated overnight before the measurement.

4.3.6. Rheological analysis of gels

The shear-thinning behaviors of peptide gels (WWHS, WWHO, WWHD, and WWHE) were analyzed by conducting rheological measurements on an Anton Paar MCR 102 rheometer with 25 mm parallel plate configuration and a shear gap of 0.3 mm. Oscillatory shearing tests were performed on 200 μ L of gels (1.33% w/v) at room temperature. Amplitude sweep (0.01-100% of strain) and frequency sweep (0.01-100 rad/s of angular frequency) studies were conducted to determine the linear viscoelastic (LVE) region. Subsequently, the self-healing property of gels were assessed by applying six alternative cycles of extreme (30%) and mild strain (0.1%) at a constant angular frequency of 10 rad/s.

4.3.7. Swelling and degradation study

For stability experiments, the gels (WWHS, WWHO, WWHD, and WWHE) were fabricated and incubated at 37 °C with PBS (pH 7.4) in an incubator shaker (120 rpm) for up to 14 days and the weight change of gels was monitored at various time periods to assess their stability. The swelling and degradation of gels were measured using following equation:

$$\% \text{ Swelling/Degradation} = \frac{W_t - W_i}{W_i} \times 100 \quad \text{Equation 4.1}$$

where, W_t is the weight of swollen gel at time t and W_i is the initial weight.

4.3.8. Antioxidant properties

ABTS assay was performed to evaluate the radical scavenging capacity of the peptides and gels following the protocol reported earlier.³⁸

4.3.9. In vitro binding of peptides towards hydroxyapatite (HAp)

Time-dependent adsorption of peptides to HAp was determined by RP-HPLC method. Peptides were dissolved in phosphate buffer saline at a concentration of 0.5 and 1.0 mM upon heating. In a 2 mL microcentrifuge tube, 5 mg of HAp and 1 mL of peptide solution at two different concentrations (0.5 and 1.0 mM) were mixed by vortexing for 1 min and the mixture was kept inside an orbital shaker at 37 °C with 100 rpm. Each mixture was cultured for 2, 4, and 12 h, and the tubes were centrifuged at 7000 rpm for 5 min. The supernatant was removed and syringe filtered. The concentration of peptide remaining in the supernatant was determined by RP-HPLC using ACN:water (50:50) with 0.1% TFA

as the mobile phase. Area under the curve (AUC) was measured from the HPLC chromatogram, which was proportional to the concentration of the peptide. Standard peptide solutions with variable concentrations were also prepared for calibration. The concentration of peptides adsorbed on the surface of HAp was calculated as the difference between initial and unloaded concentration of peptides in solution. To observe the effect of peptide concentration on adsorption phenomenon, 1 mL of peptide solution of different concentrations (0.5, 1.0, 1.5 and 2.0 mM) were mixed with 5 mg of HAp and kept inside an orbital shaker at 37 °C with 100 rpm for 12 h. Followed by centrifugation, the supernatant was collected and syringe filtered. The concentration of peptides adsorbed on the HAp surface was determined by RP-HPLC as described earlier. Binding affinities of the peptides were determined by fitting the experimental data with following linearized form of Langmuir isotherm equation:

$$\frac{[A]}{[SA]} = \frac{[A]}{S_{tot}} + \frac{1}{K_{ads}[S_{tot}]} \quad \text{Equation 4.2}$$

where, [A] and [SA] are the concentrations of adsorbate in solution and adsorbed on the HAp surface. S_{tot} is the total number of surface site available on HA and K_{ads} is the adsorption or binding equilibrium constant. The adsorption of peptides on HAp surface was further confirmed by FT-IR and thermal gravimetric analysis (TGA). In TGA study, the temperature of the peptide bound HAp particles were increased from 30 to 800 °C using a heating rate of 10 °C/min under N₂ atmosphere.

4.3.10. Cell culture studies

The murine pre-osteoblast cells (MC3T3-E1, passage 5-6) were cultured in MEM- α , supplemented with 10% FBS and 1% Pen-Strep antibiotic solution at 37 °C with 5% CO₂ in a humidified atmosphere. The experiments involving long-term cell culture studies, medium was changed every 72 h and the cells were harvested using a solution of trypsin-EDTA at around 70-80% confluency. The cells were further redispersed in complete media and seeded in dishes or cell culture plates to conduct various cell culture studies.

Cytocompatibility studies. The cytocompatible nature of peptides was evaluated via MTT and live-dead staining assays as per the protocols reported earlier.³⁹ Pre-osteoblast cells were first seeded with a cell density of 1×10^5 into a 96 well plate (100 μ L/well) followed by an incubation for 24 h. Meanwhile, peptides (2 mg) and peptide gels (1.33% w/v, 150 μ L, freeze-dried) were sterilized under UV for 30 min and 1 mL of complete MEM- α was added to it. Samples were incubated at 37 °C for 24 h and the extracts were passed through a syringe filter for further use. Cells were incubated with these sample extracts (200 μ L) for 1, 3, and 7 days. The treated cells were incubated with MTT for 3.5 h to evaluate the cytocompatibility. The reduced form of tetrazolium dye was converted into formazan crystals, which is soluble in DMSO. The absorbance of the solubilized formazan in DMSO was measured at 595 nm, which is directly correlated to cellular viability. The experiment was performed in triplicates and the data were represented as mean \pm SD. The cell viability was calculated using the following equation:

$$\% \text{ Cell viability} = \frac{\text{Absorbance for sample}}{\text{Absorbance for control}} \times 100 \quad \text{Equation 4.3}$$

The live-dead staining of the pre-osteoblast cells were performed according to the protocol reported earlier.³⁹ The cells were seeded in 48 well plate at a density of 2×10^4 cells/well at 37 °C in a humidified environment containing 5% CO₂ for 24 h. Followed by the withdrawal of media, sample extracts (200 µL) were added and incubated for another 3 days. Next, samples were aspirated and the adhered cells were stained with a mixture (150 µL) of two dyes: calcein AM and ethidium bromide staining live and dead cells. The cells were incubated for another 30 min avoiding any exposure to light. A fluorescence microscope was used to visualize the stained cells.

Cytoskeletal staining. The F-actin filament of the live cells were stained with Alexa Fluor 588 phalloidin. To perform this experiment, the cells were seeded on a coverslip and incubated for 24 h at 37 °C in a humidified environment containing 5% CO₂. The media was replaced with gel extracts and incubated for 3 days. After the incubation period, cells were washed with PBS and fixed with 4% solution of paraformaldehyde for 30 min, followed by washing with PBS. Next, 0.1% triton X-100 was used to permeabilize cells for 15 min. The permeabilized cells were treated with a solution of Alexa Fluor 488 phalloidin to stain F-actin for 30 min in dark conditions. DAPI solution (1 µg/mL) was used to further stain the nuclei of the cells for 10 min followed by washing with PBS. The stained coverslips were further mounted on to the glass slide with the help of a mounting solution and visualized under a fluorescent microscope and the images were captured at a magnification of 63×.

In vitro cell migration. Migration of MSCs is a predominant phenomenon to promote intramembranous ossification, which helps in bone regeneration. Scratch assay was carried out on pre-osteoblast cells to assess the regenerative potential of peptides and gels. In a treated 6 well plate, MC3T3 was cultured at a density of 1×10^5 cells/well until the cells achieved 100% confluency. A scratch in a form of straight line was made on the monolayer of cells with a 200 µL sterile tip. The cells were washed with PBS to remove the debris and peptide/gel extracts were added to the respective wells and cell migration was observed for 48 h. Images were acquired at certain interval of time under inverted microscope (Evos XL core, Invitrogen) to observe the healing of scratch due to the migration of cells.

Encapsulation of cells. Peptide gels (WWHS, WWHO, WWHD, and WWHE) were used as a scaffold for the encapsulation of MSCs. Around 2 mg of peptides were dissolved in a 100 µL of NaOH solution of pH 9 and mixed with 50 µL of cell suspension (5×10^3 cells/mL suspended in complete MEM-α medium) followed by even distribution into the wells of 48-well plate to form a monolayer of cell. A 200 µL of complete media was added on gels and kept at 37 °C in a humidified environment containing 5% CO₂. Cell viability was assessed by staining the cells with a mixture of calcein AM and ethidium bromide.

4.3.11. ROS scavenging assay

The effects of peptides and gels on the scavenging of intracellular reactive oxygen species (ROS) in living cells were quantitatively determined in H₂O₂ stressed MC-3T3 cells using H₂-DCFDA, which is an oxygen sensitive fluorescent probe. A 100 µL of cell suspension with a density of 1×10^4 cells/mL

were incubated in Nunc-coated 96-well black plate at 37 °C in a humidified environment with 5% CO₂. After 24 h, the medium was removed and 100 µL of sample extracts (peptides/gels incubated for 24 h with incomplete medium and syringe-filtered) were added to each well and incubated for another 24 h. The cells were then exposed to H₂O₂ solution (0.5 mM) to instigate ROS production, after which the medium was removed, washed with PBS, and exposed to 25 µM of DCFDA solution for 1 h in dark condition. The solution was aspirated and PBS was added followed by the measurement of fluorescent intensity on a plate reader at excitation and emission wavelengths of 485 and 530 nm. Cells without any sample extracts were treated as a negative control, whereas 1 mg/mL of ascorbic acid was considered as a positive control. The same protocol as previously described was followed for qualitative analysis of ROS production within the cells. A treated 48-well plate was taken instead of black 96-well plate and 2×10^4 cells/well were seeded. The fluorescence microscope's FITC channel was utilized to visualize the intracellular DCFDA in cells. The MTT assay was further performed to evaluate the protective effect of peptides and gels towards the viability of the oxidative stress-induced MC-3T3-E1 cells.

4.3.12. In vitro osteogenic activity

Alkaline phosphatase and calcium deposition assays, as well as gene expression analysis were performed to assess the osteogenic potential of peptides and gels. Cells with a density of 1×10^5 /mL were cultured in a 48-well plate for 24 h. After aspirating the media, cells were treated with 200 µL extracts of peptides and gels in complete MEM- α and incubated for 7 and 14 days. The cell media was replenished with sample extracts, every 72 h. Osteogenic media (OM) composed of complete MEM- α containing 100 nM dexamethasone, 50 µg/mL ascorbic acid, and 10 mM β -glycerophosphate disodium salt hydrate was considered as a positive control, while complete MEM- α without sample extracts was treated as the negative control.

Alkaline phosphatase (ALP) estimation. In vitro ALP activity was estimated following the protocol described earlier in the literature with little modifications.³⁶ Media was removed at day 7 and 14, and cells were washed with DPBS followed by lysis of cells with 200 µL, 0.2% triton X for 30 min in order to rupture the cell membrane and release the ALP molecules. Subsequently, 200 µL of p-nitrophenyl phosphate (pNPP) solution was added to each well containing cell lysates and incubated at 37 °C for another 90 min in dark. The final absorbance was measured at 405 nm using a plate reader.

Calcium deposition assay. Calcium deposition on the MC 3T3 cells were assessed by Alizarin Red S (3,4-Dihydroxy-9,10-dioxo-9,10-dihydroanthracene-2-sulfonic acid) stain. Alizarin Red S is commonly used to stain deposits of calcium in tissues. It works by binding calcium species in cells and producing red colored crystals under a bright field microscope. On day 7 and 14 of cell culturing, cells were washed with DPBS and fixed with 4% paraformaldehyde solution for 10 min at 4 °C. Followed by washing with DI water, fixed cells were stained with 500 µL of alizarin red S solution (40 mM, pH= 4.1-4.3) for 1 h in dark. After staining, the cells were washed with DI water to remove the excess dye and the cells were visualized under an inverted microscope to observe the red crystals. To further quantify the total amount of calcium deposited in the mineralized cells, 200 µL of 10% cetyl pyridyl chloride solution was added

to each well and incubated for 30 min in dark condition. Around 100 μ L of dissolved crystals were transferred to 96-well plate and the absorbance was measured at 562 nm.

Effect on MC3T3-E1 differentiation. To evaluate the effect of peptide and gels on osteogenic differentiation, the expression of osteogenesis related marker genes, such as alkaline phosphatase (ALP), runt-related transcription factor 2 (RUNX2), collagen type I (COL I) osteocalcin (OCN), and osteopontin (OPN) at mRNA level were examined in MC 3T3 cells. In a 6-well plate, cells were seeded at a density of 1×10^4 cells/mL and cultured for 24 h. Next, media was removed and 1 mL of extracts of peptides and gels were added. After every 72 h, media was replenished and on day 7 and 14, and total cellular RNA was isolated by lysis in TRIzol and subjected to cDNA synthesis. The levels of specific genes were assessed by quantitative real-time polymerase chain reaction (qRT-PCR). The GAPDH was used as a housekeeping gene to normalize expression levels. The sequences of gene primers are shown in **Table A4 in Appendix**.

Effect on MC 3T3-E1/RAW 264.7 indirect co-culture. To further study the effect of peptides and gels on osteogenic differentiation, 12 well plate with inserts of 0.4 μ m pore size were used for the indirect coculture study of MC-3T3 and RAW 264.7 (murine leukemic monocyte macrophage cell lines). RAW 264.7 cells with a concentration of 1×10^5 cells/mL were seeded on the 12-well plate and MC-3T3 cells at a density of 1×10^5 cells/mL were placed on the inserts. The co-culture system was cultured in complete MEM- α at 37 $^{\circ}$ C in 5% CO₂ and fully humidified atmosphere for 24 h to allow the cells to form a monolayer. The co-culture system was maintained under both basal and osteogenic conditions with and without 50 ng/mL of receptor activator of nuclear factor kappa B ligand (RANKL) protein. MC 3T3 cells were incubated with the extracts of peptides and gels for 7 days and media was replaced every 72 h. On day 7, expression of RANKL, a gene related to the differentiation state of osteoblasts was measured in MC 3T3-E1 cells by RT-PCR. Simultaneously, the expression of TRAP (tartrate resistant acid phosphate), a marker for osteoclast differentiation and resorbing activity of bone was measured in RAW 264.7 cells by RT-PCR.

4.3.13. Polarization of macrophage and inflammatory response

The gene expression levels of the M1 phenotype macrophage marker, TNF- α , iNOS, and M2 phenotype macrophage marker, IL-10, were measured by RT-PCR. Briefly, RAW 264.7 cells were incubated with the extracts of peptides and peptide gels for 7 days. The cells were then collected and the total RNA was extracted using TRIzol, followed by reverse transcription into cDNA using cDNA synthesis kit (Bio-Rad). Finally, the quantitative analysis of gene was performed by RT-PCR. The results were normalized to the expression levels of GAPDH.

4.3.14. Statistical analysis

The studies were performed in triplicates and presented as average values and standard deviations from the mean value. The data were further analyzed by Student's t-test. *p values ≤ 0.05 were considered significant and ns represents non-significant difference.

4.4. Results and discussion

The aim of this work was to investigate the role of polar and charged amino acids in tetrapeptides for their binding affinities towards HAp surface and promoting the differentiation of MSCs. Since the mineralization of HAp crystals into the gaps of collagen fibrils enhances the rigidity of the bone, the HAp binding peptides can offer a route for controlling the adsorption of calcium phosphate biominerals and regulate the bone tissue regeneration process.⁴⁰ We have designed and developed six self-assembling, nanostructured peptide scaffolds (WWHS, WWHJ, WWHP, WWHO, WWHD, and WWHE) and evaluated their antioxidant, HAp binding, alkaline phosphatase increment, calcium deposition, cell migration, immunomodulation properties, and inducing the expression of osteogenic markers (**Figure 4.1**).

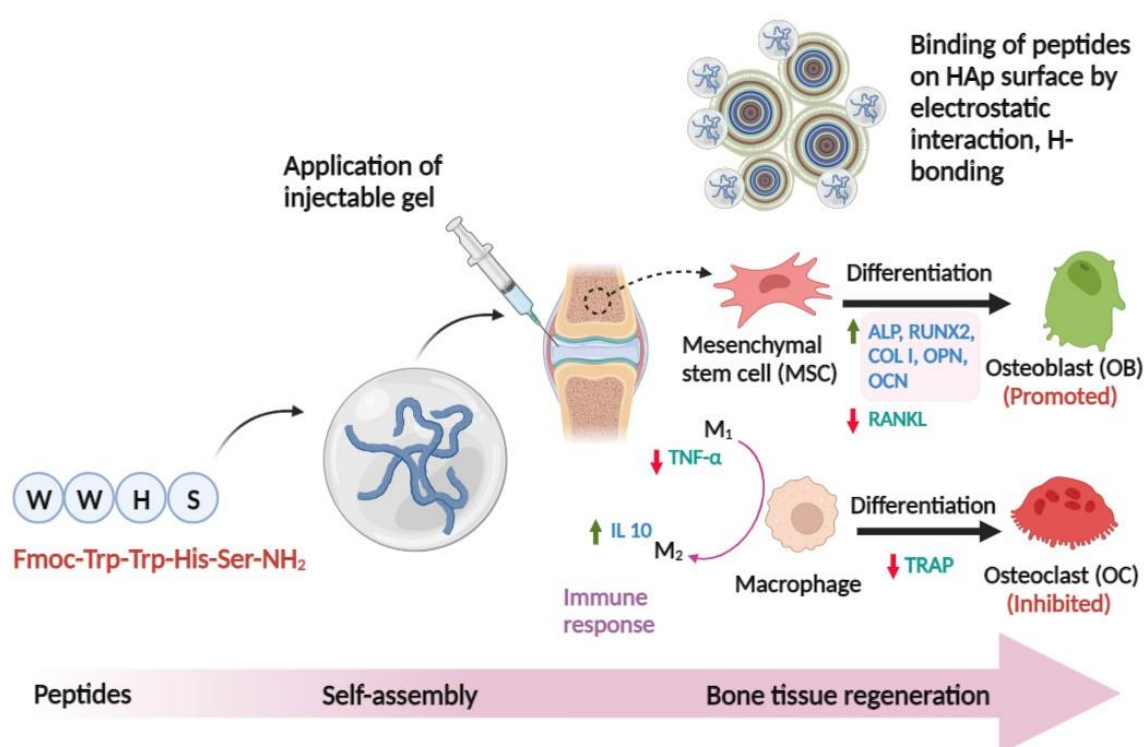


Figure 4.1. Self-assembling peptides and their application in bone tissue regeneration by binding to the hydroxyapatite (HAp) surface, potentiating the differentiation of mesenchymal stem cells (MSCs), and inhibiting osteoclastogenesis.

4.4.1. Design of self-assembling peptides and characterizations

To prepare supramolecular scaffolds from ultrashort peptides, we have chosen a self-assembling, aromatic tripeptide unit (Fmoc-Trp-Trp-His-NH₂, WWH) as previously reported by our group⁴⁰ and incorporated different polar and charged amino acids (Ser, pSer, Pro, Hyp, Asp, or Glu) at the C-terminus to make it amphiphilic and anionic at physiological pH. It is evident from the literature that peptides rich in negatively charged groups augment the bone mineralization process to a significant extent.^{41,42}

Extensive studies were also carried by researchers, which showed that collagen and non-collagenous proteins (osteopontin, dentin, fetuin, bone sialoprotein, etc.) found in bone ECM play a pivotal role in mineralization of bone by nucleating HAp crystals. So, in this work, we have designed the collagenous and non-collagenous protein inspired peptides, Fmoc-Trp-Trp-His-Ser-NH₂ (WWHS), Fmoc-Trp-Trp-His-pSer-NH₂ (WWHJ), Fmoc-Trp-Trp-His-Pro-NH₂ (WWHP), Fmoc-Trp-Trp-His-Hyp-NH₂ (WWHO), Fmoc-Trp-Trp-His-Asp-NH₂ (WWHD), and Fmoc-Trp-Trp-His-Glu-NH₂ (WWHE) by integrating amino acids, which are present in these proteins (**Figure 4.2A**). Ser and pSer are found in osteopontin, Pro and Hyp are the integral parts of collagenous protein, and Asp and Glu are present in bone sialoprotein (BSP).⁴³ All peptides were synthesized using an Fmoc-based SPPS approach taking rink amide resin as a solid support to generate amide group at C-terminus, which is reported to be proteolytically stable compared to the peptide acids. The peptides were characterized by RP-HPLC, ¹H NMR, and mass spectrometry. The RP-HPLC showed that peptides were 90-95% pure and the retention times were found to be 3.9, 5.9, 4.1, 4.3, 4.0, and 5.4 min for WWHS, WWHJ, WWHP, WWHO, WWHD, and WWHE (**Figure A50, Appendix**). The molecular weight derived from the mass spectrometry matched with their theoretical values (**Figure A51-56, Appendix**). The ¹H NMR spectra of peptides along with their assigned peaks are included in the **Appendix (Figure A57-62)**.

Furthermore, the amphiphilic nature of peptides enables them to get self-assembled into various nanostructures. We observed hydrogelation of four peptides, WWHS, WWHO, WWHD and WWHE, in a pH-triggered approach. Vial inversion method was used to monitor the gel formation. The peptide containing proline residue (WWHP) was in solution state even after changing the pH, whereas phosphoserine containing peptide (WWHJ) was precipitated after adding NaOH solution of pH 9. This is more likely due to the presence of highly negatively charged pSer group, which is hindering the self-assembly process. WWHS and WWHO instantly formed gels, which can be attributed to the presence of additional hydrogen bonding by the side chains of S and O. The zeta potential of peptides was measured in alkaline borate buffer of pH 8 and all peptides were found to possess negative charge at their surface as confirmed by negative zeta potential values (WWHS: -2.67 mV; WWHJ: -32.9 mV; WWHP: -16.3 mV; WWHO: -18.8; WWHD: -29.0 mV, and WWHE: -30.7 mV) (**Figure 4.2B**). The presence of phosphate and carboxylate group in WWHJ, WWHD, and WWHE decorate the surface of peptides with more negative charges. According to the literature, negatively charged nanostructures preferentially bind to the highly positively charged collagen fibrils and help in the nucleation of biominerals for successful regeneration of bone.⁴² The nanoscale architecture of the self-assembled peptide scaffolds was evaluated by SEM and FESEM. We envisioned that the amphiphilic structure of peptides will guide the development of porous, nanostructured assemblies, which will benefit the stem cell adhesion and proliferation by mimicking the composition and nanoarchitecture of bone and providing biochemical cues.

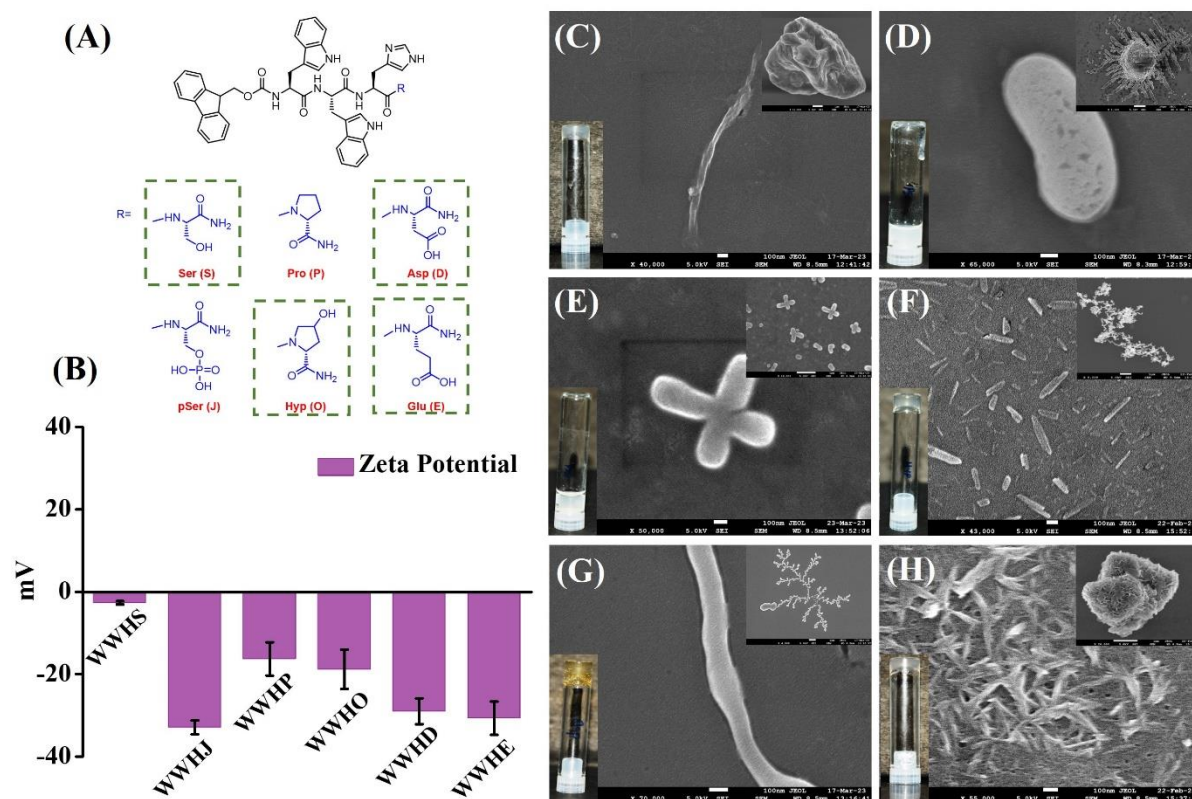


Figure 4.2. (A) Structure of self-assembling tetrapeptides, WWHS, WWHJ, WWHP, WWHO, WWHD, and WWHE. (B) Zeta potential of peptides. (C-H) FESEM micrographs of self-assembled peptides. Scale bar: 100 nm and 1 μ m (inset). (C) WWHS. (D) WWHJ. (E) WWHP. (F) WWHO. (G) WWHD. (H) WWHE.

The micrographs obtained from SEM reveals the porous morphology of peptide gels (WWHS, WWHO, WWHD, and WWHE), which can provide a bone-like microenvironment and promote cell infiltration and exchange of nutrients (**Figure A63, Appendix**). Interestingly, change of the 4th amino acid in the tetrapeptide sequence altered their microscopic structure in self-assembled state as demonstrated by the FESEM images (**Figure 4.2C**). The peptides with Ser (WWHS), Asp (WWHD), and Glu (WWHE) form long, entangled nanofibrillar structure with a dimension of less than 100 nm, which has the propensity to imitate bone ECM. Peptides comprising of pSer (WWHJ), Pro (WWHP), and Hyp (WWHO) were self-assembled into nanorod-like structures, which can help in proliferation, differentiation, and biomineralization of osteoblasts. The nanorods with a size around 200 nm were present as cluster in the self-assembled form of WWHP, whereas WWHO exhibited nanorod structure with less width (~ 100 nm) and were scattered. This phenomenon can be supported by the fact that a slightly elevated hydrophilicity of WWHO due to the presence of hydroxyl group dispersed the nanorods in aqueous solution and the absence of hydroxyl group in Pro made it less hydrophilic, which propagates the self-assembly process into a shape of clustered nanorod. Large amount of negative charge on the surface of pSer inhibited the self-assembly process and formed nanorods with a width of around 430 nm in aqueous solution. Thus, these peptides can be used as an injectable scaffold (gels) or can be integrated on the implant surface to promote ossification.

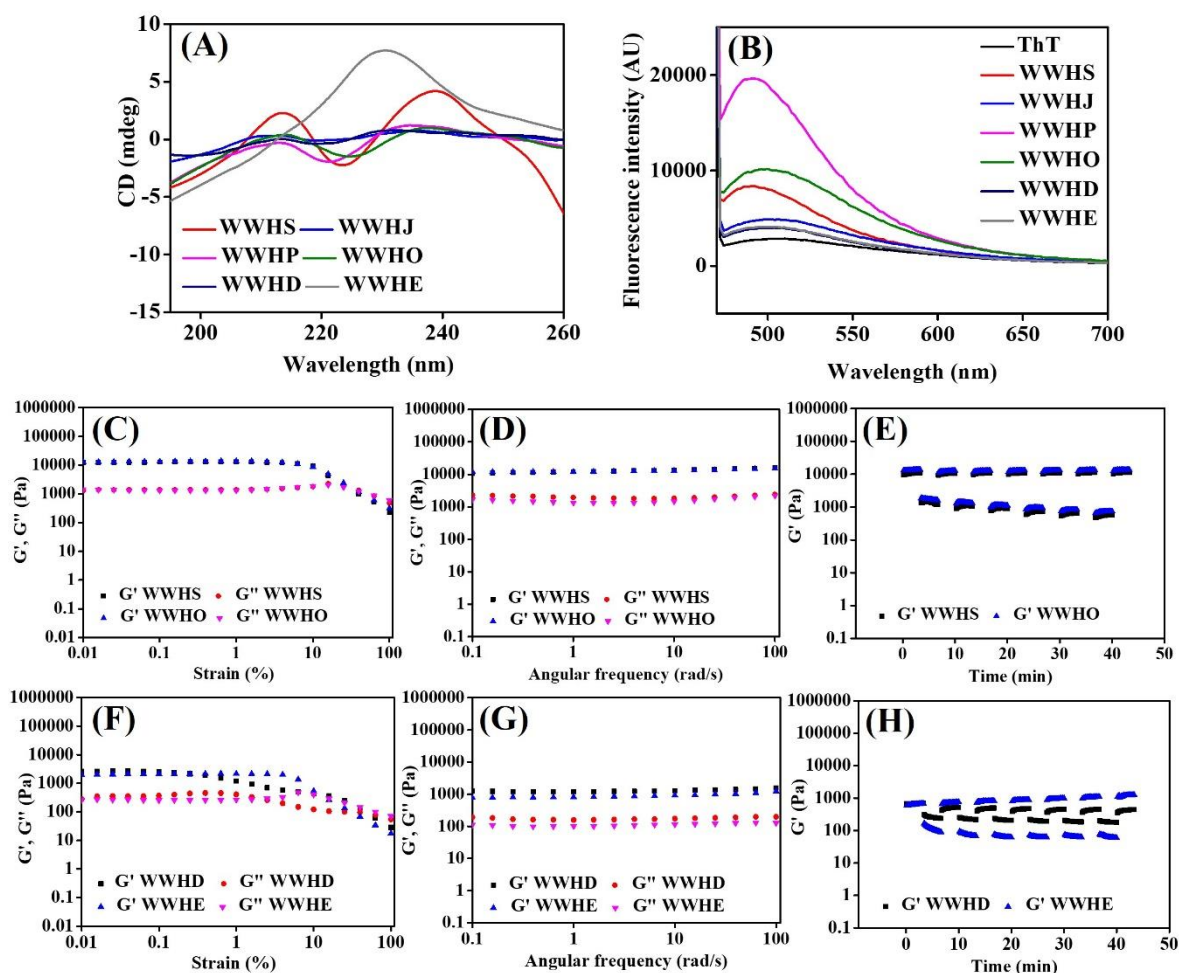


Figure 4.3. (A-B) Secondary structure formed by peptides. (A) CD spectra. (B) ThT assay. (C-H) Rheological analysis of supramolecular peptide gels, WWHS, WWHO, WWHD, and WWHE. (C, F) Amplitude sweep depicting storage and loss modulus at a constant angular frequency of 10 rad s⁻¹. (D, G) Frequency sweep at a constant strain of 1%. (E, H) Storage modulus at alternating strains of 30 and 1% for six cycles.

The aromatic amino acids (Trp and His) and the Fmoc group at the N-terminus of the peptide sequence induced the self-assembly process by facilitating intermolecular hydrophobic π - π stacking interactions. To confirm the secondary structure of peptides, CD, FT-IR spectroscopy, and thioflavin-T assay were performed. β -sheet structures of all peptides were evident from the CD spectra. A broad negative band around 215-225 nm and a broad positive peak around 195-210 nm justified the presence of β -sheet structure in the nano assembly (**Figure 4.3A**). In case of WWHJ, WWHD, and WWHE, the negative band around 220 nm, which confirms the assembly as disordered secondary structure or random coil, was not prominent. The inter and intramolecular hydrogen bonding is an essential driving force for self-assembly process of peptides, which is validated by the FT-IR spectra. The C=O stretching vibration was determined by the amide I region with distinct peak in the region of 1620-1690 cm⁻¹, which suggested the presence of β -sheet like secondary structure (**Figure A64, Appendix**). The characteristic peak at amide II (1480-1575 cm⁻¹) and amide III (1229-1390 cm⁻¹) regions were dedicated to the

bending motion of N-H coupled to C-N stretching, which opens a possibility of the presence of β -sheet conformation in self-assembled peptides. Thioflavin-T (ThT) assay was further conducted to ascertain the formation of β -sheet structures. The hydrophobic region of peptides was responsible for the binding with ThT, which leads to significant enhancement of the fluorescence intensity (between 490-500 nm) compared to unbound ThT and confirmed the presence of β -sheets in the self-assembled structures of WWHS, WWHP, and WWHO peptides, whereas, the fluorescence intensity was not that much augmented for WWHJ, WWHD, and WWHE, which further suggests the absence of prominent β -sheet structure in their assembly (**Figure 4.3B**).

4.4.2. Rheological measurements

The stability and mechanical stiffness of peptide gels were investigated by rheological studies (**Figure 4.3C-H**). The storage modulus of all gels were 10 times greater than their respective loss modulus, which confirms the viscoelastic property of gels. Gels, fabricated from WWHS and WWHO exhibited higher storage and loss modulus than those from WWHD and WWHE (G' : ~ 12 kPa and G'' ~ 1.4 kPa for Ser and Hyp containing peptides, whereas G' ~ 2.3 kPa and G'' ~ 0.2 kPa for peptide gels containing Asp and Glu, **Figure 4.3C, F**). The linear viscoelastic region (LVR) was observed at around 6% strain for WWHS and WWHO gels, which decreased to 4% and 0.4% for WWHE and WWHD gels. The dynamic frequency exhibited that the storage and loss modulus have a good tolerance to external shear stress and is essentially angular frequency independent. (**Figure 4.3D, G**).

The thixotropic properties of gels were measured by step-strain method, where gels were subjected to high and low strain alternatively for six cycles (**Figure 4.3E, H**). The storage modulus was declined upon administration of high strain but the gels were able to regain their storage modulus and get back to their original shape after withdrawal of the strain. This phenomenon illustrates the self-healing property of the peptide gels, which is an essential criterion for the injectable gels. The mechanical stability of the Ser and Hyp containing peptide gels were found superior than peptide gels with Asp and Glu because of the additional hydrogen bonding interaction with the hydroxyl group present in the side chain of Ser and Hyp. The results are comparable with the peptide gels reported earlier for the purpose of biomineralization.^{44,45} Swelling and degradation study of all these four gels was performed for 14 days and the data is reported in **Figure A65, Appendix**.

4.4.3. Hydroxyapatite binding studies

A major objective of our study was to produce peptides, which can physically or chemically bind with HAp and demonstrate high attraction to bone. We hypothesize that the peptides will provide favorable ionic and H-bonding interactions between the negative charges on the functional groups of amino acids (hydroxyl, carboxylic, and phosphate) and calcium ions within the main mineral component of bone (HAp at physiological pH).⁴⁶ Murphy *et al.* have reported that peptides containing poly(aspartic acid), poly(glutamic acid) or bisphosphonates exhibited remarkable ionic attraction towards HAp.⁴² Ling *et al.* has also discussed the role of non-collagenous proteins enriched with acidic and phosphorylated amino acid in regulating the nucleation and growth of HAp for bone mineralization.^{43,47} Bang *et al.* had

compared the HAp binding affinities of a set of peptides with positive (containing basic amino acids) and negative charge (containing acidic amino acids) and illustrated that the positively charged peptides (KNFQSRSH) exhibited better binding signal towards HAp and utilized them for biomedical imaging of bone.⁴⁸ Gungormus *et al.* also reported the ionic interaction of positively charged histidine binding peptides with phosphate ions of HAp.⁴⁵ Thus, the exact mechanism of binding of peptides towards HAp is still controversial. The interaction of collagen peptides (Pro-Hyp-Gly) with HAp has been demonstrated theoretically and experimentally.⁴⁹

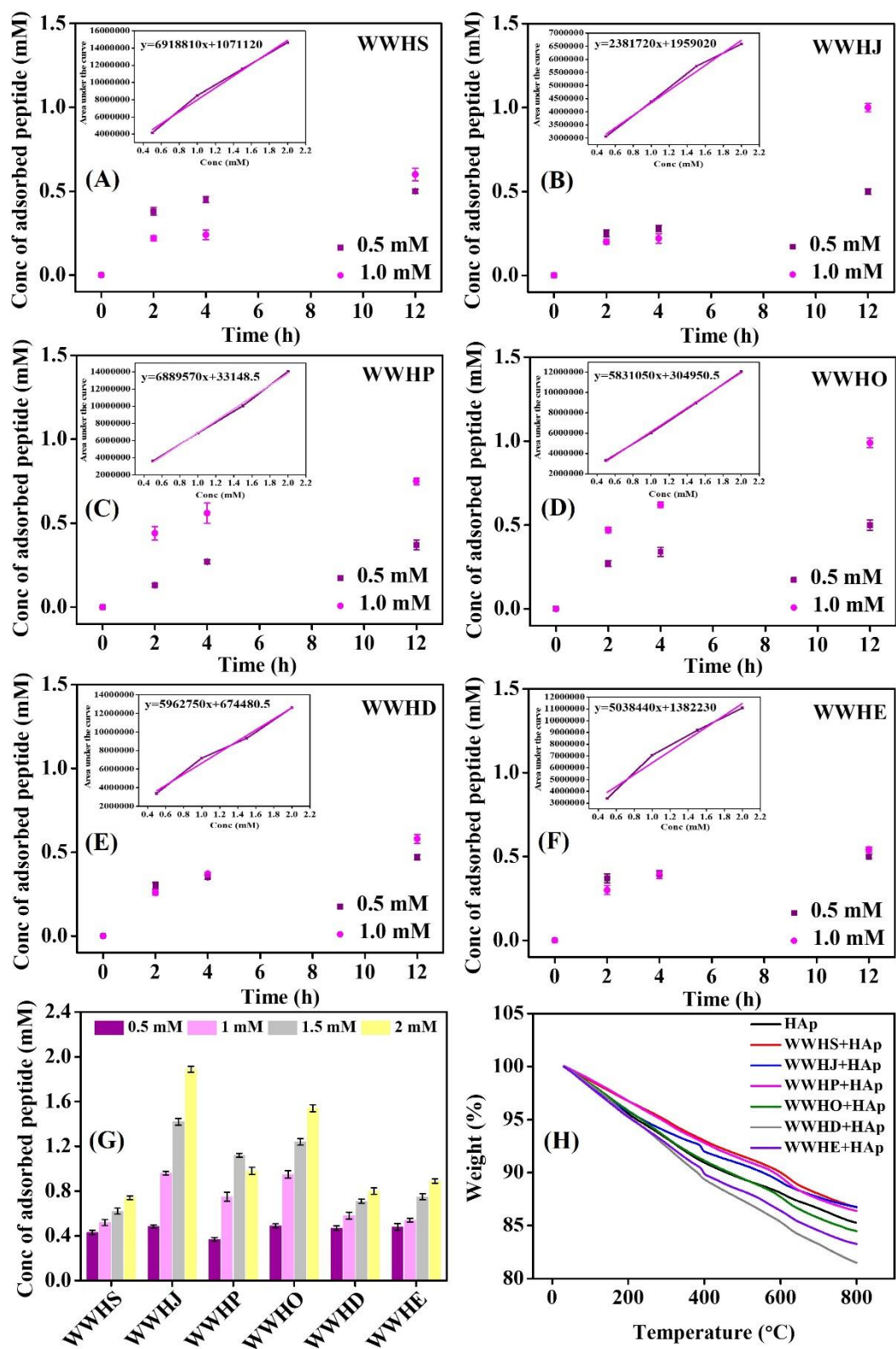


Figure 4.4. Binding of peptides on the surface of HAp. (A-F) Adsorption of peptides (0.5 and 1.0 mM) on HAp surface at different time intervals. (G) Concentration (0.5, 1.0, 1.5 and 2.0 mM)-dependent adsorption of peptides on HAp surface. (H) TGA data of bare HAp and peptide bound HAp.

In our case, we have determined the concentration of adsorbate bound on the surface of HAp by HPLC method. As shown in **Figure 4.4A-F**, the concentration of adsorbate on the adsorbent surface was

elevated with time and in case of WWHJ and WWHO, around 95% of peptide was bound on the surface of HAp at both the concentrations (0.5 and 1.0 mM). This could be due to the higher interactions of phosphate group of phosphoserine (J) and hydroxyl and amine group of hydroxyproline (O) with the Ca^{2+} , PO_4^{3-} and OH^- of HAp. The binding affinity of Ser and Pro containing residues were also significant with more than 90% of peptide in bound state at 0.5 mM concentration and 60-75% binding was observed when the initial concentration of peptide solution was increased to 1.0 mM. The peptides containing Asp and Glu with carboxyl functionality also provided remarkable binding affinity towards HAp surfaces. It has been observed in most of the cases that the concentration of peptides bound on the HAp surfaces increased with the increasing concentration of the peptides in solution (**Figure 4.4G**). The major interactions responsible for this binding are H-bonding and ionic interactions. The oxygen atom of the carboxylate and carboxyl groups interacted with the surface calcium ions by ionic interactions ($\text{Ca}\cdots\text{OCO}^-$, $\text{Ca}\cdots\text{O}=\text{C}$). Hydrogen bonding can form between hydrogen atoms of amine group and phosphate and hydroxyl oxygen atoms ($\text{NH}\cdots\text{OPO}_3$, $\text{NH}\cdots\text{OH}$).⁵⁰ The carboxyl group can also be engaged with hydrogen bonding interactions with the surface hydroxyl group of HAp ($-\text{C}=\text{O}\cdots\text{HO}-$). The imidazole ring of histidine can also be protonated at physiological pH and take part in hydrogen bond and ionic interactions. This study suggests that amino acids with side chains bearing either acidic or basic residues are more prone to strong interaction with the HAp surfaces. Nano structures of the self-assembled peptide can also have impact on the binding due to their enhanced surface area.

The data was fitted into the linear form of Langmuir adsorption isotherm and the binding constant (K_{ads}) was determined (**Figure A66, Appendix**).⁵¹ The binding affinities of peptides follow the sequence, WWHP < WWHS < WWHE < WWHD < WWHJ < WWHO indicating the participation of all the side chains of amino acids to some extent with a dominance of hydroxyl and negative charged functionalities (**Table A3, Appendix**). The thermogravimetric analysis (TGA) was also performed with the peptide bound HAp and a significant weight loss was observed around the region of 400-600 °C, which further confirmed the binding of peptides to the HAp surface (**Figure 4.4H**). FT-IR spectra elucidated the vibration of PO_4^{3-} at 1030, 605, and 565 cm^{-1} as well as bands corresponding to N-H stretching at 1640 cm^{-1} associated with adsorption of peptides on HAp surface (**Figure A67, Appendix**).⁵² Therefore, the above-mentioned studies proved that these peptides can provide significant bone-binding properties and can also be used further for targeted drug delivery and imaging to bone.

4.4.4. Cell viability and migration studies

Cell proliferation is the first stage of bone tissue regeneration. At this stage, the MSCs proliferate while maintaining its potency. Biomaterials, intended for the ossification, should be biocompatible and safe to ensure the proliferation of stem cells. To assess the cytocompatibility of peptides and gels, MTT assay was performed on pre-osteoblast cell line (MSCs) and macrophages (RAW 264.7). The number and viability of MSCs increased (1, 3 and 7 days) when treated with the extracts of peptide gels (WWHS, WWHO, WWHD and WWHE) and peptides (WWHJ and WWHP) indicating the cytocompatibility of the samples. Peptides containing proline and hydroxyproline exhibited highest proliferation of stem cells

(>170%) after 7 days, whereas peptides composed of Ser, pSer, Asp, and Glu demonstrated 150% proliferation of MSCs (**Figure 4.5A-C**). It is evident from the literature that collagen helps in spreading and proliferation of pre-osteoblast cells and Pro and Hyp are the major residues of collagen, which justifies the significant proliferative property of WWHP and WWHO. Since macrophages are the precursors of bone absorbing cells, osteoclasts, we were interested to know the fate of macrophages after treating with the extracts of peptides and peptide gels. The viability of RAW 264.7 was checked at 1st and 3rd day and the cells were found compatible with a viability of 90-100% (**Figure A68, Appendix**).

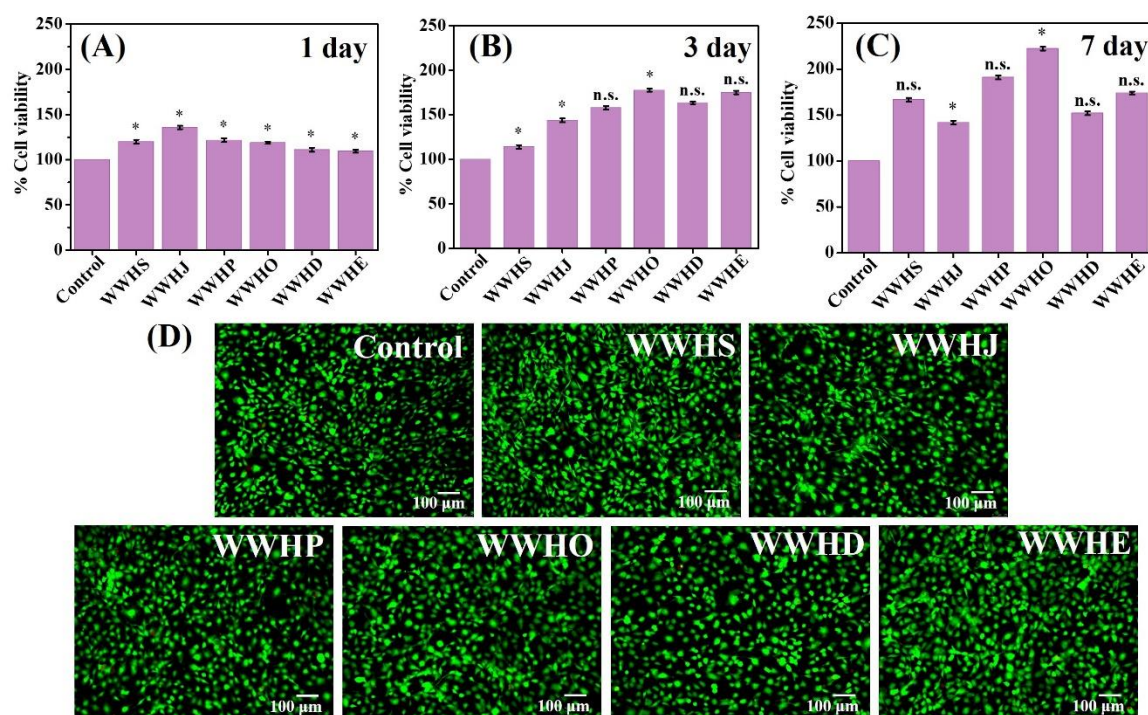


Figure 4.5. (A-C) Cell viability of MC3T3-E1 cells in the presence of the extracts of peptides (WWHJ and WWHP) and gels (WWHS, WWHO, WWHD, and WWHE) using MTT assay at 1, 3, and 7 days. Data are presented as mean \pm SD, $n = 3$, and * $p < 0.05$ indicates statistically significant data. (D) Fluorescence microscopy images of MC3T3-E1 cells after live-dead staining at 3 days. Cells without any treatment was considered as a control. Scale bar: 100 μ m.

The cytocompatible nature of peptides and gels were also verified by live/dead staining on MSCs. The growth and spindle-shaped morphology of MC3T3-E1 were seen under the fluorescence microscope, demonstrating that the peptides and gels were not cytotoxic and can promote cell proliferation. The abundance of green emission indicated that the sample will not have an impact on the viability of pre-osteoblast cells during the process of bone repair (**Figure 4.5D**).

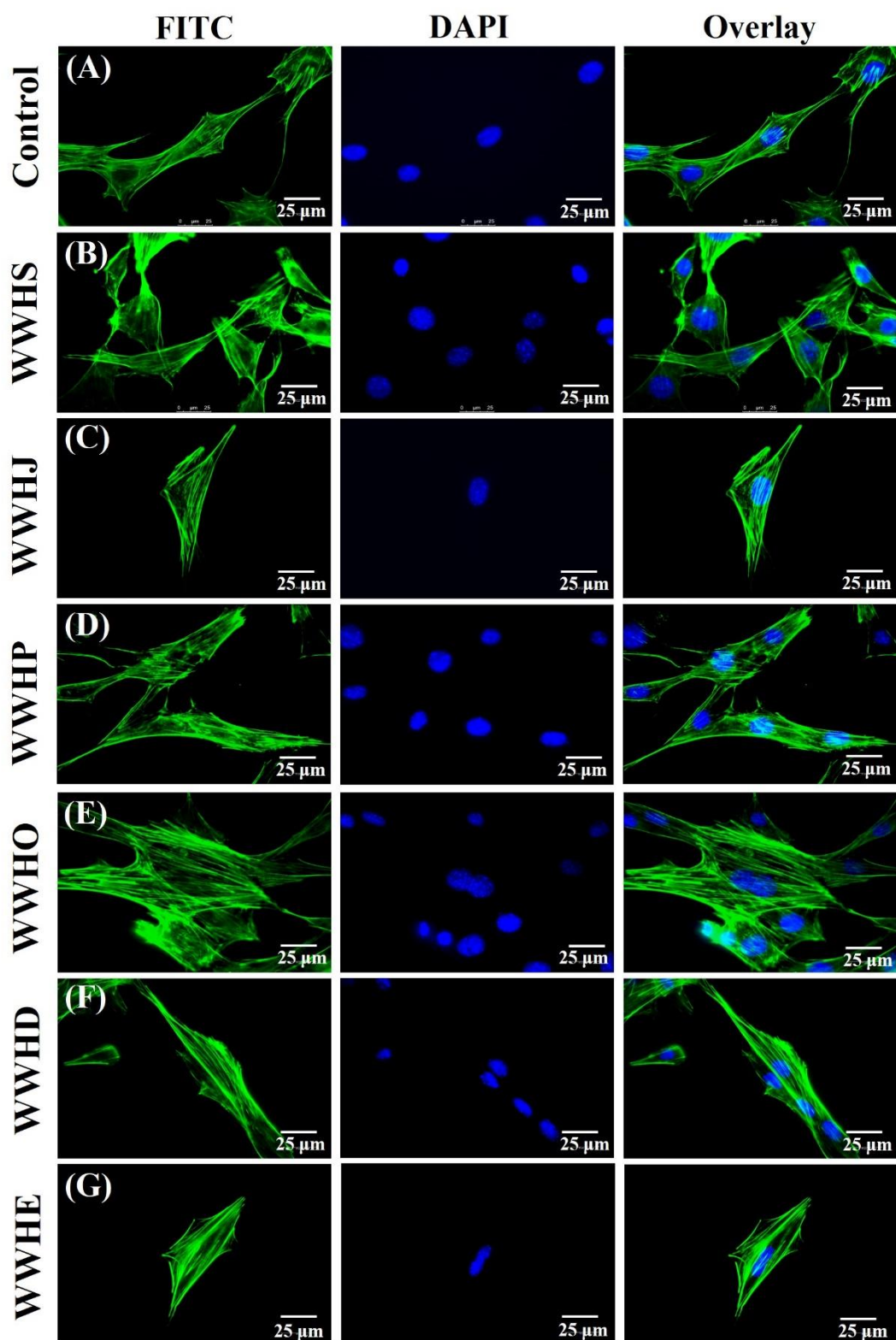


Figure 4.6. (A-G) Cytoskeletal staining of MC3T3-E1 cells with Alexa Fluor phalloidin (green) and DAPI (blue) after treating with the extracts of peptides and gels. Cells without any treatment was considered as a control. Scale bar: 25 μm .

The investigations conducted so far clearly demonstrated the cytocompatible nature of peptides and peptide gels, which produced a desirable surface for the pre-osteoblast cells to support growth and proliferation over a time period of 7 days. In order to visualize the morphology of MSCs

(mononucleated, fibroblast like shape with extended cytoplasmic projection) upon interaction with the extracts of peptides and gels, cells were stained with Alexa Fluor 488 phalloidin, which turns the cytoskeleton green and DAPI stains the nucleus blue (**Figure 4.6**). This intact morphology of MSCs after treatment with peptides and gels for 3 days is related to the cellular viability.

Other than proliferation, migration of MSCs is a fundamental step in bone fracture healing because MSCs need to firstly migrate to the bone surface before they can participate in bone formation. It is also reported in the literature that enhancing migration of MSCs may offer a cutting-edge method for restoring the bone loss and other bone diseases, such as osteoporosis, fracture, and osteoarthritis (OA). Thus, we have investigated the potential role of our peptides and gels for endorsing the migration of mesenchymal stem cells. From **Figure A69, Appendix**, we have observed that after the treatment of cells with extracts of peptides and gels, the cells started migrating within 12 h and healed the scratch by 48 h as compared to negative control (untreated). The percentage area of healing of scratch was also calculated using ImageJ software and depicted in **Figure A70, Appendix**. After successfully completing these preliminary requisites, these collagen and non-collagen derived peptides can be taken further for developing materials to successfully regenerate bones.

4.4.5. Radical scavenging properties

Levels of reactive oxygen species (ROS) inside bone cells are one of the primary causes of osteoporosis. Under stressed condition, ROS override the body's natural antioxidant defenses, leading to bone loss and skeletal fragility.³³ Thus, the introduction of antioxidant material has gained interest for decelerating bone resorption process and evoke bone formation. The ROS scavenging activity of peptides and gels were evaluated by ABTS assay. **Figure 4.7A** shows the antioxidant properties of peptides and gels by scavenging the colored free radicals, ABTS^{•+} by reducing them into a colorless solution. They exhibited more than 90% radical scavenging activities. The result was compared with ascorbic acid (1 mg/mL), which was taken as a positive control and ABTS radical without samples were considered as a negative control.

To verify the influence of the peptides and gels in reducing the level of intracellular ROS, nonfluorescent dichloro-dihydro-fluorescent dichloro-fluorescein (DCFH-DA) was used, which gets converted into fluorescent dichloro-fluorescein (DCF) in presence of ROS. As depicted in **Figure 4.7B**, the fluorescence intensity was enhanced by the H₂O₂ treatment, which was significantly reduced when the MSCs were pretreated with the antioxidant peptides and gels. This result confirms the radical scavenging potential of the peptides and gels by subsiding the ROS production caused by the H₂O₂ treatment. For qualitative analysis, MC3T3 cells were observed under the fluorescence microscope to observe the intracellular ROS localization. As presented in **Figure 4.7C**, the H₂O₂-treated MSCs have maximum green fluorescence, indicating an increase in the intracellular ROS as opposed to the control (untreated), which showed much less green fluorescence. Pretreatment of cells with peptides and gels quenched the green fluorescence, leading to the scavenging of free radicals. The viability of cells was also determined in order to validate the protective quality of peptides and gels during the oxidative stress

caused by the H_2O_2 treatment. MTT (**Figure A71, Appendix**) assay suggested that peptides and gels can effectively elevate the survival rate in the range of 75-90% compared to the control group.

4.4.6. Encapsulation of stem cells

We encapsulated MSCs into the peptide gels fabricated from WWHS, WWHO, WWHD, and WWHE peptides to better understand the viability of MSCs inside the gel microenvironment. The cells were stained using the live/dead staining protocol using a mixture of calcein AM and ethidium bromide. It is evident from **Figure 4.7D**, that the MSCs are viable inside the three-dimensional matrix of gels. The green fluorescence authenticates the presence of live cells inside the gel scaffold.

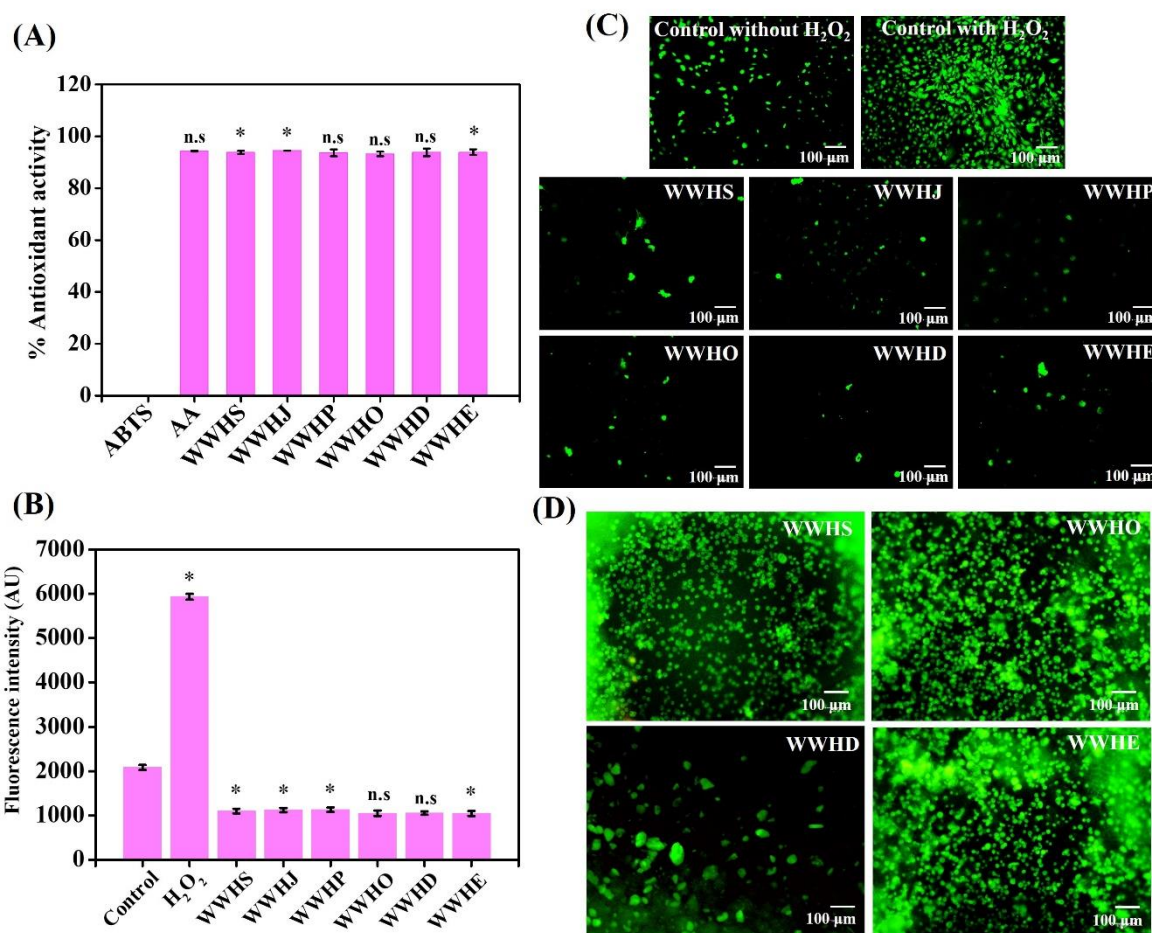


Figure 4.7. (A) Antioxidant properties of peptides using ABTS assay, and ABTS^{•+}, and ascorbic acid (AA) were used as negative and positive controls. (B-C) Effects of extracts of peptides and gels on ROS. (B) Fluorescence intensity of MC 3T3 cells after treatment with extracts, followed by the treatment with DCFDA. Cells without exposure to H_2O_2 were considered as a control. Data are presented as mean \pm SD, $n = 3$, and * $p < 0.05$ indicates statistically significant data and ns not significant difference. (C) Fluorescence microscopy images of MC 3T3 cells treated with gel extracts and DCFDA. Scale bar: 100 μ m. (D) Fluorescence microscopy images of calcein AM and ethidium bromide-stained MSCs encapsulated into the gels (WWHS, WWHO, WWHD, and WWHE). Scale bar: 100 μ m.

4.4.7. Osteogenic differentiation studies

All the above findings encouraged us to further study the osteoinductive effects of peptides and gels on pre-osteoblast cells. We performed experiments to quantify the traditional osteogenic biomarkers. We anticipate that these studies will further demonstrate the successful use of these collagen and non-collagen mimicking peptides for bone tissue regeneration.

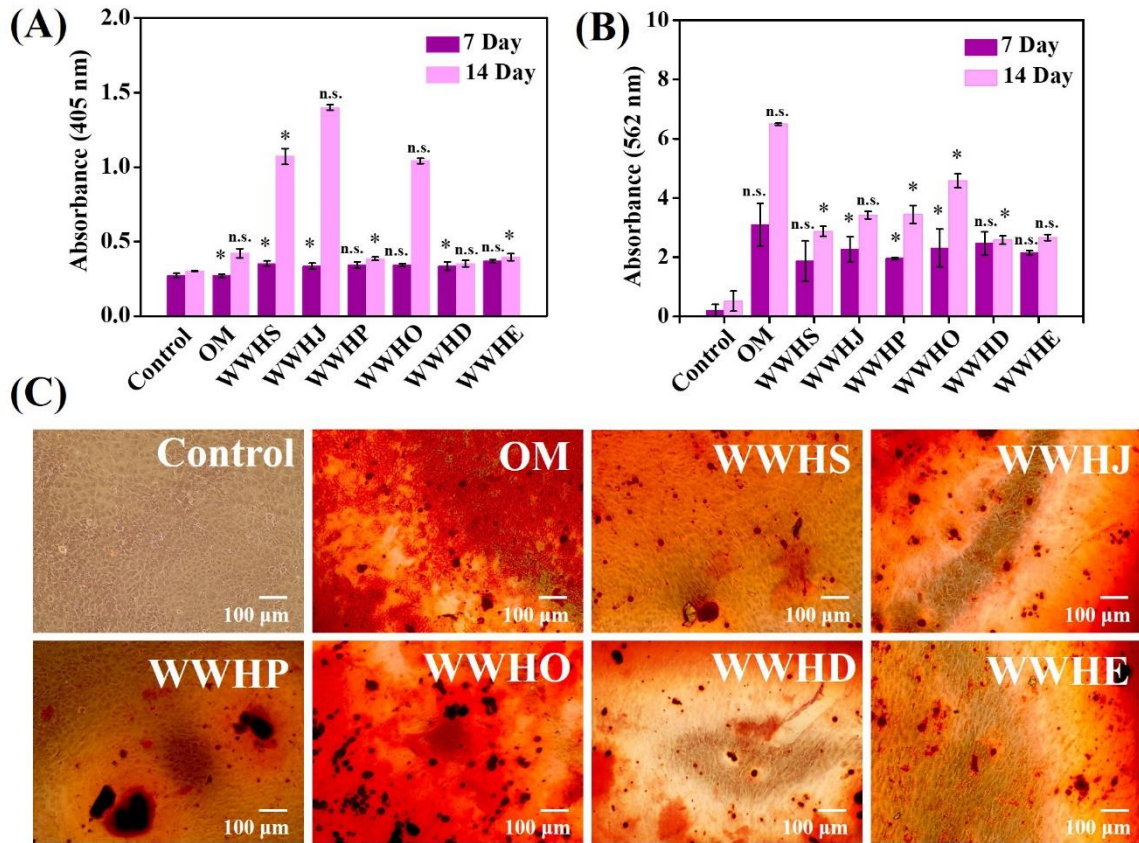


Figure 4.8. Osteogenic differentiation of MC3T3-E1 in the presence of extracts of peptides and gels. (A) Alkaline phosphatase (ALP) activity of MSCs after 7 and 14 days. Alizarin Red S staining was used to demonstrate the calcium deposition. (B) Quantitative analysis of calcium deposits on mineralized MSCs after 7 and 14 days. Data are presented as mean \pm SD, $n = 3$, and $*p < 0.05$ indicates statistically significant data and ns indicates non-significant difference. (C) Microscopic images of MSCs after 14 days of treatment. Red precipitates indicate the calcium nodules. Scale bar: 100 μ m.

Alkaline phosphatase (ALP) estimation. During osteogenic differentiation, MSCs go through several modifications including development into osteoprogenitor cells, differentiation into pre-osteoblasts, and ultimately maturation into functional osteoblasts. Alkaline phosphatase (ALP) activity is considered a biochemical marker for the initial involvement of MSCs along the osteoblast lineage. Elevated ALP activity is considered a prerequisite for enriching the bone formation site with inorganic phosphates, as it reflects the early stages of osteogenic differentiation. Over the course of 7 and 14 days, MSCs were cultured with the extracts of peptides and gels and it was observed that on 7th day, almost all samples exhibited similar activity to promote ALP in cells (**Figure 4.8A**). At 14th day, WWHJ demonstrated

highest ALP activity, which was around 4.6-fold greater than the control (containing basal media) and 3.3-fold greater than the osteogenic media (OM). These data are comparable with the peptide gels reported in the literature for the application in bone tissue engineering. Cells treated with the extracts of WWHO and WWHS gels also significantly stimulated the ALP production in pre-osteoblast cells. Unlike these compounds, WWHP, WWHD, and WWHE raised the ALP production in a good to moderate manner. This result is attributable to the differentiating capabilities of the collagen and non-collagen protein derived peptides. Since pSer containing peptide helped in stimulating the ALP level to the most, we assume that it can catalyze the phosphate ester present in WWHJ to generate inorganic phosphate, which can be used in the formation of hydroxyapatite in situ.

Estimation of calcium content. The differentiation of MSCs into osteoblasts causes significant changes in several biological characteristics, including an increased rate of calcium deposition. Calcium ions are required for the formation of HAp crystals, and the deposition of calcium in the ECM provides the structural integrity and strength to the bone tissue. Alizarin Red S staining is generally used to investigate the extracellular deposition of calcium because of its high affinity for calcium ions and it forms a red-colored complex that can be visualized under a microscope or quantified using spectrophotometry.⁵³ The MSCs after treating with the extracts of peptides and gels act as biological cues to induce osteogenic differentiation and showed a development of definite amount of calcium nodules after 7 and 14 days of culturing. The deposited calcium nodule was quantified by solubilizing them in 10% cetyl pyridyl chloride solution and measuring absorbance at 405 nm and it exhibited a moderate increase in intensity with time (**Figure 4.8B, A72, Appendix**). Additionally, the red-stained calcium nodules, which indicated the presence of extracellular calcium deposition, were seen using an inverted microscope. The data were compared with cells treated with osteogenic media (OM), and it was found that WWHO, WWHJ, and WWHS were more effective in increasing matrix mineralization than other peptides. The negative charge of these peptides helps in the deposition of calcium ions, resulting in highest mineralization.

Gene expression studies. The information gathered so far from the investigations motivated us to scrutinize the impact of these peptides on the expression of standard osteogenic markers (ALP, RUNX 2, OPN, OCN, and COL 1) by real time PCR (RT PCR) studies. After incubation with the extracts of peptides and gels for 7 and 14 days, expressions of typical osteogenesis-related mRNAs were evaluated in MC3T3-E1 cells and are depicted in **Figure 4.9A-E**. A significant change in gene expression occurred after 14 days of culture. The maximum increase in fold of alkaline phosphatase (ALP) expression was observed in case of WWHO, which was 11-folds higher than the control (basal medium without any treatment) and 2-folds higher than OM at 14th day of incubation (**Figure 4.9A**). Expression of ALP was also higher than OM in case of WWHJ (6-folds) and WWHP (8-folds). Runt-related transcription factor 2 (RUNX2) is another critical transcription factor that regulates osteoblast differentiation, bone development, bone remodeling, and bone repair, and plays a significant role in osteogenesis. **Figure 4.9B** displays excellent upregulation of RUNX 2 by the peptides and gels at both 7th and 14th day. WWHJ

influenced the upregulation at the highest level (91-folds) compared to control, whereas other peptides and gels also promoted the levels of RUNX 2 in the range of 45-75 folds at 14th day. Osteopontin (OPN), a glycoprotein is also involved in the regulation of bone remodeling. WWHO, WWHJ, WWHS, and WWHP helped in the potentiation of the OPN level in MSCs in the range between 40-90 folds. The other two peptide gels, WWHD and WWHE, also increased its level by 35-folds (**Figure 4.9C**). Osteocalcin (OCN) plays a role in calcium metabolism. It is known to interact with calcium ions, and it has been suggested that OCN may help in regulating calcium homeostasis in the body and mineralization of bone matrix. Peptides containing pSer, Asp, and Glu (WWHJ, WWHD and WWHE) demonstrated the OCN upliftment to the maximum level (6-8 folds), which was comparable with osteogenic media (**Figure 4.9D**). Collagen type I (COL 1) is the main component of the organic matrix of bone and provides the structural framework for bone formation. It provides a favorable substrate for the attachment and migration of cells involved in bone regeneration. **Figure 4.9E**, illustrates the impact of the collagen and non-collagen derived peptides on the level of COL 1. WWHP and WWHO exhibited the maximum rise in COL 1 level by 25-folds, which can be attributed to the fact that Pro and Hyp are the integral part of collagen protein. Peptides (WWHD and WWHE) composed of noncollagenous protein derived amino acids were also able to enhance the COL 1 level by 12 and 17-folds. Overall, these data authenticate the differentiating capability of MSCs by our peptides, which is a desirable trait for scaffolds to treat bone related disorders.

The effects of these peptides were assessed in a co-culture system of MC-3T3-E1 and RAW 264.7 cells because restoring the equilibrium between bone resorption by osteoclasts and bone formation by osteoblasts is crucial for the treatment of bone-related disorders, particularly osteoporosis. RANKL (Receptor Activator of Nuclear Factor Kappa-B Ligand) and TRAP (Tartrate-Resistant Acid Phosphatase) are involved in the process of osteogenesis, which is the formation and development of bone tissue.⁵⁴ RANKL is secreted by osteoblast and binds to its receptor RANK, which is present on the surface of osteoclast precursor cells, leading to their differentiation into mature osteoclasts, which are responsible for bone resorption. TRAP, on the other hand, is an enzyme that is highly expressed by mature osteoclasts and is involved in the degradation of bone matrix. It is often used as a marker for osteoclast activity and upregulated in mature osteoclasts as they become active in resorbing bone during osteogenesis. As displayed in **Figure 4.9F**, the expression of RANKL was downregulated in osteoblast-like cells, which revealed an excellent inhibitory effect on RANKL induced osteoclastogenesis by the peptide and gel extracts. The expression of TRAP in RAW 264.7 was also reduced at 7th day, which further confirmed the retardation of bone resorption as desirable in the treatment of osteoporosis.

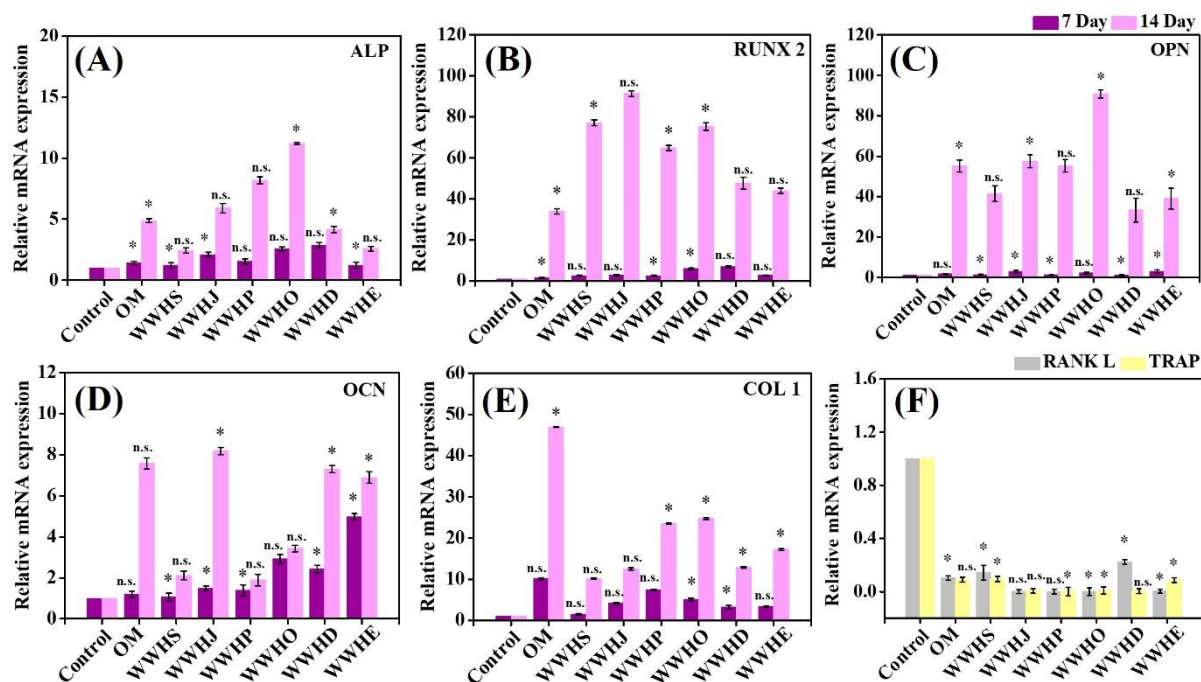


Figure 4.9. qRT PCR data. (A-E) Expression of osteogenesis related genes (ALP, RUNX 2, OPN, OCN, and COL 1) by MC3T3-E1 cells after culturing with osteogenic media (OM) and extracts of peptides and gels for 7 and 14 days. (F) Relative mRNA expression of osteoclastic factors RANKL and TRAP by MC3T3-E1 and RAW 264.7 after treatment for 7 days in an indirect coculture system. Data are presented as mean \pm SD, n = 3, *p < 0.05 indicates statistically significant data and ns non-significant difference.

The inflammatory response of macrophages was evaluated by RT-PCR. The expression of typical M1 related gene (TNF- α and iNOS) was distinctly downregulated after treatment with the extracts of peptides and gels (**Figure A73, Appendix**). In contrast, the expression of IL-10, marker for M2 macrophage were significantly enhanced. Thus, it is obvious from the study that these collagen and non-collagen protein derived peptides guided the phenotypic switch to M2 macrophages and augmented the secretion of anti-inflammatory factors. The in vitro osteogenic differentiation potential of these scaffolds are equivalent to the self-assembled peptide gels, polymeric and peptide modified polymer derivatives, hybrid biopolymers, and nanoparticles reported in the literature by Alshehri *et al.*,³⁴ Mahendiran *et al.*,⁵⁵ Tang *et al.*,³⁵ and Gilarska *et al.*²³.

4.5. Conclusions

In this work, we have developed ultrashort, amphiphilic peptide-based scaffolds capable of binding with hydroxyapatite and promoting the osteogenic differentiation for the effective regeneration of bone. We use a simple strategy of synthesizing six tetrapeptides inspired from collagen and non-collagenous proteins, which contain overall negative charge and different functionalities, such as phosphate, hydroxyl, and carboxyl groups. Out of six peptides, four peptides were self-assembled into gels with distinct nanostructures and the other two were self-assembled into clusters with nanorod-like

morphology. The studies provided a critical insight on the role of amino acids, such as Ser, pSer, Pro, Hyp, Asp, and Glu, on interactions with hydroxyapatite, the major inorganic content of bone, and mineralization. The nanostructures fabricated from the self-assembly of peptides can mimic the extracellular matrix and provide biochemical cue to the stem cells for adhesion and proliferation. In vitro cell culture studies confirmed the cytocompatible nature of these peptides towards pre-osteoblasts and their ability to promote cell proliferation and migration. It was also evident that the peptides after incubation with pre-osteoblasts enhanced the production of alkaline phosphatase (ALP) and deposition of calcium, which are the biochemical markers of ossification. They also provided protection against reactive oxygen species/oxidative stress and promoted M2 macrophage polarization with downregulation of TNF α and iNOS, and upregulation of IL-10. The differentiation of mesenchymal stem cells to pre-osteoblasts and their role in accelerating the bone formation was further confirmed by investigating the expression of several osteogenic biomarkers. The ability of these scaffolds to reduce the osteoclastogenesis process was validated by coculturing pre-osteoblast and macrophages, which highlights their excellent therapeutic value for osteoporosis. Overall, this work reports the rational design and fabrication of self-assembled, short bio-inspired peptide motifs and their promising application towards successfully developing scaffolds for bone-tissue engineering. This facile approach put forward a cell free and growth factor free yet bioactive, nanostructured platforms to induce bone regeneration.

References

- (1) Koons, G. L.; Diba, M.; Mikos, A. G. Materials Design for Bone-Tissue Engineering. *Nature Reviews Materials* **2020**, 5 (8), 584–603. <https://doi.org/10.1038/s41578-020-0204-2>.
- (2) Ansari, M. Bone Tissue Regeneration: Biology, Strategies and Interface Studies. *Progress in Biomaterials* **2019**, 8 (4), 223–237. <https://doi.org/10.1007/s40204-019-00125-z>.
- (3) Wu, A.-M.; Bisignano, C.; James, S. L.; Abady, G. G.; Abedi, A.; Abu-Gharbieh, E.; Alhassan, R. K.; Alipour, V.; Arabloo, J.; Asaad, M.; Asmare, W. N.; Awedew, A. F.; Banach, M.; Banerjee, S. Global, Regional, and National Burden of Bone Fractures in 204 Countries and Territories, 1990–2019: A Systematic Analysis from the Global Burden of Disease Study 2019. *The Lancet Healthy Longevity* **2021**, 2 (9), e580–e592. [https://doi.org/10.1016/S2666-7568\(21\)00172-0](https://doi.org/10.1016/S2666-7568(21)00172-0).
- (4) Pinna, A.; Torki Baghbaderani, M.; Vigil Hernández, V.; Naruphontjirakul, P.; Li, S.; McFarlane, T.; Hachim, D.; Stevens, M. M.; Porter, A. E.; Jones, J. R. Nanoceria Provides Antioxidant and Osteogenic Properties to Mesoporous Silica Nanoparticles for Osteoporosis Treatment. *Acta Biomaterialia* **2021**, 122, 365–376. <https://doi.org/10.1016/j.actbio.2020.12.029>.
- (5) Schmidt, A. H. Autologous Bone Graft: Is It Still the Gold Standard? *Injury* **2021**, 52, S18–S22. <https://doi.org/10.1016/j.injury.2021.01.043>.
- (6) Sohn, H.-S.; Oh, J.-K. Review of Bone Graft and Bone Substitutes with an Emphasis on Fracture Surgeries. *Biomaterials Research* **2019**, 23 (1), 9. <https://doi.org/10.1186/s40824-019-0157-y>.
- (7) Hao, Z.; Li, H.; Wang, Y.; Hu, Y.; Chen, T.; Zhang, S.; Guo, X.; Cai, L.; Li, J. Supramolecular Peptide Nanofiber Hydrogels for Bone Tissue Engineering: From Multihierarchical Fabrications to Comprehensive Applications. *Advanced Science* **2022**, 9 (11), 2103820. <https://doi.org/10.1002/advs.202103820>.
- (8) Ahmadian, Z.; Correia, A.; Hasany, M.; Figueiredo, P.; Dobakhti, F.; Eskandari, M. R.; Hosseini, S. H.; Abiri, R.; Khorshid, S.; Hirvonen, J.; Santos, H. A.; Shahbazi, M.-A. A Hydrogen-Bonded Extracellular Matrix-Mimicking Bactericidal Hydrogel with Radical Scavenging and Hemostatic Function for PH-Responsive Wound Healing Acceleration. *Advanced Healthcare Materials* **2021**, 10 (3), 2001122. <https://doi.org/10.1002/adhm.202001122>.
- (9) Bahraminasab, M.; Janmohammadi, M.; Arab, S.; Talebi, A.; Nooshabadi, V. T.; Koohsarian, P.; Nourbakhsh, M. S. Bone Scaffolds: An Incorporation of Biomaterials, Cells, and Biofactors. *ACS Biomater. Sci. Eng.* **2021**, 7 (12), 5397–5431. <https://doi.org/10.1021/acsbiomaterials.1c00920>.
- (10) Patel, A.; Zaky, S. H.; Schoedel, K.; Li, H.; Sant, V.; Beniash, E.; Sfeir, C.; Stolz, D. B.; Sant, S. Design and Evaluation of Collagen-Inspired Mineral-Hydrogel Nanocomposites for Bone Regeneration. *Acta Biomaterialia* **2020**, 112, 262–273. <https://doi.org/10.1016/j.actbio.2020.05.034>.
- (11) Wang, Y.; Azaïs, T.; Robin, M.; Vallée, A.; Catania, C.; Legriel, P.; Pehau-Arnaudet, G.; Babonneau, F.; Giraud-Guille, M.-M.; Nassif, N. The Predominant Role of Collagen in the Nucleation, Growth, Structure and Orientation of Bone Apatite. *Nat Mater* **2012**, 11.
- (12) Zhang, D.; Wu, X.; Chen, J.; Lin, K. The Development of Collagen Based Composite Scaffolds for Bone Regeneration. *Bioactive Materials* **2018**, 3 (1), 129–138. <https://doi.org/10.1016/j.bioactmat.2017.08.004>.
- (13) Pittenger, M. F.; Mackay, A. M.; Beck, S. C.; Jaiswal, R. K.; Douglas, R.; Mosca, J. D.; Moorman, M. A.; Simonetti, D. W.; Craig, S.; Marshak, D. R. Multilineage Potential of Adult Human Mesenchymal Stem Cells. *Science* **1999**, 284 (5411), 143–147. <https://doi.org/10.1126/science.284.5411.143>.
- (14) Petite, H.; Viateau, V.; Bensaïd, W.; Meunier, A.; de Pollak, C.; Bourguignon, M.; Oudina, K.; Sedel, L.; Guillemain, G. Tissue-Engineered Bone Regeneration. *Nature Biotechnology* **2000**, 18 (9), 959–963. <https://doi.org/10.1038/79449>.
- (15) Takamine, Y.; Tsuchiya, H.; Kitakoji, T.; Kurita, K.; Ono, Y.; Ohshima, Y.; Kitoh, H.; Ishiguro, N.; Iwata, H. Distraction Osteogenesis Enhanced by Osteoblastlike Cells and Collagen Gel. *Clinical Orthopaedics and Related Research* **2002**, 399.
- (16) Nabavi, M. H.; Salehi, M.; Ehterami, A.; Bastami, F.; Semyari, H.; Tehrani, M.; Nabavi, M. A.; Semyari, H. A Collagen-Based Hydrogel Containing Tacrolimus for Bone Tissue Engineering. *Drug Delivery and Translational Research* **2020**, 10 (1), 108–121. <https://doi.org/10.1007/s13346-019-00666-7>.

- (17) Mishra, R.; Varshney, R.; Das, N.; Sircar, D.; Roy, P. Synthesis and Characterization of Gelatin-PVP Polymer Composite Scaffold for Potential Application in Bone Tissue Engineering. *European Polymer Journal* **2019**, *119*, 155–168. <https://doi.org/10.1016/j.eurpolymj.2019.07.007>.
- (18) Tang, G.; Tan, Z.; Zeng, W.; Wang, X.; Shi, C.; Liu, Y.; He, H.; Chen, R.; Ye, X. Recent Advances of Chitosan-Based Injectable Hydrogels for Bone and Dental Tissue Regeneration. *Frontiers in Bioengineering and Biotechnology* **2020**, *8*.
- (19) Saleem, M.; Rasheed, S.; Yougen, C. Silk Fibroin/Hydroxyapatite Scaffold: A Highly Compatible Material for Bone Regeneration. *Science and Technology of Advanced Materials* **2020**, *21* (1), 242–266. <https://doi.org/10.1080/14686996.2020.1748520>.
- (20) Gharaei, R.; Tronci, G.; Goswami, P.; Davies, R. P. W.; Kirkham, J.; Russell, S. J. Biomimetic Peptide Enriched Nonwoven Scaffolds Promote Calcium Phosphate Mineralisation. *RSC Adv.* **2020**, *10* (47), 28332–28342. <https://doi.org/10.1039/D0RA02446E>.
- (21) Lin, C.; Wang, Y.; Lai, Y.; Yang, W.; Jiao, F.; Zhang, H.; Ye, S.; Zhang, Q. Incorporation of Carboxylation Multiwalled Carbon Nanotubes into Biodegradable Poly(Lactic-Co-Glycolic Acid) for Bone Tissue Engineering. *Colloids and Surfaces B: Biointerfaces* **2011**, *83* (2), 367–375. <https://doi.org/10.1016/j.colsurfb.2010.12.011>.
- (22) Sharma, A.; Kokil, G. R.; He, Y.; Lowe, B.; Salam, A.; Altalhi, T. A.; Ye, Q.; Kumeria, T. Inorganic/Organic Combination: Inorganic Particles/Polymer Composites for Tissue Engineering Applications. *Bioactive Materials* **2023**, *24*, 535–550. <https://doi.org/10.1016/j.bioactmat.2023.01.003>.
- (23) Gilarska, A.; Hinz, A.; Bzowska, M.; Dyduch, G.; Kamiński, K.; Nowakowska, M.; Lewandowska-Łańcucka, J. Addressing the Osteoporosis Problem—Multifunctional Injectable Hybrid Materials for Controlling Local Bone Tissue Remodeling. *ACS Appl. Mater. Interfaces* **2021**, *13* (42), 49762–49779. <https://doi.org/10.1021/acsami.1c17472>.
- (24) Zhao, C.; Qazvini, N. T.; Sadati, M.; Zeng, Z.; Huang, S.; De La Lastra, A. L.; Zhang, L.; Feng, Y.; Liu, W.; Huang, B.; Zhang, B.; Dai, Z.; Shen, Y.; Wang, X.; Luo, W.; Liu, B.; Lei, Y.; Ye, Z.; Zhao, L.; Cao, D.; Yang, L.; Chen, X.; Athiviraham, A.; Lee, M. J.; Wolf, J. M.; Reid, R. R.; Tirrell, M.; Huang, W.; de Pablo, J. J.; He, T.-C. A PH-Triggered, Self-Assembled, and Bioprintable Hybrid Hydrogel Scaffold for Mesenchymal Stem Cell Based Bone Tissue Engineering. *ACS Appl. Mater. Interfaces* **2019**, *11* (9), 8749–8762. <https://doi.org/10.1021/acsami.8b19094>.
- (25) Liang, H.; Jin, C.; Ma, L.; Feng, X.; Deng, X.; Wu, S.; Liu, X.; Yang, C. Accelerated Bone Regeneration by Gold-Nanoparticle-Loaded Mesoporous Silica through Stimulating Immunomodulation. *ACS Appl. Mater. Interfaces* **2019**, *11* (44), 41758–41769. <https://doi.org/10.1021/acsami.9b16848>.
- (26) Ullah, I.; Gloria, A.; Zhang, W.; Ullah, M. W.; Wu, B.; Li, W.; Domingos, M.; Zhang, X. Synthesis and Characterization of Sintered Sr/Fe-Modified Hydroxyapatite Bioceramics for Bone Tissue Engineering Applications. *ACS Biomater. Sci. Eng.* **2020**, *6* (1), 375–388. <https://doi.org/10.1021/acsbiomaterials.9b01666>.
- (27) Attar, H.; Löber, L.; Funk, A.; Calin, M.; Zhang, L. C.; Prashanth, K. G.; Scudino, S.; Zhang, Y. S.; Eckert, J. Mechanical Behavior of Porous Commercially Pure Ti and Ti–TiB Composite Materials Manufactured by Selective Laser Melting. *Materials Science and Engineering: A* **2015**, *625*, 350–356. <https://doi.org/10.1016/j.msea.2014.12.036>.
- (28) Raja, N.; Yun, H. A Simultaneous 3D Printing Process for the Fabrication of Bioceramic and Cell-Laden Hydrogel Core/Shell Scaffolds with Potential Application in Bone Tissue Regeneration. *J. Mater. Chem. B* **2016**, *4* (27), 4707–4716. <https://doi.org/10.1039/C6TB00849F>.
- (29) Bessa, P. C.; Casal, M.; Reis, R. Bone Morphogenetic Proteins in Tissue Engineering: The Road from Laboratory to Clinic, Part II (BMP Delivery). *J Tissue Eng Regen Med* **2008**, *2*.
- (30) Haidar, Z. S.; Hamdy, R. C.; Tabrizian, M. Delivery of Recombinant Bone Morphogenetic Proteins for Bone Regeneration and Repair. Part B: Delivery Systems for BMPs in Orthopaedic and Craniofacial Tissue Engineering. *Biotechnol Lett* **2009**, *31*.
- (31) Visser, R.; Rico-Llanos, G. A.; Pulkkinen, H.; Becerra, J. Peptides for Bone Tissue Engineering. *Journal of Controlled Release* **2016**, *244*, 122–135. <https://doi.org/10.1016/j.jconrel.2016.10.024>.
- (32) Ando, K.; Imagama, S.; Kobayashi, K.; Ito, K.; Tsushima, M.; Morozumi, M.; Tanaka, S.; Machino, M.; Ota, K.; Nishida, K.; Nishida, Y.; Ishiguro, N. Effects of a Self-Assembling Peptide as a Scaffold on Bone Formation in a Defect. *PLoS ONE* **2018**, *13* (1), e0190833. <https://doi.org/10.1371/journal.pone.0190833>.

- (33) Xue, X.; Hu, Y.; Deng, Y.; Su, J. Recent Advances in Design of Functional Biocompatible Hydrogels for Bone Tissue Engineering. *Advanced Functional Materials* **2021**, *31* (19), 2009432. <https://doi.org/10.1002/adfm.202009432>.
- (34) Alshehri, S.; Susapto, H. H.; Hauser, C. A. E. Scaffolds from Self-Assembling Tetrapeptides Support 3D Spreading, Osteogenic Differentiation, and Angiogenesis of Mesenchymal Stem Cells. *Biomacromolecules* **2021**, *22* (5), 2094–2106. <https://doi.org/10.1021/acs.biomac.1c00205>.
- (35) Tang, Y.; Chen, Y.; Huang, L.; Gao, F.; Sun, H.; Huang, C. Intramembranous Ossification Imitation Scaffold with the Function of Macrophage Polarization for Promoting Critical Bone Defect Repair. *ACS Appl. Bio Mater.* **2020**, *3* (6), 3569–3581. <https://doi.org/10.1021/acsabm.0c00233>.
- (36) Pal, V. K.; Roy, S. Cooperative Calcium Phosphate Deposition on Collagen-Inspired Short Peptide Nanofibers for Application in Bone Tissue Engineering. *Biomacromolecules* **2023**, *24* (2), 807–824. <https://doi.org/10.1021/acs.biomac.2c01262>.
- (37) Robbins, K. J.; Liu, G.; Selmani, V.; Lazo, N. D. Conformational Analysis of Thioflavin T Bound to the Surface of Amyloid Fibrils. *Langmuir* **2012**, *28* (48), 16490–16495. <https://doi.org/10.1021/la303677t>.
- (38) Nenadis, N.; Wang, L.-F.; Tsimidou, M.; Zhang, H.-Y. Estimation of Scavenging Activity of Phenolic Compounds Using the ABTS^{•+} Assay. *J. Agric. Food Chem.* **2004**, *52* (15), 4669–4674. <https://doi.org/10.1021/jf0400056>.
- (39) Halder, M.; Narula, M.; Singh, Y. Supramolecular, Nanostructured Assembly of Antioxidant and Antibacterial Peptides Conjugated to Naproxen and Indomethacin for the Selective Inhibition of COX-2, Biofilm, and Inflammation in Chronic Wounds. *Bioconjugate Chem.* **2023**, *34* (4), 645–663. <https://doi.org/10.1021/acs.bioconjchem.3c00014>.
- (40) Halder, M.; Bhatia, Y.; Singh, Y. Self-Assembled Di- and Tripeptide Gels for the Passive Entrapment and PH-Responsive, Sustained Release of an Antidiabetic Drug, Glimepiride. *Biomater. Sci.* **2022**, *10* (9), 2248–2262. <https://doi.org/10.1039/D2BM00344A>.
- (41) Coleman, R. J.; Jack, K. S.; Perrier, S.; Grøndahl, L. Hydroxyapatite Mineralization in the Presence of Anionic Polymers. *Crystal Growth & Design* **2013**, *13* (10), 4252–4259. <https://doi.org/10.1021/cg400447e>.
- (42) Murphy, M. B.; Hartgerink, J. D.; Goepferich, A.; Mikos, A. G. Synthesis and in Vitro Hydroxyapatite Binding of Peptides Conjugated to Calcium-Binding Moieties. *Biomacromolecules* **2007**, *8* (7), 2237–2243. <https://doi.org/10.1021/bm070121s>.
- (43) Licini, C.; Vitale-Brovarone, C.; Mattioli-Belmonte, M. Collagen and Non-Collagenous Proteins Molecular Crosstalk in the Pathophysiology of Osteoporosis. *Cytokine & Growth Factor Reviews* **2019**, *49*, 59–69. <https://doi.org/10.1016/j.cytogfr.2019.09.001>.
- (44) Wang, Y.; Wang, J.; Gao, R.; Liu, X.; Feng, Z.; Zhang, C.; Huang, P.; Dong, A.; Kong, D.; Wang, W. Biomimetic Glycopeptide Hydrogel Coated PCL/NHA Scaffold for Enhanced Cranial Bone Regeneration via Macrophage M2 Polarization-Induced Osteo-Immunomodulation. *Biomaterials* **2022**, *285*, 121538. <https://doi.org/10.1016/j.biomaterials.2022.121538>.
- (45) Gungormus, M.; Branco, M.; Fong, H.; Schneider, J. P.; Tamerler, C.; Sarikaya, M. Self Assembled Bi-Functional Peptide Hydrogels with Biomineralization-Directing Peptides. *Biomaterials* **2010**, *31* (28), 7266–7274. <https://doi.org/10.1016/j.biomaterials.2010.06.010>.
- (46) Tang, S.; Dong, Z.; Ke, X.; Luo, J.; Li, J. Advances in Biomineralization-Inspired Materials for Hard Tissue Repair. *International Journal of Oral Science* **2021**, *13* (1), 42. <https://doi.org/10.1038/s41368-021-00147-z>.
- (47) Ling, C.; Zhao, W.; Wang, Z.; Chen, J.; Ustiyana, P.; Gao, M.; Sahai, N. Structure–Activity Relationships of Hydroxyapatite-Binding Peptides. *Langmuir* **2020**, *36* (10), 2729–2739. <https://doi.org/10.1021/acs.langmuir.9b03779>.
- (48) Bang, J.; Park, H.; Yoo, J.; Lee, D.; Choi, W. I.; Lee, J. H.; Lee, Y.-R.; Kim, C.; Koo, H.; Kim, S. Selection and Identification of a Novel Bone-Targeting Peptide for Biomedical Imaging of Bone. *Sci Rep* **2020**, *10* (1), 10576. <https://doi.org/10.1038/s41598-020-67522-4>.
- (49) Almora-Barrios, N.; de Leeuw, N. H. Modelling the Interaction of a Hyp-Pro-Gly Peptide with Hydroxyapatite Surfaces in Aqueous Environment. *CrystEngComm* **2010**, *12* (3), 960–967. <https://doi.org/10.1039/B917179G>.
- (50) Almora-Barrios, N.; de Leeuw, N. H. A Density Functional Theory Study of the Interaction of Collagen Peptides with Hydroxyapatite Surfaces. *Langmuir* **2010**, *26* (18), 14535–14542. <https://doi.org/10.1021/la101151e>.

- (51) Wang, K.; Wang, X.; Li, H.; Zheng, S.; Ren, Q.; Wang, Y.; Niu, Y.; Li, W.; Zhou, X.; Zhang, L. A Statherin-Derived Peptide Promotes Hydroxyapatite Crystallization and *in Situ* Remineralization of Artificial Enamel Caries. *RSC Adv.* **2018**, 8 (3), 1647–1655. <https://doi.org/10.1039/C7RA12032J>.
- (52) Chen, P.-H.; Tseng, Y.-H.; Mou, Y.; Tsai, Y.-L.; Guo, S.-M.; Huang, S.-J.; Yu, S. S.-F.; Chan, J. C. C. Adsorption of a Statherin Peptide Fragment on the Surface of Nanocrystallites of Hydroxyapatite. *J. Am. Chem. Soc.* **2008**, 130 (9), 2862–2868. <https://doi.org/10.1021/ja076607y>.
- (53) Huang, W.; Yang, S.; Shao, J.; Li, Y.-P. Signaling and Transcriptional Regulation in Osteoblast Commitment and Differentiation. *FBL* **2007**, 12 (8), 3068–3092.
- (54) Tu, M.-G.; Chen, Y.-W.; Shie, M.-Y. Macrophage-Mediated Osteogenesis Activation in Co-Culture with Osteoblast on Calcium Silicate Cement. *J Mater Sci: Mater Med* **2015**, 26 (12), 276. <https://doi.org/10.1007/s10856-015-5607-z>.
- (55) Mahendiran, B.; Muthusamy, S.; Janani, G.; Mandal, B. B.; Rajendran, S.; Krishnakumar, G. S. Surface Modification of Decellularized Natural Cellulose Scaffolds with Organosilanes for Bone Tissue Regeneration. *ACS Biomater. Sci. Eng.* **2022**, 8 (5), 2000–2015. <https://doi.org/10.1021/acsbiomaterials.1c01502>.

CHAPTER - 5

Immobilization of self-assembling peptides on ceria nanoparticles for biocatalysis

Immobilization of self-assembling peptides on ceria for biocatalysis

5.1. Introduction**5.1.1. Biocatalysis**

Biocatalysis refers to the use of natural catalysts, such as enzymes or whole cells, to perform chemical transformations.¹ These catalysts accelerate the rate of chemical reactions by providing an alternative pathway with lower activation energy, allowing reactions to occur under milder conditions. Enzymes are proteins that act as highly efficient biocatalysts in living organisms.² They possess specific active sites that can bind to substrates and facilitate their conversion into products. Enzymes are incredibly selective, often catalyzing specific reactions and producing specific products, which makes them valuable tools in various industries.³ Biocatalysis offers several advantages over traditional chemical catalysis. Firstly, enzymes are usually highly specific, which means they can perform reactions with high selectivity, minimizing the formation of unwanted by-products.⁴ Secondly, enzymes often work under mild conditions, including lower temperatures and pressures, which can reduce energy consumption and lower production costs. Moreover, biocatalysis is often more environment friendly as it can avoid the use of toxic or hazardous chemicals, and it finds application in a wide range of industries, including pharmaceuticals, agriculture, food and beverage, biofuels, and manufacturing. Examples of biocatalytic reactions include the production of antibiotics, synthesis of fine chemicals, degradation of environmental pollutants, and conversion of biomass into biofuels. Overall, biocatalysis harnesses the power of biological catalysts to enable more sustainable and efficient chemical processes, with significant potential for advancing industries and reducing environmental impact.

5.1.2. Challenges

While biocatalysis offers numerous benefits, there are also several challenges associated with the use of biocatalysts. The lack of availability of these enzymes in large quantity is the major concern for the industrial use.⁵ Additionally, some enzymes may be derived from rare or difficult-to-cultivate organisms, making them less accessible, which significantly increases their costs. Many biocatalysts, especially enzymes, can be sensitive to environmental conditions such as temperature and pH.⁶ They may undergo denaturation or loss of activity over time, reducing their stability and shelf-life. Maintaining the stability of biocatalysts during storage and industrial processes can be a challenge. There are issues related to the use of enzymes in the development of heterogeneous catalysts.^{7,8} The enzymes are attached to solid surfaces either through adsorption or covalent bonding. Adsorption-based immobilizations invariably result in a loss of adsorbed protein during the course of subsequent cycles. On the other hand, covalent connections are generated through numerous chemical processes that may cause the connected enzyme to become denatured.⁹ As a result, it is increasingly difficult to reuse the catalysts and the cost-effectiveness of the final product purification is also reduced.

5.1.3. Self-assembling peptides as biocatalyst

In order to surmount the challenges, artificial enzymes or compounds that mimic enzymes are a promising alternative.^{1,10,11} An enzyme's effective catalytic activity comes from supramolecular interactions that form a three-dimensional structure within the protein molecule. The correct spatial arrangement of the amino acids inside these structures produces the catalytic pockets needed to bind a particular substrate and carry out chemical reactions.¹² The minimalistic approach to develop artificial biocatalysts that have the same catalytic efficiency, stereoselectivity, and specificity as genuine enzymes is to imitate their catalytic site by incorporating the amino acids found in the catalytic pocket.

Self-assembling peptides can act as biocatalysts by organizing into well-defined structures or scaffolds that provide an environment for catalytic reactions to occur.^{13,14} These peptides have the unique ability to spontaneously form ordered structures through non-covalent interactions, such as hydrogen bonding, electrostatic interactions, and hydrophobic interactions. The self-assembling peptides can be designed to incorporate catalytic residues or functional groups within their sequence, allowing them to perform specific enzymatic reactions. The catalytic activity of self-assembling peptides can be influenced by factors such as the peptide sequence, secondary structure, and the microenvironment created by the self-assembled structure.¹⁵ Proline-containing peptides, for instance, are known to catalyze the Mannich, Michael, Aldol, and Acyl Transfer processes.^{16,17} In a similar way, ester hydrolysis reactions are widely known to be catalyzed by histidine (His).^{18,19} For the regeneration of hydrolase and esterase activities, a variety of His-containing hydrogels and nanofibrils have been developed. Similarly, hydrogel-trapped hemin chloride has been found to have peroxidase-like activity.²⁰ In this regard, hydrolytic enzymes, such as lipase and α -chymotrypsin, have drawn a lot of attention due to their prevalence in living things and growing economic significance.²¹ Therefore, much effort has been made to develop artificial esterase and phosphatase.²²

Several design techniques have been used to generate peptide-based artificial enzymes, such as short helices, α -helical coiled coils and barrels, β -hairpins, and β -peptide bundles. For instance, Korendovych *et al.* developed a set of heptapeptides that form β -sheets and by the self-assembly of these peptides, they obtained a Zn(II)-coordinated structure.²³ This structure mimicked the catalytic center of natural carbonic anhydrase and demonstrated catalytic activity towards carbonic anhydrase substrates. Numata *et al.* developed an enzyme-like catalyst by incorporating the conventional serine-protease catalytic triad to peptides that can self-assemble into fibrils and resemble amyloids.²⁴ The formation of this β -sheet backbone was essential to imitate the protease binding site. Gulseren *et al.* reported esterase mimicking catalytic nano-system with essential residues, Ser, His, and Asp in the peptide sequence.²⁵ Mikolajczak *et al.* developed peptide-gold nanoparticle conjugates as sequential cascade catalyst for hydrolysis followed by hydrogenation reactions.²⁶ Dowari *et al.* reported the immobilization of peptide amphiphile containing Asp (Ser) His triad on silica surface for hydrolase mimicking properties.²⁷ Reja *et al.* has developed nanotubes from self-assembled lipidated short peptide (C₁₀-FFVK) for aldolase mimicking properties.²⁸ Overall, self-assembling peptide provide a versatile platform for creating functional

materials with catalytic capabilities, and expanding the scope of biocatalysis beyond traditional enzymes.

5.1.4. Research gap

There has been a lot of reports available in the literature, where self-assembled peptides have been extensively explored to develop artificial enzymes. The major limitation associated with such system is that they are in homogenous solution with the reaction mixture and cannot be removed once the reaction is over. Unbranched, linear peptides reported so far can only expose their single binding pocket to the substrate, which limits the rate of reaction. Additionally, there are very few reports on the use of these artificial enzymes for societal welfare, and the potential of peptides to exhibit multiple catalytic activities simultaneously. Developing multifunctional peptide catalysts that can perform multiple types of reactions or exhibit synergistic effects has the potential to open new possibilities in biocatalysis.

5.2. Objectives

The main aim of this work is to develop multifunctional, heterogenous catalyst with esterase, phosphatase, and haloperoxidase mimicking potential and use them for pesticides detection (organophosphorus and carbamate), bone tissue regeneration, and anti-biofouling applications. We have immobilized self-assembled, nanofibrous catalytic peptide on ceria nanoparticle and evaluated their potential to act as a biocatalyst. Ceria nanoparticles (CeNP) were fabricated using hydrothermal method and thiolated (TC) using (3-mercaptopropyl)trimethoxysilane, which was further conjugated to peptide amphiphile (PA) by “thiol-ene” reaction. The branched peptide amphiphile containing catalytic triad ‘Ser-His-Asp’, when immobilized on the thiolated ceria surface, generated a heterogenous catalyst (TCP) with a greater number of catalytic sites. CeNPs were selected due to their haloperoxidase mimicking properties. Peptide conjugated ceria nanoparticles were thoroughly characterized and they were found to mimic esterase, phosphatase, and haloperoxidase enzyme. This enzyme mimicking activity further motivated us to evaluate their role in pesticide detection, bone tissue regeneration, and anti-biofouling material preparation. Therefore, our strategy addresses the aforementioned research gap and contributes to advancing the field of peptide-based biocatalysis and unlock their full potential as versatile catalysts.

5.3. Experimental Section

5.3.1. Materials

All the solvents and chemicals were of high analytical quality and utilized without further purification unless otherwise stated. Rink amide AM resins (0.80 mmol/g loading) was procured from Novabiochem. Fmoc protected amino acids, such as Fmoc-Lys(Alloc)-OH, Fmoc-Lys(Fmoc)-OH, Fmoc-His(trt)-OH, Fmoc-Ser(trt)-OH, Fmoc-Asp(OtBu)-OH were purchased from BLD Pharm, India. 1-bis(dimethylamino)methylene]-1H-1,2,3-triazolo[4,5-b] pyridinium 3-oxide hexafluorophosphate (HATU), trifluoroacetic acid (TFA), N, N-diisopropylethylamine (DIEA), triisopropyl silane (TIS), lauric acid, 5,5'-dithiobis-2-nitrobenzoic acid (DTNB) and 3-mercaptopropyl trimethoxysilane

(MPTMS) were bought from TCI Chemicals, India. Dimethyl sulfoxide (DMSO) and HPLC grade solvents, such as acetonitrile, methanol, and isopropyl alcohol were purchased from Merck and used for reverse phase high-pressure liquid chromatography (RP-HPLC). Piperidine, N, N dimethyl formamide (DMF), and dichloromethane (DCM) were bought from Spectrochem and Rankem Laboratories. *p*-Nitrophenyl phosphate (pNPP) and *p*-nitrophenyl acetate (pNPA) were procured from Sisco Research Laboratories Pvt. Ltd. (SRL), India. Cerium nitrate hexahydrate 99.9% AR and Irgacure 2959 were purchased from Loba Chemie and Sigma Aldrich. PolyPrep chromatography columns from Bio-Rad were used for solid-phase peptide synthesis (SPPS). Deionized water (DI, 18.2 MΩ cm) was obtained from a Milli-Q system and used in all experiments. MC3T3-E1 cells (CRL-2593, Subclone-4) were purchased from ATCC. Minimum Essential Medium alpha (MEM-α), 0.25% trypsin/EDTA, penstrep, SYBR™ Green Master Mix, and trizol were purchased from Thermo Fisher Scientific. MTT reagent (3-(4,5-dimethylthiazol)-2,5-diphenyltetrazolium bromide), ascorbic acid, and fetal bovine serum (FBS) were procured from Himedia. *E. coli* (MTCC 1687) were purchased from CSIR-IMTECH, Chandigarh. For antibacterial studies, Luria broth (Himedia) was used as culture media.

5.3.2. Synthesis of branched peptide amphiphile (PA) and characterization

The branched peptide amphiphile was synthesized using standard 9-fluorenylmethoxycarbonyl (Fmoc)-based SPPS method. Rink amide AM resin was employed as a solid support. The amino acids were coupled using a mixture of HATU (2.85 equiv.) and DIEA (5.7 equiv.) and 20% piperidine in DMF (3 mL) was used to deprotect Fmoc group. The synthesized peptide was cleaved from the resin by using a cocktail comprising 3mL of 95% v/v TFA, 2.5% v/v TIS, and 2.5% v/v water. Subsequently, the amide terminated peptide/PA (C₁₂-SHD)₂KK(Alloc)-NH₂ was cleaved, and precipitated from 30 mL of cold diethyl ether, which was followed by centrifugation and drying under vacuum. The purity of these peptides was determined by using a RP-HPLC equipped with Xbridge BEH C₁₈ column (250 × 4.6 mm, 5 μm) and a gradient flow of acetonitrile/water for 35 min with 0.1% TFA as a mobile phase at a flow rate of 1 mL/min. The peptides were further characterized by mass (XEVO G2-XS QTOF) and ¹H NMR (JEOL JNM-ECS, 400 MHz) analysis.

5.3.3. Secondary structures of the peptide

The secondary structure of the peptide was determined by circular dichroism (CD) and Thioflavin T (ThT) assay. CD analysis was performed on a CD spectrometer (JASCO J-1500) using a quartz cuvette with a 0.1 cm path length. In order to induce the formation of secondary structures, peptide solutions were prepared in DI water and incubated at room temperature for five days prior to the investigation. Spectra of the peptides were recorded at a concentration of 0.5 mM in the region of 195-350 nm at a continuous scanning rate of 200 nm/min. Fluorescence spectra was used to analyze the binding of peptides with ThT according to a previously described method.²⁹ The fluorescence was recorded using a Tecan multimode microplate reader at an excitation wavelength of 440 nm. As a blank, ThT solution was used that contained no peptides.

5.3.4. Preparation of cerium oxide nanoparticles (CeNPs)

A conventional hydrothermal technique was used for the preparation of CeNPs.³⁰ A 60 mL of 4 M NaOH was used to make a suspension of 0.4 g of cerium nitrate hexahydrate (1 mmol) followed by stirring for 30 min. The mixture was transferred to a 100 mL Teflon-lined stainless-steel autoclave and incubated for 24 h at 100 °C. After centrifuging, the CeNPs were washed with water and ethanol, and dried at 70 °C to get a distinctive dark yellow powder.

5.3.5. Preparation of thiol functionalized CeNPs (TC)

The surface of CeNP was activated by dehydrating the sample at 80 °C overnight. Around 75 mg of CeNPs were dispersed in 15 mL of toluene in a round bottom flask and ultrasonicated for 30 min.³¹ To this suspension, MPTMS (0.6 mL) was added, and the suspension was refluxed at 110 °C overnight followed by centrifugation. The resulting thiol functionalized ceria nanoparticles (TC) were washed with toluene and ethanol and air-dried at 50 °C overnight.

5.3.6. Synthesis of peptide conjugated ceria nanoparticles (TCP)

The branched peptide amphiphile was conjugated with the thiol functionalized ceria via thiol-ene reaction.^{32–34} In general, 20 mg of TC was dispersed in 1 mL of methanol and sonicated for 15 min followed by the addition of 2 mM, 5 mL solution of PA. Radical initiator (Irgacure 2959, 0.2 equiv. 2.81 mg) was added to the mixture and the suspension was exposed to UV light (365 nm) with stirring at room temperature for 1 h. The peptide-functionalized ceria nanoparticles (TCPs) were centrifuged at 6,000 rpm, washed thoroughly with methanol, and finally dried overnight at 50°C.

5.3.7. Characterization

All the materials (CeNPs, TCs, and TCPs) were characterized by various spectroscopic and microscopic techniques for their chemical and physical properties.

Chemical properties. Crystallinity of all materials were determined by PXRD using Rigaku Miniflex diffractometer in the range of 10-80 with Cu K α (λ = 0.154 nm) radiation. EDX (Bruker Splash 6130) and XPS (Thermo Fisher Scientific, K-alpha) analysis were performed to confirm the elemental distribution and electronic state of elements. Thermogravimetric analysis (TA Instruments, USA, SDT-650) was done under N₂ flow (100 mL/min) from 40-800 °C at a ramp of 10 °C/min to validate the thiol modification on the surface of CeNPs and conjugation with the peptide amphiphile on thiolated ceria surface.

Physical properties. Particle size distribution was measured on a DLS Microtrac/Nanotrac Flex instrument. Field emission scanning electron microscope (FESEM) was used to study the morphological characteristics of nanomaterials by employing the drop-casting method on silicon wafer.

5.3.8. Ellman's assay

Ellman's assay was used to quantify the functionalization of CeNPs with thiol group.³⁵ Working solution of DTNB (Ellman's reagent) was prepared by dissolving 4 mg of DTNB and 20.5 g of sodium acetate

in 5 mL of DI water. About 50 μL of this Ellman's reagent was mixed with 2.5 mL of tris buffer (1 M, pH: 8) to make the blank solution. Samples were suspended in tris buffer and 250 μL of each sample (1 mg/mL) was added to the blank solution and incubated for 15 min at room temperature. The absorbance was measured at 412 nm, and the quantity of the surface thiol group was determined by dividing absorbance by the extinction co-efficient of the reagent ($13,600 \text{ M}^{-1}\text{cm}^{-1}$).

5.3.9. Measurement of the esterase-mimicking activity

The esterase-mimicking activity was measured using *p*-nitro phenyl acetate (pNPA) as a substrate.²⁷ All the nanomaterials (CeNP, TC, TCP, and PA) were dispersed in 20 mM phosphate buffer of pH 7 at a concentration of 1 mg/mL. The suspension was thoroughly vortexed and sonicated for 10 min to get a homogeneous suspension. The catalytic suspension (100 μL) was added into the well of a 96-well plate followed by the addition of 6 μL of pNPA solution (12.5 mM in ACN). The absorbance was measured at 405 nm, every 15 min for 150 min. Catalyst without pNPA was considered as the reference and its absorbance was recorded simultaneously. The absorbance value of the reference well was subtracted from the sample data to eliminate the contribution of the catalyst. Absorbance of the substrate without catalyst was observed to check their self-hydrolysis potential and these values were further subtracted to obtain the values coming from the catalysis only. The calibration curve of *p*-nitrophenol (pNP) was used to determine the amount of pNP formed and subsequently the rate of hydrolysis was also calculated using the extinction coefficient of pNP, which is $13014 \text{ M}^{-1}\text{cm}^{-1}$. In order to calculate the kinetic parameters, pNPA concentrations between 0.2 and 1.5 mM were used and the data was fitted to the Michaelis-Menten equation.

5.3.10. Measurement of phosphatase-mimicking activity

The phosphatase-mimicking activity was measured using *p*-nitro phenyl phosphate (pNPP) as a substrate and its working solution was prepared (12.5 mM) in 25 mM tris buffer of pH 8. The experiment was performed in the similar way as mentioned above.

5.3.11. Reusability of catalyst

We used a different method for the reusability test because the 96-well plate was not suitable for it. In this instance, the catalysts were suspended (1 mg/mL) in 940 μL of 20 mM phosphate buffer, pH 7 using the same procedure as previously described. Substrate (60 μL of a 12.5 mM solution of pNPA and pNPP in ACN or Tris buffer) was added to this suspension, and the sample was agitated on a mechanical shaker for 45 min. The sample was immediately centrifuged, the supernatant was transferred to the cuvette, and the solution's absorbance was measured at 405 nm. The absorbances of only the catalyst (same concentrations as used for the samples and similar treatment, without adding the substrate) or the substrate (same concentrations as used for the samples) were recorded at 405 nm and subtracted from the data obtained for the samples in order to remove any absorbance that might come from the catalyst or the substrate. The entire process was carried out six times. PNP's calibration curve was used to determine how much PNP was produced in each case. The catalysts were cleaned with water five times,

then with ACN five times, and vacuum-dried at 50 °C for 12 h after each cycle. The dried catalyst was then used in additional cycles using the same procedure.

5.3.12. Measurement of haloperoxidase-mimicking activity

The haloperoxidase-mimicking potential of the catalyst was investigated by a protocol reported earlier with little modifications.³⁶ Initially, phenol red (0.6 mg, 50 μ M) and ammonium bromide (0.1 mg, 25 μ M) were dissolved in water, which was followed by the addition of H₂O₂ (1 μ L, 300 μ M). The pH of the solution was maintained between 5 and 6 and each sample (1 mg/mL) was incubated with this reactant solution for 5 h at room temperature and the absorbance was recorded in the range of 400-600 nm using a UV-Vis spectrophotometer.

5.3.13. Acetylcholinesterase (AChE)-mimicking activity

Stock solutions of acetylthiocholine and DTNB (40 mg, 100 mM) were prepared in 1 mL DMSO. About 1 mg of each material (CeNP, TC, TCP, and PA) were suspended in 1 mL of PBS, and 10 μ L of DTNB and acetylthiocholine were added to the suspension of catalysts and absorbance data was collected at 405 nm, every 15 min for 150 min. The rate of reaction was obtained by using molar extinction coefficient of 13600 M⁻¹cm⁻¹.

5.3.14. Ca mineralization

The capability of the catalysts to imitate alkaline phosphatase (ALP) enzyme was assessed by Ca mineralization study.^{22,37} Wells of a 24-well plate were coated with 1 mg/mL suspension of all the materials (CeNP, TC, TCP, and PA) and dried over night at 37 °C. An osteogenic solution was prepared containing 15 mM of β -glycerophosphate as a source of Pi, 20 mM of CaCl₂ as a source of Ca²⁺ in Tris-HCl buffer (25 mM, pH 7.4). About 800 μ L of this solution was added into each well and incubated at 37 °C for 7 days. Every day, osteogenic solution was replenished with fresh osteogenic solution. At 7th day, after removing the solution, wells were washed with distilled water and allowed to air dry. The mineralized calcium developed due to the ALP-mimicking enzyme was further measured by using 0.1% Alizarin Red S (3,4-Dihydroxy-9,10-dioxo-9,10-dihydroanthracene-2-sulfonic acid) staining. After staining, the excess dye was removed and wells were washed with distilled water and the 10% cetylpyridinium chloride was added to dissolve the calcium-bound dye. Finally, the absorbance was measured at 562 nm to quantify the mineralized calcium using a Tecan multimode microplate reader. Wells containing only osteogenic solution without any sample were treated as a control.

5.3.15. Cell culture study

The murine pre-osteoblast cells (MC3T3-E1, passage 5-6) were cultured in MEM- α , supplemented with 10% FBS and 1% Pen-Strep antibiotic solution at 37 °C with 5% CO₂ in a humidified atmosphere. For experiments involving long term cell culture studies, medium was changed every 72 h and the cells were harvested using a solution of trypsin-EDTA at around 70-80% confluency. The cells were further redispersed in complete media and seeded in dishes or cell culture plates to conduct various cell culture studies. Osteogenic media (OM) composed of complete MEM- α containing 100 nM dexamethasone, 50

µg/mL ascorbic acid, and 10 mM β-glycerophosphate disodium salt hydrate was considered as a positive control, while complete MEM-α without sample was treated as the negative control.

Cytocompatibility study. The cytocompatible nature of the nanomaterials (CeNP, TC, TCP, and PA) was evaluated via MTT assay as per the protocols reported earlier.³⁸ Pre-osteoblast cells were first seeded with a cell density of 1×10^5 cells into a 96 well plate (100 µL/well) and after an incubation for 24 h, the media was replaced with the suspension of nanomaterials in varying amounts (50, 100, 300 and 500 µg). After 48 h of incubation, the treated cells were incubated with 20 µL of MTT solution (5 mg/mL in PBS) for 3.5 h to evaluate their cytocompatibility. The absorbance of the solubilized formazan in DMSO was measured at 595 nm, which is directly correlated to the cellular viability. The experiment was performed in triplicate and the data were represented as mean ± SD. The cell viability was calculated using the following equation:

$$\% \text{ Cell viability} = \frac{\text{Absorbance for sample}}{\text{Absorbance for control}} \times 100 \quad \text{Equation 5.1}$$

Alkaline phosphatase (ALP) estimation. Alkaline phosphatase (ALP) is essential for bone remodeling, resorption, and mineralization of carbonated apatite. In vitro ALP activity was estimated following the protocol described earlier in the literature with little modifications.³¹ Cells with a density of 1×10^5 cells/mL were cultured in a 48-well plate for 24 h. After aspirating the media, cells were treated with suspension of nanomaterials (50, 100, 300, and 500 µg) in the complete MEM-α and incubated for 7 days. The cell media was replenished with nanoparticle suspension every 72 h. Media was removed at day 7 and cells were washed with DPBS followed by lysis of cells with 200 µL of 0.2% triton X for 30 min in order to rupture the cell membrane and release the ALP molecules. Subsequently, 200 µL of p-nitrophenyl phosphate (pNPP) solution was added to each well containing cell lysates and incubated at 37 °C for another 90 min in dark. The final absorbance was measured at 405 nm using a plate reader.

Calcium deposition assay. The propensity of the nanomaterials to mimic the ALP enzyme was further confirmed by calcium deposition study on the MC-3T3 cells by Alizarin Red S staining. The media was replaced with the suspension of nanomaterials and osteogenic media every 72 h. On day 7 of cell culturing, cells were washed with DPBS and fixed with 4% paraformaldehyde solution for 10 min at 4 °C. Followed by washing with DI water, fixed cells were stained with 500 µL of alizarin red S solution (40 mM, pH = 4.1-4.3) for 1 h in dark. After staining, the cells were washed with DI water to remove the excess dye and then the cells were visualized under an inverted microscope to observe the red crystals. To further quantify the total amount of calcium got deposited in the mineralized cells, 200 µL of 10% cetylpyridyl chloride solution was added to each well and incubated for 30 min in dark condition, and 100 µL of dissolved crystals was transferred to 96-well plate and the absorbance was measured at 562 nm.

5.3.16. Anti-biofouling test

The anti-biofouling property of nanomaterials was evaluated using bacteria *E. coli*. Suspension of nanomaterials (1 mg/mL) were casted on 24-well plates and air dried for 24 h.³⁹ Meanwhile, *E. coli* was grown till mid-log phase in Luria broth (LB) media overnight and optical density was adjusted to 0.1 at 600 nm. Samples were incubated with 500 μ L of bacterial suspension, 4.4 mM NH_4Br , and 0.42 mM H_2O_2 for 24 h at 37 $^\circ\text{C}$ inside an incubator. Wells containing bacterial suspension, NH_4Br , and H_2O_2 without samples were considered as controls. After 24 h of incubation, the suspension was removed and the wells were gently washed with distilled water to remove the weakly attached bacteria. Afterwards, the biofilm was air-dried and stained with crystal violet (0.1%) for 15 min and washed again with distilled water to remove the excess dye. Finally, 33% acetic acid solution was added to dissolve the crystal violet bound with the biofilm and the absorbance was measured at 590 nm to quantify the biofilm formation.

5.3.17. Statistical analysis

The studies were performed in triplicates and presented as average values and standard deviations from the mean value. The data were further analyzed statistically using Student's t-test. * Represents p value ≤ 0.05 , ns represents non-significant.

5.4. Results and discussion

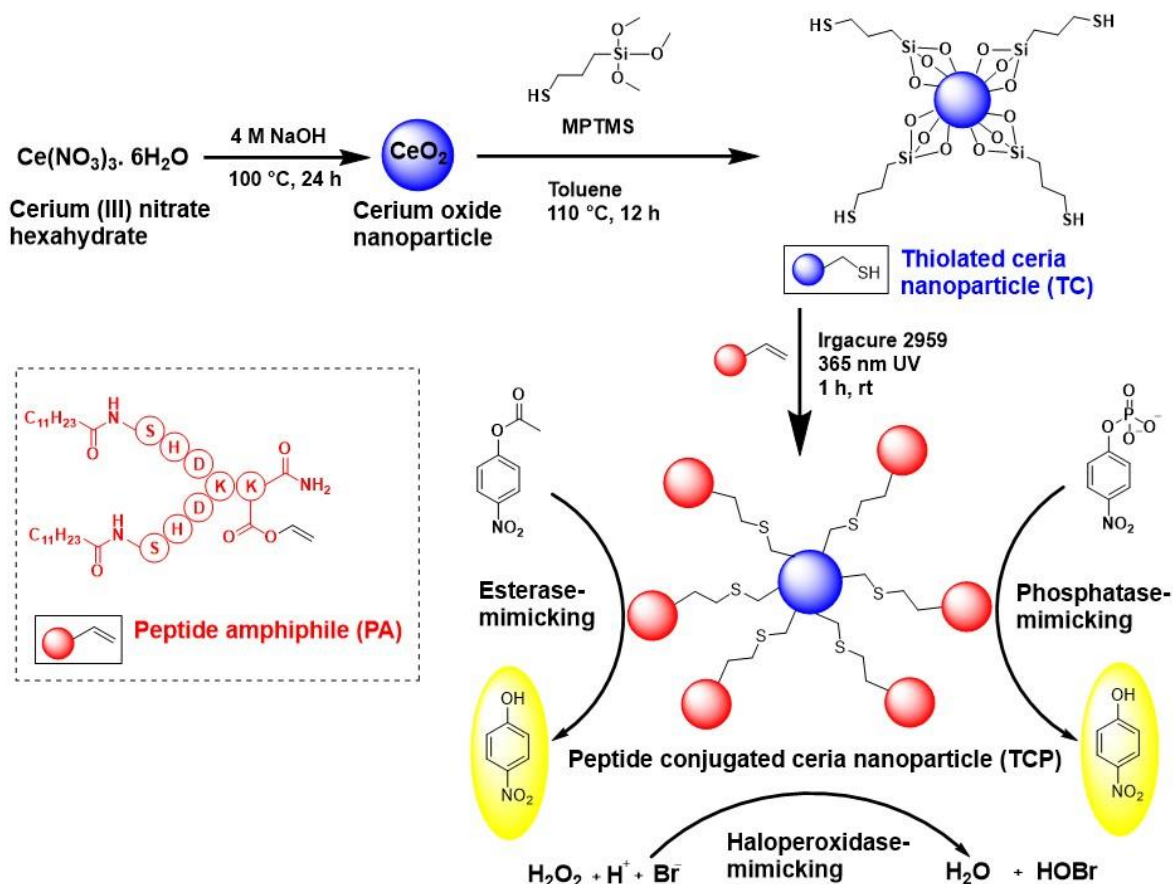


Figure 5.1. Fabrication of thiol-functionalized ceria nanoparticles and their conjugation to branched peptide amphiphile via thiol-ene conjugation for esterase, phosphatase, and haloperoxidase-mimicking activity.

The aim of this work was to develop artificial enzyme as multifunctional biocatalyst to mimic esterase, phosphatase, and haloperoxidase activity for pesticide detection, bone tissue regeneration, and anti-biofouling material application. In order to achieve this goal, we have synthesized self-assembled, branched peptide amphiphile (PA) containing the catalytic triad (Ser: S; His: H; and Asp: D) present in serine protease enzyme and conjugated it on the surface of thiol-modified ceria nanoparticle (CeNP). Immobilization of peptide on nanoparticles helps us to fabricate heterogenous biocatalyst that is recyclable. The hydrolase-mimicking properties were rendered by the self-assembled peptide and CeNP imparted the haloperoxidase-mimicking properties. These enzyme-mimicking properties were further explored for various applications (**Figure 5.1**).

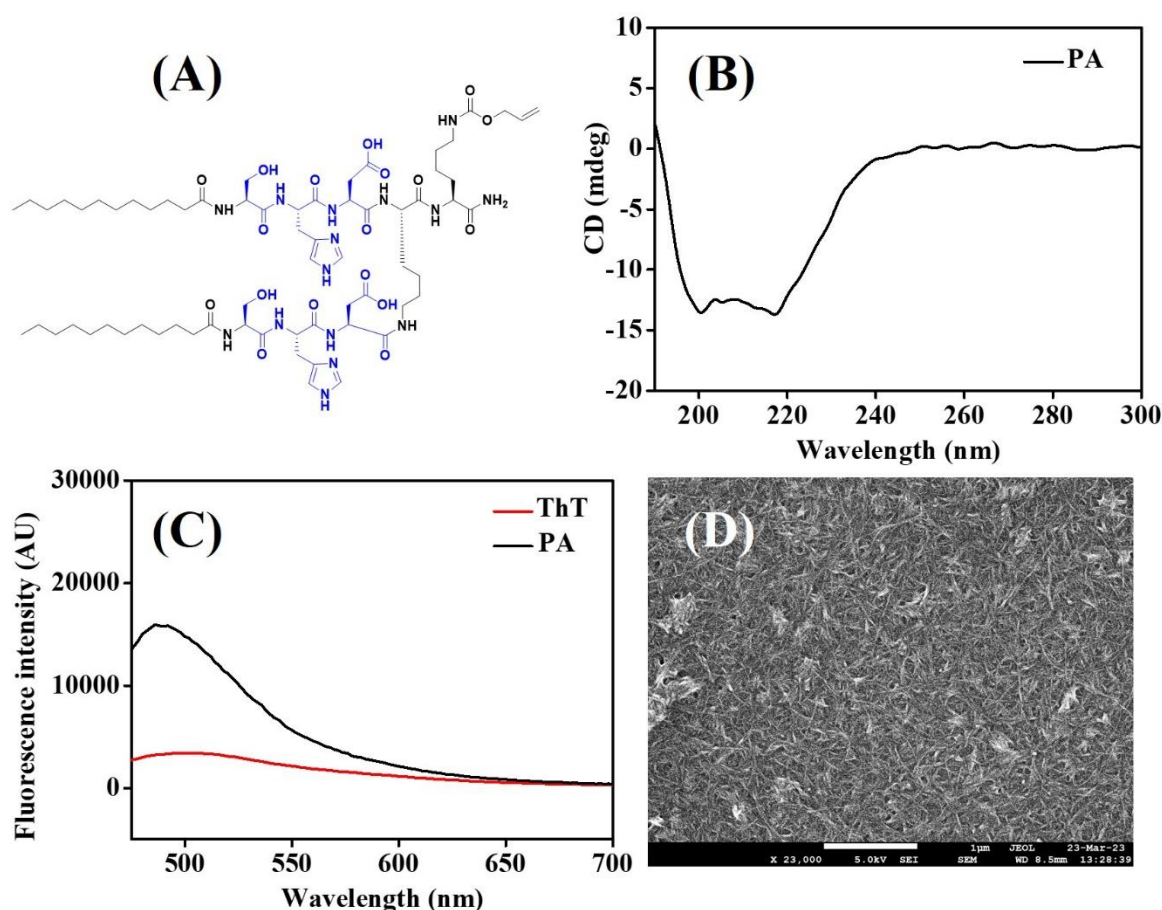


Figure 5.2. Characterization of self-assembled, branched amphiphilic peptide (PA). (A) Structure. (B) CD spectrum. (C) ThT assay. (D) FESEM micrograph. Scale bar 1 μm .

5.4.4. Design, synthesis, and characterization of peptide amphiphile (PA)

We have rationally designed the self-assembled, peptide amphiphile (PA) by incorporating the catalytic triad (S, H, and D) to mimic the catalytic site of serine protease, which belongs to the class of hydrolase

enzyme (**Figure 5.2A**). The branched peptide was synthesized in order to provide two catalytic sites in a single molecule of peptide. Based on the literature review, we hypothesized that the participating amino acids from the nearby peptides will work together to increase the activity of the peptide in its self-assembled state and the local substrate concentration will be higher at the surface of the aggregates. Therefore, we incorporated hydrophobic chain (C₁₂) at the N-terminus of the peptide to make it amphiphilic. As our aim was to conjugate the peptide to the nanoparticle by thiol-ene conjugation, we did not deprotect the Alloc-protecting group in the peptide sequence.

Fmoc-based SPPS technique was used to synthesize the peptide and rink amide resin was used as a solid support to generate carboxamide group at C-terminus. The peptide was characterized by RP-HPLC, ¹H NMR, and mass spectrometry. The RP-HPLC showed that the peptide is 90-95% pure and the retention time was found to be 4.6 min (**Figure A74, Appendix**). The MW derived from the mass spectrometry matched with their theoretical values (**Figure A75, Appendix**). The ¹H NMR spectrum of the peptide along with the assigned peaks is included in the **Appendix (Figure A76)**. The secondary structure of the self-assembled peptide was investigated by CD spectroscopy and ThT assay. A broad negative peak around 215-220 nm signifies the formation of β -sheet like morphology, and a negative band in the range of 190-200 nm suggests the presence of random coil like structure (**Figure 5.2B**). Thus, CD study confirms the presence of β -sheet morphology along with random coil like structure in the self-assembled peptide. ThT assay demonstrated the enhancement in fluorescence intensity in the range of 490-500 nm, which signifies the binding of the ThT to the hydrophobic region of the peptide and further confirms the β -sheet morphology (**Figure 5.2C**). Unbound ThT without any sample was considered as a control. The nanoscale architecture of the self-assembled peptide was evaluated by FESEM investigations. The microscopic image suggests the formation of long nanofibers by the peptide in its self-assembled form (**Figure 5.2D**). The width of the nanofibers was calculated by ImageJ software and it was found to be below 20 nm, which can be attributed to the long hydrophobic carbon chain attached at the N-terminus of the peptide.

5.4.5. Preparation and functionalization of ceria nanoparticles (CeNPs)

CeNPs were fabricated using hydrothermal method by hydrolyzing a ceria precursor, cerium nitrate hexahydrate in a basic environment. The surface was modified post synthesis using MPTMS to obtain thiol modified ceria nanoparticles (TCs). The thiol grafting on the surface was quantified by Ellman's assay, which suggested a 1306.88 $\mu\text{mol/g}$ of thiol density. The nanoparticles were characterized by XRD, TGA, elemental mapping, and XPS. The morphology and size of nanoparticles were confirmed by FESEM and DLS, which have been discussed below.

5.4.6. Immobilization of peptide on ceria surface

Our objective was to develop a multifunctional peptide-based catalyst in which the hydrolase mimicking peptide amphiphile (PA) was immobilized on a ceria surface to produce a heterogeneous catalyst. Immobilization on solid surface is expected to maintain its catalytic efficiency. Additionally, the assembly of catalytic peptides on a solid surface increases the proposed peptide catalyst's robustness

and reusability features in an integrated manner. With this aim, peptide amphiphile (PA) was conjugated on the surface of thiolated ceria (TC) via thiol-ene click reaction. The successful grafting was further confirmed by Ellman's assay, which showed that the free thiol density on the ceria surface has reduced after conjugation with peptide.

5.4.7. Characterizations

All nanomaterials (CeNP, TC, and TCP) were characterized by PXRD, TGA, Elemental mapping, FESEM, and DLS. XRD patterns of materials were investigated to determine their crystal structure (**Figure 5.3A**). CeNPs showed characteristic sharp peaks at 28.38, 32.82, 47.16, and 56.1° corresponding to 111, 200, 220, and 311 planes.³⁶ This data suggested that CeNPs have a fluorite-type crystalline nature as per the JCPDS file no. 34-0394.⁴⁰ Neither surface modification with thiol groups nor further integration of peptide on it changed the PXRD pattern or induced any new peak. However, the intensity of the peaks was significantly reduced. This data suggests that after modification on the surface of the ceria, the crystallinity was decreased.

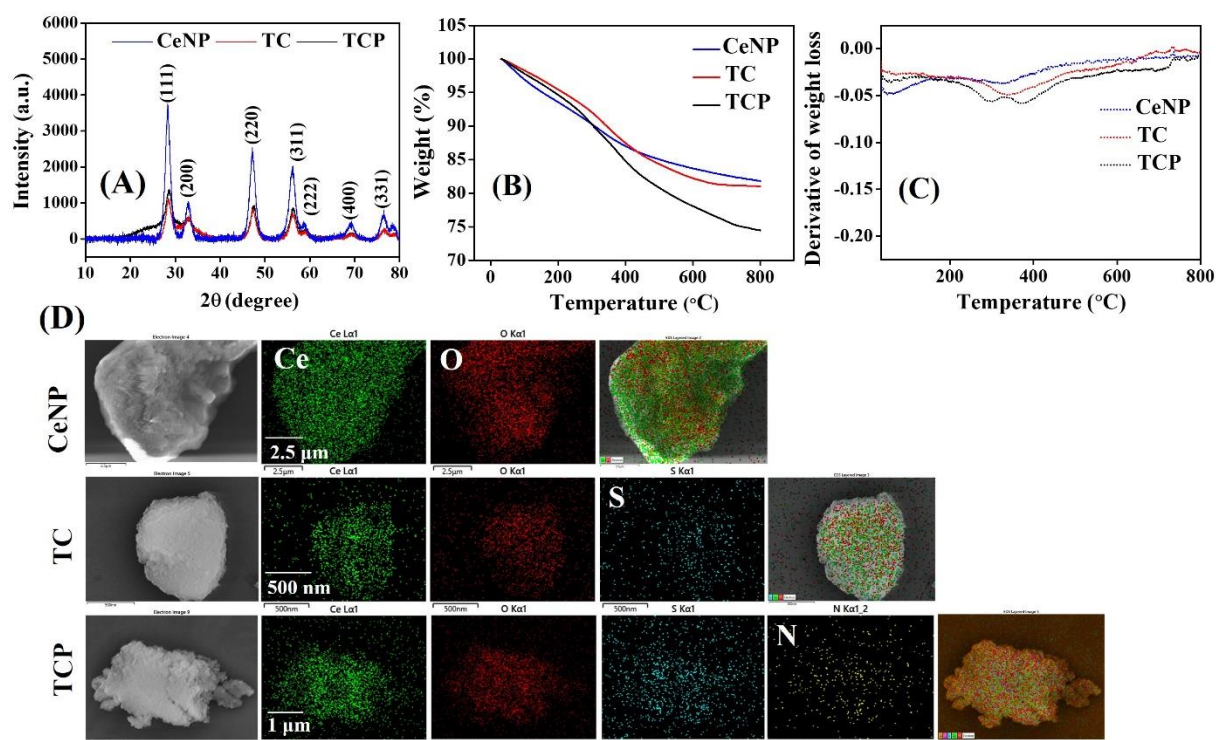


Figure 5.3. Characterization of Ceria nanoparticle (CeNPs), thiol-modified ceria nanoparticle (TC), and peptide-functionalized ceria nanoparticle (TCP). (A) XRD patterns. (B) TGA curve. (C) DTG curve. (D) Elemental mapping.

Successful grafting of thiol group and peptide on the ceria surface was further confirmed by TGA. The percentage mass loss was observed from the TGA curve (**Figure 5.3B**), whereas the derivative thermogravimetry curve (DTG) demonstrated the rate of material weight change upon heating (**Figure 5.3C**). The weight loss at 100 °C signified the loss of adsorbed water molecules from the nanomaterials. The weight loss from 250-400 °C in the DTG curve was due to the loss of organic moiety from the ceria surface.²⁷ This data confirms the functionalization of CeNP with thiol (-SH) and peptide. EDX mapping

was performed to understand the elemental distribution in all nanomaterials (**Figure 5.3D**). It was observed from the elemental mapping that the CeNP surfaces were functionalized with thiol and peptide amphiphile. FESEM images revealed that the CeNPs have a spherical morphology. Grafting of thiol groups and peptide on the surface of CeNPs did not change the morphology of nanoparticles (**Figure 5.4A-C**). It is interesting to note that conjugation of branched peptide amphiphile on the surface of CeNPs reduced their aggregation, thus increasing the stability. The size of nanoparticles increased a little after functionalization. The particle size distribution is evident from the DLS study. The size of CeNPs, TC, and TCP were found to be 41.6, 49.7, and 54.3 nm (**Figure 5.4D-F**).

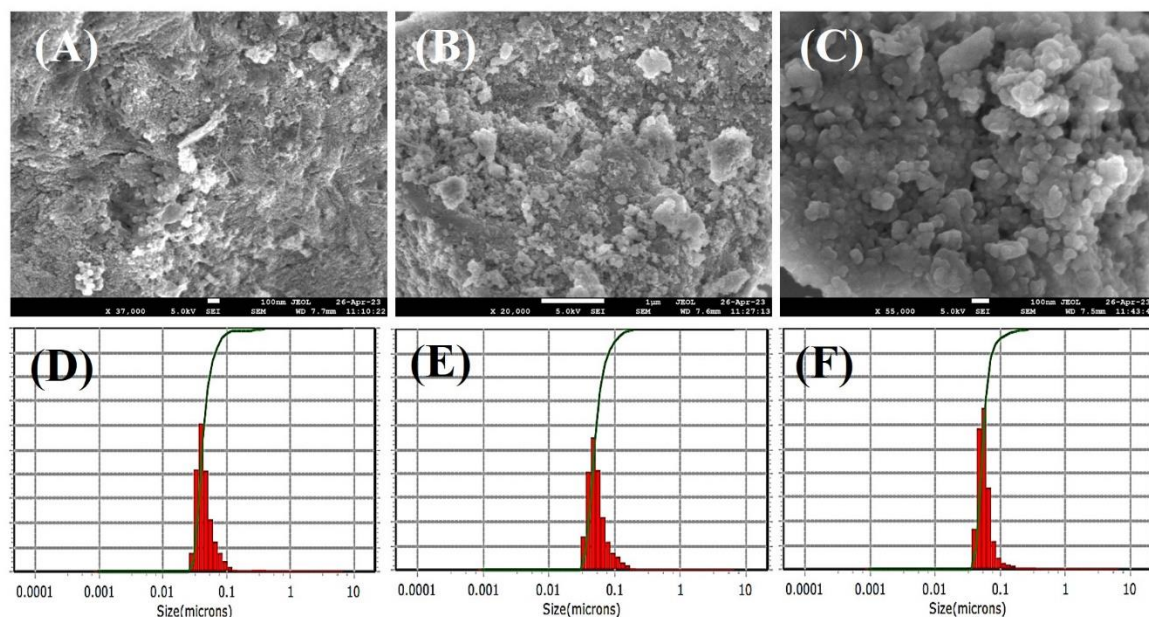


Figure 5.4. FESEM images and particle size distribution studies by DLS. (A, D) CeNPs. (B, E) TCs. (C, F) TCPs. Scale bar: (A, C) 100 nm. (B) 1 μm.

The oxidation state of the components of the nanocomposite was revealed by XPS spectra (**Figure A77, Appendix**). High-resolution Ce 3D spectrum of TCP showed spin-orbit coupling peaks corresponding to Ce 3d_{3/2} and Ce 3d_{5/2}. The peaks designated at II (884.9 eV), IV (898.0 eV), and VI (903.0 eV) corresponds to the Ce³⁺ oxidation state, whereas peaks at I (882.1 eV), III (888.5 eV), V (900.6 eV), VII (907.0 eV), and VIII (916.3 eV) corresponds to the Ce⁴⁺ oxidation state.³⁶ The ratio of Ce³⁺ to Ce⁴⁺ was calculated as 0.57 (**Table A5, Appendix**). The oxygen vacancy in the material was assessed using the expression $\text{Ce}^{3+} / (\text{Ce}^{3+} + \text{Ce}^{4+}) \times 100$, and found to be 37%. TCPs with 37% oxygen vacancy can demonstrate efficient catalytic activity, as this activity is enhanced by oxygen vacancy.

5.4.8. Catalytic activity

The individual and cooperative role of amino acids in the catalytic pockets of enzymes are best understood using peptide nano catalysts, which are simple to synthesize and modify. Histidine residues can be used to create peptide amphiphile nano catalysts with catalytic domains. Here, we developed branched, amphiphilic peptide with two catalytic domains, composed of Ser-His-Asp. The artificial enzyme can undergo self-assembly to resemble the folding mechanism of the natural enzyme.

Accordingly, we integrated a catalytic peptide on the surface of CeNPs to evaluate their multiple enzymes mimicking properties.

The esterase-mimicking activity was assessed using pNPA as a substrate, which upon hydrolysis generate yellow colored product, pNP ($\lambda_{\text{max}} = 405 \text{ nm}$). Autohydrolysis of pNPA was considered as a blank and the value was subtracted from the final absorbance value (**Figure 5.5A**). The peptide amphiphile exhibited maximum absorbance, which signifies the highest amount of p-nitrophenol production due to hydrolysis of substrate by esterase-mimicking enzyme. The activity was reduced when the PA was conjugated on the ceria nanoparticle surface but it was better than CeNPs and TCs. The overall velocity was also determined and it was found to be 0.57, 0.64, 0.82, and 1.42 $\mu\text{M}/\text{min}$ for CeNP, TC, TCP, and PA (**Figure 5.5B**). The esterase-mimicking activity was comparable with the catalyst reported by Gulseren *et al.*²⁵

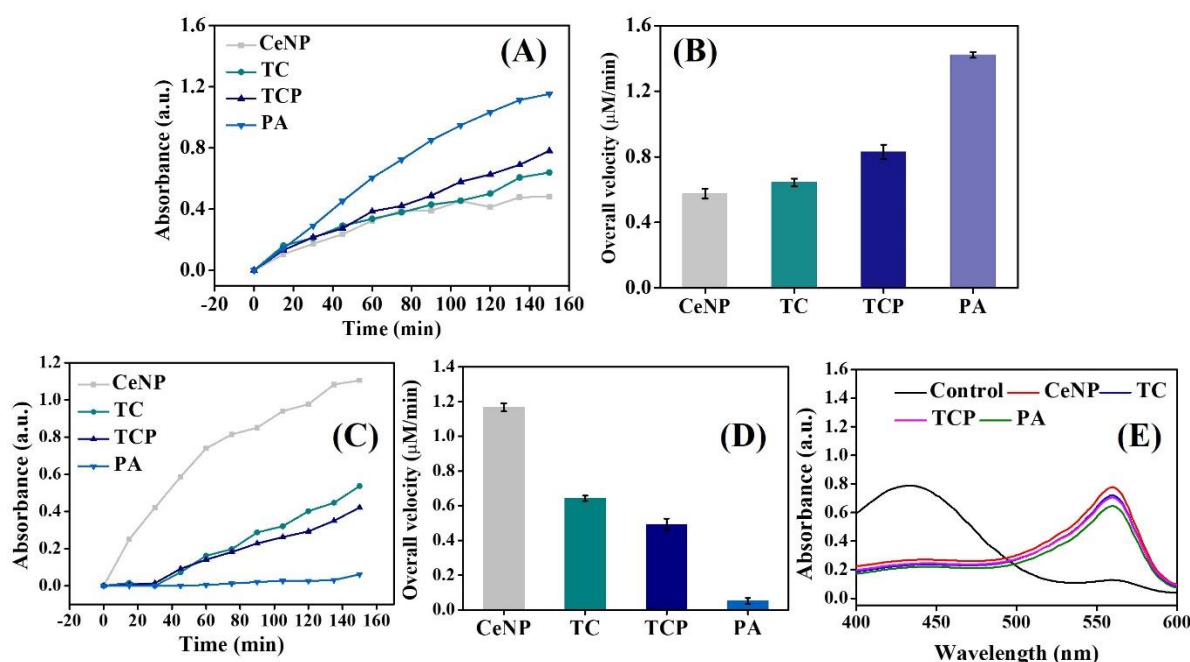


Figure 5.5. Catalytic activity for pNPA hydrolysis. (A) Absorbance of pNP vs time. (B) Overall velocity of the reaction catalyzed by CeNP, TC, TCP, and PA. (C-D) Catalytic activity for pNPP hydrolysis. (C) Absorbance of pNP vs time. (D) Overall velocity of the reaction catalyzed by CeNP, TC, TCP, and PA. (E) UV-Vis spectra for the haloperoxidase-mimicking activity indicating the conversion of phenol red ($\lambda_{\text{max}} = 432 \text{ nm}$) to bromophenol blue ($\lambda_{\text{max}} = 590 \text{ nm}$).

The phosphatase-mimicking activity was determined using pNPP as a substrate. It was very fascinating to note that the CeNPs exhibited the highest rate of hydrolysis of phosphoester bond (**Figure 5.5C**). This dephosphorylation by CeNPs was due to the reversible $\text{Ce}^{3+}/\text{Ce}^{4+}$ redox pair and the oxygen vacancy of the nanoceria was thought to be the active site of the dephosphorylation.⁴¹ After the functionalization of CeNPs with thiol and peptide, the phosphoesterase activity was reduced. Although, the overall velocity of TCP was better than PA (**Figure 5.5D**). A catalyst's recyclability is one of the main issues for the industrial use. We have carried out a single batch of catalysis followed by the removal of the catalyst by filtration, washing, and drying in order to determine whether the heterogenous catalyst (TCP) can be

recycled after each usage. The catalyst was reused for the subsequent batch after drying. The same procedure was carried out five times (**Figure A78, Appendix**), and no significant loss of activity was observed even during the fifth cycle. This demonstrates that the catalyst can be recycled using a simple and affordable process.

A class of peroxidase enzyme called haloperoxidase catalyzes the oxidation of halides.³⁹ The material's haloperoxidase-like activity was assessed utilizing the phenol red bromination assay. In the presence of halide ions and peroxide, phenol red can be brominated to generate bromophenol blue using a catalyst that resembles haloperoxidase. A successful reaction is indicated by a drop in the absorbance intensity of phenol red ($\lambda_{\text{max}} = 432 \text{ nm}$) and a corresponding increase in the absorbance intensity of bromophenol blue ($\lambda_{\text{max}} = 590 \text{ nm}$). It can be observed from **Figure 5.5E** that CeNPs exhibited highest haloperoxidase-mimicking activity with a shift of wavelength from 430 to 590 nm and the absorbance was highest at 590 nm among other nanomaterials. TCP also exhibited significant potential in bromination of phenol red while showing haloperoxidase-mimicking activity.

5.4.9. Applications of biocatalyst

The heterogenous biocatalyst, developed in this work was explored for several applications.

Acetylcholine esterase mimicking activity. Acetylcholinesterase is an enzyme found on the postsynaptic membrane and at the neuromuscular junction.⁴² Its primary function is to hydrolyze acetylcholine into choline and acetate. The breakdown of acetylcholine by acetylcholinesterase allows for the precise control over nerve impulses, preventing overstimulation or prolonged activation of postsynaptic receptors. Additionally, by clearing acetylcholine from the synapse, acetylcholinesterase helps prepare the postsynaptic neuron for subsequent signals, ensuring efficient synaptic communication. The two main types of pesticides that have been frequently used in agricultural are organophosphates (Ops) and carbamates, which can irreversibly inhibit AChE and pose a serious threat to human nervous, respiratory, and cardiovascular system. Therefore, it is highly desirable to identify OPs and carbamates selectively.⁴³ In order to estimate the AChE-mimicking property of the catalyst, we carried out experiment on acetylthiocholine, which is an analogue of acetylcholine and can produce thiocholine upon hydrolysis by AChE. The generated thiocholine was estimated by colorimetric method using Ellman's reagent (**Figure A79, Appendix**). PA displayed highest efficiency in hydrolysis of acetylthiocholine followed by TCP. CeNP and TC exhibited very less activity, which suggests the importance of catalytic triad in the artificial enzyme. The acetylcholine esterase (AChE)-mimicking potential of the catalyst was confirmed, which can be later investigated for pesticide detection.

Alkaline-phosphatase mimicking activity. Alkaline phosphatase (ALP) is an enzyme, which hydrolyses the phosphoester bond, found in various tissues throughout the body, including the liver, bone, intestines, and placenta.^{22,37,44} It plays several important roles in biological processes, such as energy production, signal transduction, bone formation, and gene maintenance. It is particularly important in bone formation and mineralization. ALP is produced by osteoblasts, which are responsible for building

and maintaining bone. Alkaline phosphatase helps to remove phosphate groups from various molecules, thus, allowing the deposition of calcium and phosphate ions to form hydroxyapatite, the mineralized matrix of bone. Therefore, we assessed the potential of our catalyst to imitate ALP to further use it for the application of bone tissue regeneration.

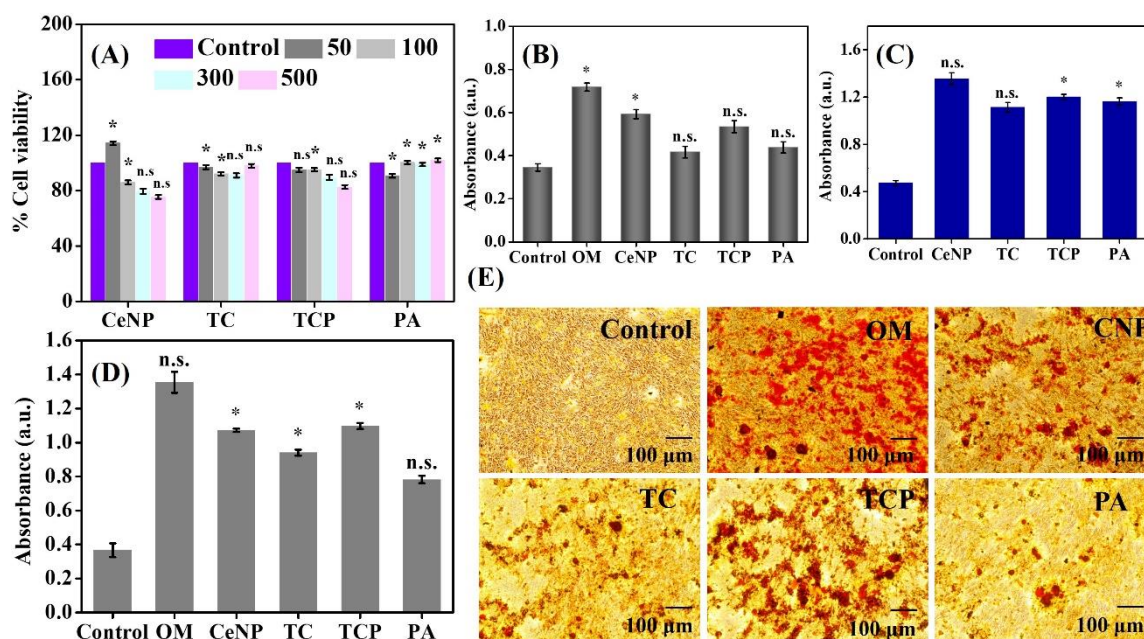


Figure 5.6. (A) Cytocompatibility study on MC3T3-E1 cells in presence of nanomaterials (CeNPs, TC, TCP, and PA) at different concentrations (50, 100, 300, and 1 µg/mL) using MTT assay at 48 h. (B) Alkaline phosphatase (ALP) activity of nanomaterials on MC3T3-E1 cells on 7th day. (C-E) Evaluation of the calcium deposited by Alizarin Red S staining. (C) On the surface of well plate. (D) On the surface of MC3T3-E1 cells. (E) Microscopic images of MC3T3-E1 cells after 7 days of treatment with nanomaterials. Red precipitates illustrate the calcium nodules. Data are presented as mean \pm SD, $n = 3$, and * $p < 0.05$ indicates statistically significant data.

We evaluated the cell viability of mesenchymal stem cells (MC3T3-E1) at different concentrations of nanomaterials (50, 100, 300 and 500 µg/mL). It was evident from **Figure 5.6A** that with higher concentration, CeNPs exhibited toxicity, whereas PA helped in the proliferation of cells upon increasing the concentration. Surface modification of CeNPs with thiol and PA decreased its toxicity and enhanced the cell viability. As far as ALP assay was concerned, CeNPs exhibited highest ALP activity on MSCs at 300 µg/mL concentration, which can be attributed to their inherent phosphatase-mimicking properties owing to their reversible $\text{Ce}^{3+}/\text{Ce}^{4+}$ redox pair and oxygen vacancy at the outer shell⁴¹ (**Figure 5.6B**). Modification of their surface with thiol and peptide could interfere with their oxidation state and deteriorate their ALP-mimicking potential on MSCs.

Considering the phosphatase like catalytic behavior of nanomaterials, we anticipated that they will have a great potential in stimulating osteogenic activity of natural ALP. In order to verify this, 24-well plates were coated with nanomaterials and incubated with the osteogenic solution containing β -

glycerophosphate and CaCl_2 for 7 days. Alizarin red S staining was carried out to quantify the amount of calcium deposition on the surface of the well. As shown in **Figure 5.6C**, the deposited calcium on the surface of well coated with nanomaterial was higher compared to the control (osteogenic media without any sample) confirming the ALP-like catalytic property of the nanomaterials, which accelerated the hydrolysis of β -glycerophosphate. The phosphatase-mimicking activity was again evaluated on the MC3T3-E1 cells and similar trend was observed where TCP allowed significant calcium deposition (**Figure 5.6D**). Control signifies the cells with complete media and OM denotes the cells treated with osteogenic media. Furthermore, inverted microscopy revealed the red-stained calcium nodules representing the extracellular calcium accumulation (**Figure 5.6E**). The results are comparable to the work reported earlier by Wang and coworkers and Gulseren *et al.*³⁷

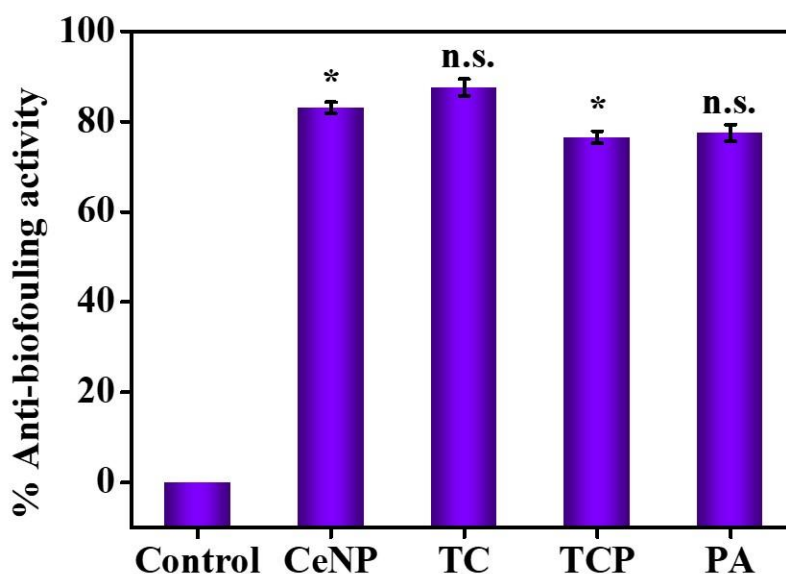


Figure 5.7. Anti-biofouling activity of CeNPs, TC, TCP, and PA against *E. coli*. Data are presented as mean \pm SD, $n = 3$, and * $p < 0.05$ indicates statistically significant data.

Finally, the haloperoxidase-like activity of the nanomaterials was exploited for the development of anti-biofouling materials.⁴⁵ The non-specific surface adherence of microorganisms is known as biofouling, which can harm the materials' performance and decrease its effectiveness by causing corrosion on metallic surfaces and bacterial infections on surgically implanted medical equipment.^{46,47} Haloperoxidase can catalyze the oxidation of halides with hydrogen peroxide to generate hypohalous acids, such as HOBr, which is known to disrupt the quorum sensing of microorganisms, thus inhibiting biofilm formation, the initial step for biofouling of a surface. We determined the inhibition of biofilm formation by crystal violet staining method and it was observed from the **Figure 5.7**, that the heterogenous catalyst (TCP) demonstrated around 80% anti-biofouling activity. Therefore, the material can be a good candidate to integrate on the surface of implant or any object as a coating material to prevent the adhesion of bacteria.

5.5. Conclusions

In summary, we have developed self-assembling, branched peptide amphiphile containing catalytic triad, 'Ser-His-Asp' to mimic the active site of serine protease, which can effectively bind with esters and hydrolyze the bond. This hydrolase mimetic catalyst was immobilized on the surface of ceria nanoparticles using thiol-ene click reaction, which exhibits haloperoxidase-mimicking properties due to their reversible change between the two oxidation states, $\text{Ce}^{3+}/\text{Ce}^{4+}$. The nanofibrous morphology of the self-assembling peptide was not retained upon conjugation with the ceria nanoparticles and the heterogenous catalyst developed a spherical shape, with a diameter of 54.3 nm. Integration of the peptide on the nanoparticle surface minimized the aggregation of nanoparticles and made the catalyst recyclable without loss of activity. The peptide-based nanomaterial showed multifunctional catalyst activity by mimicking the esterase, phosphatase, and haloperoxidase enzyme. The enzyme mimicking potential of the biocatalyst was further explored for various applications. In future, the acetylcholinesterase (AChE)-mimicking property can be used for the detection of pesticides, like organophosphates and carbamates. Alkaline phosphatase (ALP)-like activity can be exploited to develop material for bone tissue regeneration and anti-biofouling applications. Thus, the catalyst created might be quite valuable for industrial applications. Overall, this work showcases benefits of developing multifunctional heterogenous biocatalyst to reduce the problem of instability associated with peptide based homogenous catalyst. We also exploited the potential enzyme-mimicking role of the catalyst in different fields for human welfare.

References

- (1) Hamley, I. W. Biocatalysts Based on Peptide and Peptide Conjugate Nanostructures. *Biomacromolecules* **2021**, 22 (5), 1835–1855. <https://doi.org/10.1021/acs.biomac.1c00240>.
- (2) Yi, D.; Bayer, T.; Badenhorst, C. P. S.; Wu, S.; Doerr, M.; Höhne, M.; Bornscheuer, U. T. Recent Trends in Biocatalysis. *Chem. Soc. Rev.* **2021**, 50 (14), 8003–8049. <https://doi.org/10.1039/D0CS01575J>.
- (3) Bell, E. L.; Finnigan, W.; France, S. P.; Green, A. P.; Hayes, M. A.; Hepworth, L. J.; Lovelock, S. L.; Niikura, H.; Osuna, S.; Romero, E.; Ryan, K. S.; Turner, N. J.; Flitsch, S. L. Biocatalysis. *Nat Rev Methods Primers* **2021**, 1 (1), 46. <https://doi.org/10.1038/s43586-021-00044-z>.
- (4) Schmid, A.; Dordick, J. S.; Hauer, B.; Kiener, A.; Wubbolts, M.; Witholt, B. Industrial Biocatalysis Today and Tomorrow. *Nature* **2001**, 409 (6817), 258–268. <https://doi.org/10.1038/35051736>.
- (5) Rudroff, F.; Mihovilovic, M. D.; Gröger, H.; Snajdrova, R.; Iding, H.; Bornscheuer, U. T. Opportunities and Challenges for Combining Chemo- and Biocatalysis. *Nature Catalysis* **2018**, 1 (1), 12–22. <https://doi.org/10.1038/s41929-017-0010-4>.
- (6) Alvarez, G.; Shahzad, T.; Andanson, L.; Bahn, M.; Wallenstein, M. D.; Fontaine, S. Catalytic Power of Enzymes Decreases with Temperature: New Insights for Understanding Soil C Cycling and Microbial Ecology under Warming. *Global Change Biology* **2018**, 24 (9), 4238–4250. <https://doi.org/10.1111/gcb.14281>.
- (7) Mokhtar, N. F.; Abd. Rahman, R. N.; Muhd Noor, N. D.; Mohd Shariff, F.; Mohamad Ali, M. S. The Immobilization of Lipases on Porous Support by Adsorption and Hydrophobic Interaction Method. *Catalysts* **2020**, 10 (7), 1–14. <https://doi.org/10.3390/catal10070744>.
- (8) Basso, A.; Serban, S. Industrial Applications of Immobilized Enzymes—A Review. *Molecular Catalysis* **2019**, 479, 110607. <https://doi.org/10.1016/j.mcat.2019.110607>.
- (9) Sabater, S.; Mata, J. A.; Peris, E. Catalyst Enhancement and Recyclability by Immobilization of Metal Complexes onto Graphene Surface by Noncovalent Interactions. *ACS Catal.* **2014**, 4 (6), 2038–2047. <https://doi.org/10.1021/cs5003959>.
- (10) Federsel, H.-J.; Moody, T. S.; Taylor, S. J. C. Recent Trends in Enzyme Immobilization—Concepts for Expanding the Biocatalysis Toolbox. *Molecules* **2021**, 26 (9), 1–20. <https://doi.org/10.3390/molecules26092822>.
- (11) Garcia, A. M.; Kurbasic, M.; Kralj, S.; Melchionna, M.; Marchesan, S. A Biocatalytic and Thermoreversible Hydrogel from a Histidine-Containing Tripeptide. *Chem. Commun.* **2017**, 53 (58), 8110–8113. <https://doi.org/10.1039/C7CC03371K>.
- (12) Rufo, C. M.; Moroz, Y. S.; Moroz, O. V.; Stöhr, J.; Smith, T. A.; Hu, X.; DeGrado, W. F.; Korendovych, I. V. Short Peptides Self-Assemble to Produce Catalytic Amyloids. *Nature Chem* **2014**, 6 (4), 303–309. <https://doi.org/10.1038/nchem.1894>.
- (13) Guler, M. O.; Stupp, S. I. A Self-Assembled Nanofiber Catalyst for Ester Hydrolysis. *J. Am. Chem. Soc.* **2007**, 129 (40), 12082–12083. <https://doi.org/10.1021/ja075044n>.
- (14) Lou, Y.; Zhang, B.; Ye, X.; Wang, Z.-G. Self-Assembly of the de Novo Designed Peptides to Produce Supramolecular Catalysts with Built-in Enzyme-like Active Sites: A Review of Structure–Activity Relationship. *Materials Today Nano* **2023**, 21, 100302. <https://doi.org/10.1016/j.mtnano.2023.100302>.
- (15) Pelin, J. N. B. D.; Gerbelli, B. B.; Edwards-Gayle, C. J. C.; Aguilar, A. M.; Castelletto, V.; Hamley, I. W.; Alves, W. A. Amyloid Peptide Mixtures: Self-Assembly, Hydrogelation, Nematic Ordering, and Catalysts in Aldol Reactions. *Langmuir* **2020**, 36 (11), 2767–2774. <https://doi.org/10.1021/acs.langmuir.0c00198>.
- (16) List, B.; Lerner, R. A.; Barbas, C. F. Proline-Catalyzed Direct Asymmetric Aldol Reactions. *J. Am. Chem. Soc.* **2000**, 122 (10), 2395–2396. <https://doi.org/10.1021/ja994280y>.
- (17) Miller, S. J. In Search of Peptide-Based Catalysts for Asymmetric Organic Synthesis. *Acc. Chem. Res.* **2004**, 37 (8), 601–610. <https://doi.org/10.1021/ar030061c>.
- (18) Zhang, C.; Xue, X.; Luo, Q.; Li, Y.; Yang, K.; Zhuang, X.; Jiang, Y.; Zhang, J.; Liu, J.; Zou, G.; Liang, X.-J. Self-Assembled Peptide Nanofibers Designed as Biological Enzymes for Catalyzing Ester Hydrolysis. *ACS Nano* **2014**, 8 (11), 11715–11723. <https://doi.org/10.1021/nn5051344>.
- (19) Huang, Z.; Guan, S.; Wang, Y.; Shi, G.; Cao, L.; Gao, Y.; Dong, Z.; Xu, J.; Luo, Q.; Liu, J. Self-Assembly of Amphiphilic Peptides into Bio-Functionalized Nanotubes: A Novel Hydrolase Model. *J. Mater. Chem. B* **2013**, 1 (17), 2297. <https://doi.org/10.1039/c3tb20156b>.

- (20) Watkins, D. W.; Jenkins, J. M. X.; Grayson, K. J.; Wood, N.; Steventon, J. W.; Le Vay, K. K.; Goodwin, M. I.; Mullen, A. S.; Bailey, H. J.; Crump, M. P.; MacMillan, F.; Mulholland, A. J.; Cameron, G.; Sessions, R. B.; Mann, S.; Anderson, J. L. R. Construction and in Vivo Assembly of a Catalytically Proficient and Hyperthermostable de Novo Enzyme. *Nature Communications* **2017**, *8* (1), 358. <https://doi.org/10.1038/s41467-017-00541-4>.
- (21) Patel, S. C.; Bradley, L. H.; Jinadasa, S. P.; Hecht, M. H. Cofactor Binding and Enzymatic Activity in an Unevolved Superfamily of de Novo Designed 4-Helix Bundle Proteins. *Protein Science* **2009**, *18* (7), 1388–1400. <https://doi.org/10.1002/pro.147>.
- (22) Wang, Y.; Yang, L.; Wang, M.; Zhang, J.; Qi, W.; Su, R.; He, Z. Bioinspired Phosphatase-like Mimic Built from the Self-Assembly of De Novo Designed Helical Short Peptides. *ACS Catal.* **2021**, *11* (9), 5839–5849. <https://doi.org/10.1021/acscatal.1c00129>.
- (23) Zozulia, O.; Korendovych, I. V. Semi-Rationally Designed Short Peptides Self-Assemble and Bind Hemin to Promote Cyclopropanation. *Angew. Chem. Int. Ed.* **2020**, *59* (21), 8108–8112. <https://doi.org/10.1002/anie.201916712>.
- (24) Wong, Y.-M.; Masunaga, H.; Chuah, J.-A.; Sudesh, K.; Numata, K. Enzyme-Mimic Peptide Assembly To Achieve Amidolytic Activity. *Biomacromolecules* **2016**, *17* (10), 3375–3385. <https://doi.org/10.1021/acs.biomac.6b01169>.
- (25) Gulseren, G.; Khalily, M. A.; Tekinay, A. B.; Guler, M. O. Catalytic Supramolecular Self-Assembled Peptide Nanostructures for Ester Hydrolysis. *J. Mater. Chem. B* **2016**, *4* (26), 4605–4611. <https://doi.org/10.1039/C6TB00795C>.
- (26) Mikolajczak, D. J.; Kokscha, B. Peptide-Gold Nanoparticle Conjugates as Sequential Cascade Catalysts. *ChemCatChem* **2018**, *10* (19), 4324–4328. <https://doi.org/10.1002/cctc.201800961>.
- (27) Dowari, P.; Kumar Baroi, M.; Das, T.; Kanti Das, B.; Das, S.; Chowdhuri, S.; Garg, A.; Debnath, A.; Das, D. Development of a Hydrolase Mimicking Peptide Amphiphile and Its Immobilization on Silica Surface for Stereoselective and Enhanced Catalysis. *Journal of Colloid and Interface Science* **2022**, *618*, 98–110. <https://doi.org/10.1016/j.jcis.2022.03.076>.
- (28) Reja, A.; Afrose, S. P.; Das, D. Aldolase Cascade Facilitated by Self-Assembled Nanotubes from Short Peptide Amphiphiles. *Angewandte Chemie International Edition* **2020**, *59* (11), 4329–4334. <https://doi.org/10.1002/anie.201914633>.
- (29) Halder, M.; Bhatia, Y.; Singh, Y. Self-Assembled Di- and Tripeptide Gels for the Passive Entrapment and PH-Responsive, Sustained Release of an Antidiabetic Drug, Glimepiride. *Biomater. Sci.* **2022**, *10* (9), 2248–2262. <https://doi.org/10.1039/D2BM00344A>.
- (30) Trenque, I.; Magnano, G. C.; Bolzinger, M. A.; Roiban, L.; Chaput, F.; Pitault, I.; Briançon, S.; Devers, T.; Masenelli-Varlot, K.; Bugnet, M.; Amans, D. Shape-Selective Synthesis of Nanoceria for Degradation of Paraoxon as a Chemical Warfare Simulant. *Phys. Chem. Chem. Phys.* **2019**, *21* (10), 5455–5465. <https://doi.org/10.1039/C9CP00179D>.
- (31) Rasool, N.; Negi, D.; Singh, Y. Thiol-Functionalized, Antioxidant, and Osteogenic Mesoporous Silica Nanoparticles for Osteoporosis. *ACS Biomater. Sci. Eng.* **2023**, *9* (6), 3535–3545. <https://doi.org/10.1021/acsbiomaterials.3c00479>.
- (32) Aimetti, A. A.; Shoemaker, R. K.; Lin, C.-C.; Anseth, K. S. On-Resin Peptide Macrocyclization Using Thiol–Ene Click Chemistry. *Chem. Commun.* **2010**, *46* (23), 4061. <https://doi.org/10.1039/c001375g>.
- (33) Liu, Y.; Hou, W.; Sun, H.; Cui, C.; Zhang, L.; Jiang, Y.; Wu, Y.; Wang, Y.; Li, J.; Sumerlin, B. S.; Liu, Q.; Tan, W. Thiol–Ene Click Chemistry: A Biocompatible Way for Orthogonal Bioconjugation of Colloidal Nanoparticles. *Chem. Sci.* **2017**, *8* (9), 6182–6187. <https://doi.org/10.1039/C7SC01447C>.
- (34) Li, Y.; Yang, M.; Huang, Y.; Song, X.; Liu, L.; Chen, P. R. Genetically Encoded Alkenyl–Pyrrolysine Analogues for Thiol–Ene Reaction Mediated Site-Specific Protein Labeling. *Chem. Sci.* **2012**, *3* (9), 2766. <https://doi.org/10.1039/c2sc20433a>.
- (35) Kalantari, M.; Ghosh, T.; Liu, Y.; Zhang, J.; Zou, J.; Lei, C.; Yu, C. Highly Thiolated Dendritic Mesoporous Silica Nanoparticles with High-Content Gold as Nanozymes: The Nano-Gold Size Matters. *ACS Appl. Mater. Interfaces* **2019**, *11* (14), 13264–13272. <https://doi.org/10.1021/acsami.9b01527>.
- (36) Wang, N.; Li, W.; Ren, Y.; Duan, J.; Zhai, X.; Guan, F.; Wang, L.; Hou, B. Investigating the Properties of Nano Core-Shell CeO₂@C as Haloperoxidase Mimicry Catalyst for Antifouling Applications. *Colloids and Surfaces A: Physicochemical and Engineering Aspects* **2021**, *608*, 125592. <https://doi.org/10.1016/j.colsurfa.2020.125592>.

- (37) Gulseren, G.; Yasa, I. C.; Ustahuseyin, O.; Tekin, E. D.; Tekinay, A. B.; Guler, M. O. Alkaline Phosphatase-Mimicking Peptide Nanofibers for Osteogenic Differentiation. *Biomacromolecules* **2015**, *16* (7), 2198–2208. <https://doi.org/10.1021/acs.biomac.5b00593>.
- (38) Halder, M.; Narula, M.; Singh, Y. Supramolecular, Nanostructured Assembly of Antioxidant and Antibacterial Peptides Conjugated to Naproxen and Indomethacin for the Selective Inhibition of COX-2, Biofilm, and Inflammation in Chronic Wounds. *Bioconjugate Chem.* **2023**. <https://doi.org/10.1021/acs.bioconjchem.3c00014>.
- (39) Hu, M.; Korschelt, K.; Viel, M.; Wiesmann, N.; Kappl, M.; Brieger, J.; Landfester, K.; Thérien-Aubin, H.; Tremel, W. Nanozymes in Nanofibrous Mats with Haloperoxidase-like Activity To Combat Biofouling. *ACS Appl. Mater. Interfaces* **2018**, *10* (51), 44722–44730. <https://doi.org/10.1021/acsami.8b16307>.
- (40) Sreeremya, T. S.; Thulasi, K. M.; Krishnan, A.; Ghosh, S. A Novel Aqueous Route To Fabricate Ultrasmall Monodisperse Lipophilic Cerium Oxide Nanoparticles. *Ind. Eng. Chem. Res.* **2012**, *51* (1), 318–326. <https://doi.org/10.1021/ie2019646>.
- (41) Dhall, A.; Burns, A.; Dowding, J.; Das, S.; Seal, S.; Self, W. Characterizing the Phosphatase Mimetic Activity of Cerium Oxide Nanoparticles and Distinguishing Its Active Site from That for Catalase Mimetic Activity Using Anionic Inhibitors. *Environ. Sci.: Nano* **2017**, *4* (8), 1742–1749. <https://doi.org/10.1039/C7EN00394C>.
- (42) Sidhu, J. S.; Rajendran, K.; Mathew, A. B.; Iqbal, T.; Saini, D. K.; Das, D. Acetylcholine Structure-Based Small Activatable Fluorogenic Probe for Specific Detection of Acetylcholinesterase. *Anal. Chem.* **2023**, *95* (19), 7594–7602. <https://doi.org/10.1021/acs.analchem.3c00099>.
- (43) Qian, S.; Lin, H. Colorimetric Sensor Array for Detection and Identification of Organophosphorus and Carbamate Pesticides. *Anal. Chem.* **2015**, *87* (10), 5395–5400. <https://doi.org/10.1021/acs.analchem.5b00738>.
- (44) Uslu, C.; Narin, S.; Demirsoy, Z.; Öksüz, H. B.; Gülseren, G. Pectin Hydrogels Crosslinked via Peptide Nanofibers for Designing Cell-Instructive Dynamic Microenvironment. *International Journal of Biological Macromolecules* **2023**, *233*, 123604. <https://doi.org/10.1016/j.ijbiomac.2023.123604>.
- (45) Pütz, E.; Tutzschky, I.; Frerichs, H.; Tremel, W. In Situ Generation of H₂O₂ Using CaO₂ as Peroxide Storage Depot for Haloperoxidase Mimicry with Surface-Tailored Bi-Doped Mesoporous CeO₂ Nanozymes. *Nanoscale* **2023**, *15* (11), 5209–5218. <https://doi.org/10.1039/D2NR02575B>.
- (46) Xiong, H.; He, X.; Lou, T.; Bai, X. Synthesis and Characterization of New CNT-Loaded CeO₂ Nanoparticles for Antibacterial Applications. *Biochemical Engineering Journal* **2023**, *195*, 108931. <https://doi.org/10.1016/j.bej.2023.108931>.
- (47) Herget, K.; Hubach, P.; Pusch, S.; Deglmann, P.; Götz, H.; Gorelik, T. E.; Gural'skiy, I. A.; Pfitzner, F.; Link, T.; Schenk, S.; Panthöfer, M.; Ksenofontov, V.; Kolb, U.; Opatz, T.; André, R.; Tremel, W. Haloperoxidase Mimicry by CeO_{2-x} Nanorods Combats Biofouling. *Adv. Mater.* **2017**, *29* (4), 1603823. <https://doi.org/10.1002/adma.201603823>.

CHAPTER - 6

Conclusions and perspectives

6.1. Summary of the thesis

The aim of this thesis was to develop self-assembling peptide-based scaffolds for drug delivery, tissue regeneration, and biocatalytic applications. The inherent biocompatibility, biodegradability and tunable functionality make self-assembled peptide an ideal choice as a biomaterial. Although researchers are developing several peptide-based scaffolds, their propensity to act as a drug delivery vehicle for antidiabetic drug has been hardly explored. Moreover, peptides with only L-amino acids are more prone to proteolytic degradation. Besides, potential role of polar and charged amino acids for facilitation of bone regeneration has not been investigated. Therefore, we have developed rationally designed constructs of supramolecular nanostructures involving non-covalent interactions between amino acids with specific properties. By rationally choosing amino acids, we have integrated a wide range of properties, like cell attachment, antioxidant, antibacterial, pH-responsiveness, biomineralization, and catalytic activity along with the cytocompatibility into the peptide sequence and obtained diverse supramolecular structures with multifunctional potential in biomedical field. In particular, we have developed self-assemble peptide gel for the pH-responsive, sustained delivery of an anti-diabetic drug, glimepiride, and a multifunctional wound dressing to address the off-target side effects associated with the use of nonselective, anti-inflammatory drugs, naproxen, and indomethacin. In addition, we have investigated the effects of polar and charged amino acids in a tetrapeptide sequence on hydroxyapatite adsorption and bone tissue regeneration and have developed self-assembling peptide gel-based artificial enzyme for catalyzing reactions like hydrolysis and halogenation of organic compounds in the presence of halide ions and hydrogen peroxide. All the materials developed are summarized in the following table (Table 6.1).

Table 6.1. List of self-assembled peptide-based biomaterials developed in this thesis for biomedical applications.

Peptide Sequences	Forms/Structures	Functions
Fmoc-YY-NH ₂ (YY)	Gel forming entangled networks with tiny pores	Release of antidiabetic drug, glimepiride.
Fmoc-WW-NH ₂ (WW)	Gel with porous morphology	Release of antidiabetic drug, glimepiride.
Fmoc-WWH-NH ₂ (WWH)	Gel with porous morphology	pH sensitive release of antidiabetic drug, glimepiride.
Npx-YYk-NH ₂ (Npx-YYk)	Gel with thin, long, flexible nanofibers	Chronic wound healing

Npx-YYr-NH ₂ (Npx-YYr)	Gel with thin, long, flexible nanofibers	Chronic wound healing
Ind-YYk-NH ₂ (Ind-YYk)	Gel with nanotape-like structure	Chronic wound healing
Ind-YYr-NH ₂ (Ind-YYr)	Gel with nanotape-like structure	Chronic wound healing
Fmoc-WWHS-NH ₂ (WWHS)	Gel with long, entangled nanofibrillar structure	Bone tissue regeneration
Fmoc-WWHJ-NH ₂ (WWHJ)	Nanorod	Bone tissue regeneration
Fmoc-WWHP-NH ₂ (WWHP)	Nanorod	Bone tissue regeneration
Fmoc-WWHO-NH ₂ (WWHO)	Gel with nanorod like structure	Bone tissue regeneration
Fmoc-WWHD-NH ₂ (WWHD)	Gel with long, entangled nanofibrillar structure	Bone tissue regeneration
Fmoc-WWHE-NH ₂ (WWHE)	Gel with long, entangled nanofibrillar structure	Bone tissue regeneration
(C ₁₂ -SHD) ₂ KK(Alloc)-NH ₂ (PA)	Nanofibers	Enzyme-mimetic activity
Peptide (PA) conjugated ceria nanoparticles (TCP)	Spherical	Enzyme-mimetic activity

This thesis is organized into six chapters. **Chapter 1** is introductory and it provides an overview on the self-assembly process and self-assembling peptides along with an exhaustive literature review on the use of self-assembling peptide in various biomedical field, in particular, in drug delivery, wound healing, bone regeneration, and as enzyme mimics. The literature survey is followed by the identification of knowledge gaps in different fields and specific objectives of this thesis. The hypothesis statement and organization of the thesis are also included in this chapter. **Chapter 2** deals with the development of ultra-short peptide gels from Fmoc-YY-NH₂ (YY), Fmoc-WW-NH₂ (WW), and Fmoc-WWH-NH₂ (WWH) peptides for the pH-responsive, sustained release of the hydrophobic anti-diabetic medication, glimepiride. Gels hold promise as injectable drug repositories due to their favorable viscoelastic, self-healing, and thixotropic properties. Incorporation of histidine to the dipeptide backbone aided in the development of an acidic media-sensitive gel that can help diabetic patients by avoiding the issue of nonspecific drug release from scaffolds. Tripeptide gel's slow rate of degradation makes it suitable for a long-acting, sustained release of medication. All gels have excellent antioxidant properties, which is helpful in removing the significant amount of reactive oxygen species (ROS) produced by the oxidation of glucose in diabetes patients. All gel releasates induced pH-dependent glucose uptake in human liver cancer cell line and showed great cytocompatibility to a variety of cell lines. In order to reduce side effects and dosage frequency in diabetic patients, the self-assembled tripeptide gel developed in this work can be employed as an injectable device for a pH-sensitive, long-term, controlled/sustained drug release.

In **chapter 3**, we have created multifunctional wound healing scaffolds that possess antibacterial, antibiofilm, antioxidant, radical scavenging, and anti-inflammatory characteristics for chronic wounds. It was accomplished by synthesizing peptides with two antioxidant tyrosine amino acids, which is likely to form supramolecular gels and a cationic amino acid, such as lysine or arginine, to have antibacterial and antibiofilm capabilities. To increase their stability against degradation by proteolytic enzymes and selectivity towards the cyclooxygenase 2 enzyme, which plays a key role in inflammation, the cationic amino acids were taken in the D-form. Peptide-drug conjugates, Npx-YYk, Npx-YYr, Ind-YYk, and Ind-YYr were synthesized by covalently attaching nonsteroidal anti-inflammatory drugs, indomethacin and naproxen to tripeptides. The supramolecular gels obtained from self-assembling peptide-drug conjugates were evaluated for their surface, stability, viscoelasticity, swelling, and degradation characteristics. In cell culture, these gels' potential as a scaffold for persistent wound healing was examined. As designed, naproxen- and indomethacin-conjugated peptide gels demonstrated great proteolytic stability and selective cyclooxygenase 2 enzyme inhibition, which can be beneficial in scar-free wound healing. The gels demonstrated strong antibacterial activity against *S. aureus*, the primary pathogen responsible for chronic wounds, through a mechanism including cell wall and membrane rupture, suppression of biofilm development, and breakdown of established biofilms. They also exhibited anti-inflammatory activities, offered defense against reactive oxygen species/oxidative stress, and promoted cell proliferation in mice fibroblast and mouse macrophage-like cells. Overall, this work offers a viable method for creating multifunctional peptide-based scaffolds for wound healing that have the ability to reduce bacterial infections, biofilm development, and heightened inflammatory responses, resulting in faster wound healing.

The goal of **chapter 4** was to fabricate ultra-short, amphiphilic peptide-based scaffolds that could bind to hydroxyapatite and induce osteogenic differentiation for efficient bone repair. To achieve this, we have synthesized six tetrapeptides, Fmoc-WWHS-NH₂ (WWHS), Fmoc-WWHJ-NH₂ (WWHJ), Fmoc-WWHP-NH₂ (WWHP), Fmoc-WWHO-NH₂ (WWHO), Fmoc-WWHD-NH₂ (WWHD), and Fmoc-WWHE-NH₂ (WWHE), inspired from collagen and non-collagenous proteins that have negative charge with distinct functionalities, such as phosphate, hydroxyl, and carboxyl groups. Four out of six peptides formed self-assembled gels with distinct nanostructures and the other two formed nanorod-like clusters. The research sheds light on the role of amino acids, such as Ser, pSer, Pro, Hyp, Asp, and Glu, in establishing interactions with hydroxyapatite, the main inorganic component of bone, and aiding in mineralization. The nanostructures made from self-assembled peptides can mimic the extracellular matrix and give stem cells biochemical cues for adherence and proliferation. Studies using cell culture demonstrated that these peptides are biocompatible to pre-osteoblasts and induce their migration and proliferation. The peptides increased the levels of biochemical indicators of ossification, alkaline phosphatase (ALP) and calcium deposition, following 7 and 14 days of incubation with pre-osteoblast cells. They promoted M2 macrophage polarization by downregulating TNF- α , iNOS, and upregulating IL-10 in addition to providing the protection against reactive oxygen species and oxidative stress. The differentiation of mesenchymal stem cells into pre-osteoblasts and their potential contribution to

speeding bone production were further established by assessing the expression of a number of osteogenic indicators. By coculturing pre-osteoblasts and macrophages, the capacity of these scaffolds to inhibit the osteoclastogenesis process was also confirmed, highlighting their outstanding therapeutic value for osteoporosis. Overall, this study describes the rational design and fabrication of self-assembled, short bio-inspired peptide motifs as well as their promising potential in the development of bone-tissue engineering scaffolds. The nanostructured platforms provide a cell-free and growth factor-free strategy for bone regeneration.

Chapter 5 reports the development of a self-assembling, branching, peptide amphiphile, $(C_{12}SHD)_2KK(Alloc)-NH_2$ (PA) with the catalytic triad 'Ser-His-Asp' to mimic the active site of esterase, which can successfully bind with esters and hydrolyze the bond. This hydrolase-mimicking catalyst was immobilized on the surface of ceria nanoparticles through thiol-ene click reaction, which have haloperoxidase-mimicking capabilities due to their reversible transition between two oxidation states, Ce^{3+}/Ce^{4+} . The self-assembling PA's nanofibrous morphology was not retained after conjugation with the ceria nanoparticles, and the heterogeneous catalyst gained a spherical form with a diameter of 54.3 nm. The incorporation of the peptide on the nanoparticle surface reduced nanoparticle aggregation and made the catalyst reusable, without loss of activity. Overall, the peptide-based nanomaterial developed serves as a multifunctional catalyst capable of mimicking the enzymes, esterase, phosphatase, and haloperoxidase. The enzyme-mimicking capability of biocatalyst was investigated further for a variety of applications. In future, the acetylcholinesterase (AChE)-mimicking property can be exploited to identify pesticides, such as organophosphates and carbamates. Due to their considerable alkaline phosphatase (ALP) and haloperoxidase-mimicking characteristics, this heterogeneous biocatalyst can be used to generate materials for bone tissue regeneration and anti-biofouling applications. The catalyst developed can be highly valuable for industrial applications. The critical summary of the work done, contribution to the existing knowledge, and perspectives are provided in this chapter, which is **chapter 6** and the last chapter of this thesis.

6.2. Contribution to the existing knowledge

The aim of this thesis was to develop different types of self-assembling peptide-based scaffolds with inherent activities to meet challenges associated with the diabetic drug delivery, wound healing, bone tissue regeneration, and enzyme-mimics.

Researchers have developed formulations, such as self-assembled peptide gels, polymeric hydrogels, glycopolymer nanoparticles, polymerosomes, and microneedle array patches for the treatment of diabetes but these formulations are limited to the delivery of insulin. There are only few reports on nanoparticulate systems for the delivery of glipizide and repaglinide in diabetes but these formulations do not demonstrate long-term, controlled release patterns. Glimepiride-loaded formulations have been developed and reported to control diabetes but they face restrictions, such as early burst release, usage of plasticizers, and permeation enhancers. Our glimepiride-loaded self-assembled peptide gel provides

a pH sensitive, long term, sustained release of glimepiride to address the problem of hypoglycemia due to the high drug concentration. In addition, the gel possesses inherent antioxidant activity to provide protection against reactive oxygen species/oxidative stress resulting from the free radicals generated during oxidation of glucose, which can lead to organ damage.

Next, we have developed peptide-drug conjugate gels as multifunctional wound dressings for chronic wounds. Majority of antimicrobial peptide gels reported in the field are unable to destruct biofilm, which is critical in chronic wounds. Not much has been done for the selective inhibition of COX-2 enzyme to treat stalled inflammation associated with the chronic wounds. To address these challenges, we have developed gels from peptides with inherent antioxidant, antimicrobial, and antibiofilm properties, which were conjugated to non-steroidal anti-inflammatory drugs, naproxen and indomethacin. Using an amino acid in D-form, we were able to selectively inhibit COX-2 enzyme. The proteolytically stable conjugate gels we have prepared can be potentially useful in the treatment of wounds with persistent infection, where an increased inflammatory response to infection impairs healing.

There are various peptide-based scaffolds reported as potential materials for bone tissue regeneration but the importance of charged and polar amino acids on the adsorption of hydroxyapatite, which is the major inorganic component of bone and helps in biomineralization, has not been thoroughly investigated so far. Using six tetrapeptides by changing a single amino acid in the sequence, we were able to detect the change in morphology and functionality of the peptides with the change of a single amino acid and their ability to provide biological cues to the differentiation of mesenchymal stem cells to promote bone tissue regeneration. These cell- and growth factor-free, cost-effective scaffolds provide an avenue to develop biomaterials by simply taking amino acids in the peptide sequence, which promote ossification. These scaffolds also inhibit osteoclastogenesis and do not provoke immunogenicity, which are two important factors of any bone regenerating biomaterials but largely overlooked in many of the earlier reports.

Lastly, we have developed a heterogenous, biocatalyst-mimic from self-assembling peptide to mimic esterase, phosphatase, and haloperoxidase enzymes. The current research primarily focuses on homogenous artificial enzymes, which encounter issues, such as lack of reusability and cost effectiveness. In addition, the application of these biocatalyst-mimics in the field of human welfare is also missing. We have overcome this challenge by immobilizing a catalytic peptide amphiphile on catalytic nanoparticle, such as cerium oxide, and fabricated a heterogenous, biocatalyst-mimic, which was explored in applications, like acetylcholinesterase-mimicking (for future use in pesticide detection), bone tissue regeneration, and anti-biofouling application. Thus, our biocatalyst-mimic is not only restricted to catalyzing reactions, it can also be used for therapeutic purposes.

6.3. Future perspectives

The thesis is focused on the development of biomaterials derived from self-assembled peptides to overcome the challenges associated with antidiabetic drug delivery, wound healing, tissue regeneration,

and biocatalyst-mimic. The peptide gels developed for glimepiride delivery is likely to address the batch-to-batch variability difficulties, scale-up production, and regulatory constraints associated with combination products due to their straightforward synthesis and gel fabrication procedures. However, the usage of DMSO in gel fabrication may be a barrier to their translation and there is a need to reduce the amount of DMSO to a clinically acceptable level or dry gels can be employed. The development of multifunctional peptide-drug conjugate gels can address many critical issues related to stalled inflammation in chronic wounds. Therefore, these gels can be evaluated in diabetic rat model to evaluate their effect on diabetic wounds, which is a major challenge in chronic wound healing.

We have investigated the effect of polar and charged amino acids on bone mineralization and it has led to the development of scaffolds for bone tissue regeneration. Peptides with phosphoserine and hydroxyproline exhibited highest potential as bone tissue regenerating biomaterials. These two amino acids can be used together to fabricate a scaffold for biomineralization and ossification in future. The supramolecular gels reported in this work can also be used to coat the surface of bone implant and evaluated in an osteoporotic animal model to better understand its bone forming capabilities and inhibit bone resorption. Lastly, the acetylcholinesterase-mimicking property of the heterogenous, biocatalyst-mimic can be exploited further for the selective detection of pesticides, such as organophosphates and carbamates, which could be present in fruit juice and green tea. Moreover, its alkaline phosphatase-mimicking activity can be integrated with other bone forming biomaterials for generating better scaffolds for bone tissue regeneration. The anti-biofouling activity of the catalyst can be further evaluated against different microorganisms responsible for the formation of biofilm and it can be mixed with paints to explore it as an anti-biofouling coating material for implants or equipment.

The biomaterials and technologies developed in this thesis have demonstrated promising results and, therefore, can be further evaluated in an animal model, followed by the clinical evaluation.

APPENDIX

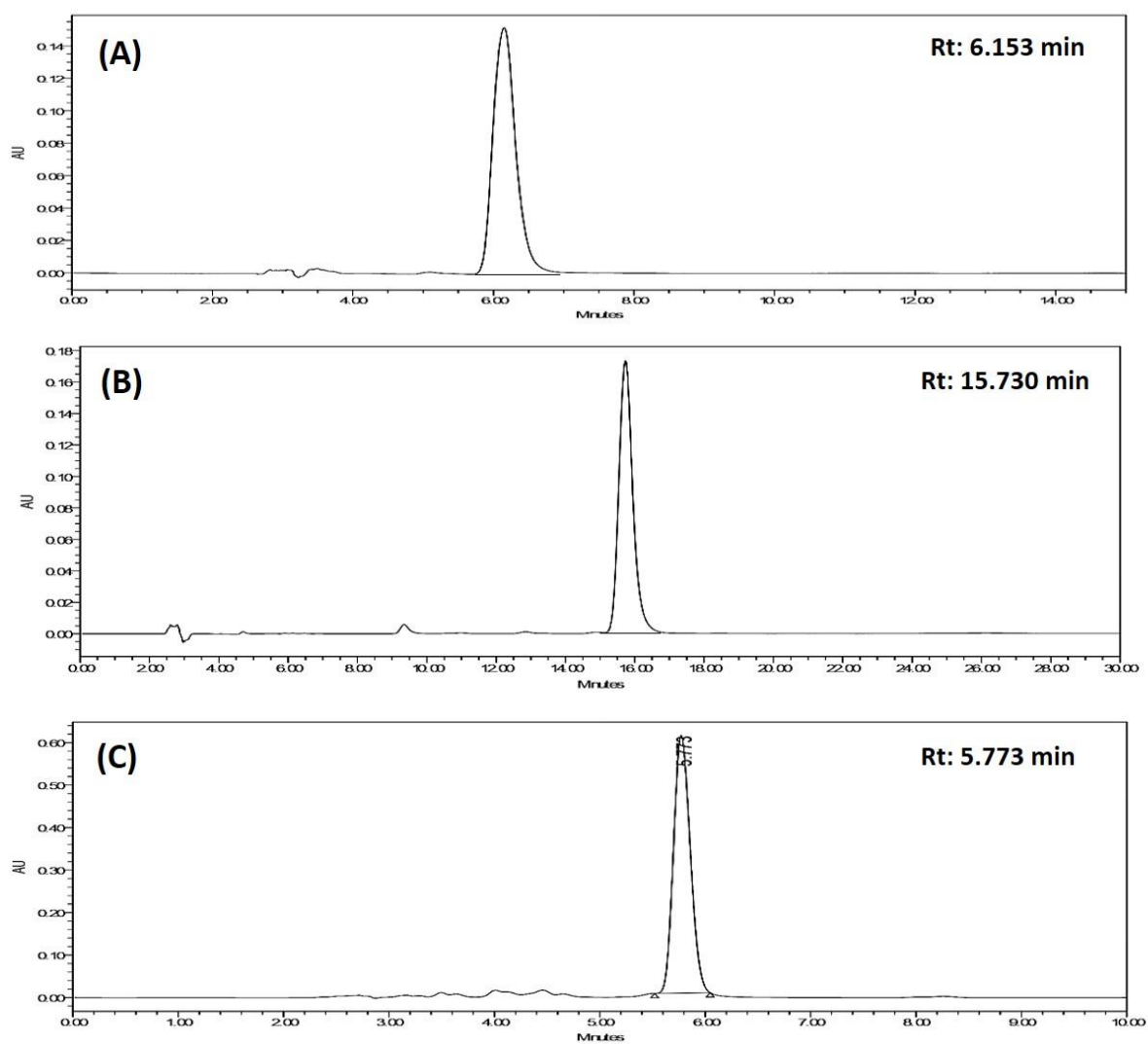


Figure A1. RP-HPLC of peptides. (A) Fmoc-YY-NH₂. (B) Fmoc-WW-NH₂. (C) Fmoc-WWH-NH₂.

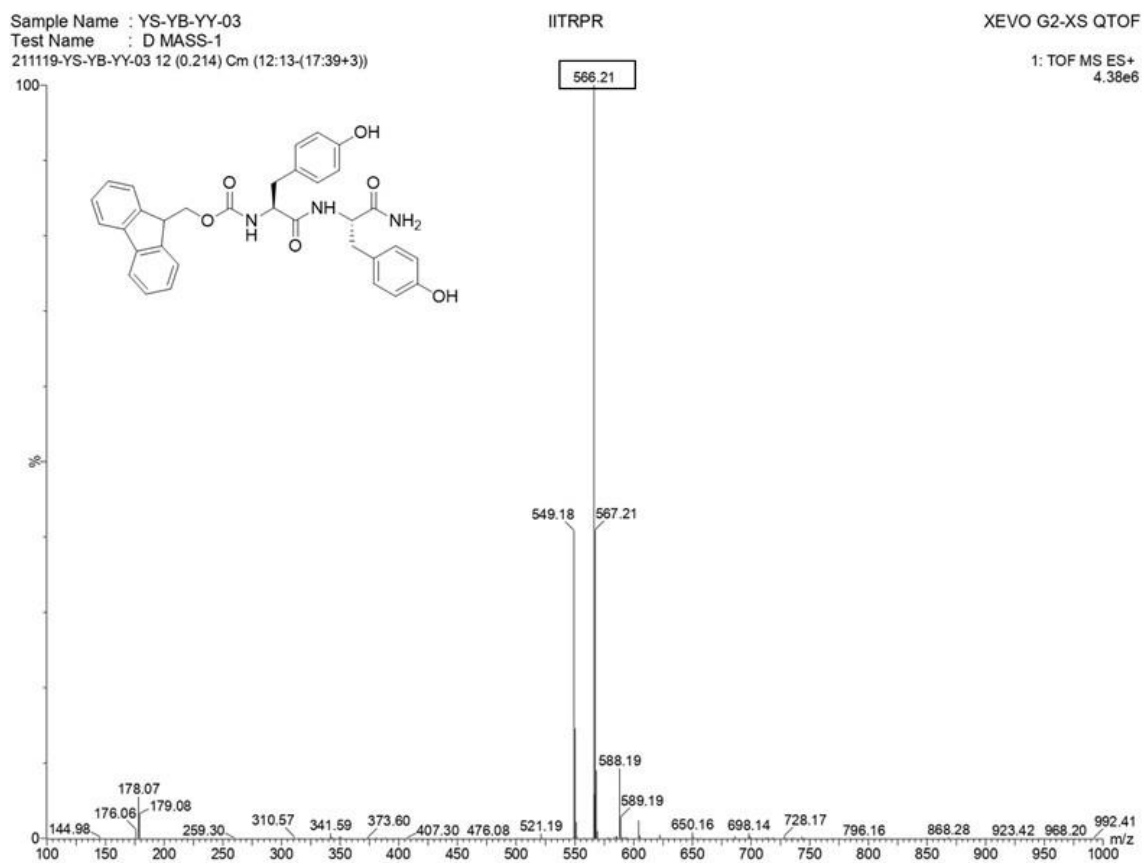


Figure A2. Mass spectrum of Fmoc-YY-NH₂ peptide.

Sample Name : YS-YB-WW-11
Test Name : D MASS-1
250220-YS-YB-WW-11 9 (0.163)

IITRPR

XEVO G2-XS QTOF

1: TOF MS ES+
1.96e7

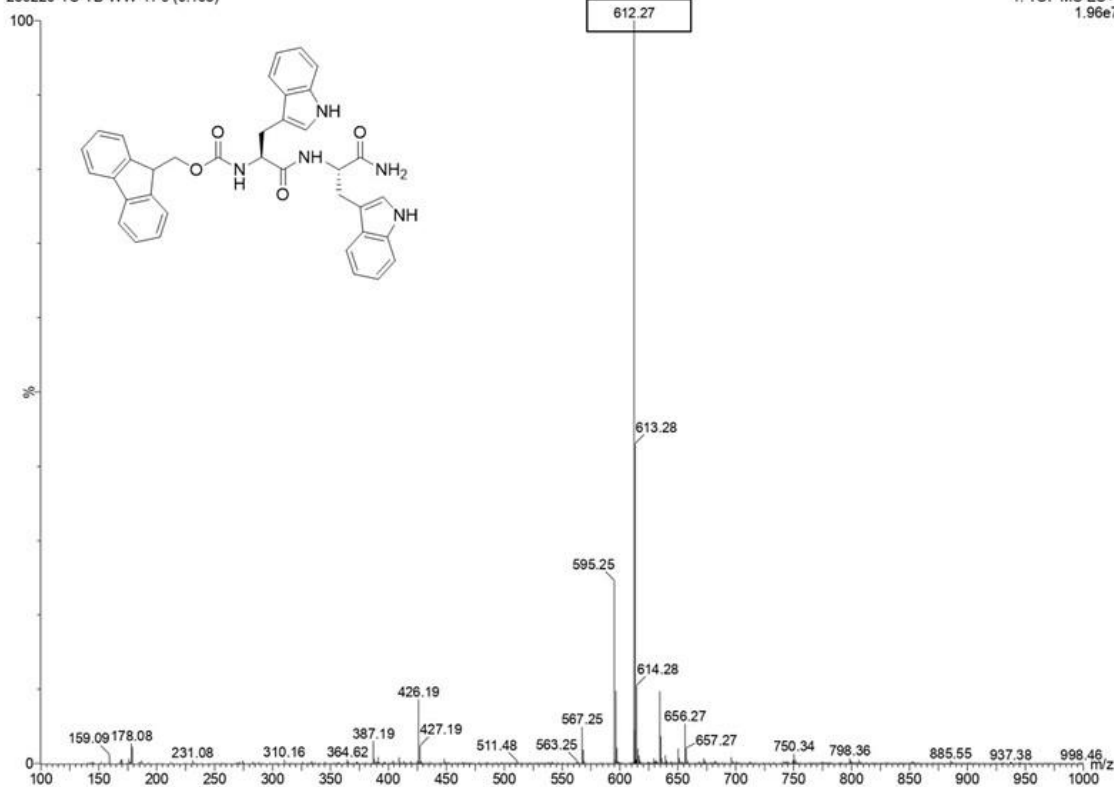


Figure A3. Mass spectrum of Fmoc-WW-NH₂ peptide.

Sample Name : YS-MH-WWLH3
Test Name : D MASS-1
261020-YS-MH-WWLH3 11 (0.197)

IITRPR

UPLC-XEVOG2XSQTOF

1: TOF MS ES+
1.26e7

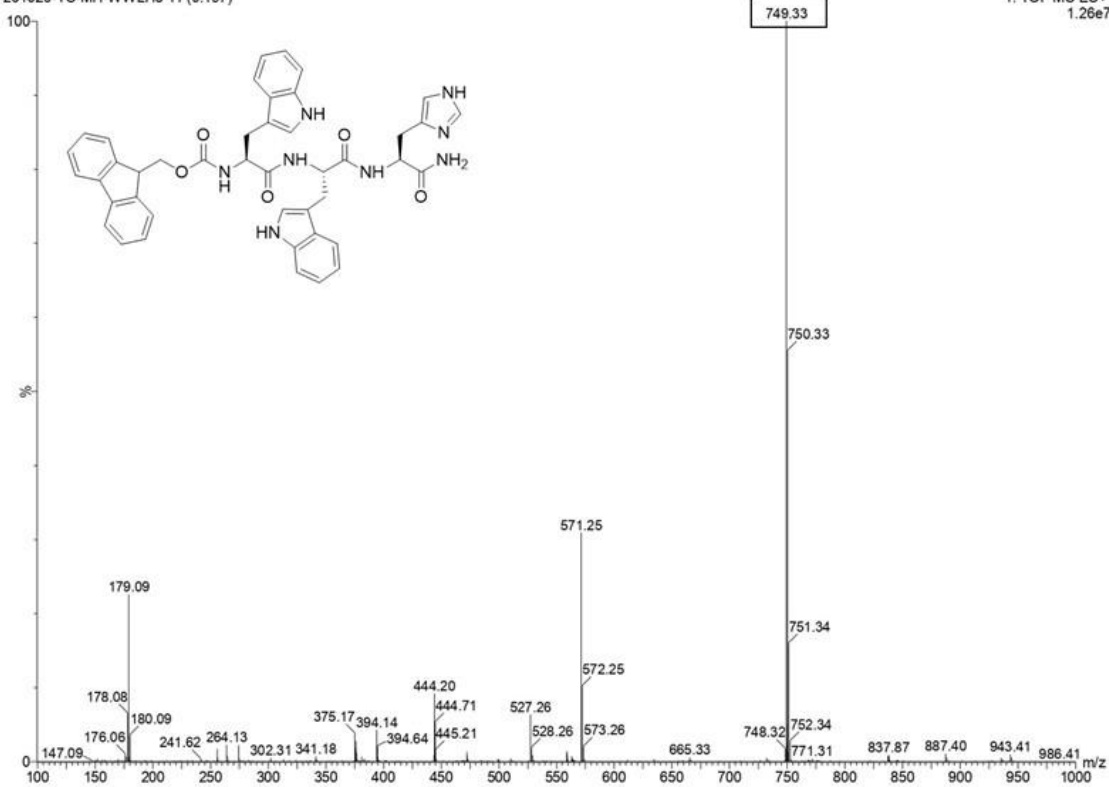


Figure A4. Mass spectrum of Fmoc-WWH-NH₂ peptide.

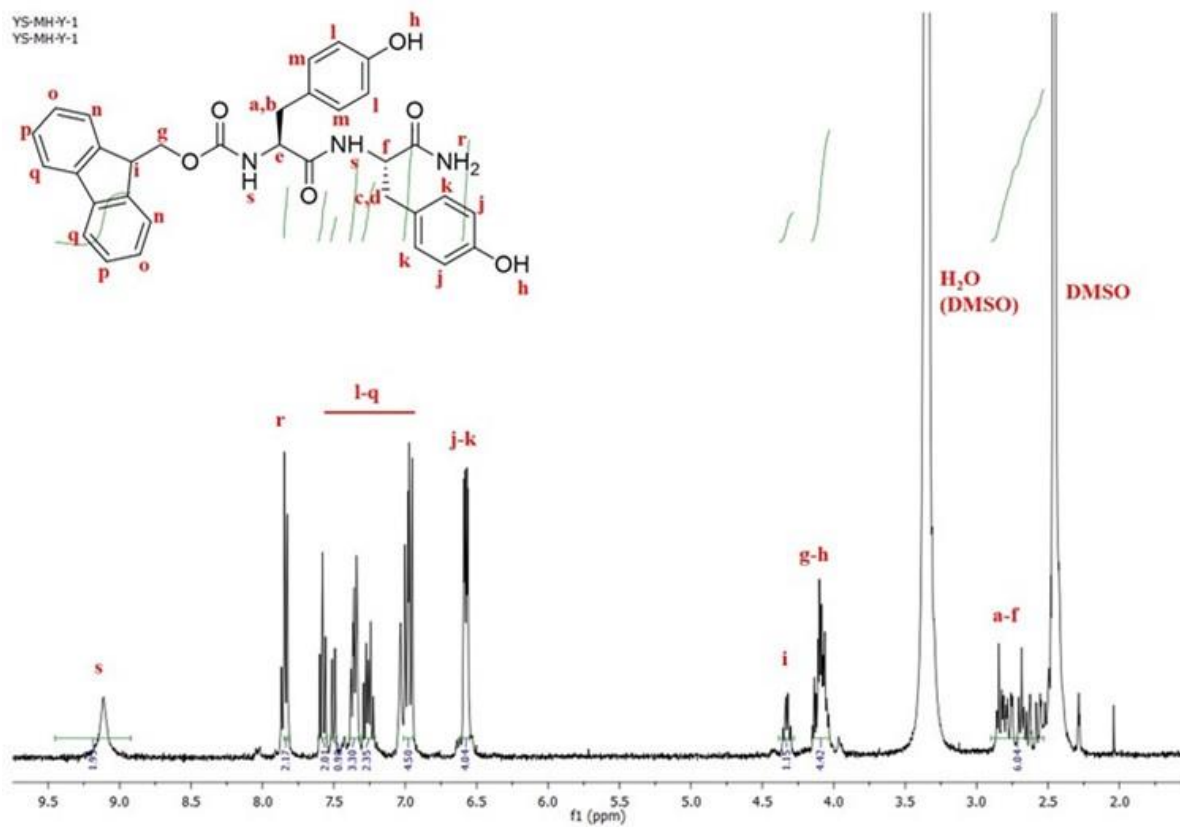


Figure A5. ¹H NMR spectrum of Fmoc-YY-NH₂ peptide.

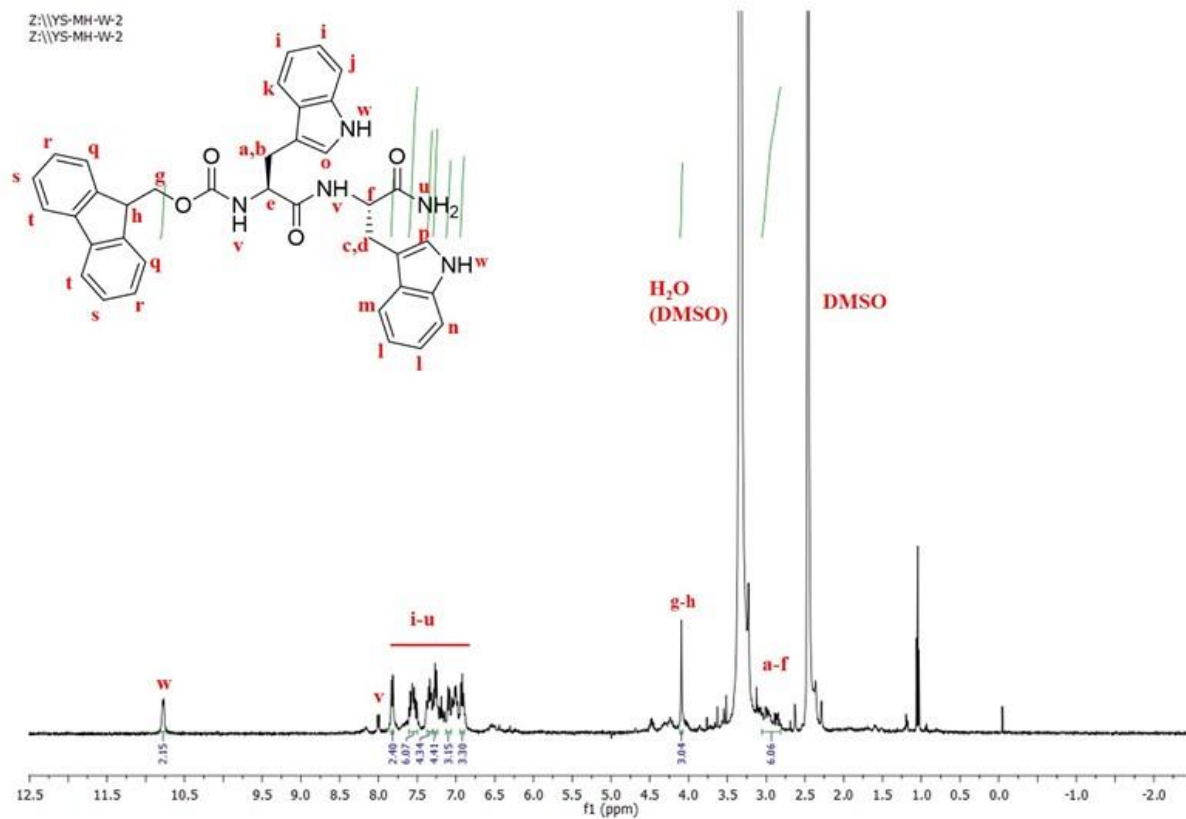


Figure A6. ¹H NMR spectrum of Fmoc-WW-NH₂ peptide.

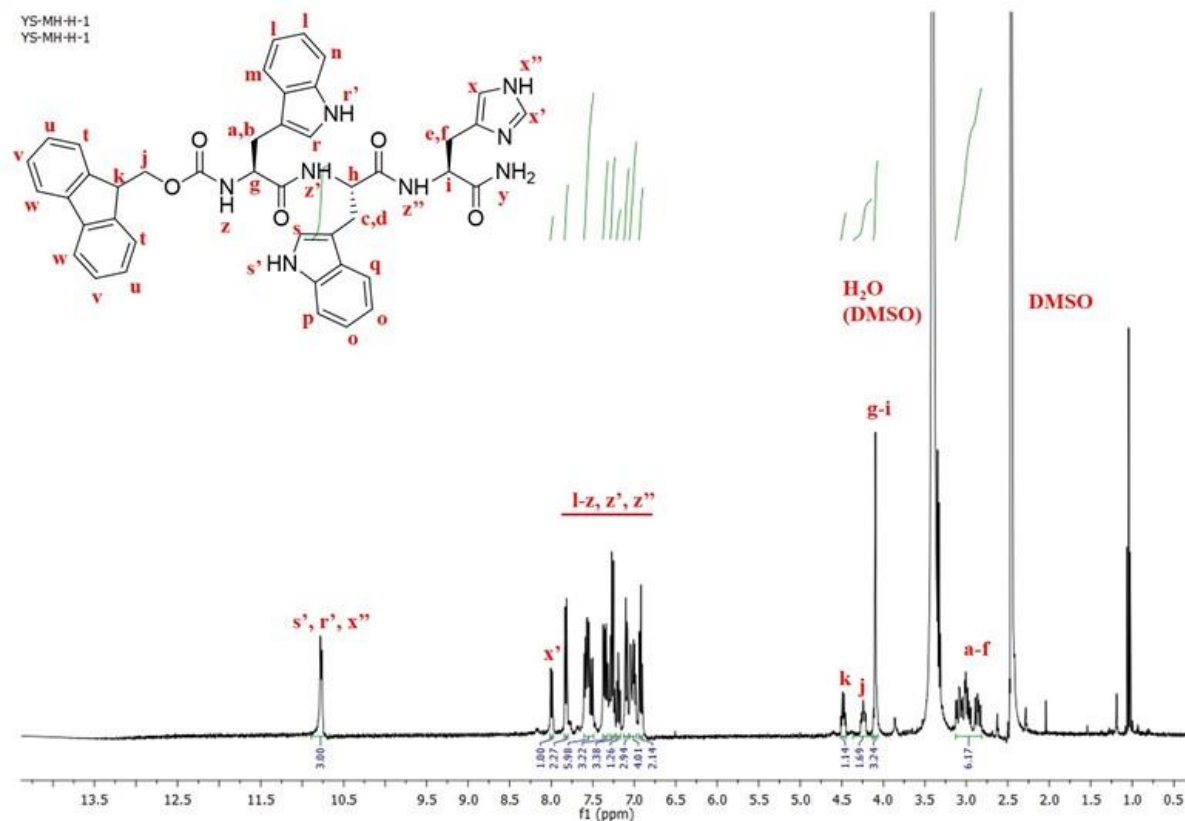


Figure A7. 1H NMR spectrum of Fmoc-WWH-NH₂ peptide.

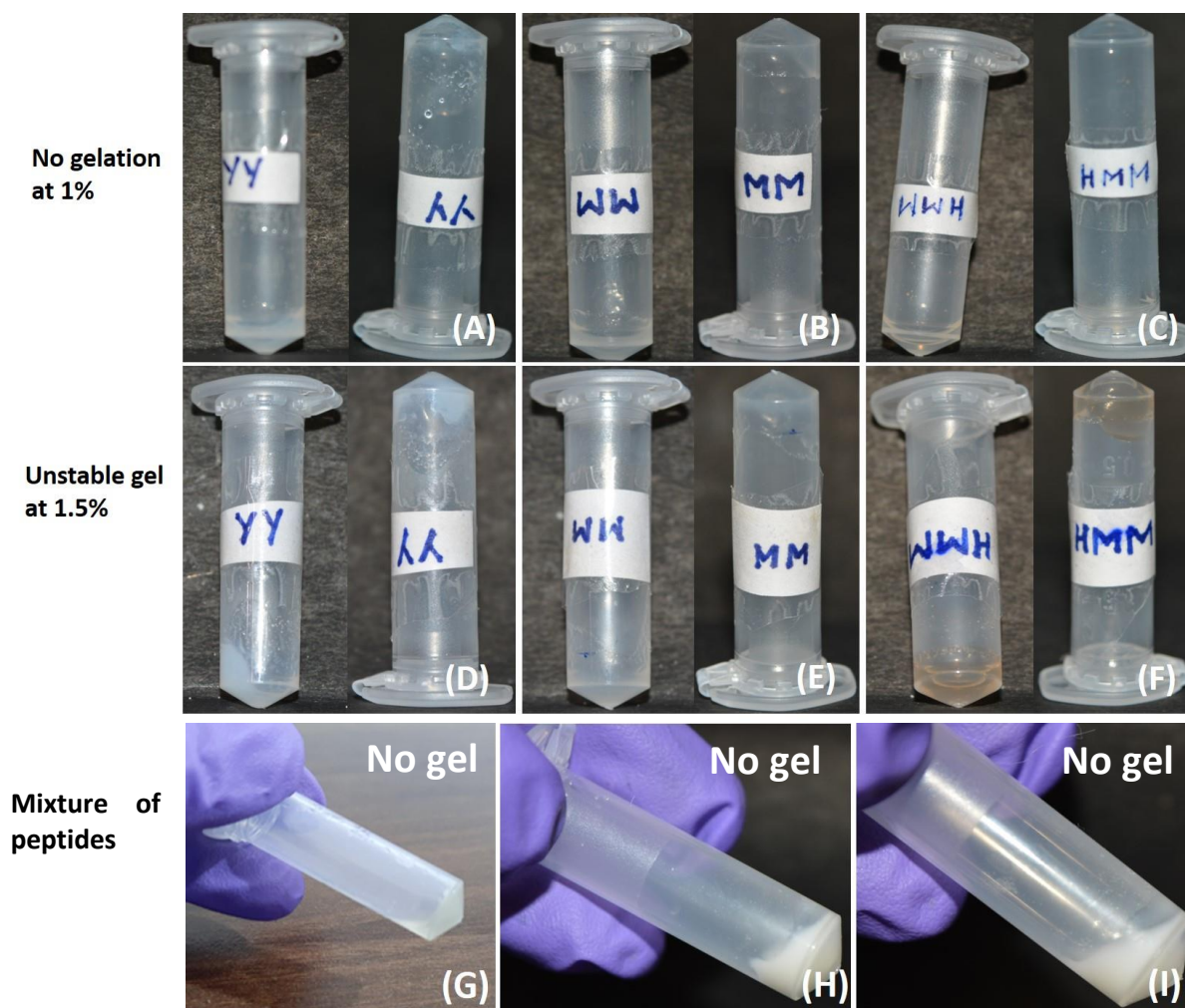


Figure A8. Images of peptide gels at different concentrations. (A, D) YY. (B, E) WW. (C, F) WWH. Combination of three peptides for gelation at different concentrations. (G) 1% w/v (H) 1.5% w/v (I) 2% w/v

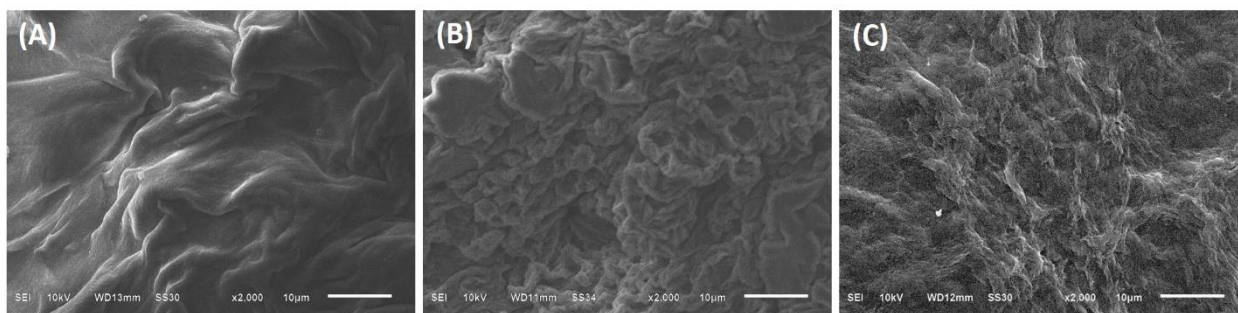


Figure A9. Scanning electron microscopy (SEM) images of dried glimepiride-loaded peptide gels (2% w/v). (A) YY. (B) WW. (C) WWH. Scale bar 10 μm .

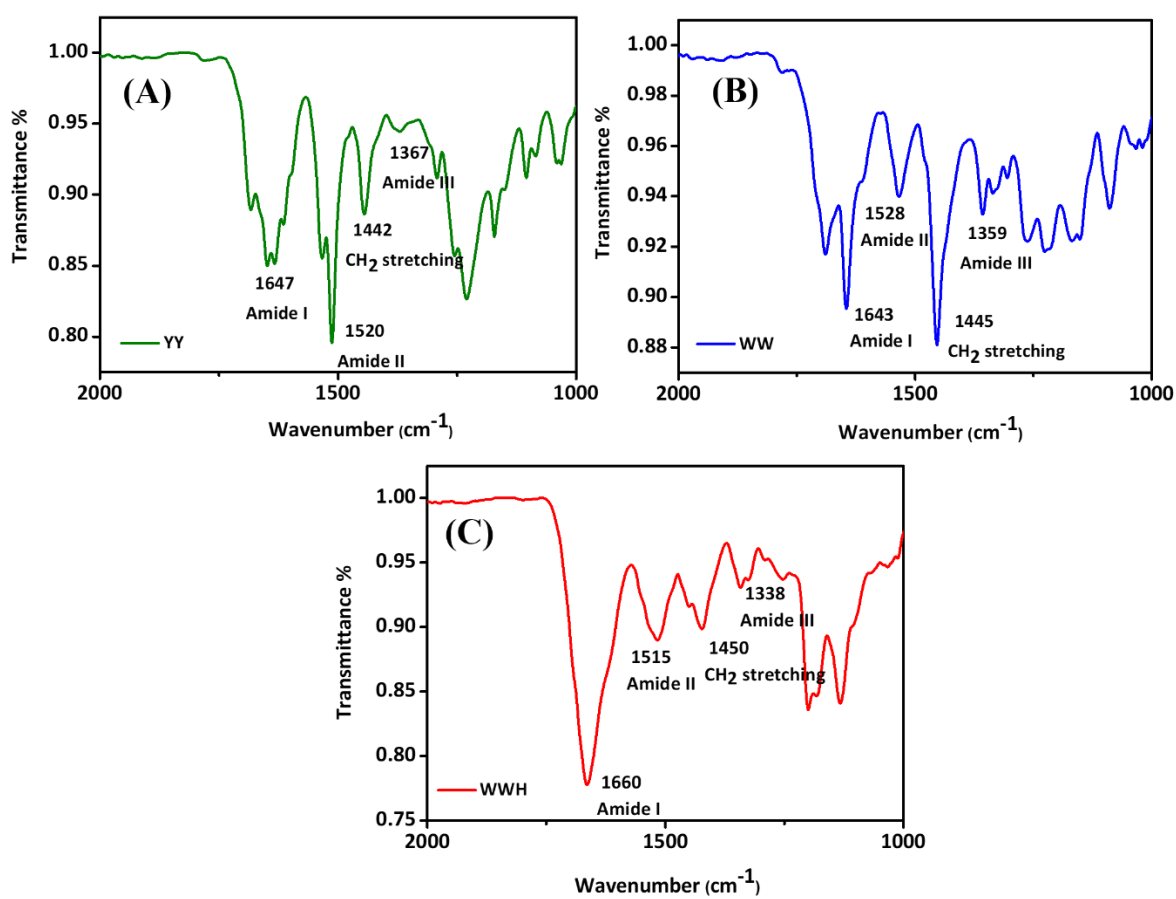


Figure A10. FTIR spectra of peptides. (A) YY. (B) WW. (C) WWH.



Figure A11. Injectability of WWH gel.

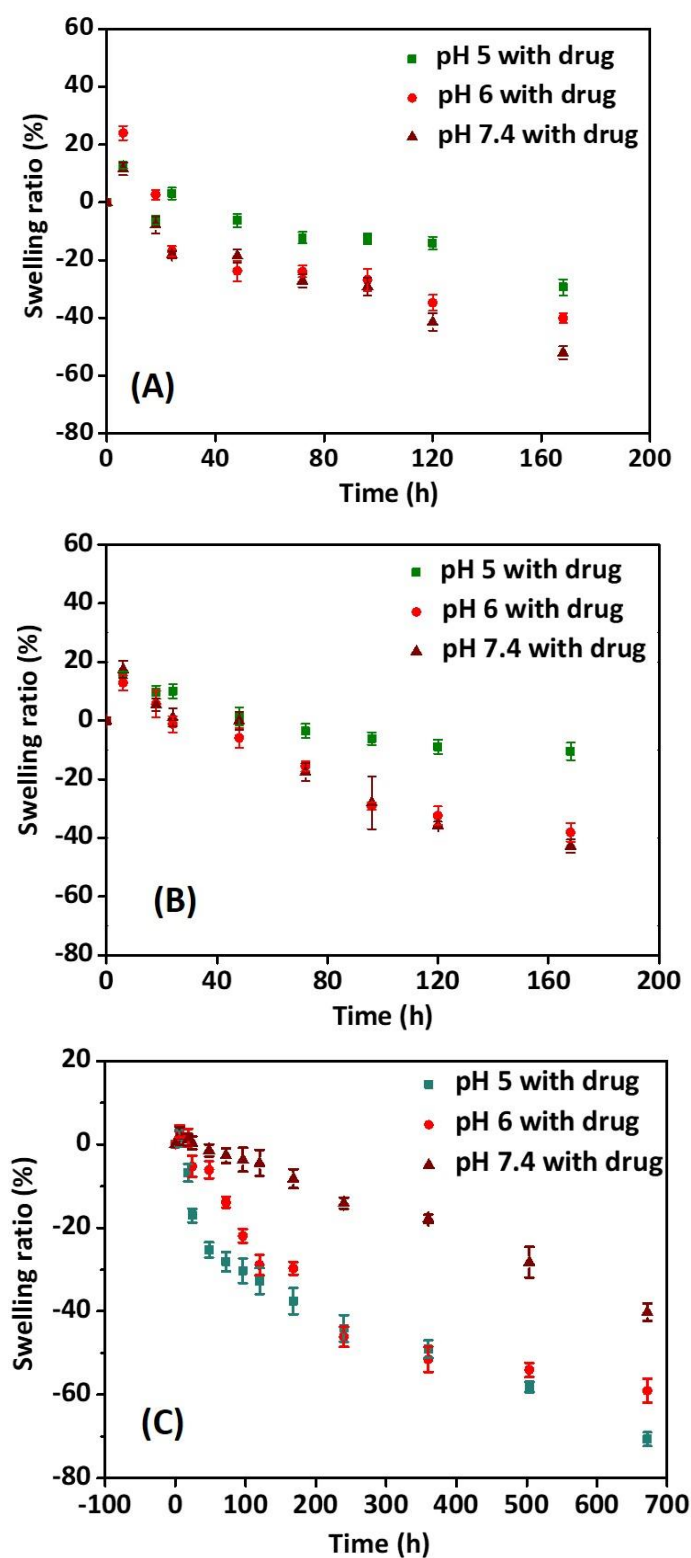


Figure A12. Swelling and degradation of glimepiride-loaded peptide gels at pH 5, 6, and 7.4. (A) YY. (B) WW. (C) WWH. Values above 0% indicate gravimetric water uptake, whereas negative values suggest degradation. Data reported are mean \pm SE ($n = 3$).

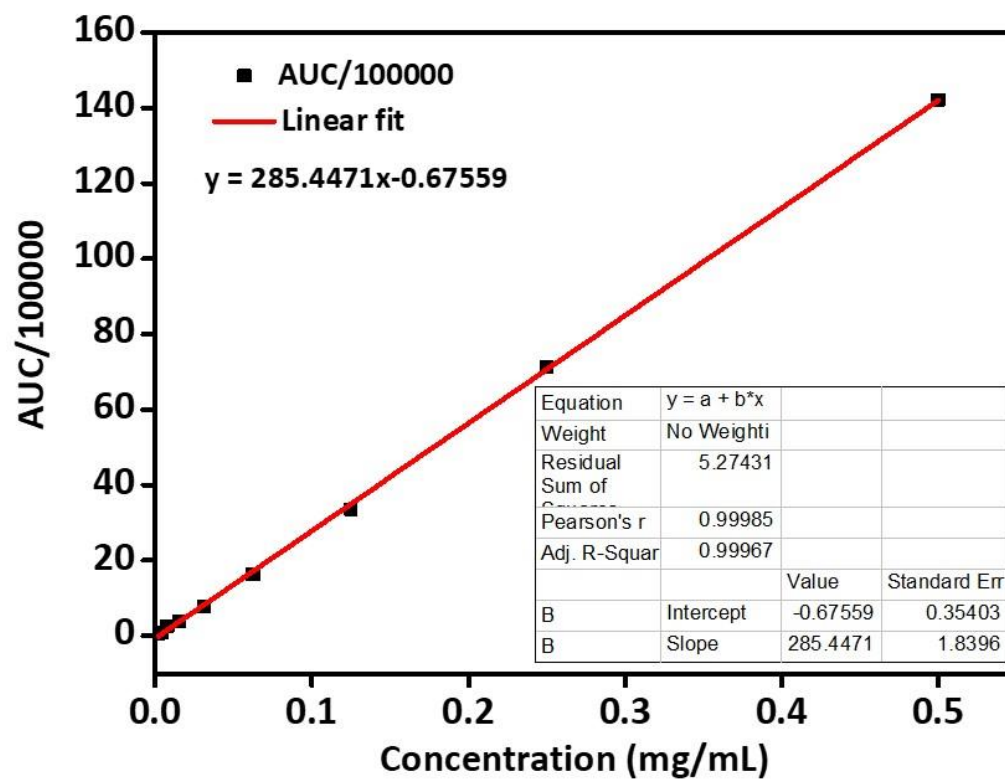


Figure A13. Standard curve of glimepiride.

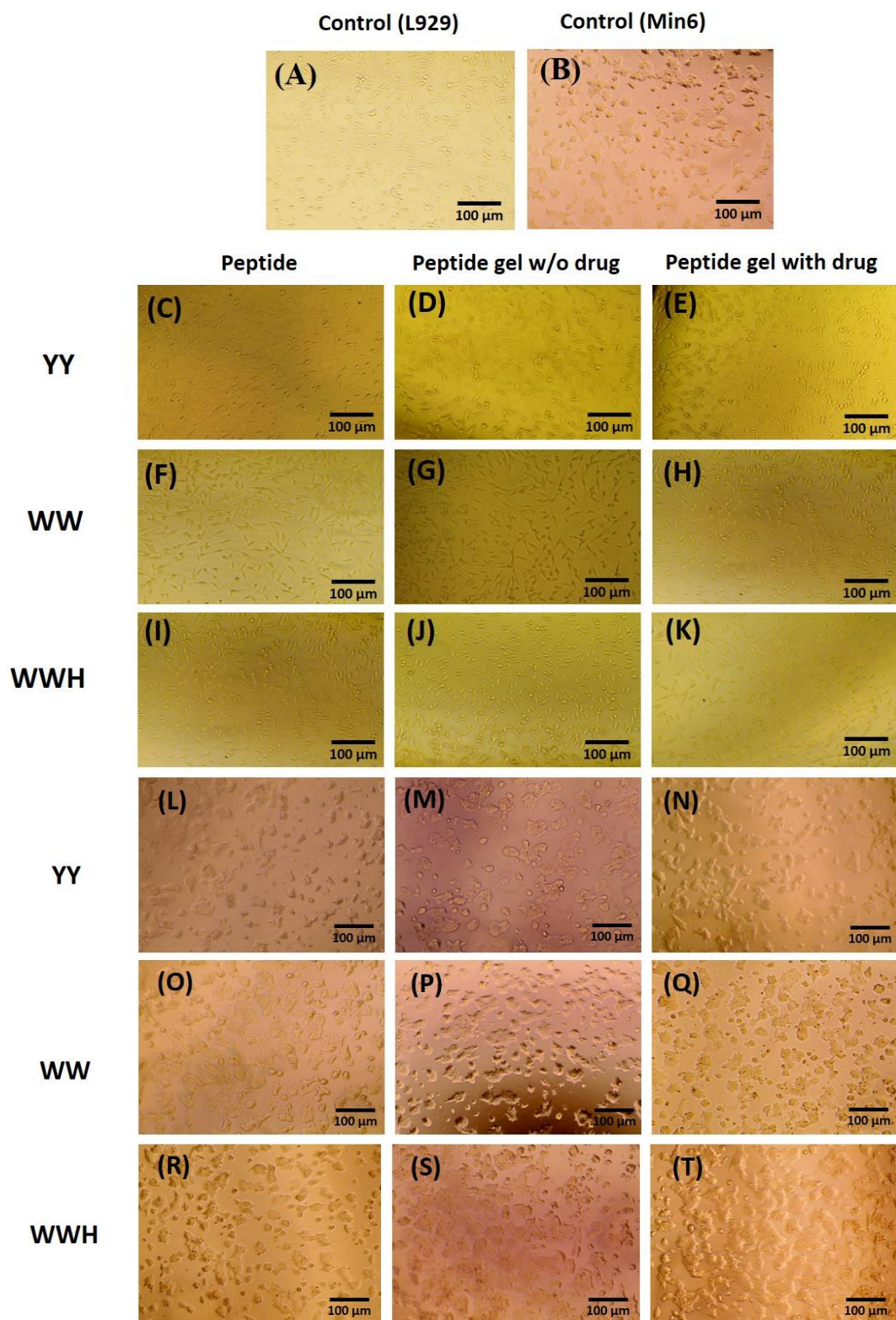


Figure A14. Images of cells after treatment with peptides, peptide gels, and glimepiride-loaded peptide gels for 24 h. (A, B) Control of L929 and Min6 cells. (C-K) L929 cells. (L-T) Min6 cells. Cells without peptides/gels were taken as a control.

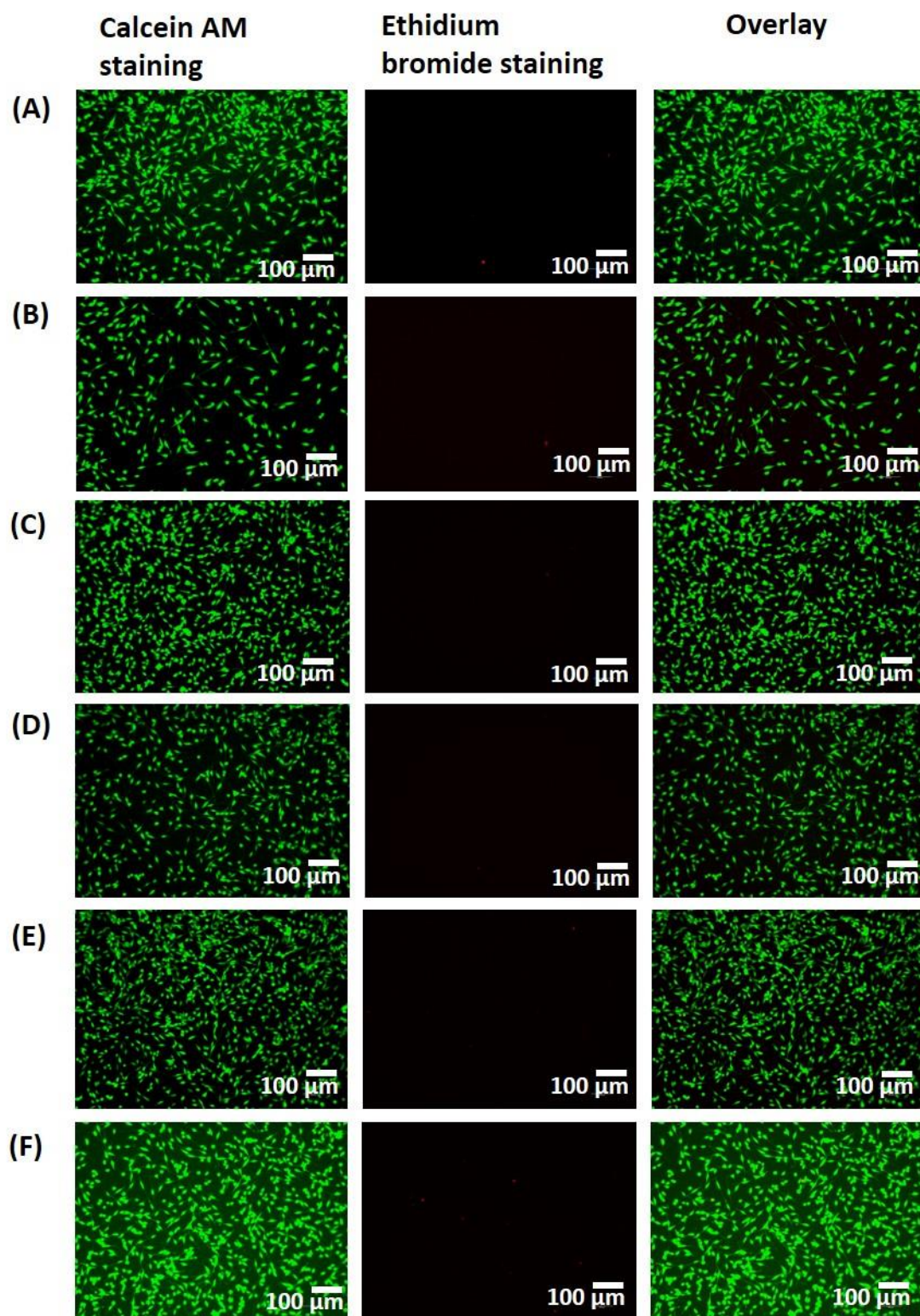


Figure A15. Fluorescence images of L929 cells stained with live and dead cell staining dyes, calcein AM and ethidium bromide, and acquired after 24 h of treatment with the releasate of peptides/gels. (A) YY peptide. (B) YY peptide gel. (C) WW peptide. (D) WW peptide gel. (E) WWH peptide. (F) WWH peptide gel. Scale bar: 100 μm .

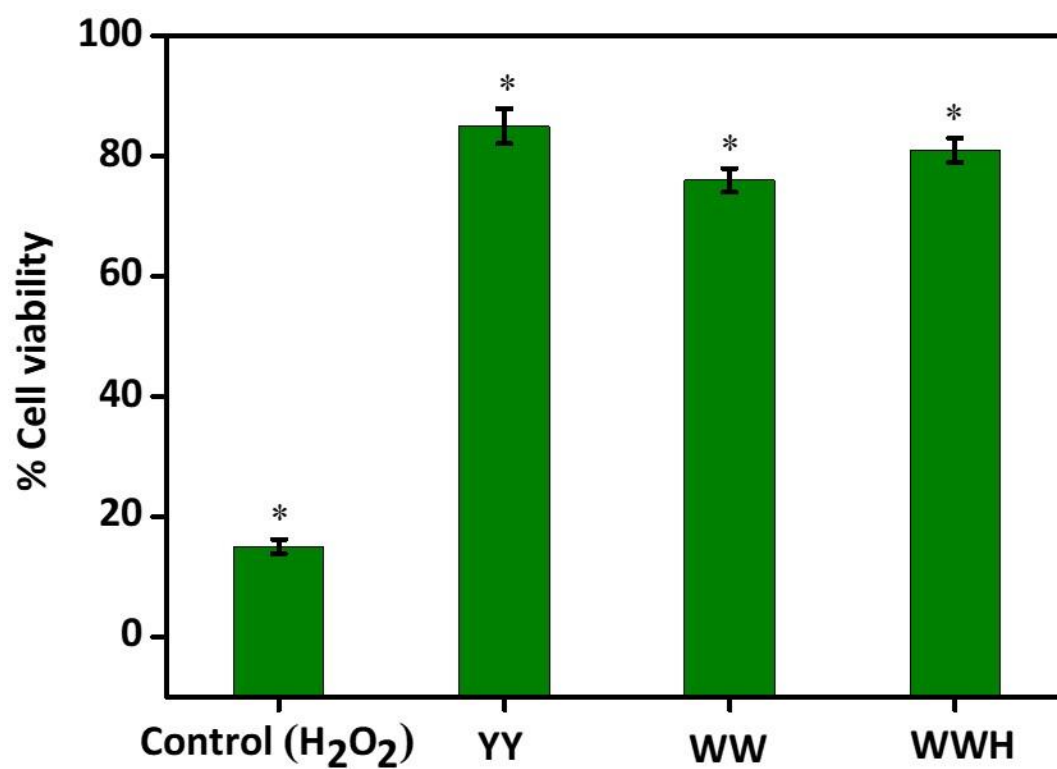


Figure A16. Effect of glimepiride-loaded peptide gels on the viability of H₂O₂-treated HepG2 cells. Data reported are mean ± SE (n = 3). Comparisons between two groups (samples to control) were carried out using Student's t-test. *p < 0.05 indicates statistically significant data.

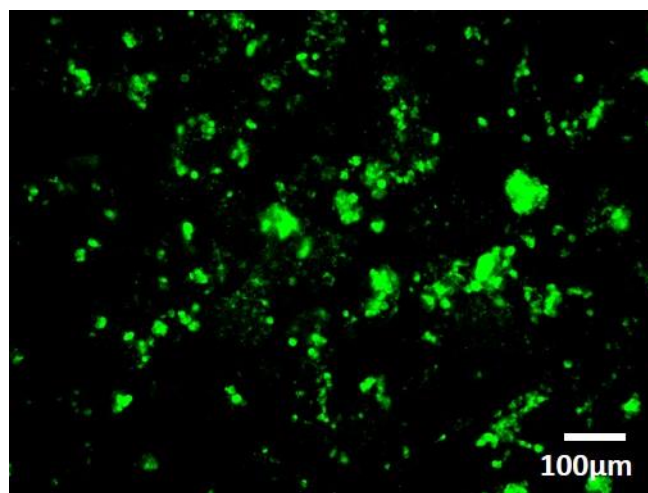


Figure A17. Fluorescence microscopy image of HepG2 cells incubated with 2-NBDG for 5 days in the presence of glimepiride solution (0.1 mg/mL).

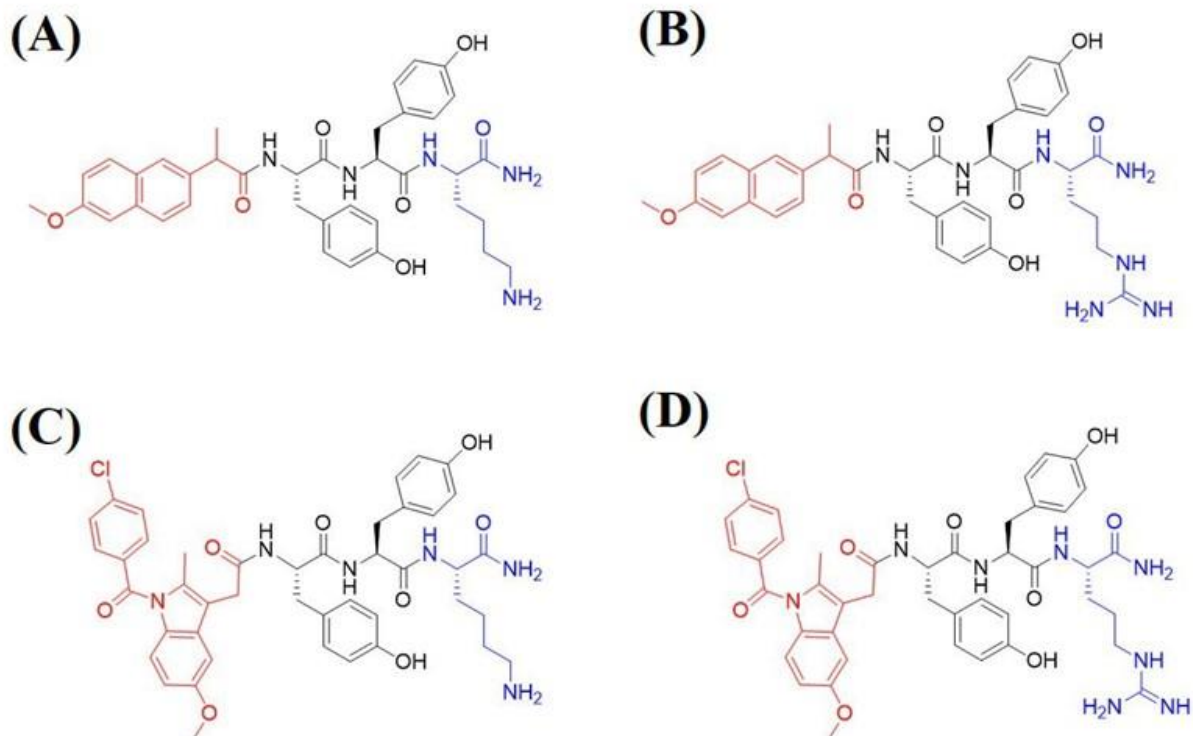


Figure A18. Structures of NSAID-peptide conjugates. (A) Npx-^LTyr-^LTyr-^LLys-NH₂ (Npx-YYK). (B) Npx-^LTyr-^LTyr-^LArg-NH₂ (Npx-YYR). (C) Ind-^LTyr-^LTyr-^LLys-NH₂ (Ind-YYK). (D) Ind-^LTyr-^LTyr-^LArg-NH₂ (Ind-YYR).

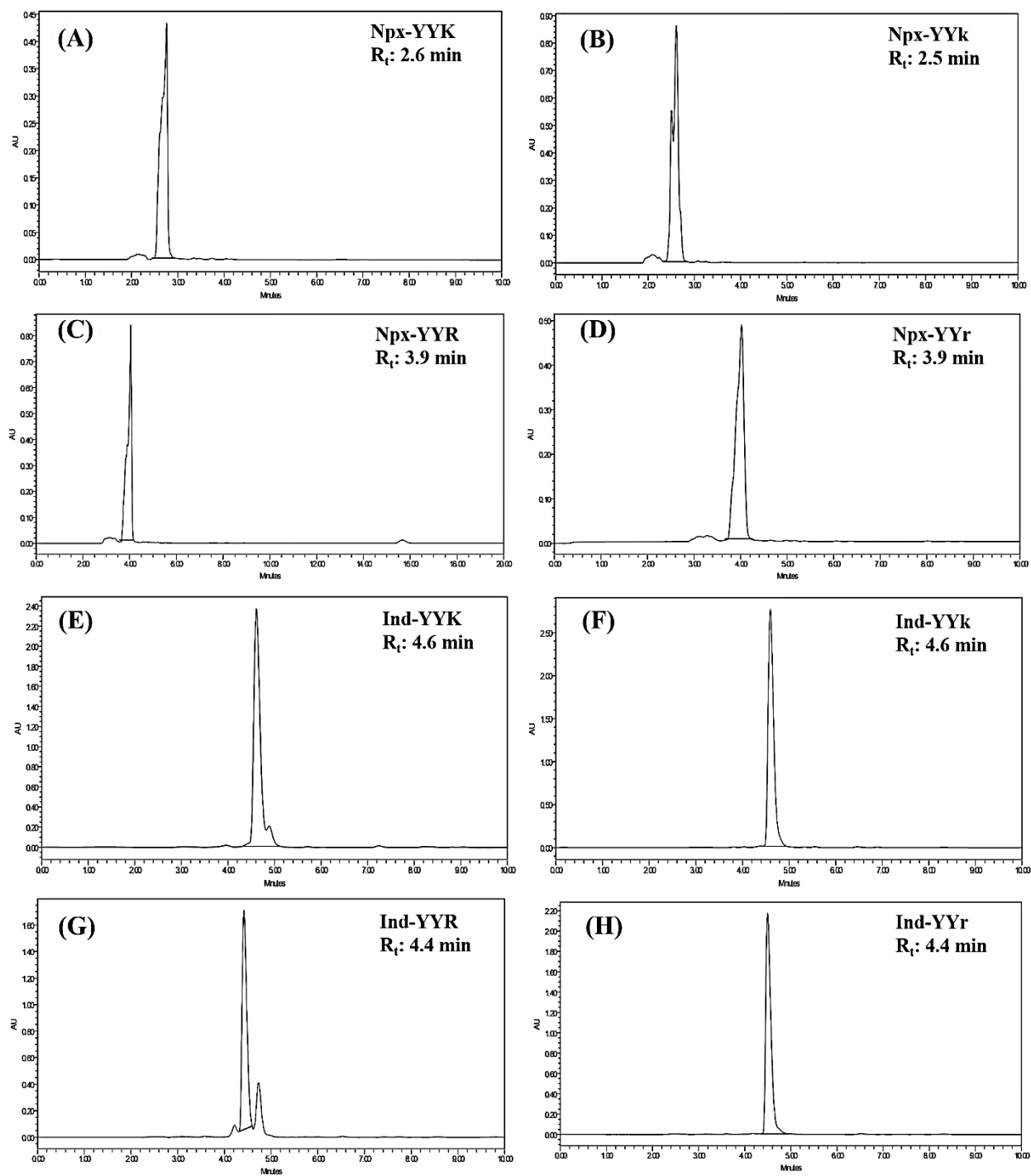


Figure A19. RP-HPLC of peptides. (A) Npx-YYK. (B) Npx-YYk. (C) Npx-YYR. (D) Npx-YYr. (E) Ind-YYK. (F) Ind-YYk. (G) Ind-YYR. (H) Ind-YYr.

Sample Name : YS-MN-YYK
Test Name : D MASS-1
270121-YS-MN-YYK 10 (0.180)

IITRPR

XEVO G2-XS QTOF

1: TOF MS ES+
1.22e7

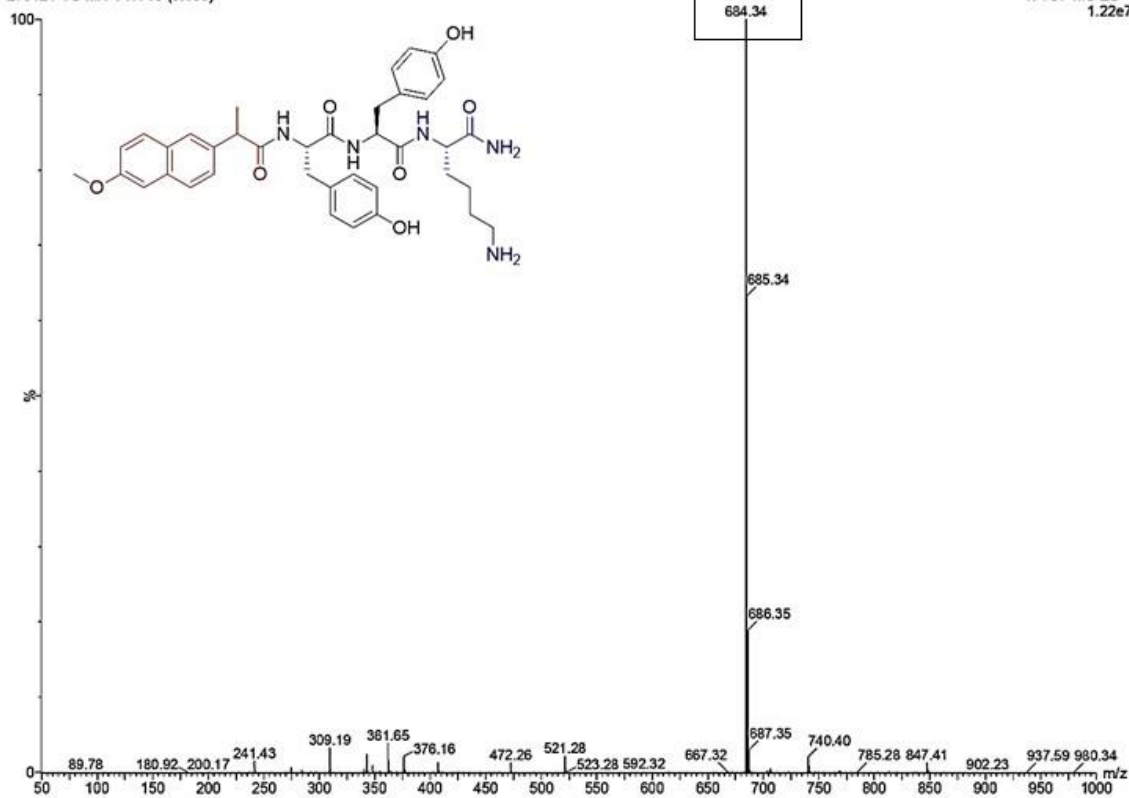


Figure A20. Mass spectrum of Npx-YYK peptide.

Sample Name : 240821_YS-MH-NKD
Test Name :
240821_YS-MH-NKD 9 (0.169)

IITRPR

XEVO G2-XS QTOF

1: TOF MS ES+
1.09e8

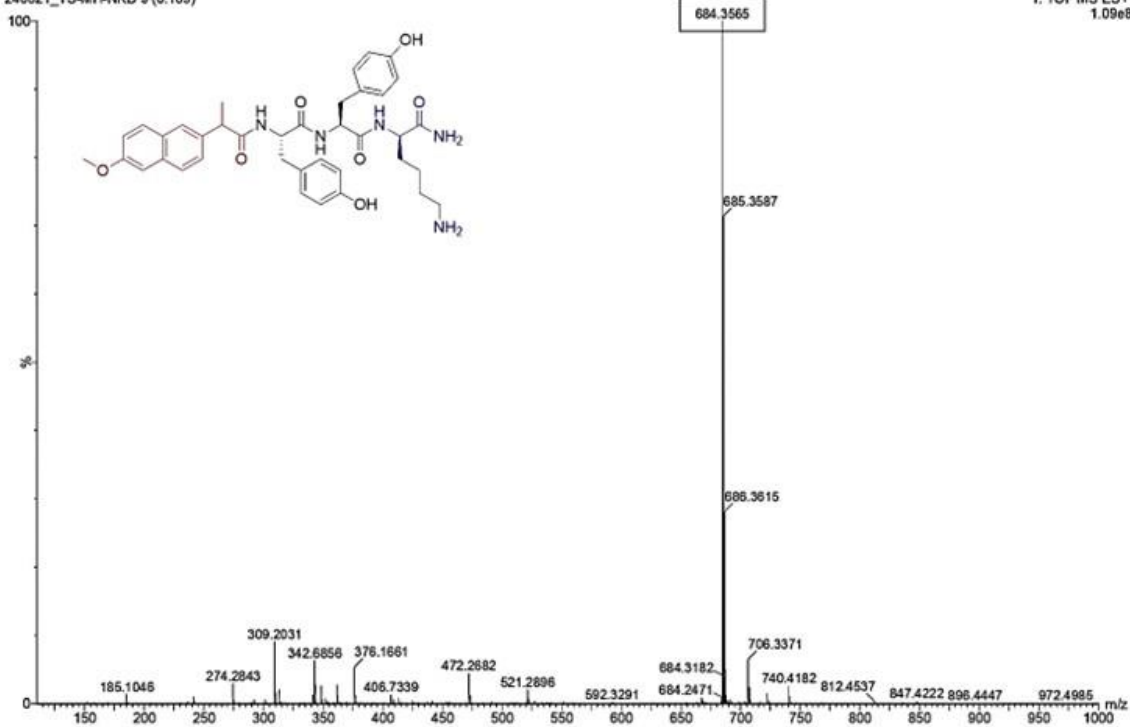


Figure A21. Mass spectrum of Npx-YYk peptide.

Sample Name : YS-MN-YYR
Test Name : D MASS-1
270121-YS-MN-YYR 11 (0.197)

IITRPR

XEVO G2-XS QTOF

1: TOF MS ES+
1.51e7

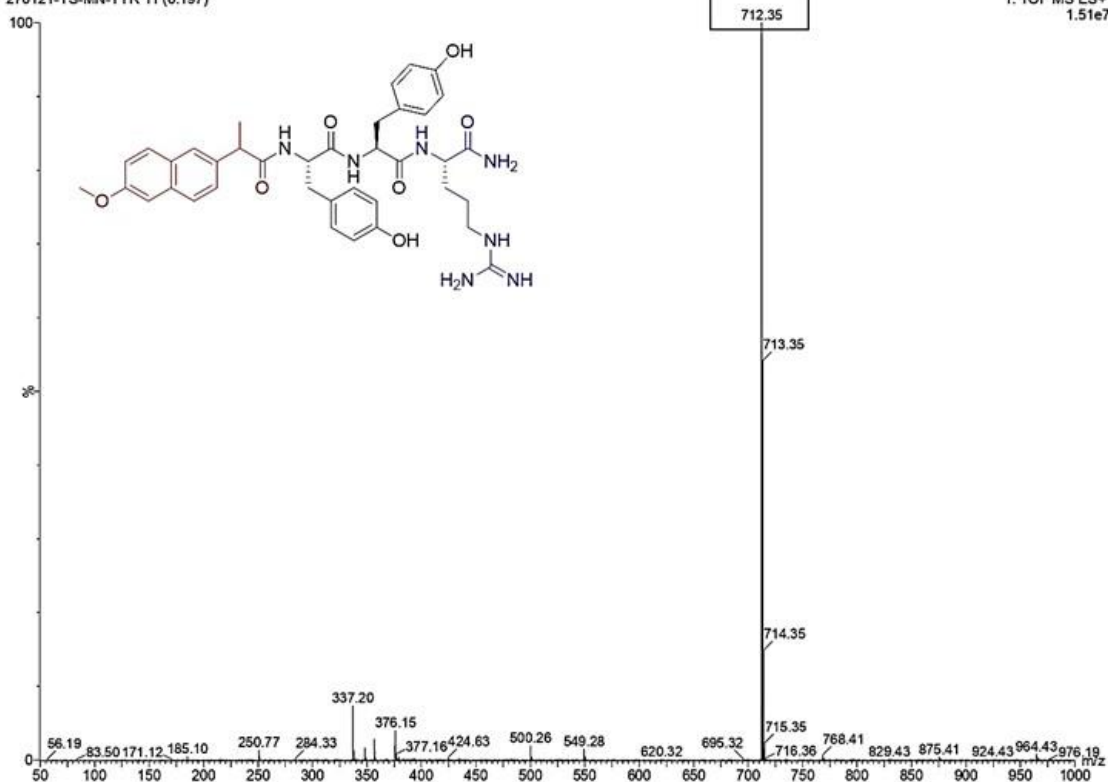


Figure A22. Mass spectrum of Npx-YYR peptide.

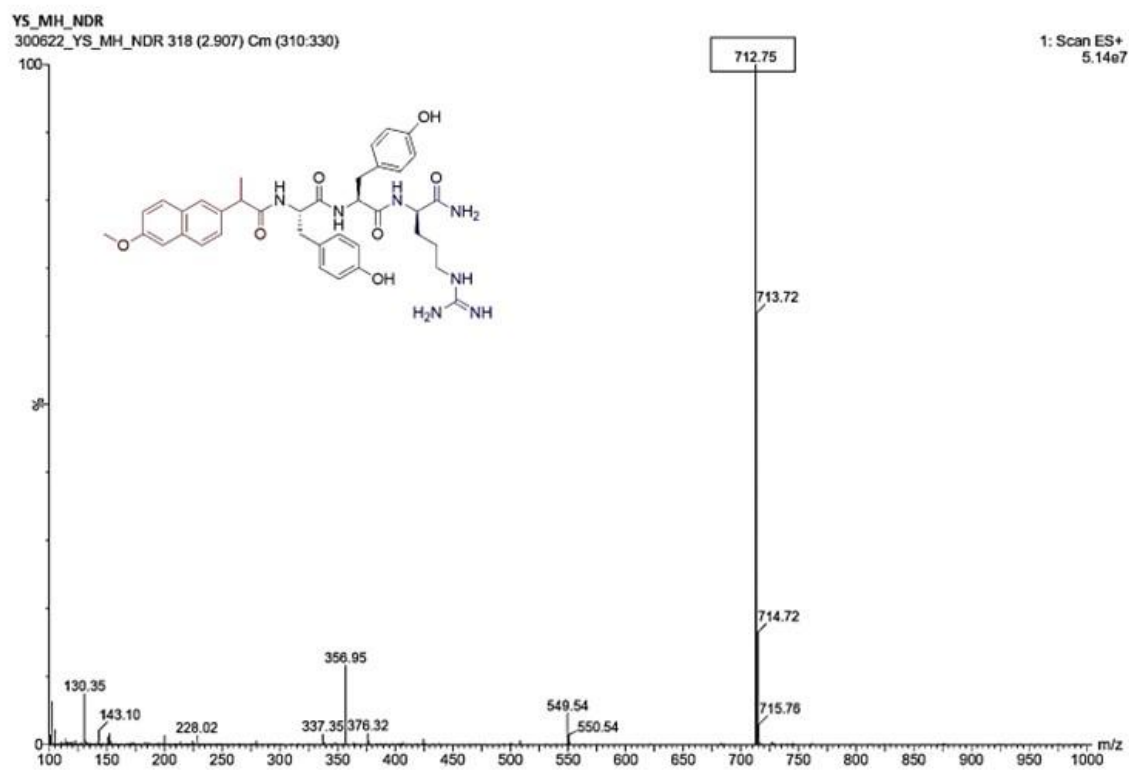


Figure A23. Mass spectrum of Npx-YYr peptide.

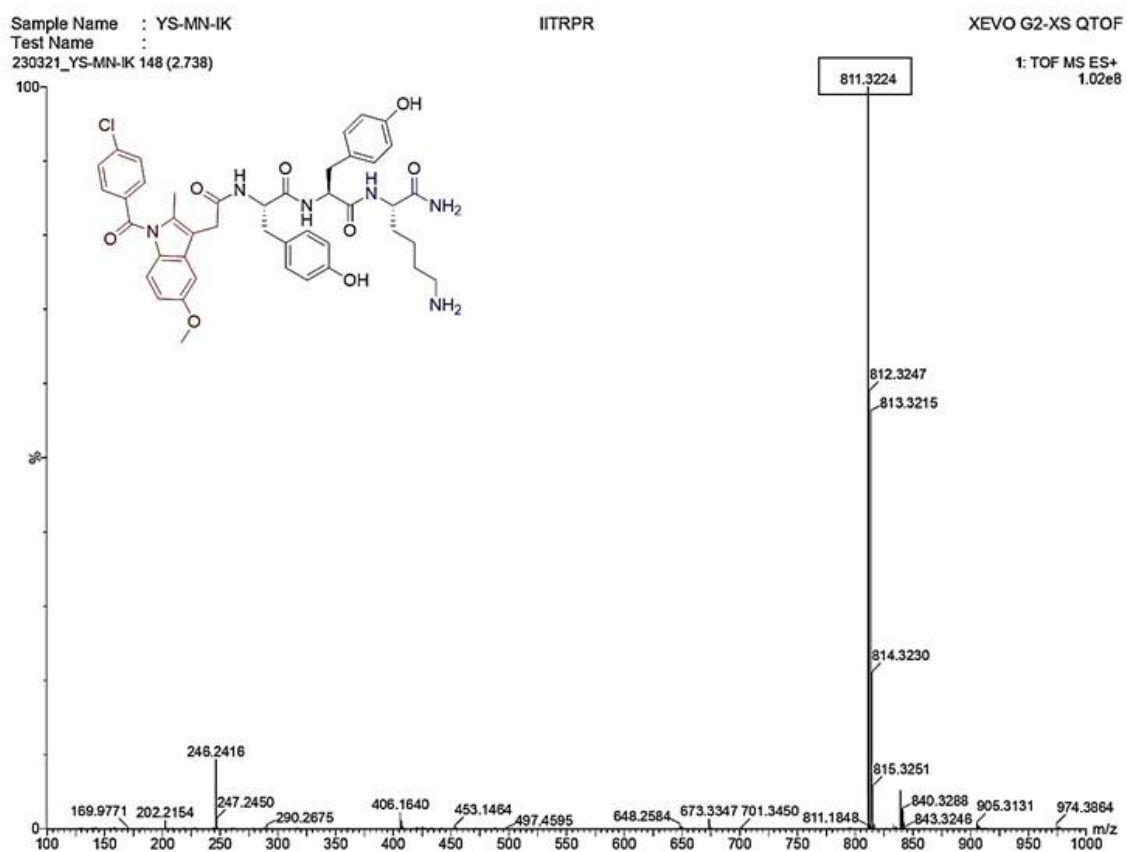


Figure A24. Mass spectrum of Ind-YYK peptide.

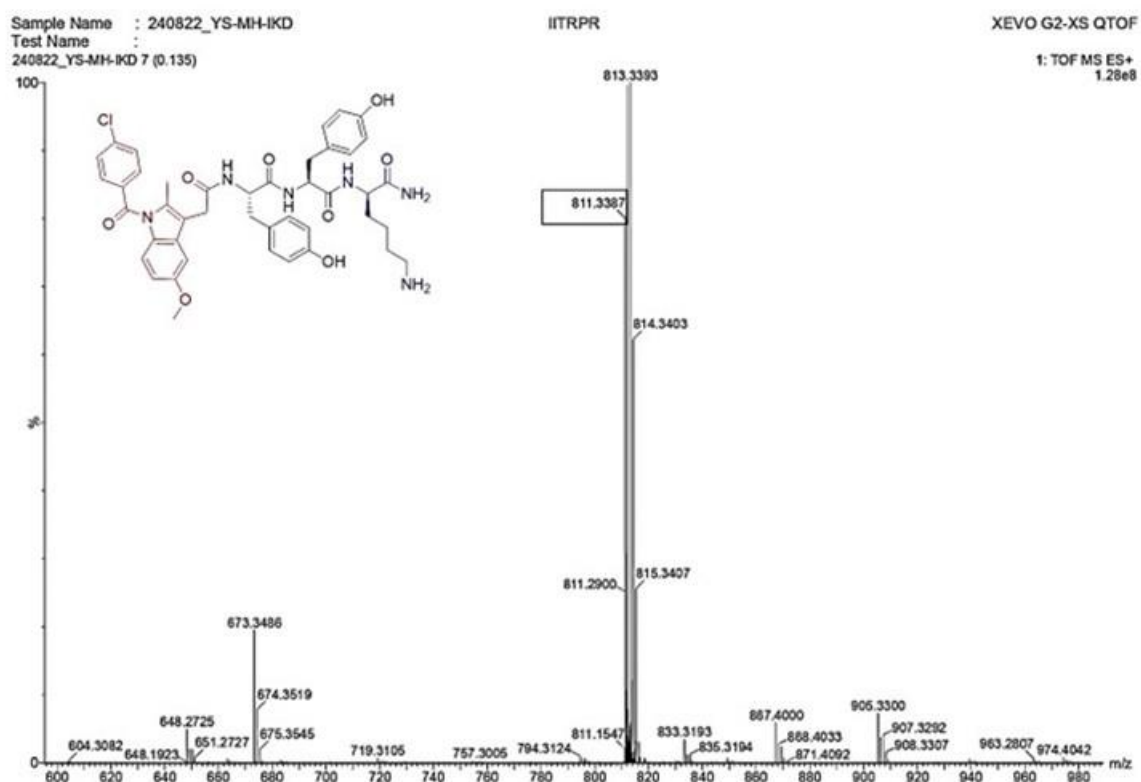


Figure A25. Mass spectrum of Ind-YYk peptide.

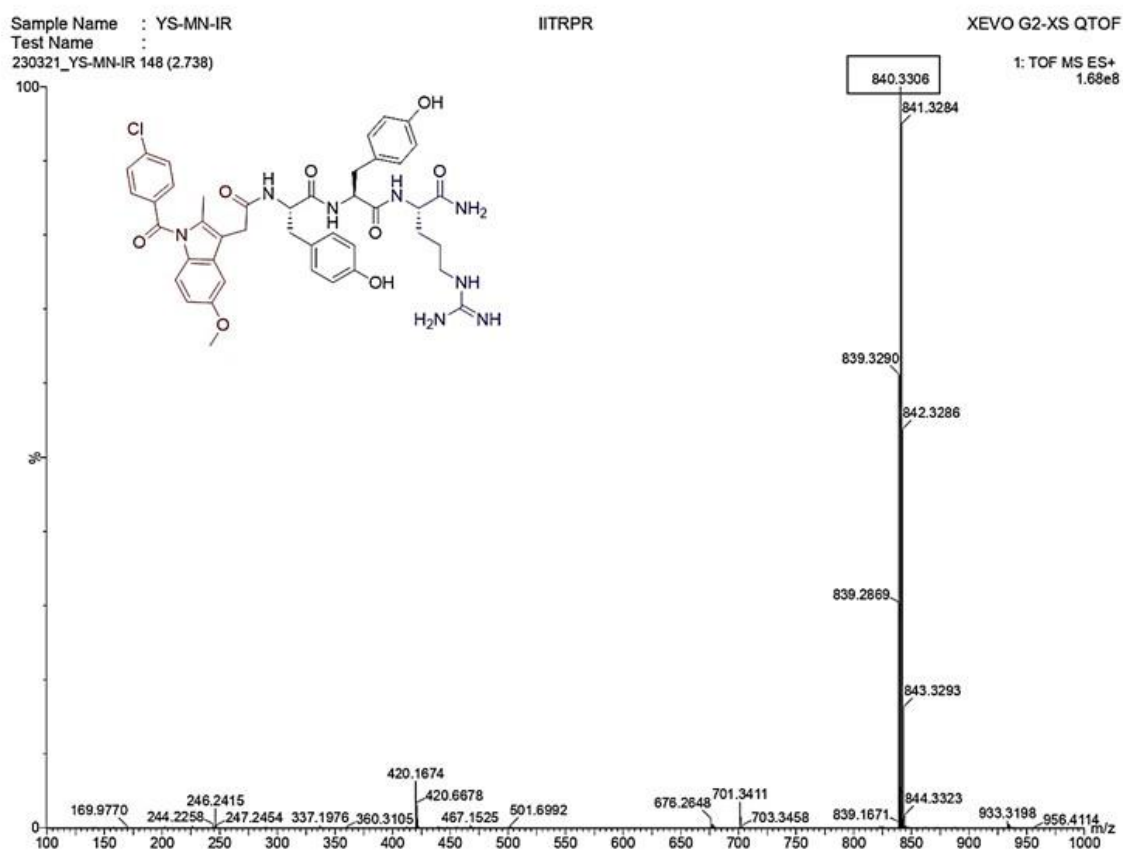


Figure A26. Mass spectrum of Ind-YYR peptide.

Sample Name : 300821_YS-MH-IDR
 Test Name :
 300821_YS-MH-IDR-POS 7 (0.135)

IITRPR

XEVO G2-XS QTOF

1: TOF MS ES+
 2.29e8

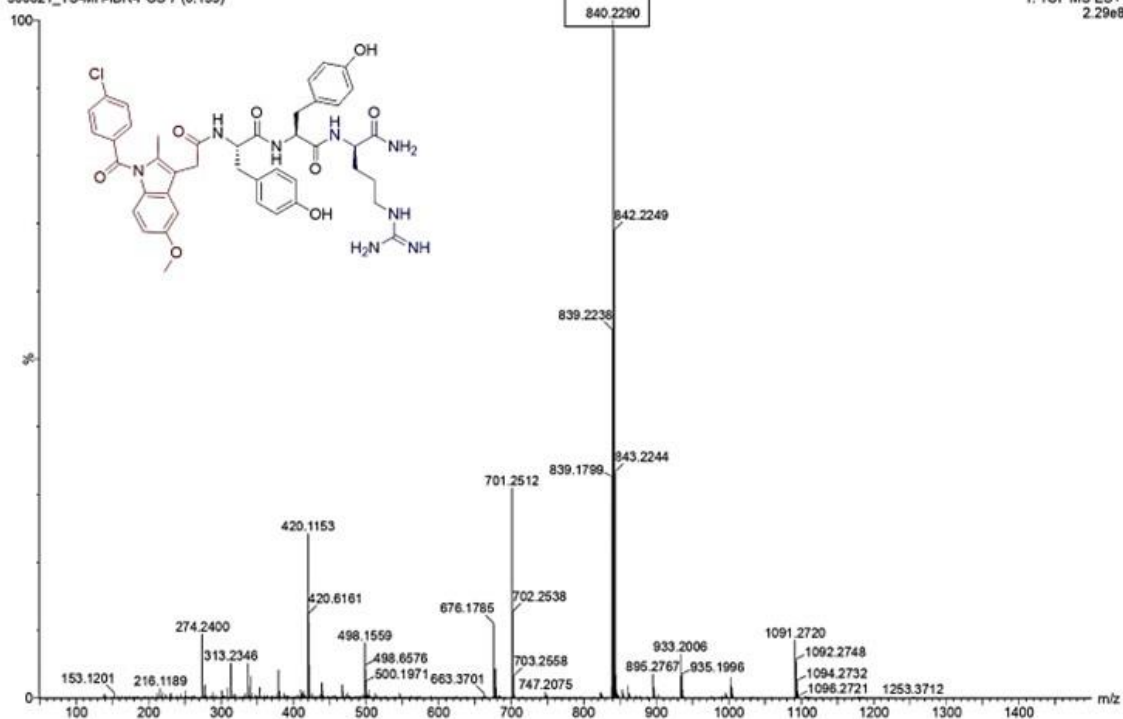


Figure A27. Mass spectrum of Ind-YYr peptide.

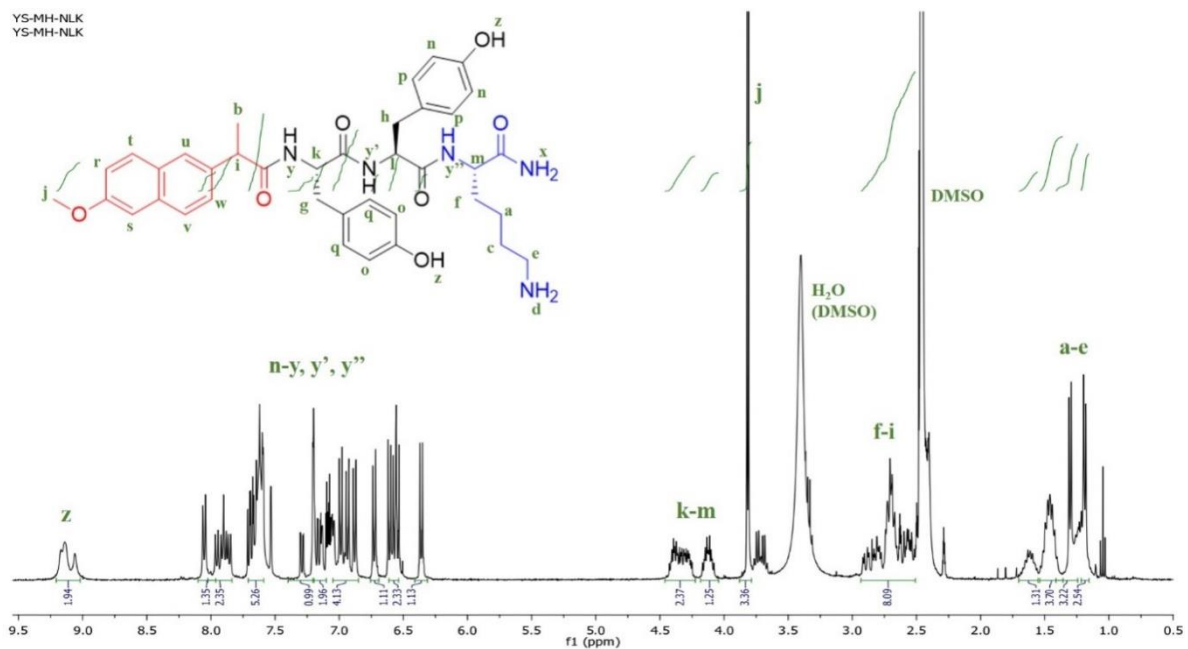


Figure A28. ^1H NMR spectrum of Npx-YYK peptide.

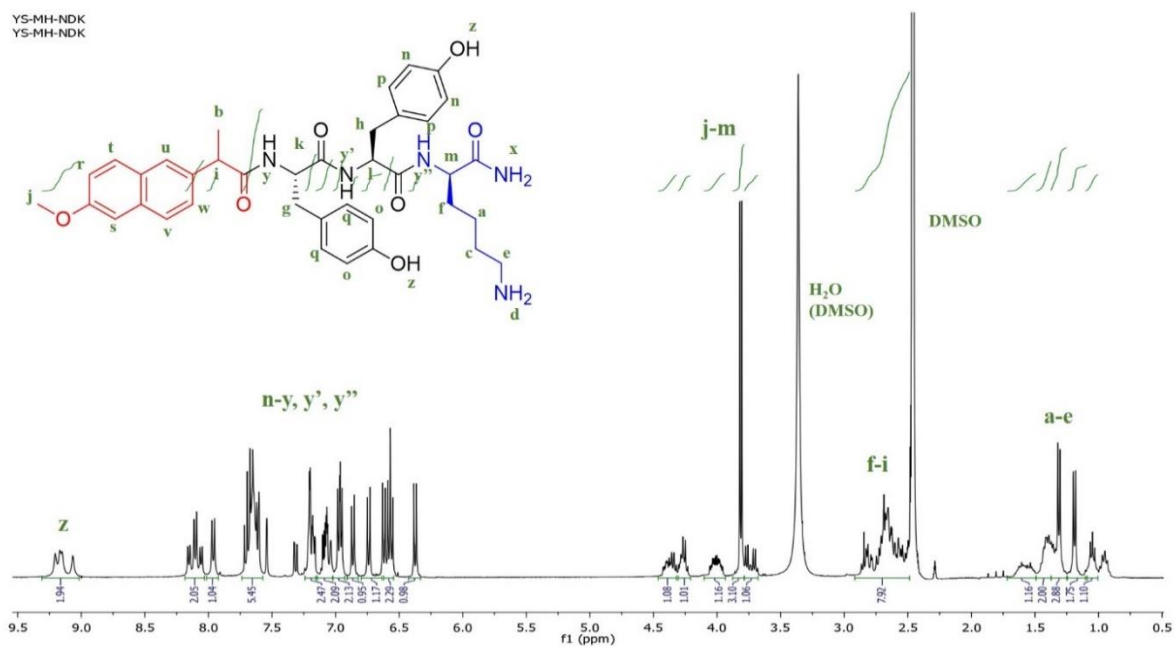


Figure A29. ^1H NMR spectrum of Npx-YYk peptide.

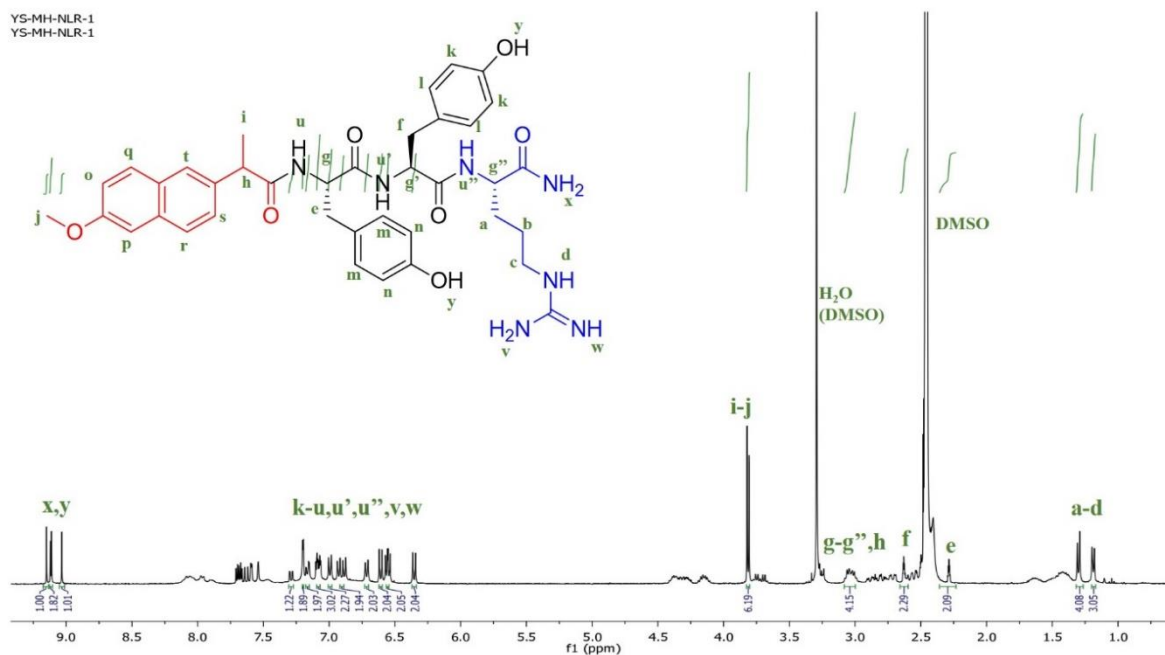


Figure A30. ^1H NMR spectrum of Npx-YYR peptide.

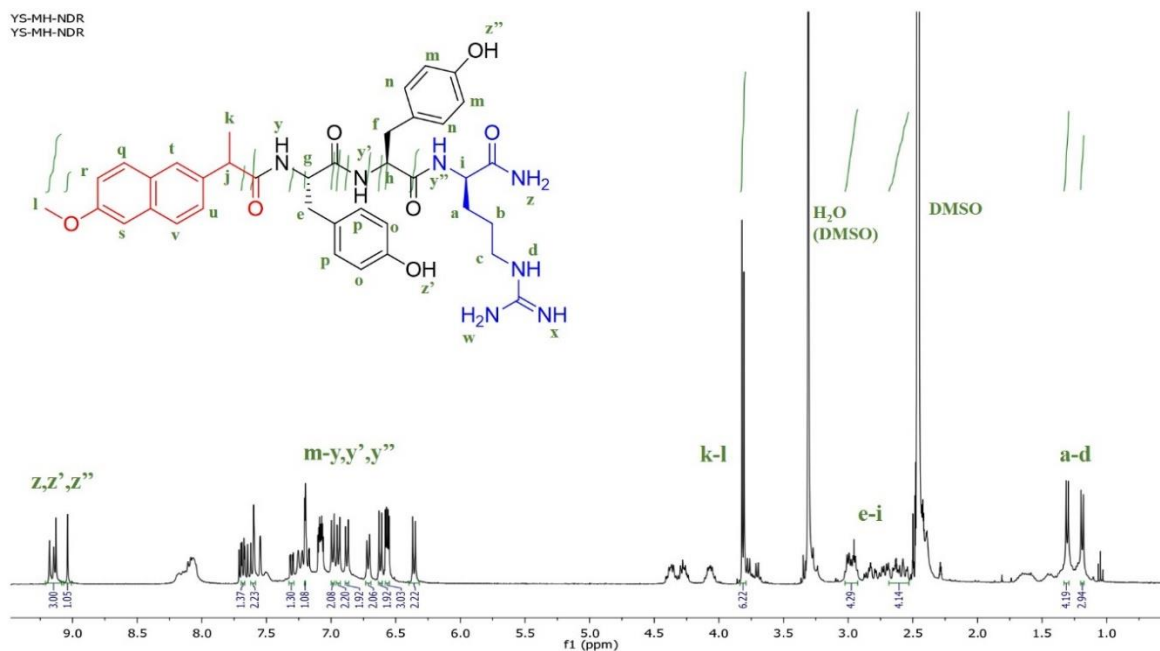


Figure A31. 1H NMR spectrum of Npx-YYr peptide.

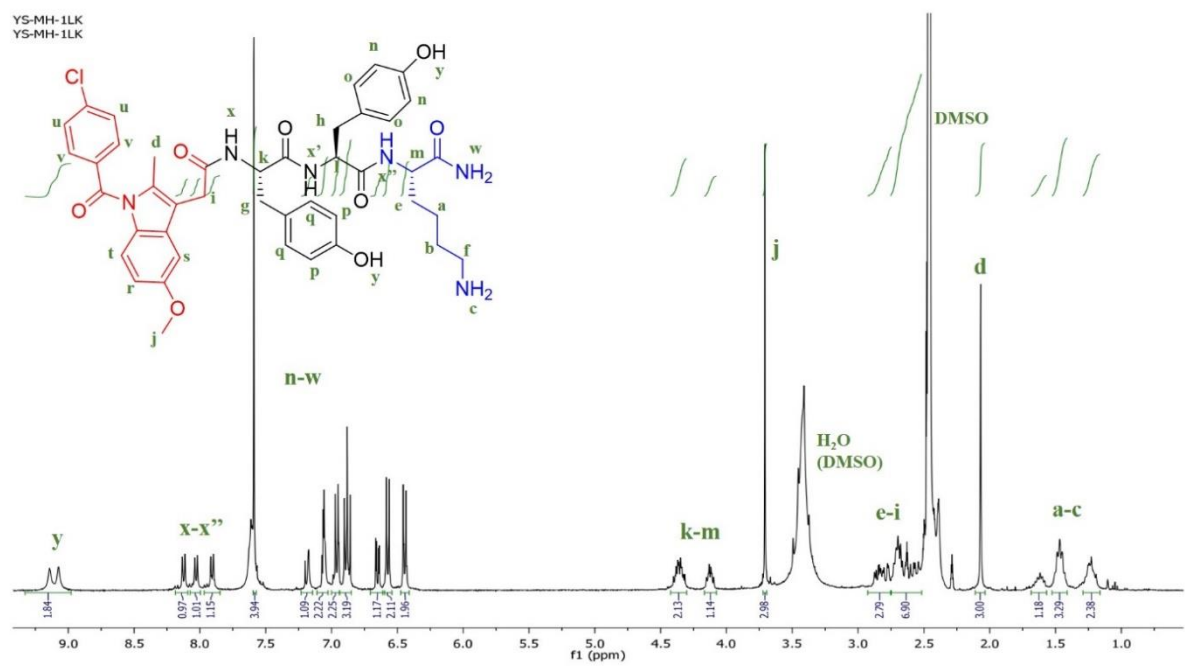


Figure A32. ¹H NMR spectrum of Ind-YYK peptide.

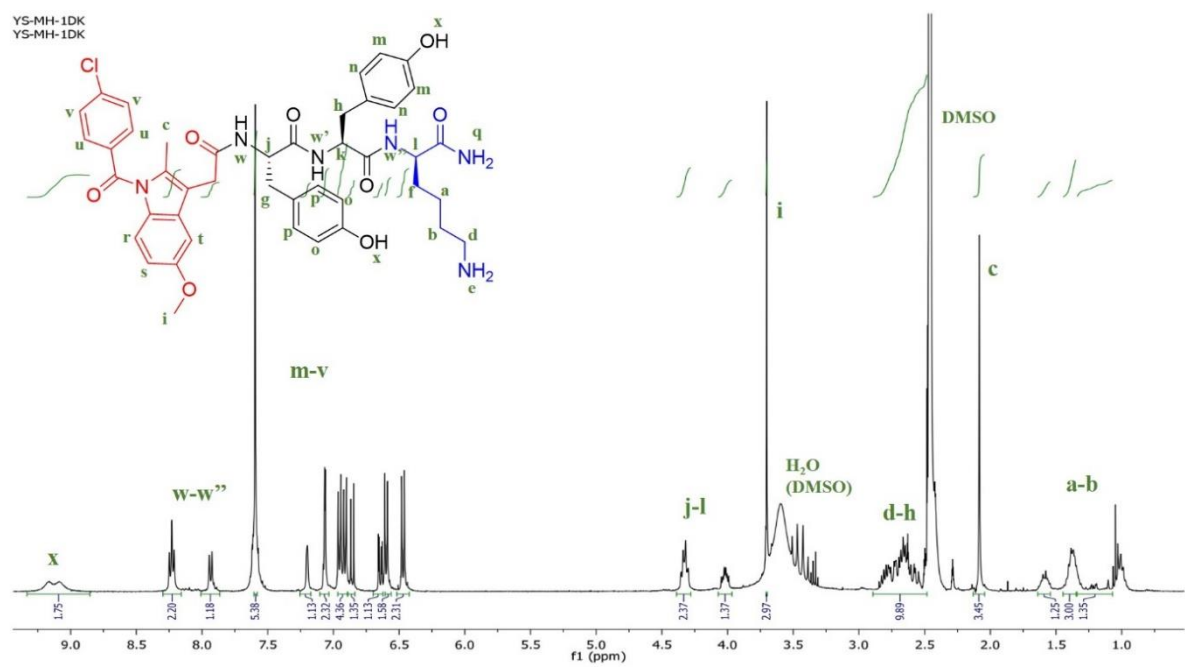


Figure A33. ^1H NMR spectrum of Ind-YYk peptide.

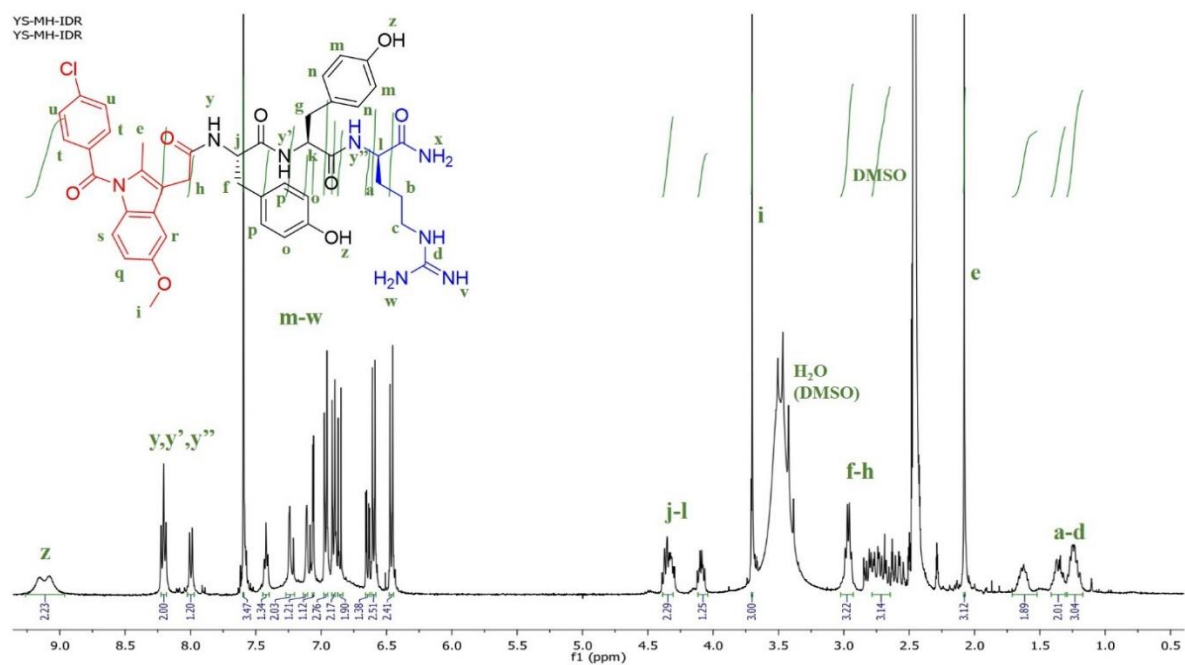


Figure A35. ^1H NMR spectrum of Ind-YYr peptide.

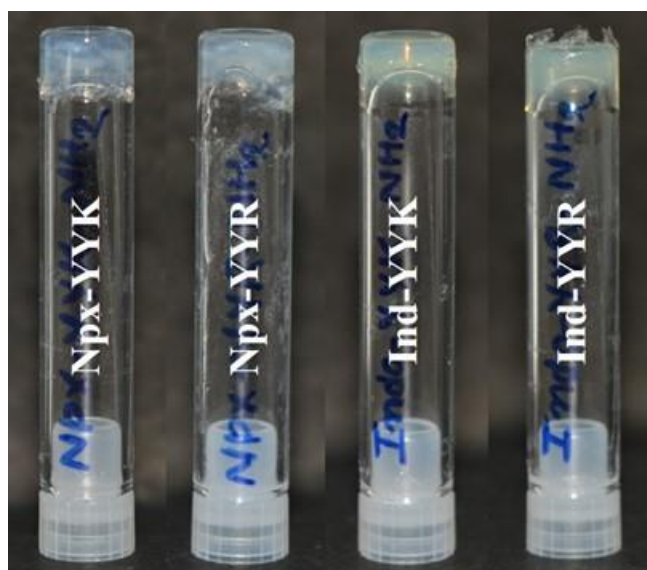


Figure A36. Images of supramolecular peptide-conjugate gels, Npx-YYK, Npx-YYR, Ind-YYK, and Ind-YYR.

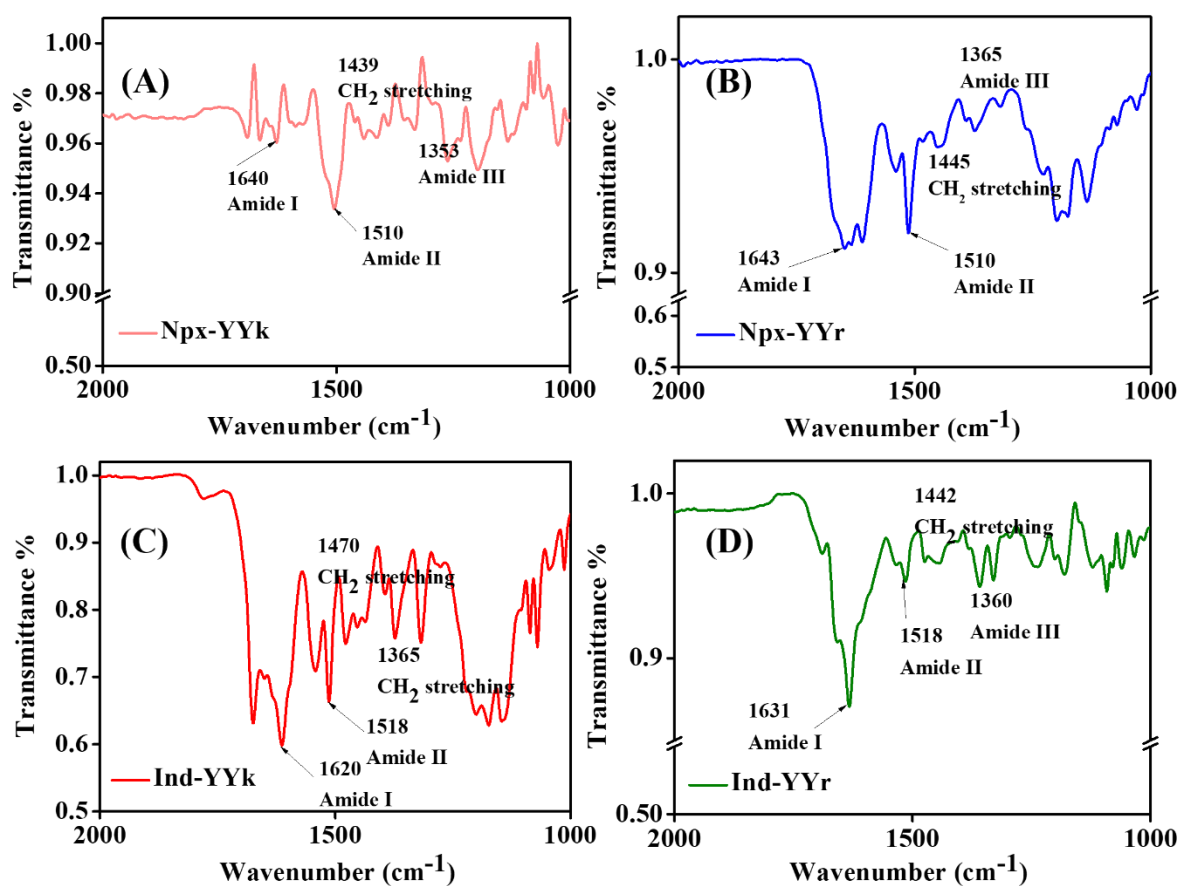


Figure A37. FTIR spectra of peptides. (A) Npx-YYk. (B) Npx-YYr. (C) Ind-YYk. (D) Ind-YYr.

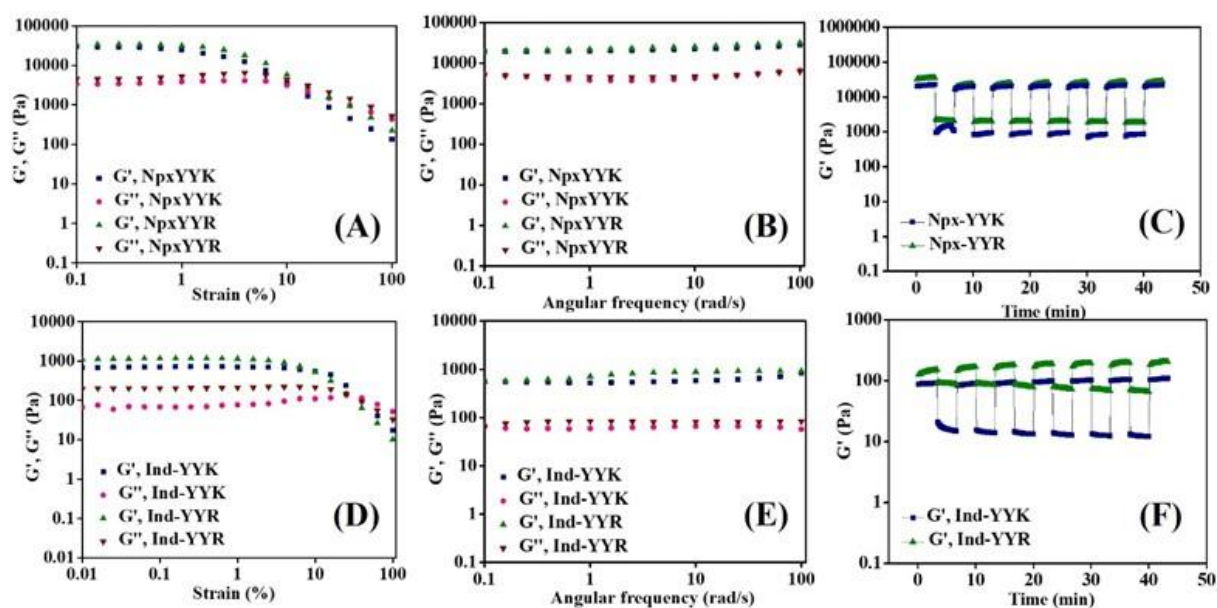


Figure A38. Rheological analysis of peptide-conjugate gels, Npx-YYK, Npx-YYR, Ind-YYK, and Ind-YYR (2% w/v). (A, D) Amplitude sweep studies demonstrating the storage and loss modulus and corresponding crossover values at a constant angular frequency of 10 rad s^{-1} . (B, E) Frequency sweep at a constant strain of 1%. (C, F) The storage modulus at alternating strains of 30% and 1% for 6 consecutive cycles.

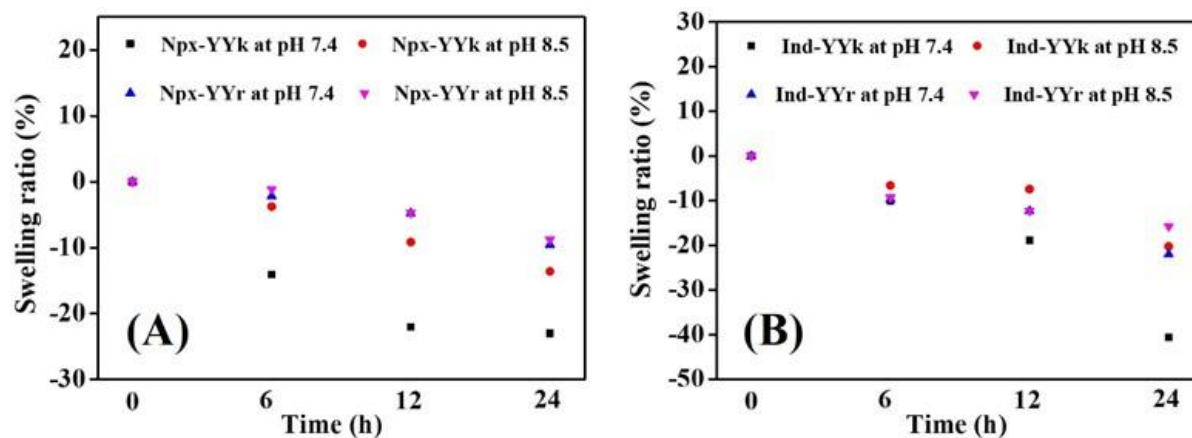


Figure A39. Swelling and degradation of peptide-conjugate gels at pH 7.4 and 8.5. (A) Npx-YYk and Npx-YYr. (B) Ind-YYk and Ind-YYr. Values above 0% indicate gravimetric water uptake (weight gain), whereas negative values suggest degradation (weight loss). Data reported are mean \pm SE ($n = 3$).

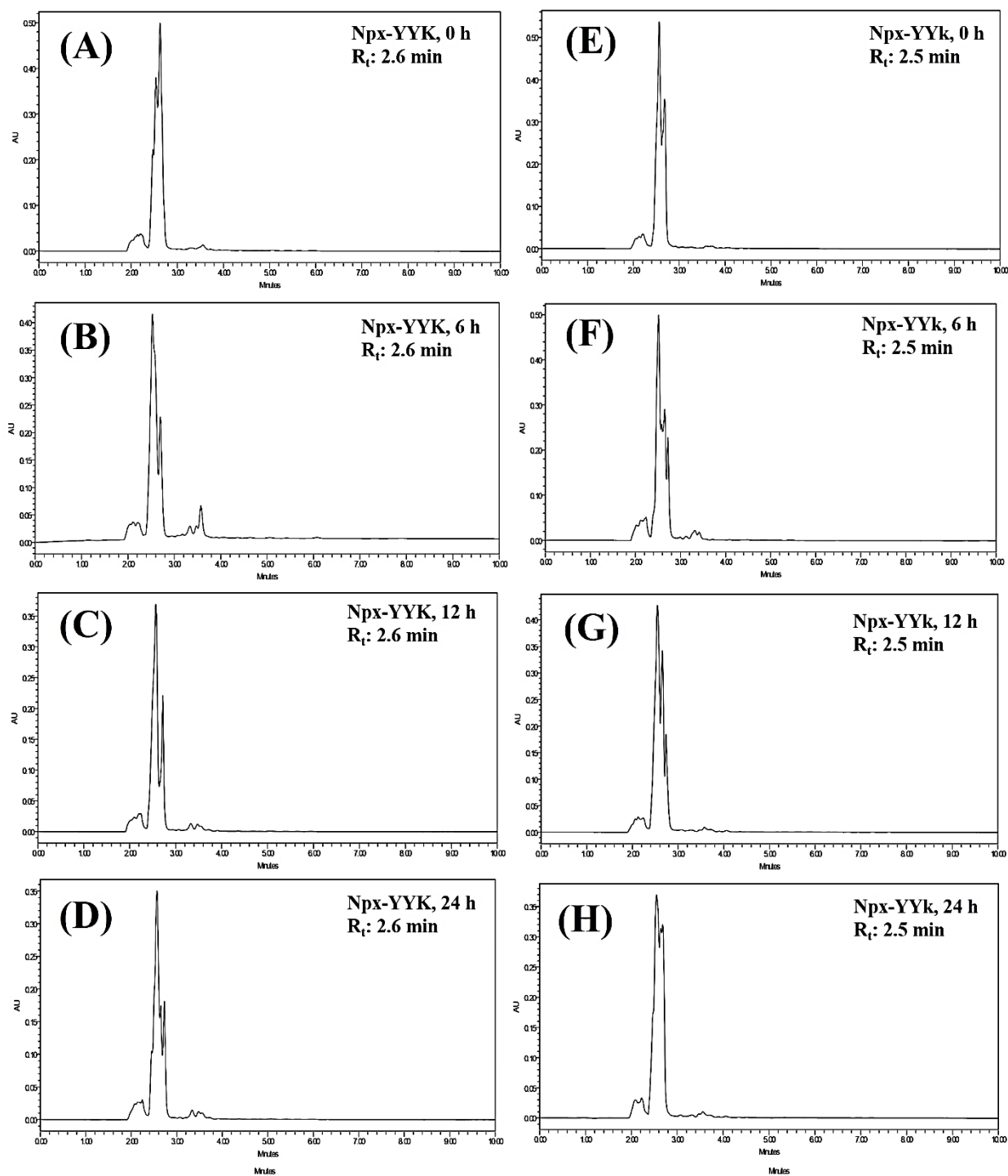


Figure A40. Proteolytic stability studies. Figure shows the RP-HPLC profiles of peptide-conjugate gels (2% w/v) incubated with a mocktail of proteolytic enzymes (proteinase K, chymotrypsin, and pepsin) at pH 7.4 for 0, 6, 12, and 24 h. (A-D) Npx-YYK. (E-H) Npx-YYk.

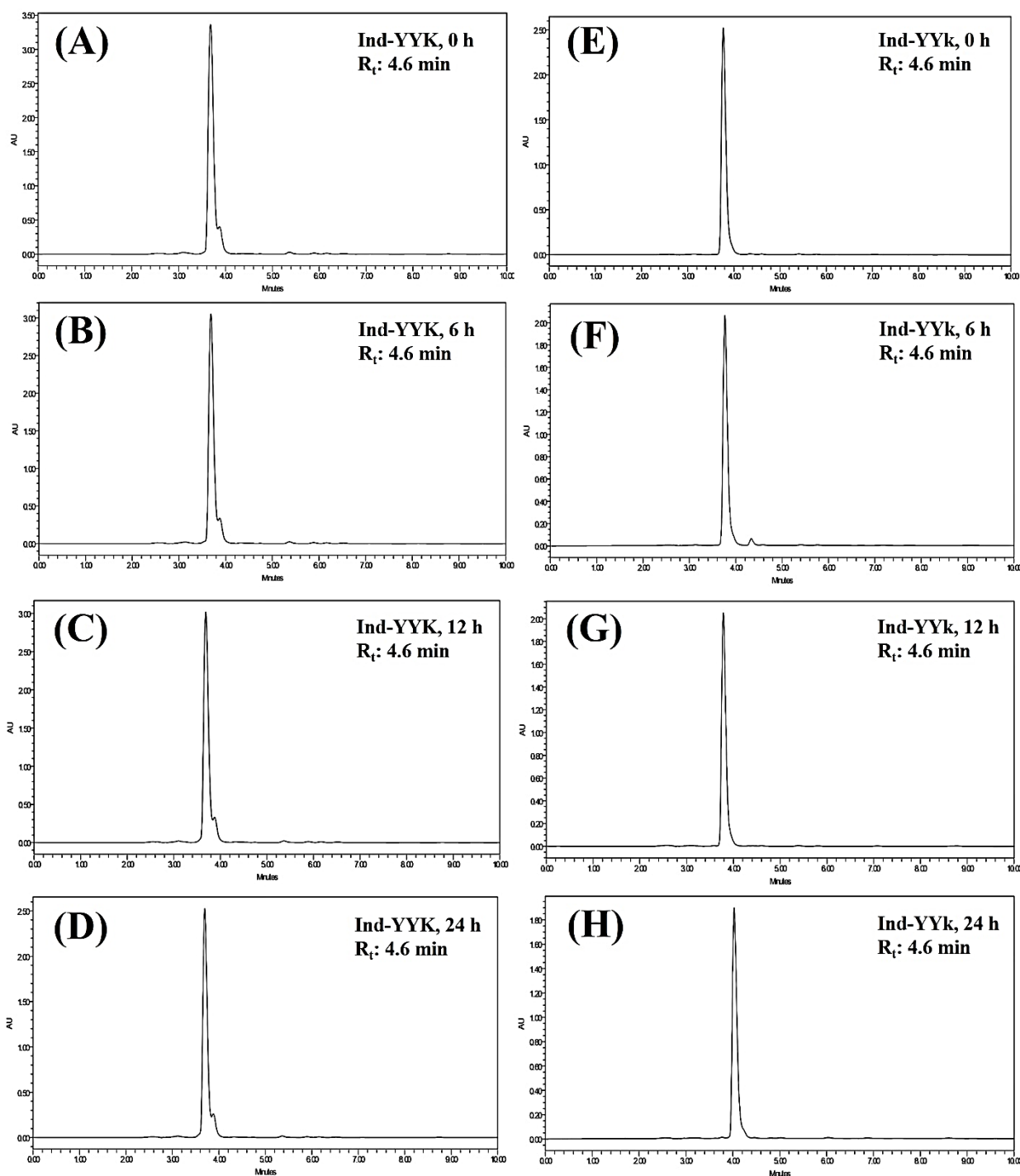


Figure A41. Proteolytic stability studies. The figure shows the RP-HPLC profiles of peptide-conjugate gels (2% w/v) incubated with a mocktail of proteolytic enzymes (proteinase K, chymotrypsin, and pepsin) at pH 7.4 for 0, 6, 12, and 24 h. (A-D) Npx-YYR. (E-H) Npx-YYr.

Figure A42. Proteolytic stability studies. The figure shows the RP-HPLC profiles of peptide-conjugate gels (2% w/v) incubated with a mocktail of proteolytic enzymes (proteinase K, chymotrypsin, and pepsin) at pH 7.4 for 0, 6, 12, and 24 h. (A-D) Ind-YYK. (E-H) Ind-YYk.

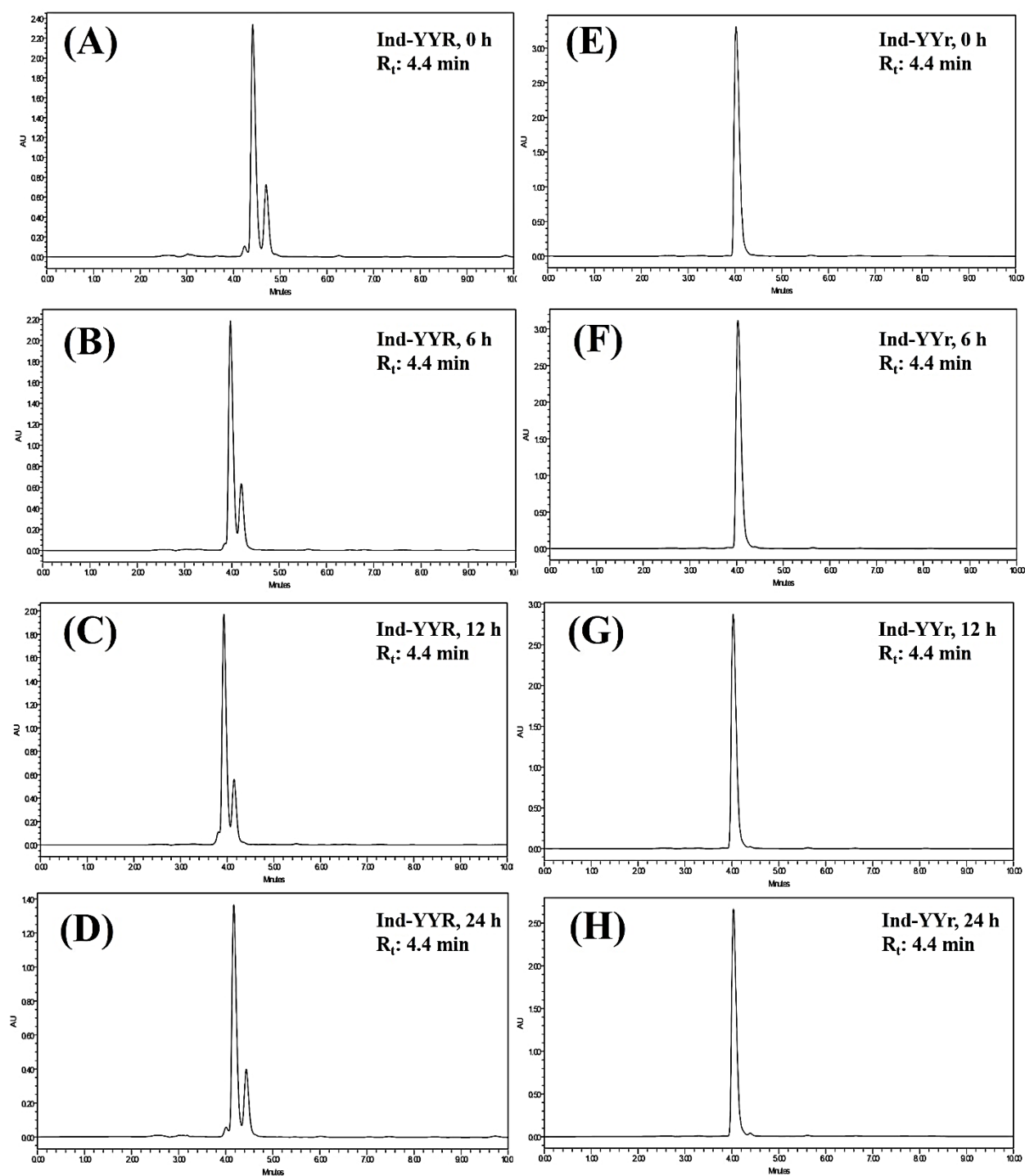


Figure A43. Proteolytic stability studies. The figure shows the RP-HPLC profiles of peptide-conjugate gels (2% w/v) incubated with a mocktail of proteolytic enzymes (proteinase K, chymotrypsin, and pepsin) at pH 7.4 for 0, 6, 12, and 24 h.(A-D) Ind-YYR. (E-H) Ind-YYr.

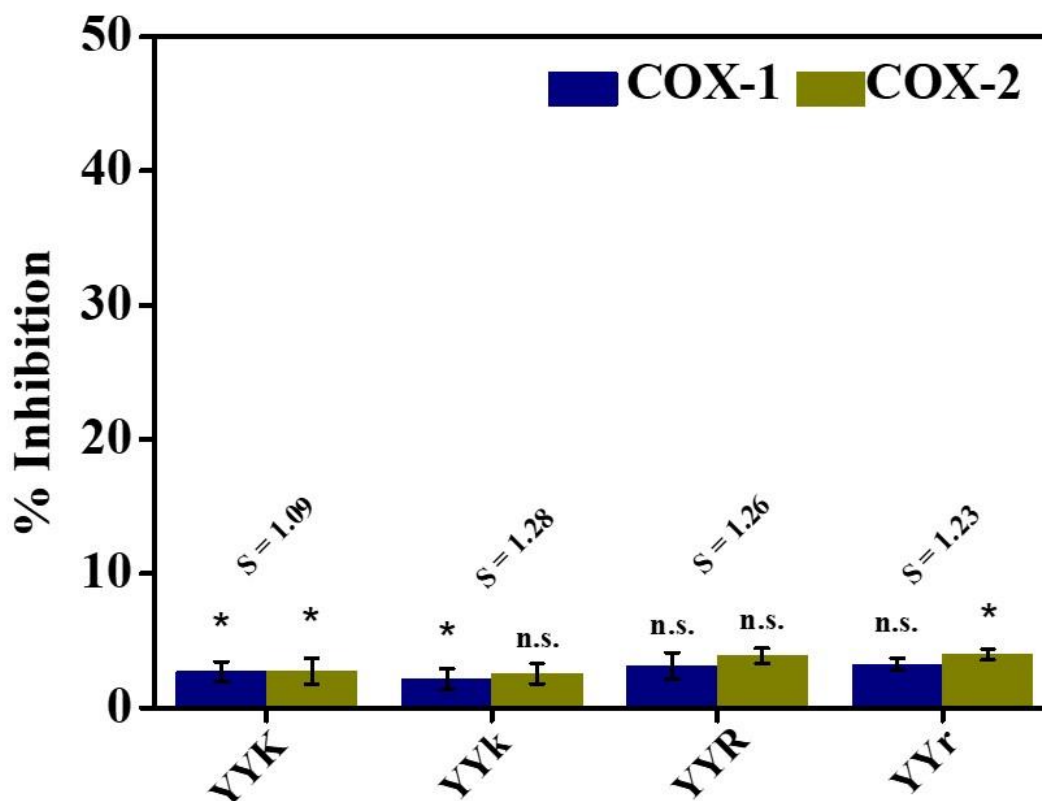
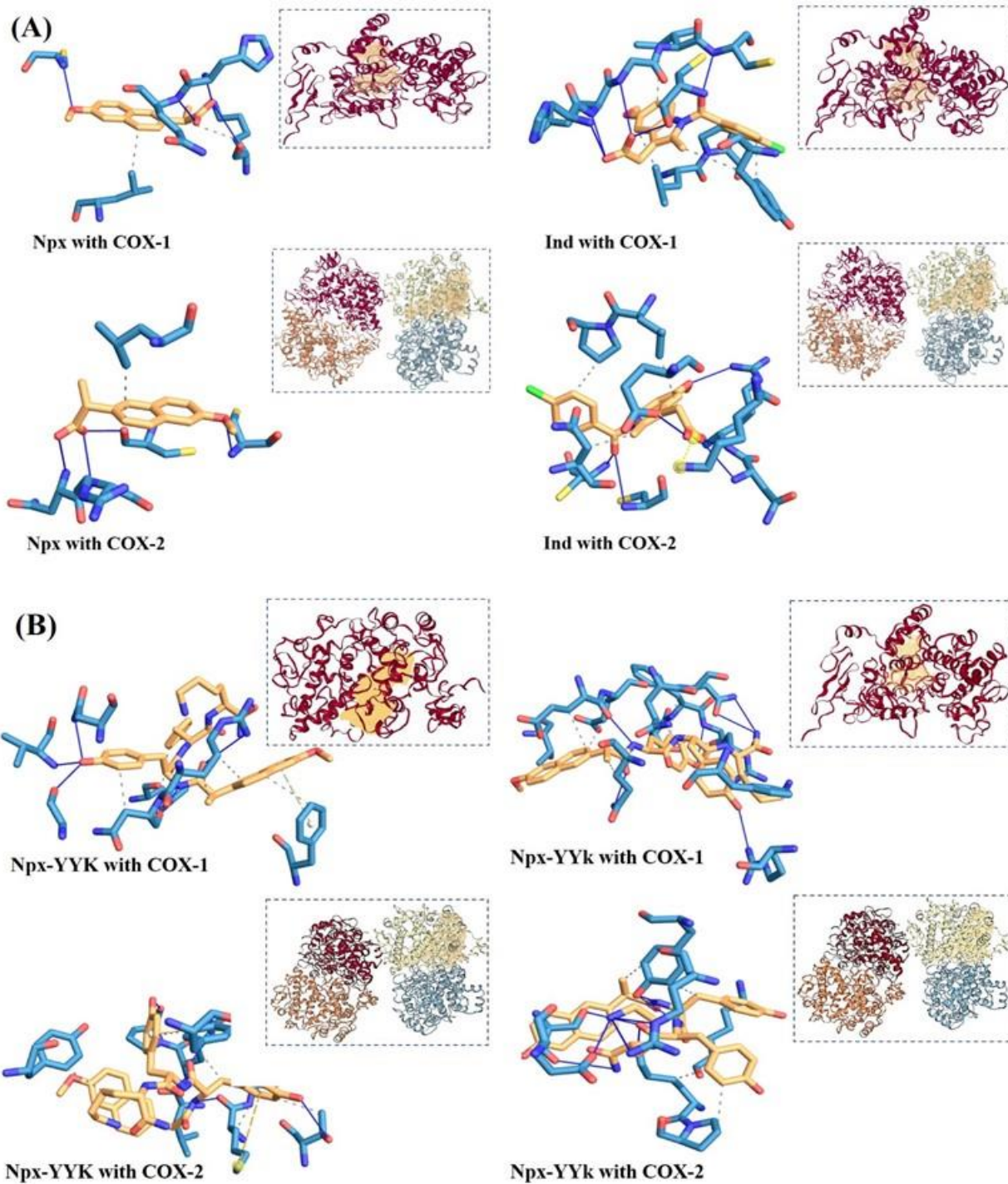


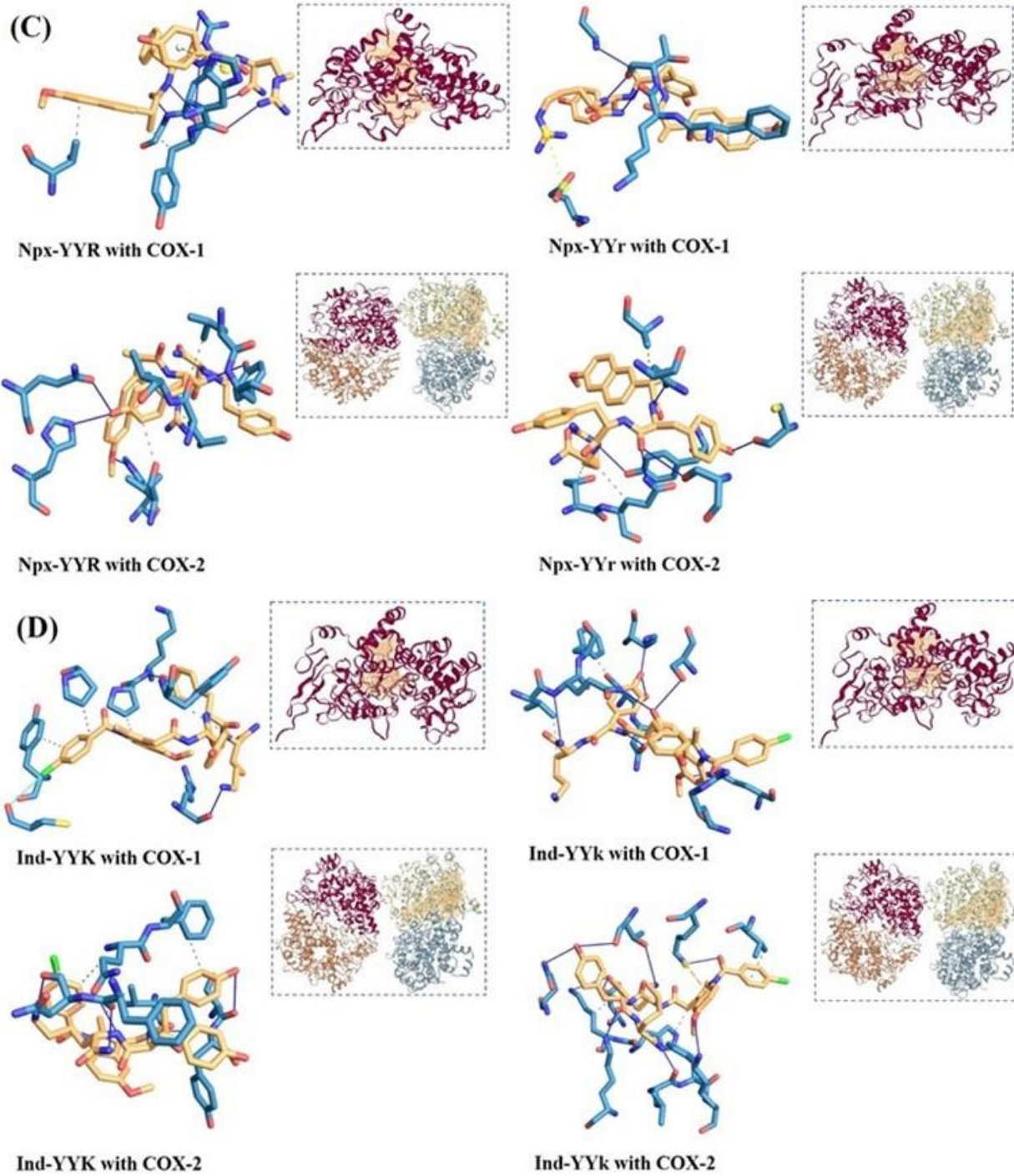
Figure A44. Percentage inhibition of COX-1 and COX-2 enzymes by peptides, YYK, YYk, YYR, and YYr. S is the selectivity index defined as the ratio of COX-2 to COX-1 inhibition. Data are presented as mean \pm SD, n = 3, and *p < 0.05 indicates statistically significant data.

Method for in silico molecular docking study

All structures of drugs (Npx and Ind) and drug-peptide conjugates (Npx-YYK, Npx-YYk, Npx-YYR, Npx-YYr, Ind-YYK, Ind-YYk, Ind-YYR, and Ind-YYr) were drawn using ChemDraw with SMILES, and PDB format was generated through smile translator using NCI/CADD Cactus (<https://cactus.nci.nih.gov/services/translate/>). Three-dimensional structures of two isoforms of cyclooxygenase enzymes, COX-1 and COX-2, were obtained from Protein Data Bank (PDB). Proteins (6Y3C for COX-1 and 1PXX for COX-2) were prepared and docked with all ligands using AutoDock (AutoDock 4-Scripps Research, GNU). Results were analyzed using PLIP: protein-ligand interaction profiler. Negative binding energy values of docked complexes were determined to evaluate the binding efficiency of ligands with proteins.



Continued....



Continued....

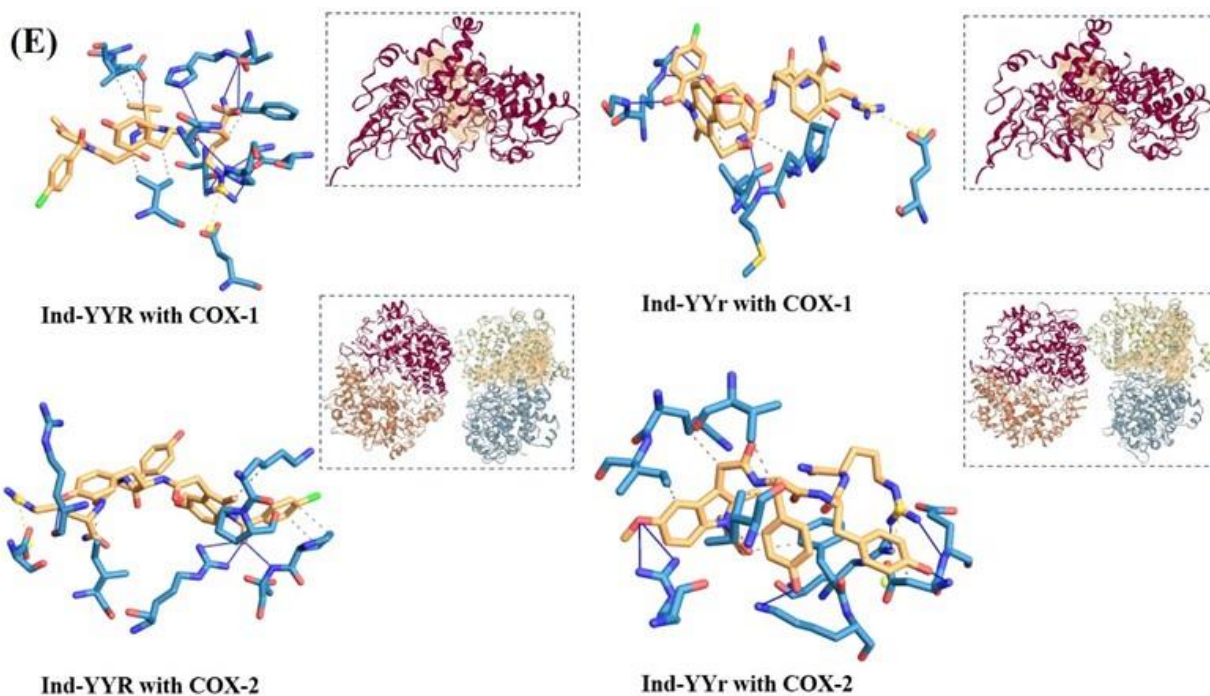


Figure A45. Binding of drugs and peptide conjugates to COX-1 and COX-2 enzymes. (A) Naproxen and indomethacin. (B-E) Peptide conjugates. Ligands are presented as a ball and stick model and enzymes are presented as ribbons.

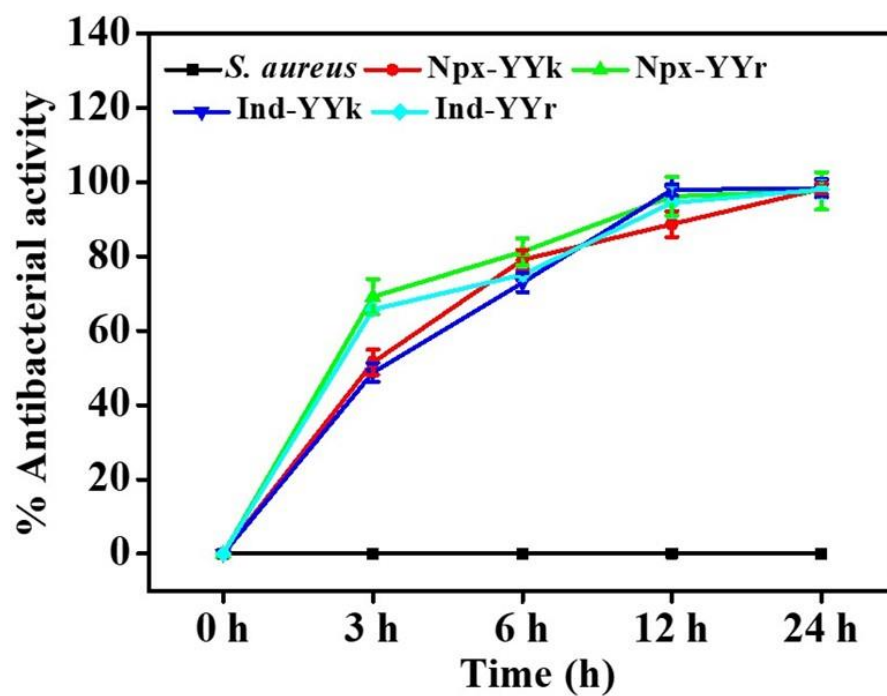


Figure A46. Antibacterial activities of peptide-conjugates, Npx-YYk, Npx-YYr, Ind-YYk, and Ind-YYr, against *S. aureus* by optical density method.

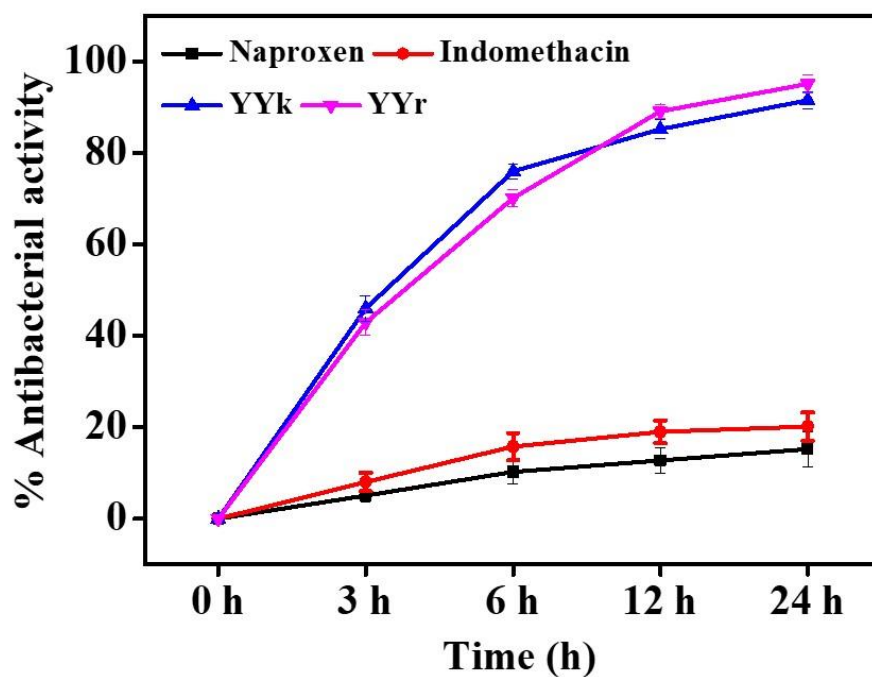


Figure A47. Antibacterial activities of naproxen, indomethacin, and unconjugated peptides, YYk, and YYr against *S. aureus* by optical density method.

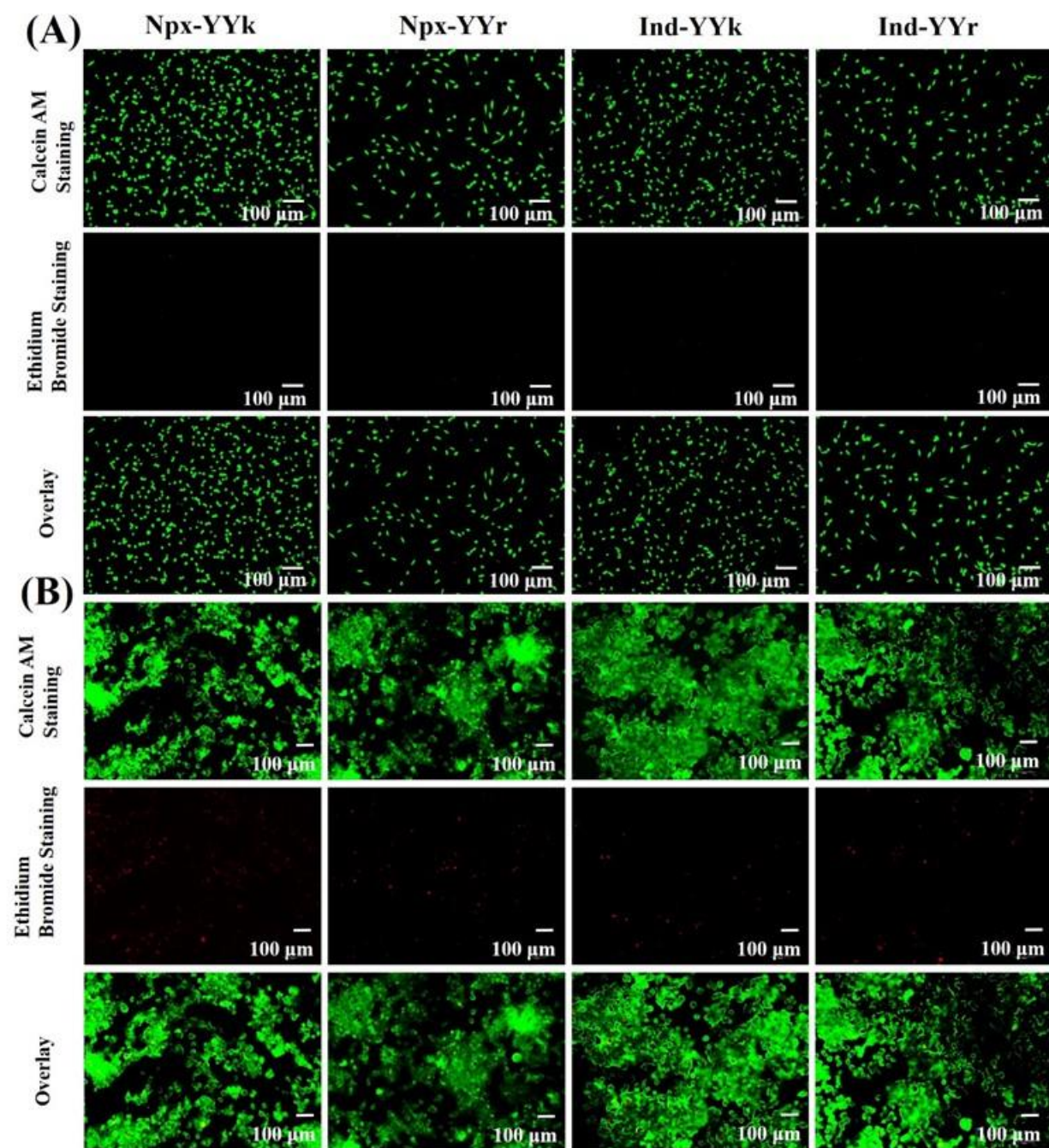


Figure A48. Live/dead staining of cells treated with extracts of Npx-YYk, Npx-YYr, Ind-YYk, and Ind-YYr for 24 h. (A) Mouse fibroblast cell line (L929). (B) Macrophage-like cell line (RAW 264.7). Scale bar: 100 μ m. Cells were stained with calcein AM and ethidium bromide. Live and dead cells show green and red fluorescence. Cells without any treatment were considered as a control.

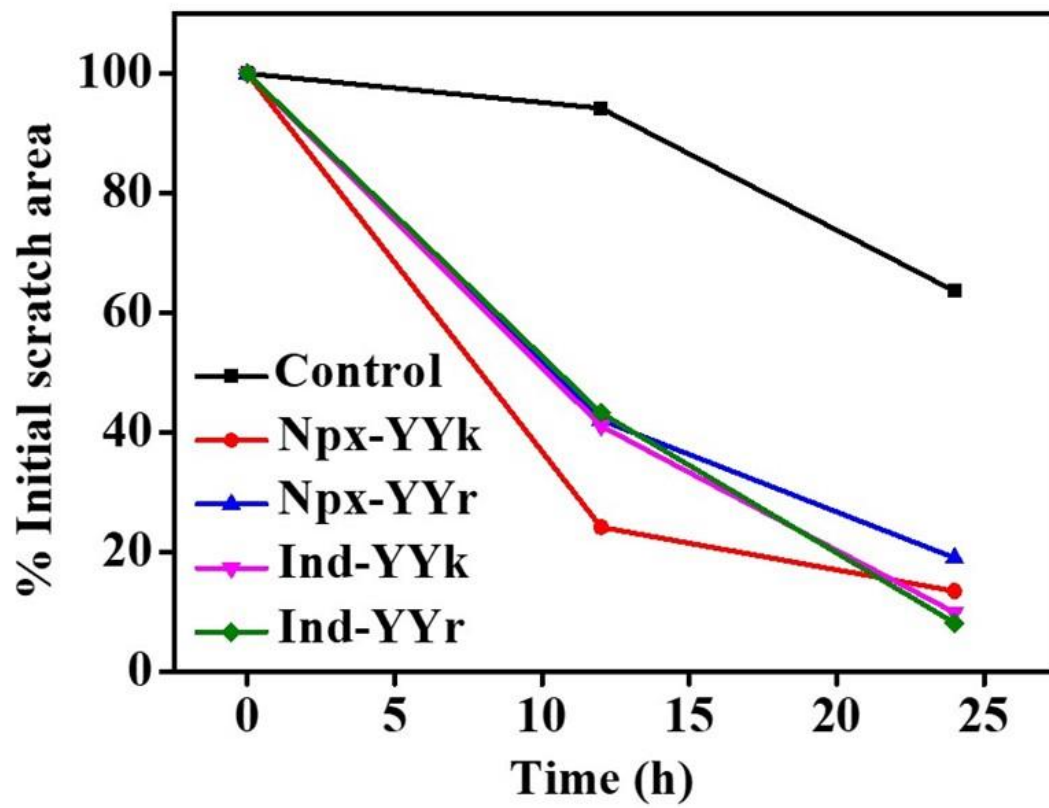


Figure A49. Quantitative analysis of the area of scratch healing.

Table A1. The primer sequences used in the RT-PCR study.

Gene	Primer Sequence (5'→3')
mGAPDH-F	AGGTCGGTGTGAACGGATTG
mGAPDH-R	GGGGTCGTTGATGGCAACA
Mu-TNF- α -F	CTGTCTTGCGTTGGGGGAG
Mu-TNF- α -R	TTAAGCTGCCTCACTCCCGT
Mu-IL-6-F	CCATCTCTCCGTCTCTCACC
Mu-IL-6-R	AGACCGCTGCCTGTCTAAAA
Mu-IL-10-F	GCTCTTACTGACTGGCATGAG
Mu-IL-10-R	CGCAGCTCTAGGAGCATGTG

Table A2. Binding energy, interactions involved, and selectivity index of naproxen, indomethacin, and conjugates to COX-1 and COX-2 (calculated by AutoDock software).

Ligand	Receptor	Binding energy	Inhibition constant	Interactions involved	Selectivity Index (S)
Naproxen	COX-1	-7.51 kcal/mol	3.14 μ M	Hydrophobic, Hydrogen bond	0.116
Naproxen	COX-2	-6.23 kcal/mol	26.93 μ M	Hydrophobic, Hydrogen bond	
Indomethacin	COX-1	-8.89 kcal/mol	305.77 nM	Hydrophobic, Hydrogen bond	0.533
Indomethacin	COX-2	-8.51 kcal/mol	573.52 nM	Hydrophobic, Hydrogen bond, Salt bridge	
Npx-YYK	COX-1	-4.33 kcal/mol	673.48 μ M	Hydrophobic, Hydrogen bond, π - π stacking	0.100
Npx-YYK	COX-2	-2.97 kcal/mol	6.71 mM	Hydrophobic, Hydrogen bond, π - π stacking	
Npx-YYk	COX-1	-3.94 kcal/mol	1.29 mM	Hydrophobic, Hydrogen bond	28.301
Npx-YYk	COX-2	-5.92 kcal/mol	45.58 μM	Hydrophobic, Hydrogen bond	
Npx-YYR	COX-1	-3.91 kcal/mol	1.36 mM	Hydrophobic, Hydrogen bond, π - π stacking	0.006
Npx-YYR	COX-2	-0.91 kcal/mol	216.25 mM	Hydrophobic, Hydrogen bond	
Npx-YYr	COX-1	-2.38 kcal/mol	17.92 mM	Hydrophobic, Hydrogen bond, Salt bridge	4.236
Npx-YYr	COX-2	-3.24 kcal/mol	4.23 mM	Hydrophobic, Hydrogen bond	

Ind-YYK	COX-1	-5.39 kcal/mol	112.40 μ M	Hydrophobic, Hydrogen bond, Halogen bond	0.003
Ind-YYK	COX-2	-2.11 kcal/mol	28.22 mM	Hydrophobic, Hydrogen bond	
Ind-YYk	COX-1	-4.74 kcal/mol	334.51 μ M	Hydrophobic, Hydrogen bond	2.342
Ind-YYk	COX-2	-5.25 kcal/mol	142.79 μM	Hydrophobic, Hydrogen bond, π - π stacking	
Ind-YYR	COX-1	-5.40 kcal/mol	110.06 μ M	Hydrophobic, Hydrogen bond, salt bridge	0.138
Ind-YYR	COX-2	-4.23 kcal/mol	797.39 μM	Hydrophobic, Hydrogen bond, salt bridge	
Ind-YYr	COX-1	-4.18 kcal/mol	860.27 μ M	Hydrophobic, Hydrogen bond, salt bridge	8.678
Ind-YYr	COX-2	-5.46 kcal/mol	99.13 μM	Hydrophobic, Hydrogen bond, salt bridge	

*Selectivity index (S) = $\frac{\text{Inhibition constant of COX 1}}{\text{Inhibition constant of COX 2}}$

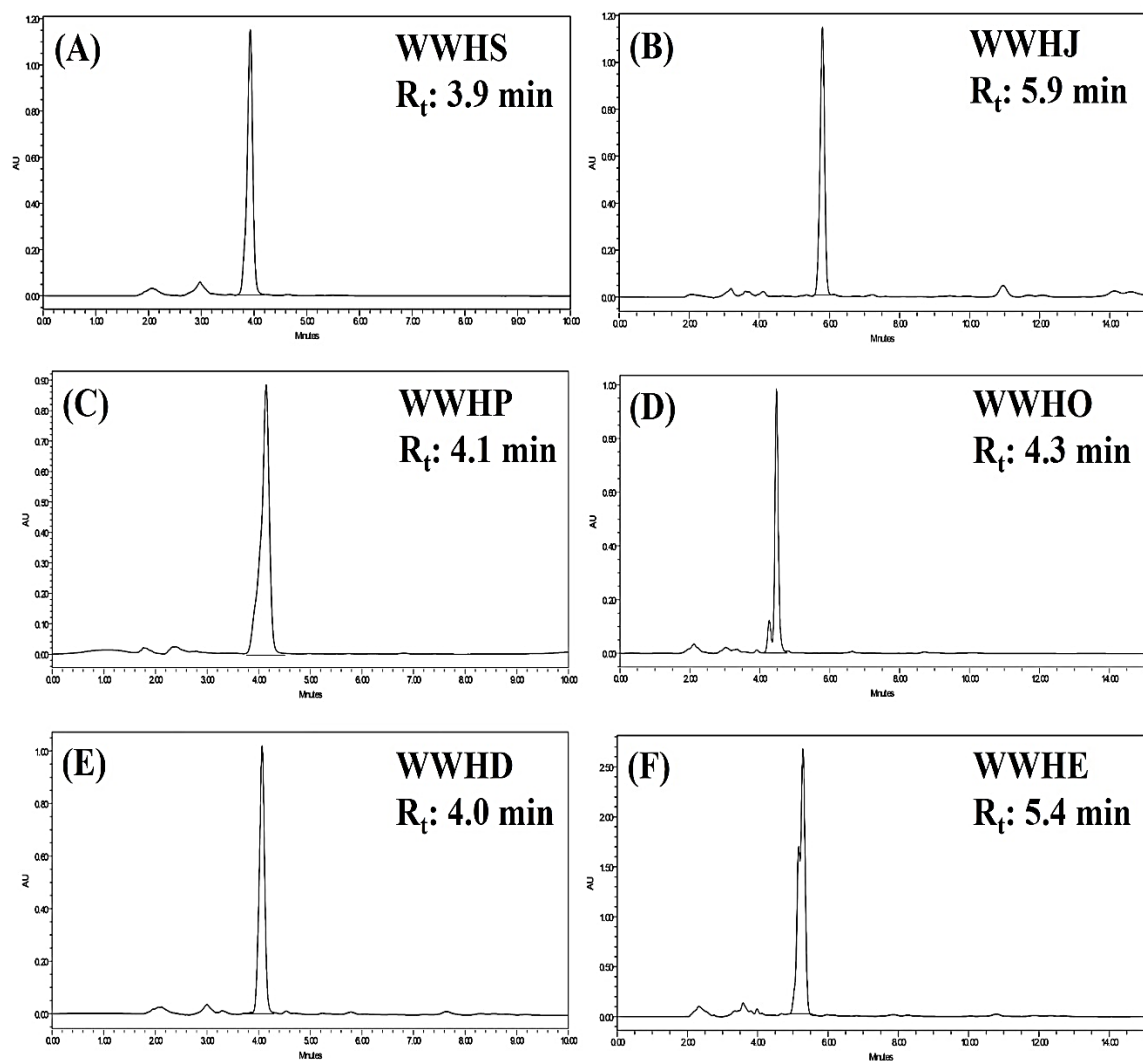
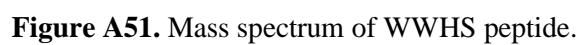
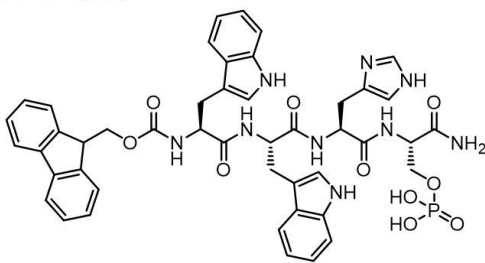


Figure A50. RP-HPLC of peptides. (A) WWHS. (B) WWHJ. (C) WWHP. (D) WWHO. (E) WWHD. (F) WWHE.

1: TOF MS ES+
2.01e7



1: TOF MS ES+
2.58e7



218

1: TOF MS ES+
7.09e7

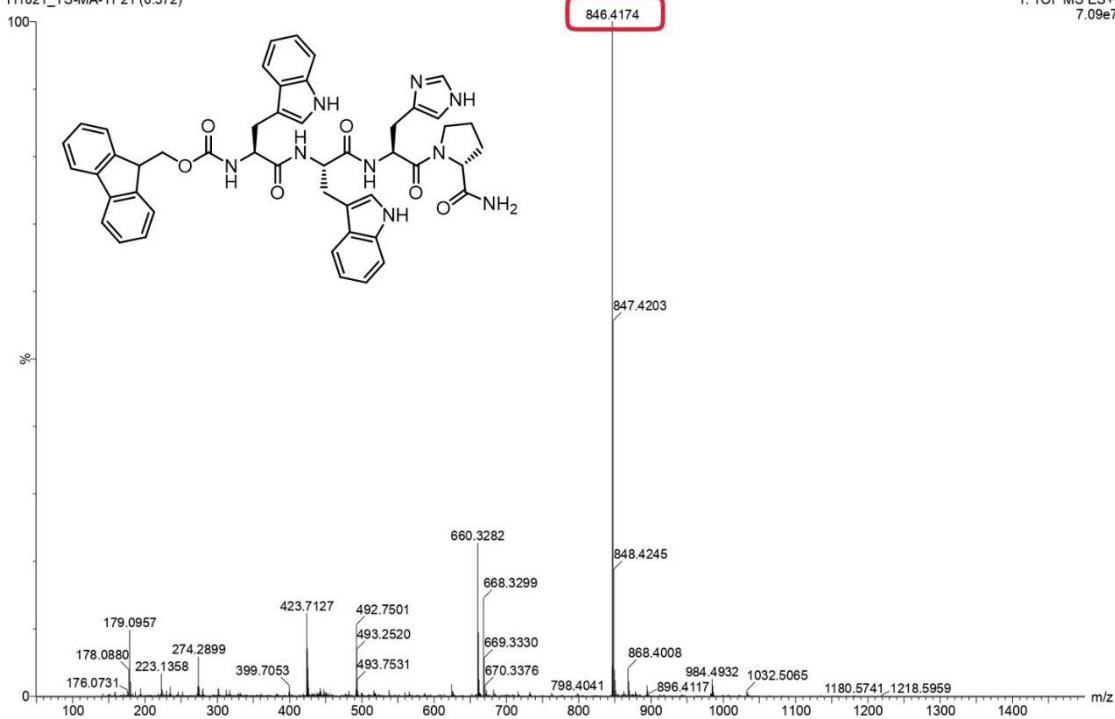


Figure A53. Mass spectrum of WWHP peptide.

Sample Name : 181021_YS-MA-12
Test Name :
181021_YS-MA-12 7 (0.135)

IITRPR

XEVO G2-XS QTOF

1: TOF MS ES+
1.88e8

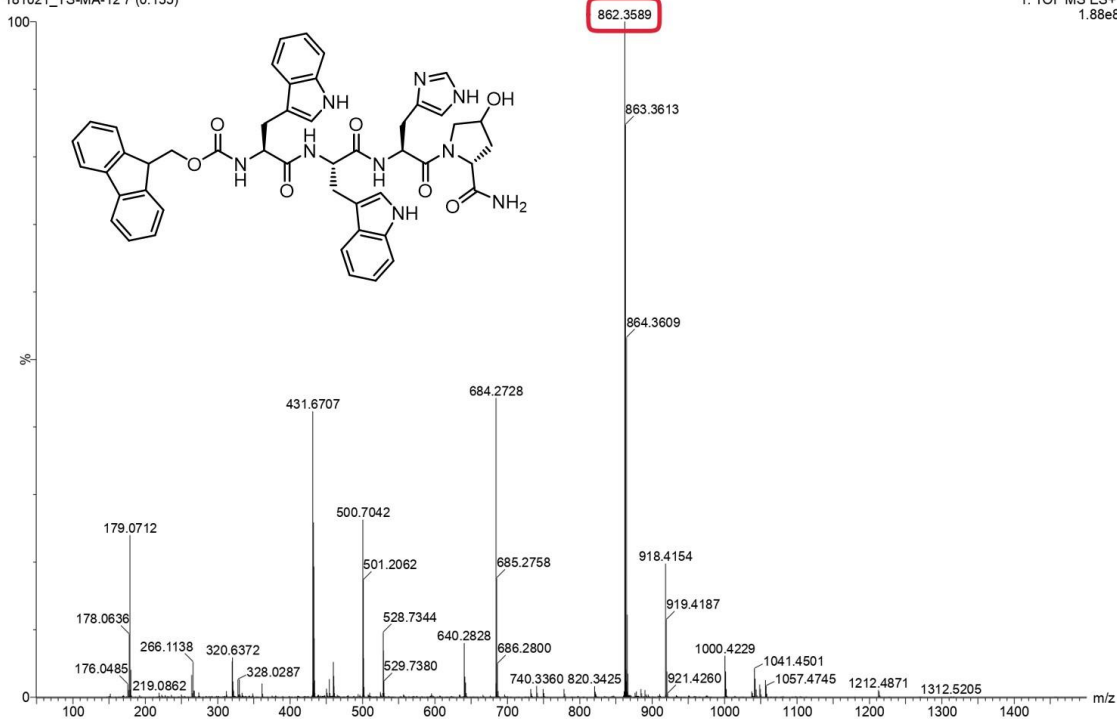


Figure A54. Mass spectrum of WWHO peptide.

Sample Name : 111021_YS-MA-10
Test Name :
111021_YS-MA-10 18 (0.321)

IITRPR

XEVO G2-XS QTOF

1: TOF MS ES+
3.16e7

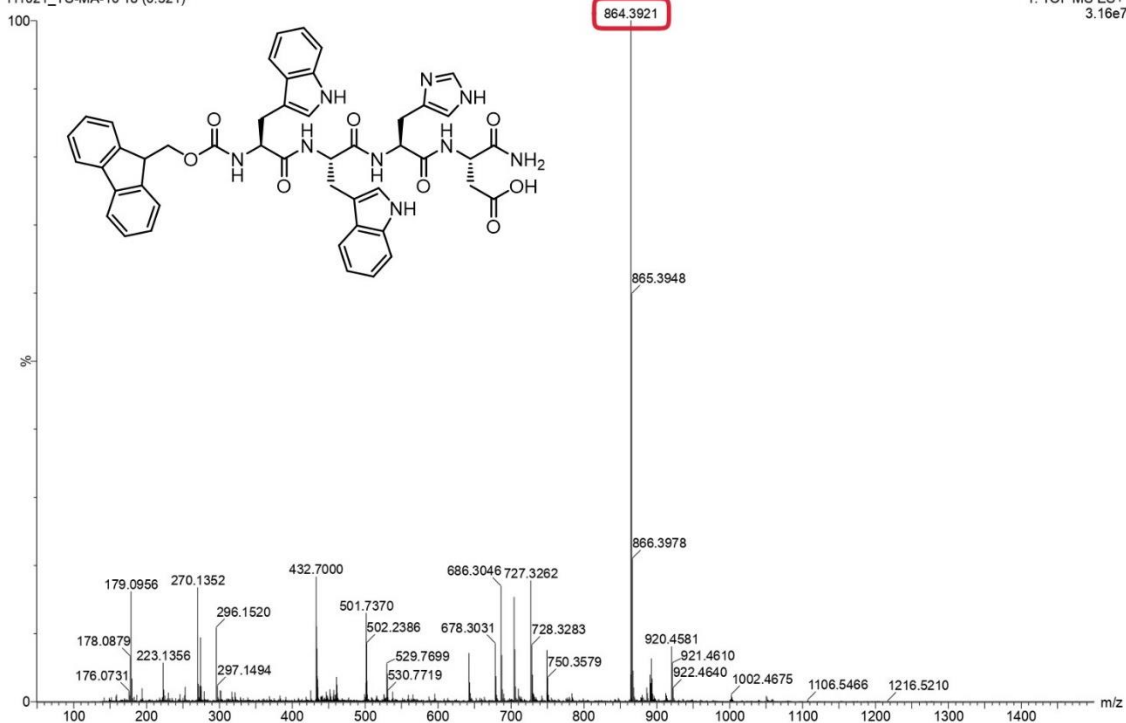


Figure A55. Mass spectrum of WWHD peptide.

Sample Name : 011121_YS-MA-13
Test Name :
011121_YS-MA-13 19 (0.338)

IITRPR

XEVO G2-XS QTOF

1: TOF MS ES+
2.74e7

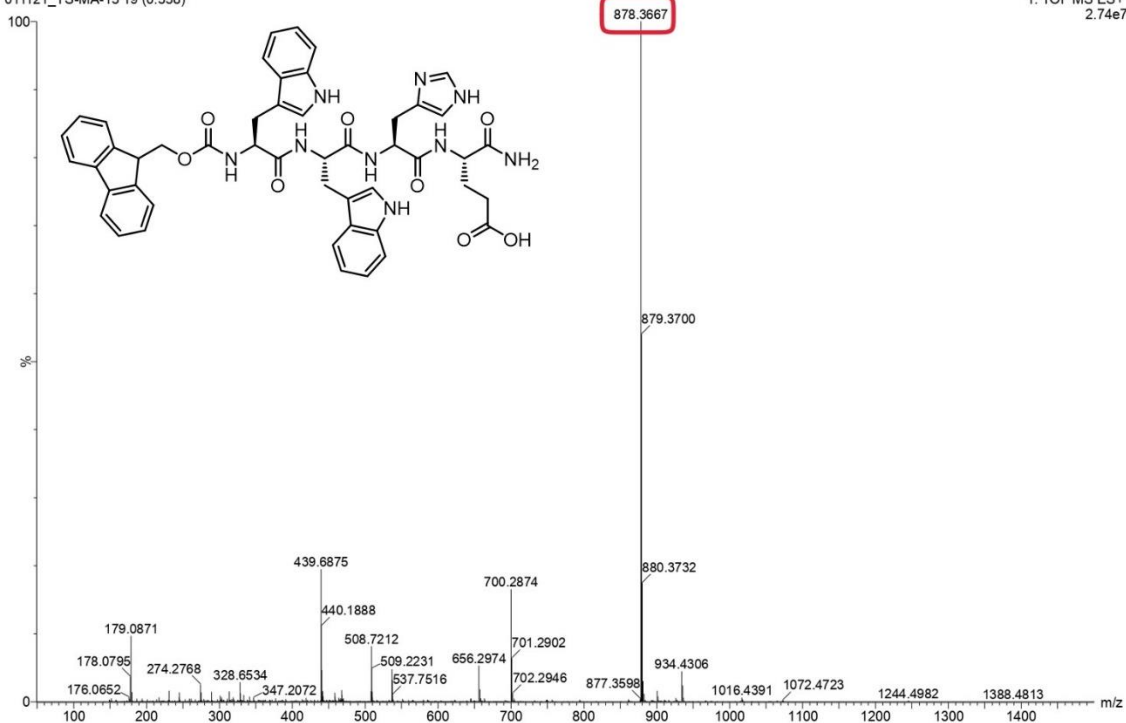


Figure A56. Mass spectrum of WWHE peptide.

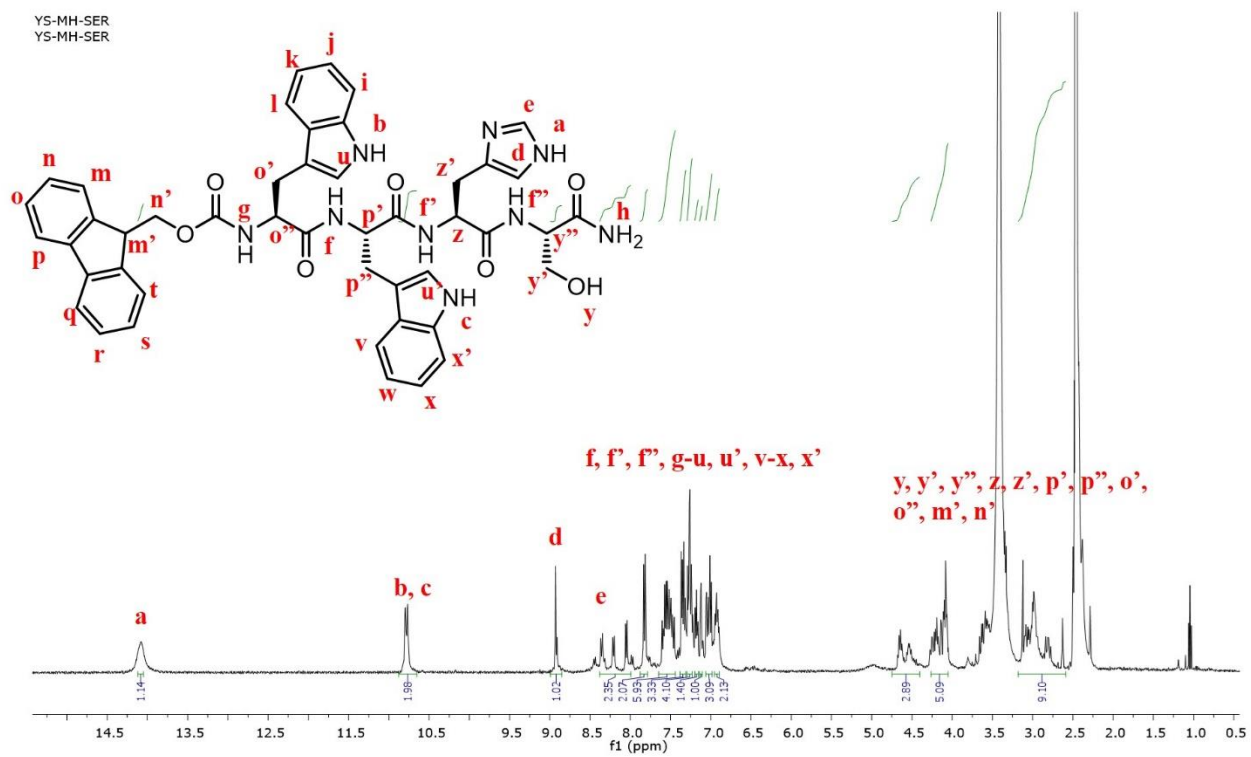


Figure A57. ^1H NMR spectrum of WWHS peptide.

YS-MH-PSE
YS-MH-PSE

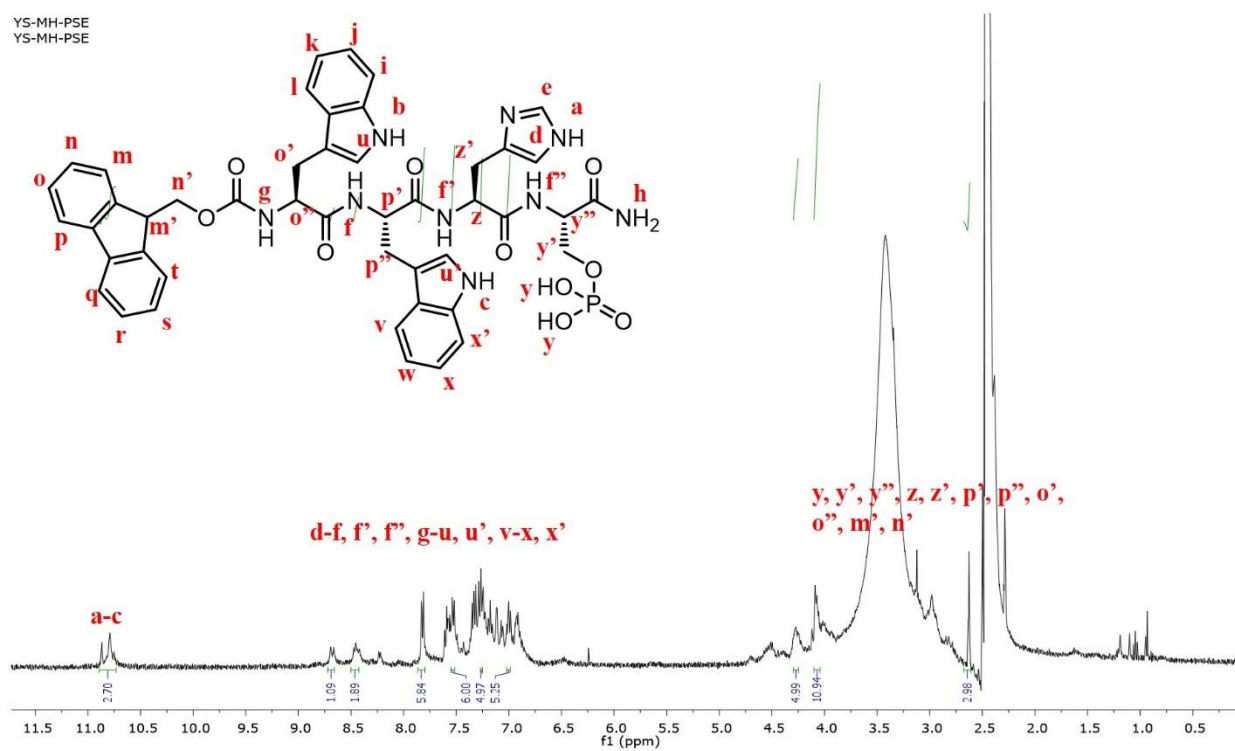


Figure A58. ^1H NMR spectrum of WWHJ peptide.

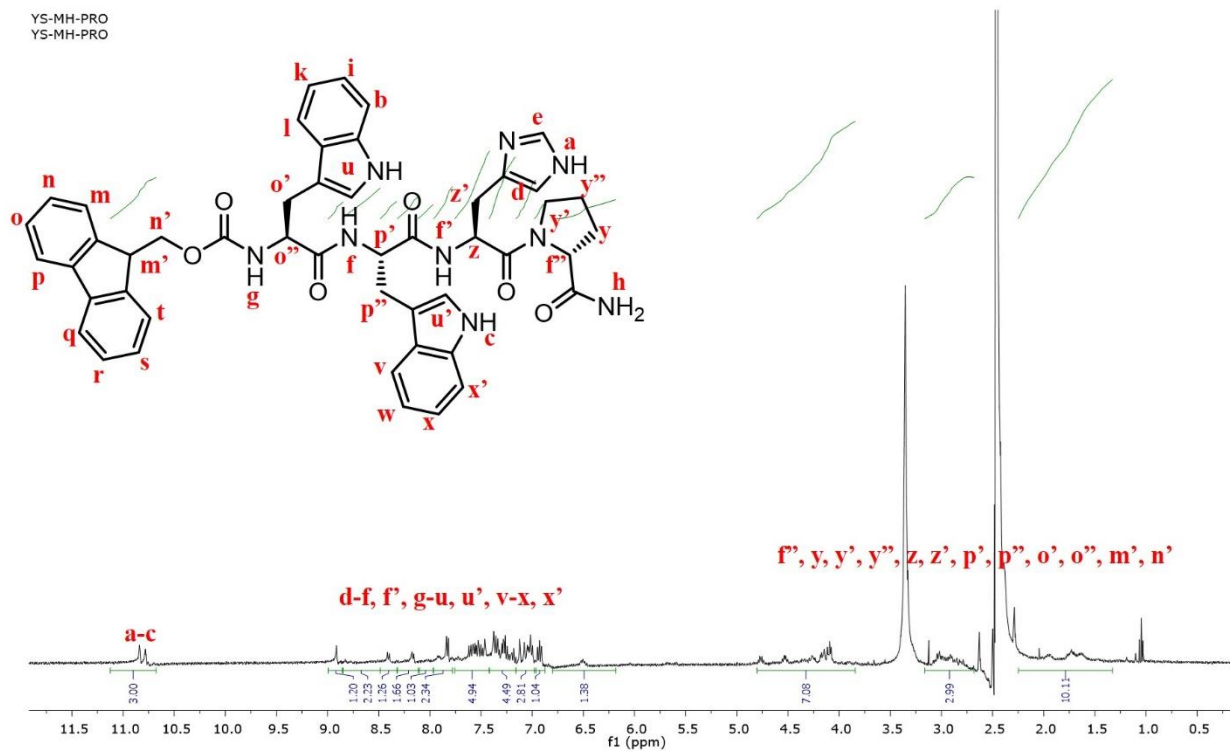


Figure A59. ^1H NMR spectrum of WWHP peptide.

YS-MH-HYP
YS-MH-HYP

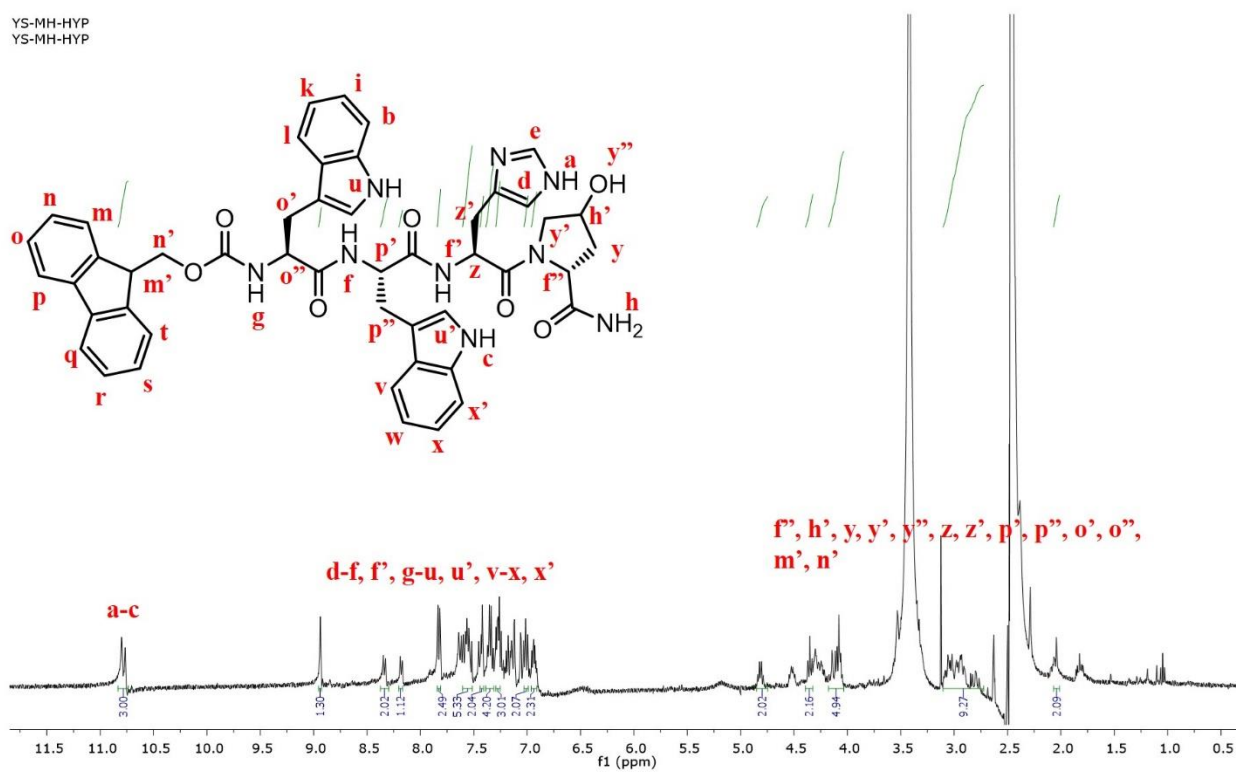


Figure A60. ^1H NMR spectrum of WWHO peptide.

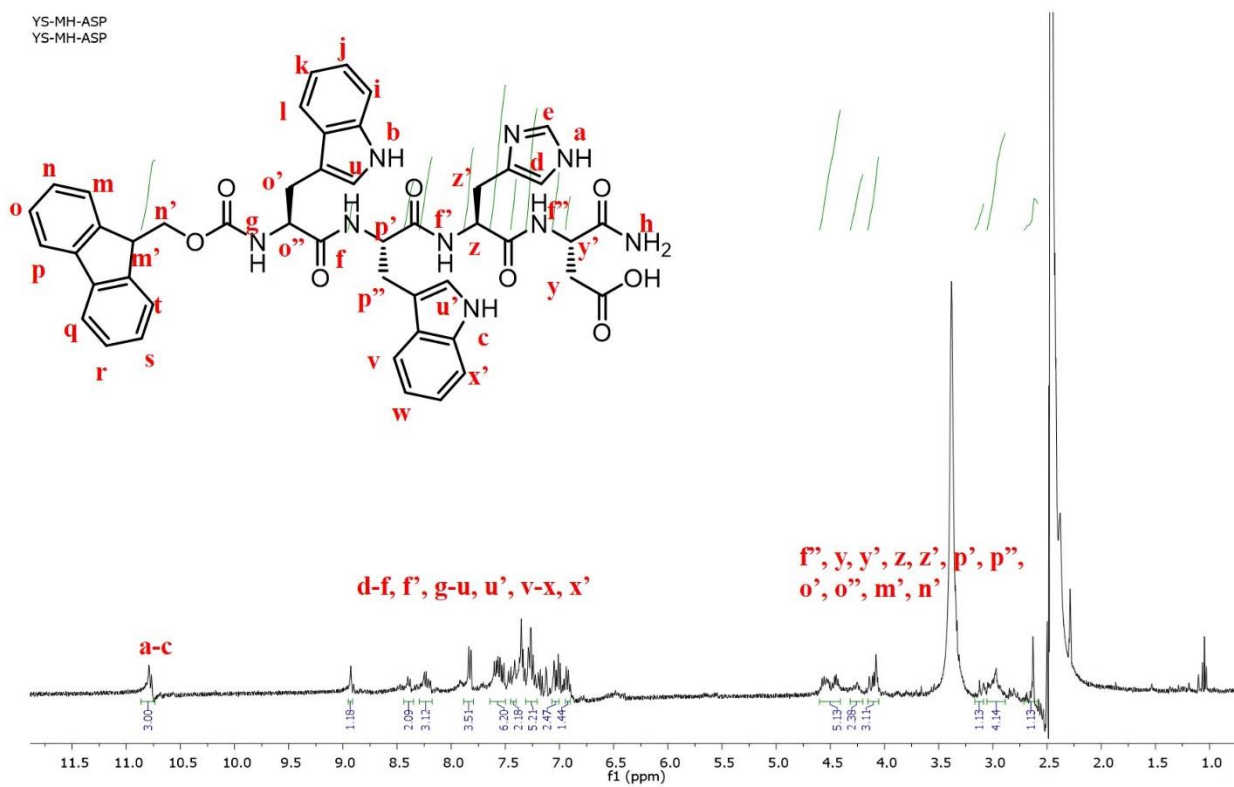


Figure A61. ^1H NMR spectrum of WWHD peptide.

YS-MH-GLU
YS-MH-GLU

Chemical structure of YS-MH-GLU is shown, featuring various protons labeled with letters (a, b, c, d, e, f, g, h, i, j, k, l, m, n, o, p, q, r, s, t, u, v, w, x, y, z, a', b', c', d', e', f', g', h', i', j', k', l', m', n', o', p', q', r', s', t', u', v, w, x', y', z, a'', b'', c'', d'', e'', f'', g'', h'', i'', j'', k'', l'', m'', n'', o'', p'', q'', r'', s'', t'', u'', v'', w'', x'', y'', z').

The ^1H NMR spectrum (ppm) shows peaks corresponding to these protons. Key peaks are labeled: a-c (aromatic, 11.0 ppm), d-f, f', g-u, v-x, x' (aromatic, 6.5-9.0 ppm), f'', y, y', y'', z, z', p', p'', o', o'', m', n' (aliphatic, 1.5-4.5 ppm).

Integration values are provided for several peaks: 3.00, 2.95, 1.16, 1.17, 2.55, 6.44, 7.00, 5.08, 2.89, 1.92, 5.05, 4.21, 5.23.

Figure A62. ^1H NMR spectrum of WWHE peptide.

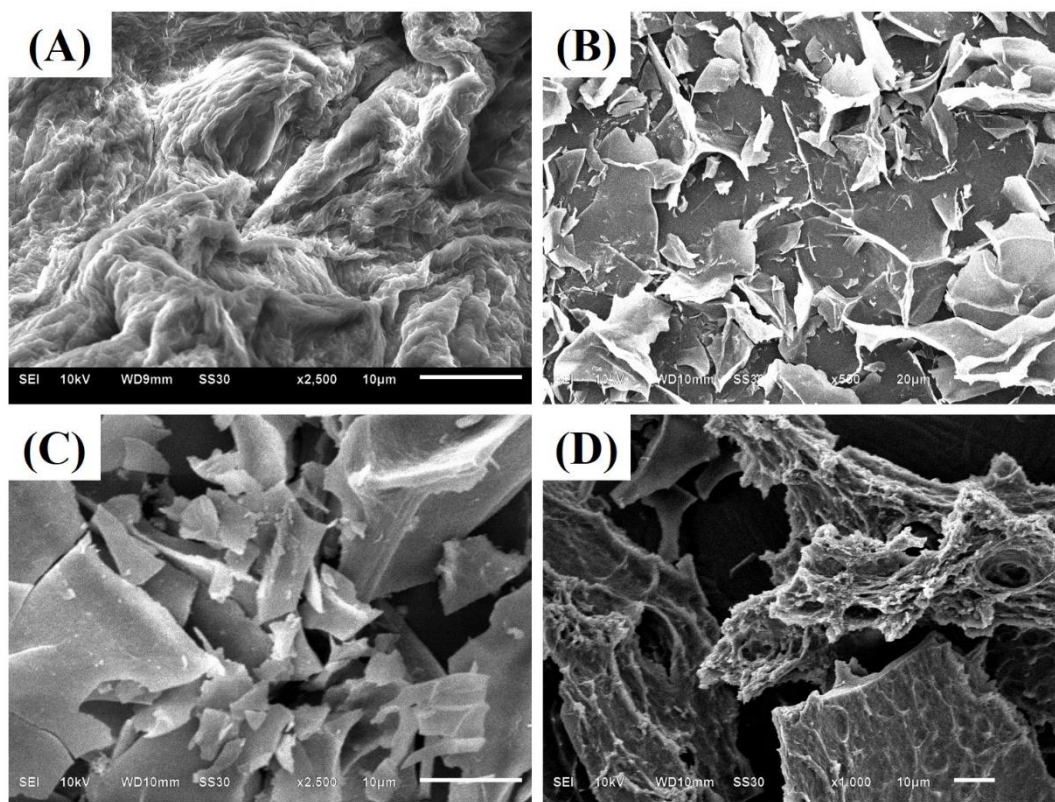


Figure A63. SEM images of peptide gels (2% w/v). (A) WWHS. (B) WWHO. (C) WWHD. (D) WWHE. Scale bar. 10 μm (A, C-D) and 20 μm (B).

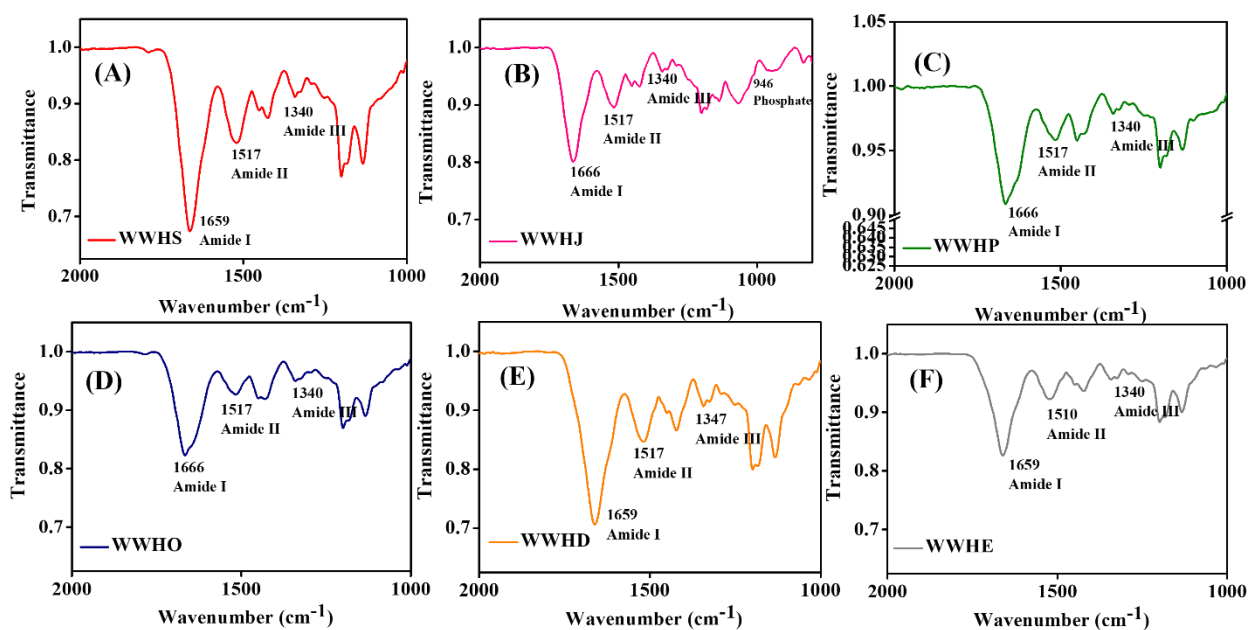


Figure A64. FTIR spectra of peptides. (A) WWHS. (B) WWHJ. (C) WWHP. (D) WWHO. (E) WWHD. (F) WWHE.

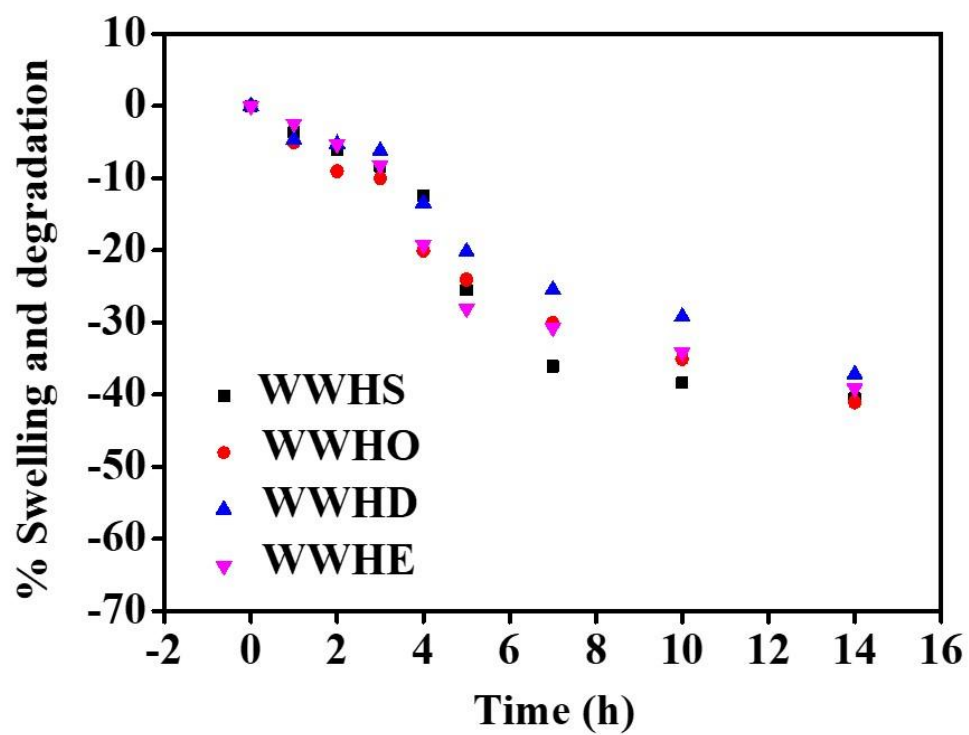


Figure A65. Swelling and degradation of peptide gels at pH 7.4 and 6.5. (A) WWHS (B) WWHJ (C) WWHP (D) WWHO (E) WWHD (F) WWHE. Values above 0% indicate gravimetric water uptake (weight gain), whereas negative values suggest degradation (weight loss). Data reported are mean \pm SE (n = 3).

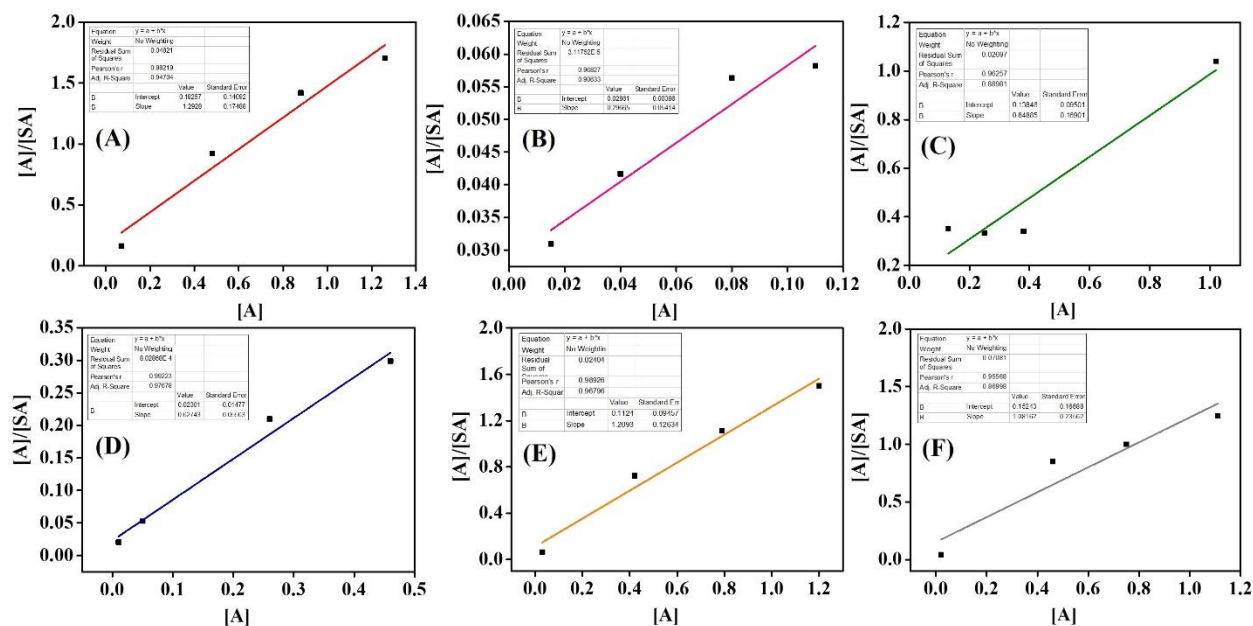


Figure A66. Hydroxyapatite and peptide binding data fitted into linear form of Langmuir adsorption isotherm model.

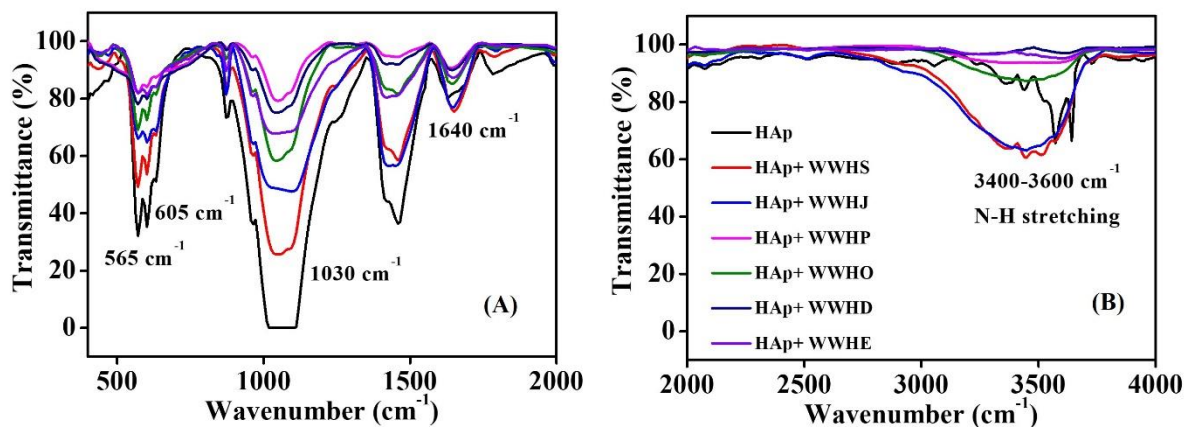


Figure A67. FTIR spectra of peptides adsorbed on HAp surface. (A) 400-2000 cm^{-1} . (B) 2000-4000 cm^{-1} .

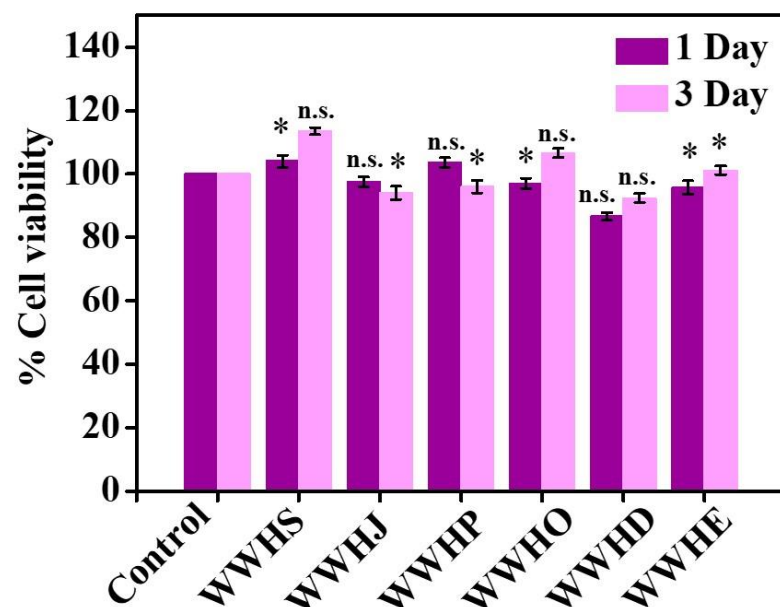


Figure A68. MTT assay of the peptide (WWHJ, WWHP) and hydrogel (WWHS, WWHO, WWHD and WWHE) extracts on RAW 264.7 for 1 and 3 days.

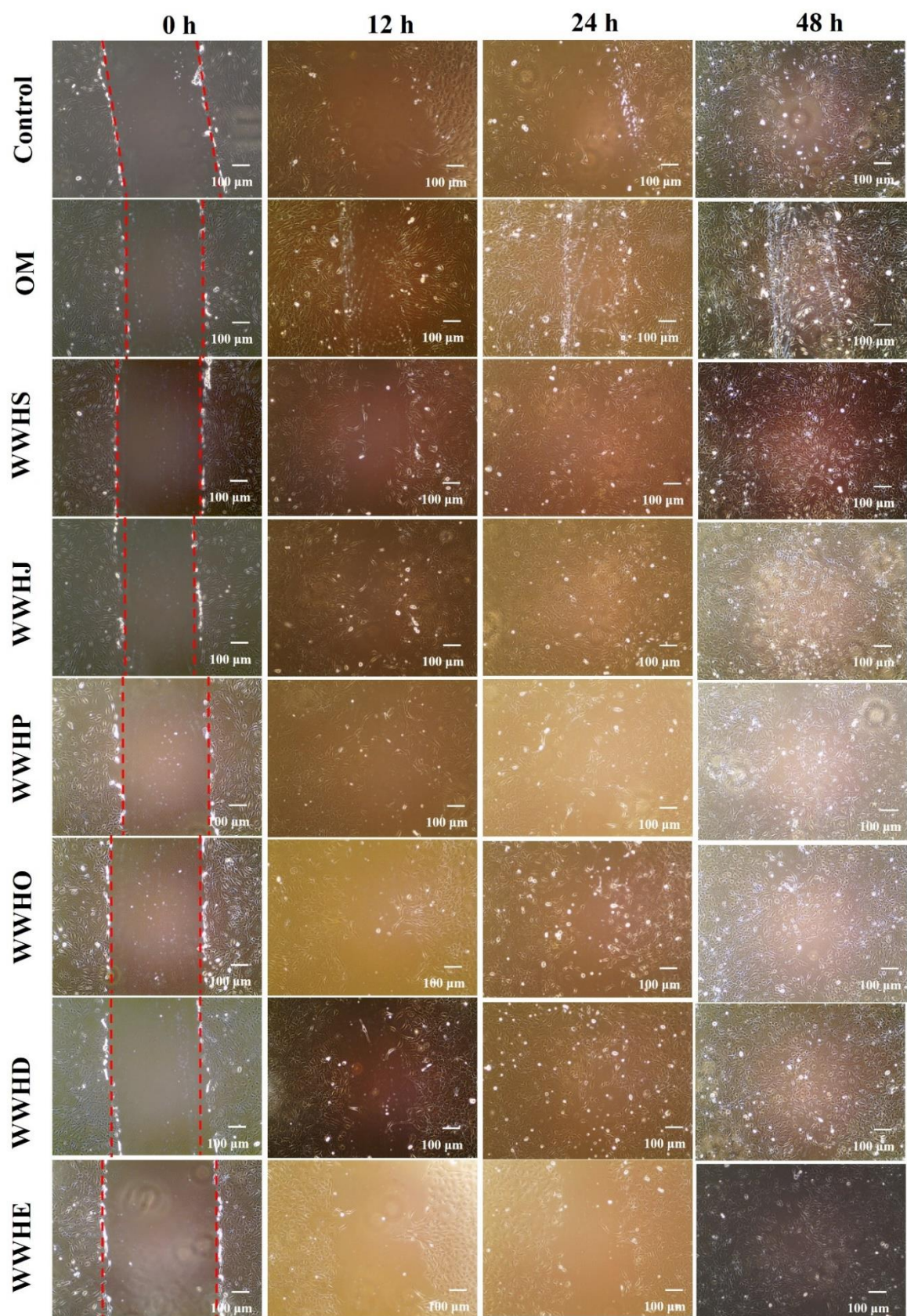


Figure A69. Images of migration of MC 3T3 E1 cells and healing of scratch at different time intervals (0, 12, 24 and 48 h). Cells without any treatment were considered as a control. Scale bar: 100 μm .

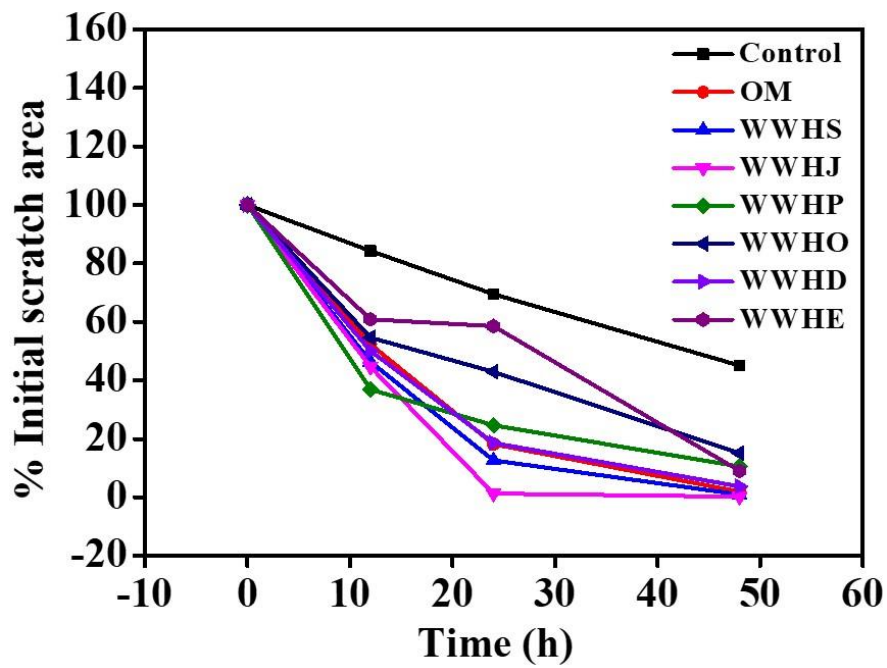


Figure A70. Quantitative analysis of the area of scratch healing.

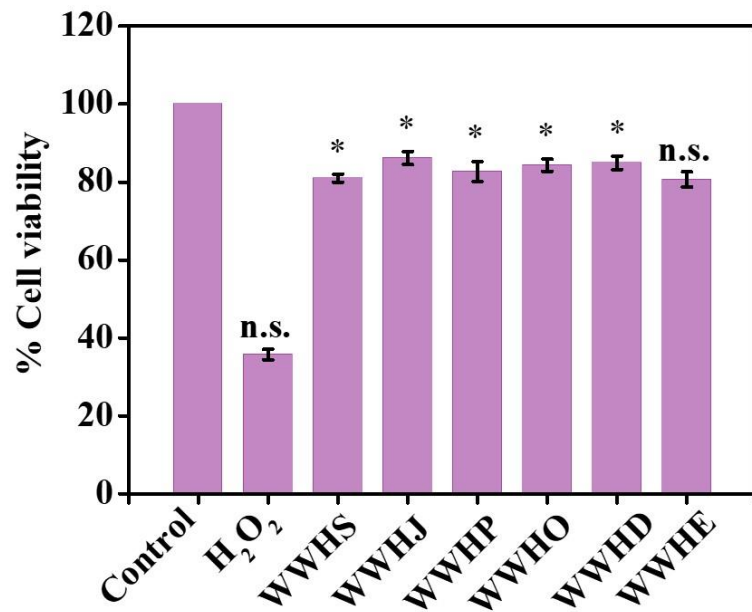


Figure A71. Viability of H₂O₂-induced MC 3T3-E1 cells after treatment with extracts peptides (WWHJ, WWHP) and hydrogels (WWHS, WWHO, WWHD and WWHE) for 24 h using the MTT assay.

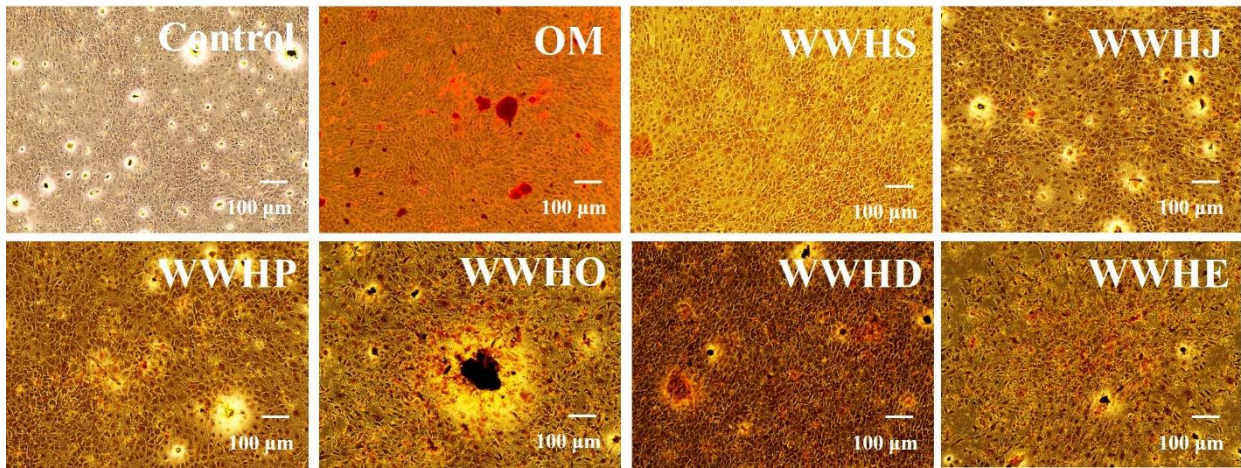


Figure A72. Alizarin Red S staining to demonstrate calcium deposition on MC 3T3-E1 cells at 7th day. Scale bar. 100 μ m.

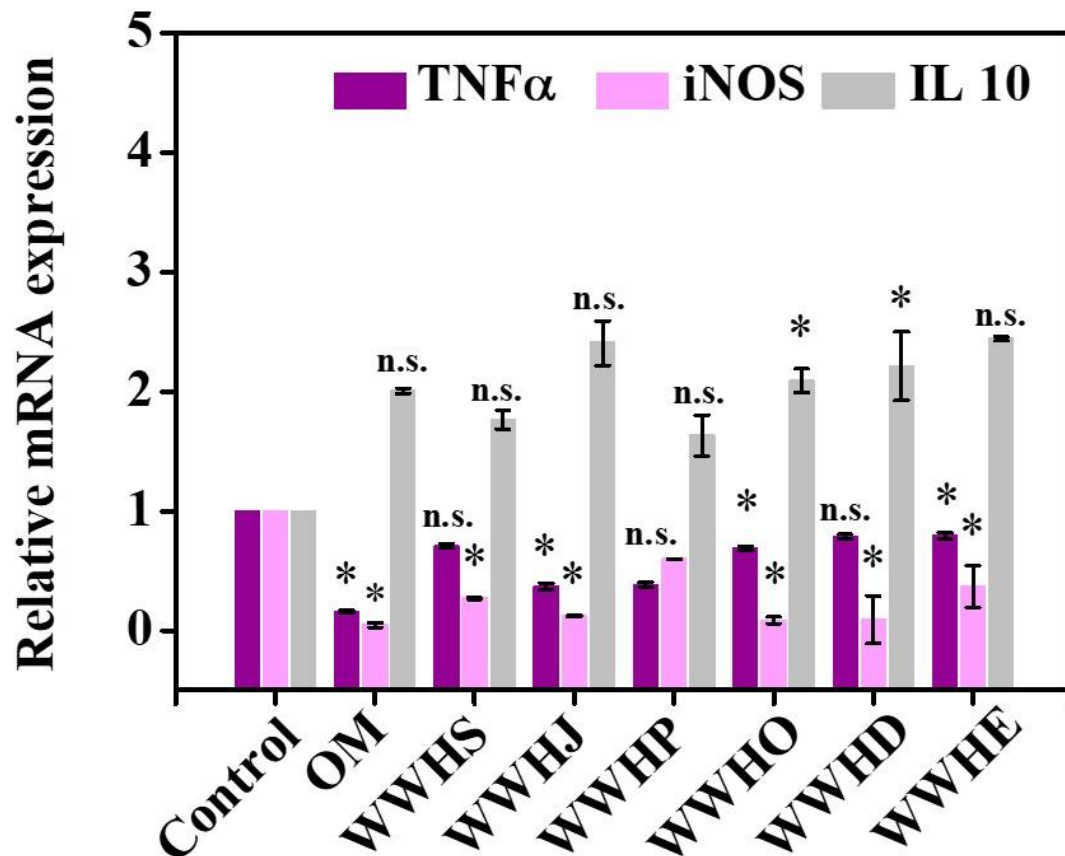


Figure A73. RT PCR data of different phenotype of macrophages. TNF α and iNOS are markers for M1 macrophages, and IL 10 is a marker for M2 macrophages. Results are shown as mean \pm SD.

Table A3. Binding Affinities (K_{ads}) of HAp binding peptides.

Peptide	r	K_{ads} (L.mol⁻¹)
WWHS	0.98219	7.06
WWHJ	0.96827	10.77
WWHP	0.96257	6.128
WWHO	0.99223	27.27
WWHD	0.98926	10.35
WWHE	9.95568	7.0971

Table A4. The primer sequences used in RT-PCR study.

Gene	Primer Sequence (5'→3')
mGAPDH-F	AGGTCGGTGTGAACGGATTG
mGAPDH-R	GGGGTCGTTGATGGCAACA
ALP-F	CTGATCAGTGTGCCCCTGCAG
ALP-R	GGAGCTTGGAACGAATGTTCTG
RUNX 2-F	TCCACCACGCCGCTGTCT
RUNX 2-R	TCAGTGAGGGATGAAATGCT
OPN-F	CTTGCTTGGGTTTGCAGTCTT
OPN-R	GGTCGTAGTTAGTCCCTCAGA
OCN-F	CAA AGG TGC AGC CTT TGT GTC
OCN-R	TCA CAG TCC GGA TTG AGC TCA
COL 1-F	CGATGGATTCCCGTTCGAGT
COL 1-R	CGATCTCGTTGGATCCCTGG
RANK L-F	CTAAGAGACATGGCCACGG
RANK L-R	GTCCAGGGGTTAGACCCAGA
TRAP-F	AGCAGCCAAGGAGGACTACGTT
TRAP-R	TCGTTGATGTCGCACAGAGG
Mu-TNF- α -F	CTGTCTTGCGTTGGGGGAG
Mu-TNF- α -R	TTAAGCTGCCTCACTCCCGT
Mu-iNOS-F	CACCAAGCTGAACTTGAGCG
Mu-iNOS-R	CGTGGCTTTGGGCTCCTC
Mu-IL-10-F	GCTCTTACTGACTGGCATGAG
Mu-IL-10-R	CGCAGCTCTAGGAGCATGTG

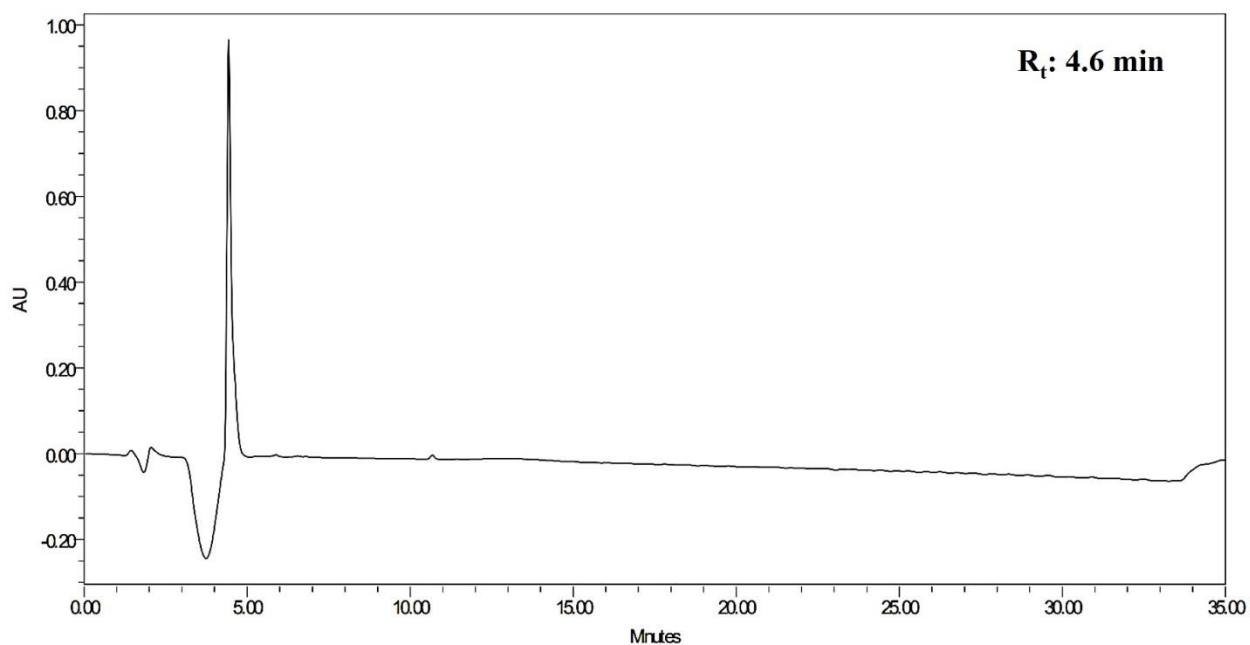


Figure A74. RP-HPLC of peptide amphiphile (PA).

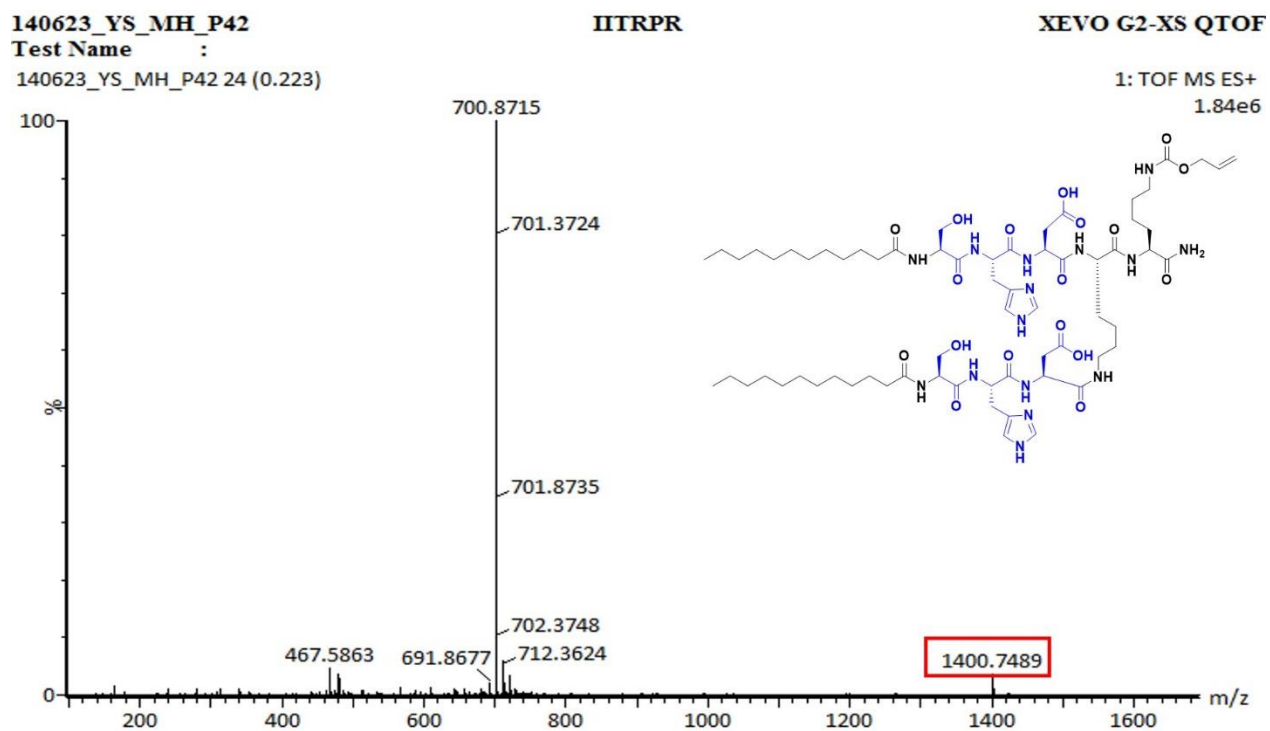


Figure A75. Mass spectrum of peptide amphiphile (PA).

YS-MH-P4
YS-MH-P4

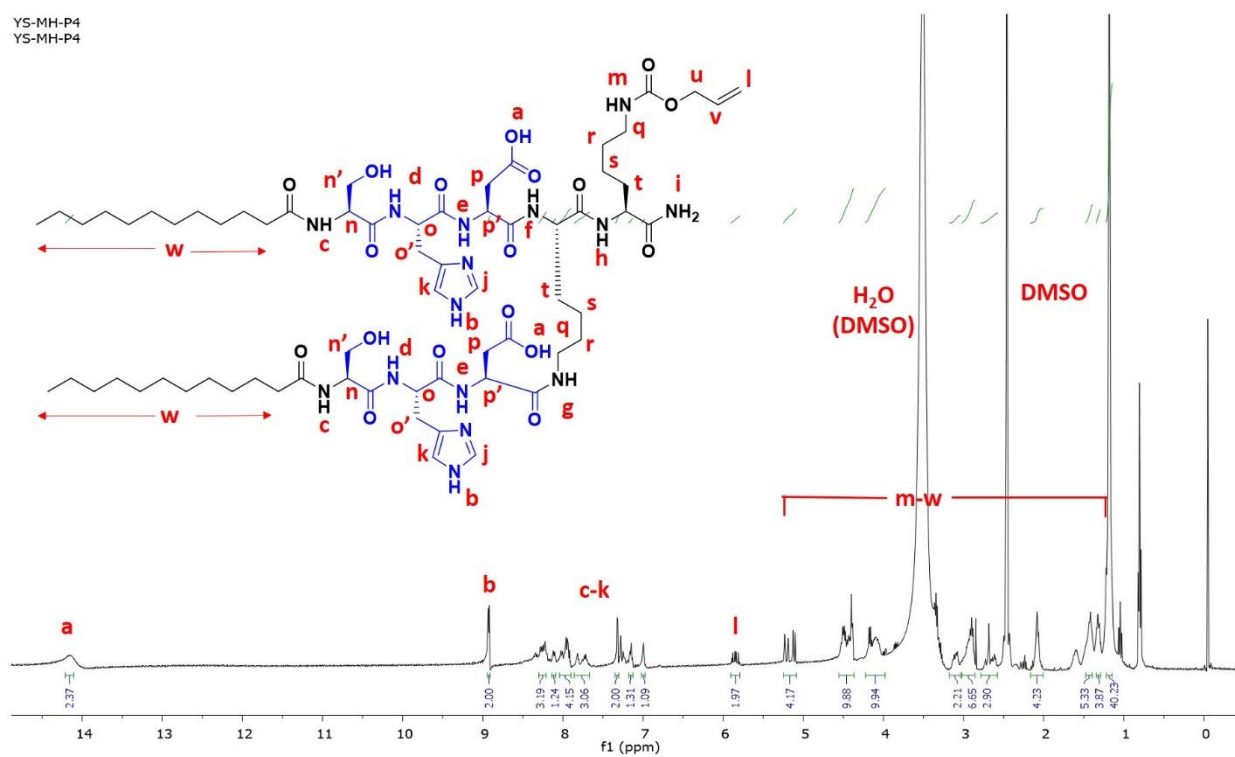


Figure A76. NMR spectra of peptide amphiphile (PA).

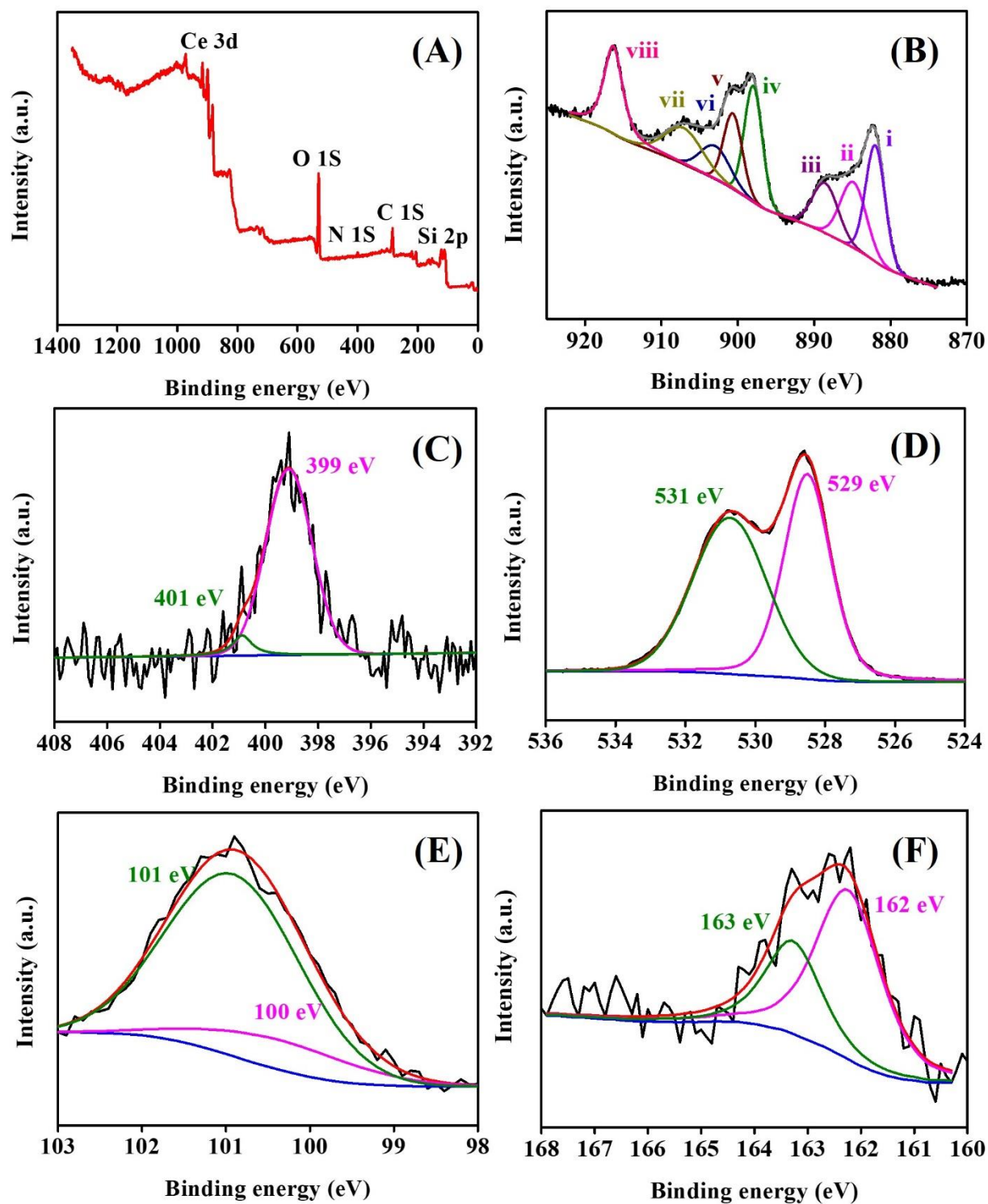


Figure A77. XPS spectra of TCP. (A) Survey scan. (B) Ce 3d. (C) N 1s. (D) O 1s. (E) Si 2p. (F) S 2p.

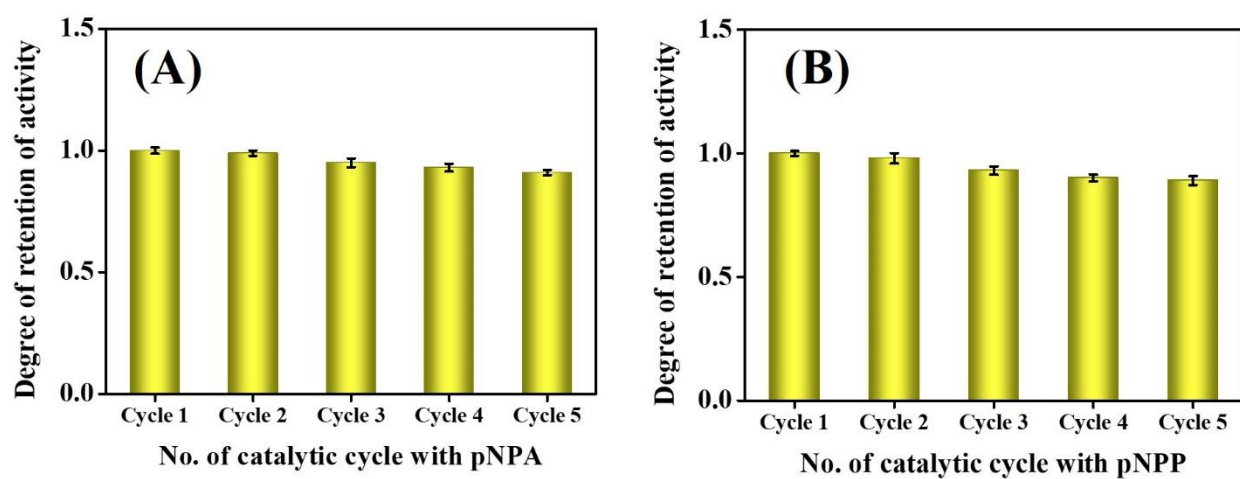


Figure A78. Recyclability of TCP. (A) Hydrolysis of pNPA. (B) Hydrolysis of pNPP.

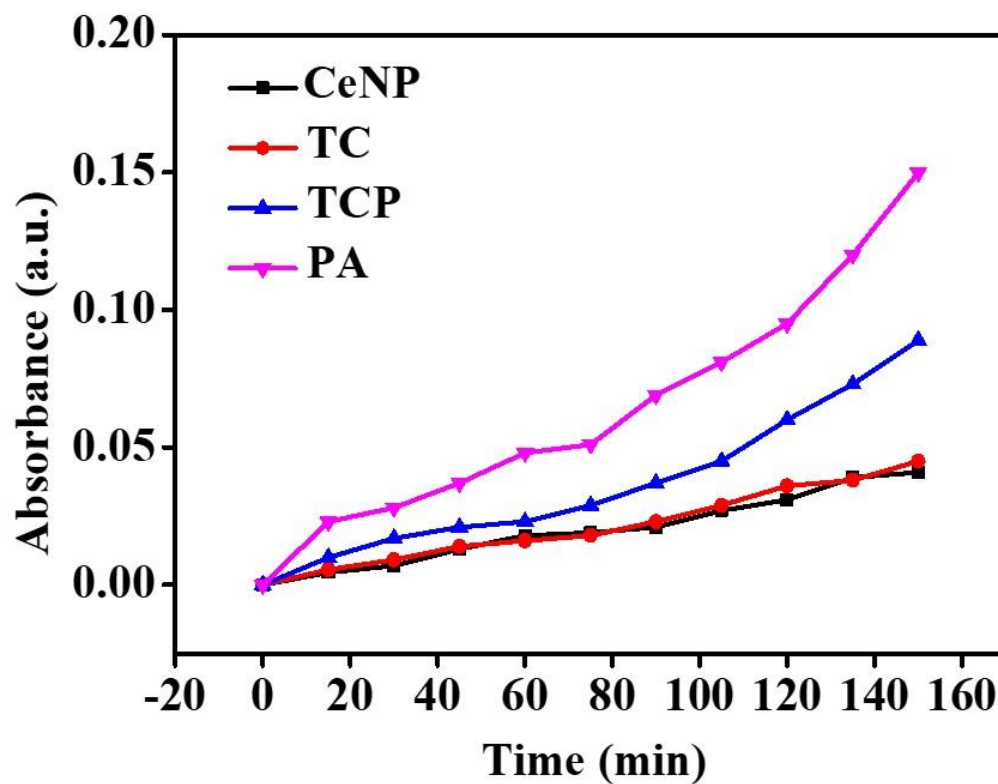


Figure A79. Catalytic activity for acetylthiocholine hydrolysis. Y-axis represents absorbance of TNB.

Table A5. Ratio of $\text{Ce}^{3+}/\text{Ce}^{4+}$ estimated using Ce 3d XPS spectrum of TCP.

Peaks	Binding energy (eV)	Area
i	882.1	18840
ii	884.9	16200
iii	888.5	13500
iv	898	17280
v	900.6	12890
vi	903	10350
vii	907	15670
viii	916.3	15750
ii, iv, vi	Ce^{3+}	43830
i, viii, v, vii, viii	Ce^{4+}	76650
	$\text{Ce}^{3+}/\text{Ce}^{4+}$	0.57
	$\text{Ce}^{3+}/(\text{Ce}^{3+}+\text{Ce}^{4+})$	37%

CURRICULUM VITAE

MOUMITA HALDER

Permanent Address: J D Apartment, R C Pandit lane, Purulia-723103, West Bengal, India

Current Address: Lab No. 309, SSB Block, Indian Institute of Technology Ropar, Rupnagar, Punjab-140001, India

Email ID. 2018cyz0011@iitrpr.ac.in, haldermoumita19@gmail.com

Phone. +91-8637094630, +91-8335849105

Gender: Female

Date of Birth: 08/08/1994

Languages: English, Hindi, and Bengali (native)

Academic Details

Degree	Board/University	Year of Passing	Percentage of marks
Doctor of Philosophy (PhD) in Chemistry	IIT Ropar	2023	9.25
M.S. (Pharm) in Medicinal Chemistry	NIPER, Mohali	2018	9.74
B. Pharm	NSHM Knowledge Campus, MAKAUT, Kolkata	2016	9.31
Higher Secondary	WBCHSE	2012	89.2%
Secondary	WBBSE	2010	85%

Research Experience

Aug 2018 to present. PhD Scholar at Department of Chemistry, IIT Ropar

Supervisor. Dr Yashveer Singh

Title of thesis. Self-assembled peptides for drug delivery, tissue regeneration, and biocatalytic applications

- Synthesis and characterization of peptides, nanoparticles

- Fabrication of supramolecular gels and characterization
- Mammalian and bacterial cell culture
- In-silico docking study

Aug 2016 to June 2018. Masters project

Supervisor. Prof. (Dr) Rahul Jain

Title of thesis. Synthesis of structurally diverse ring-substituted arylated Quinoline derivatives as antituberculosis agents

- Synthesis of heterocycles and their characterization

Teaching Assistantship

Aug 2019 to Dec 2019. Worked as a Teaching Assistant for the B. tech 1st year students in organic chemistry lab

Aug 2019 to June 2022. Mentored 3 masters students during their MSc project work in research laboratory

Experimental and Technical Skills

- Synthesis and characterization of small organic molecules, peptides, nanoparticles
- Fabrication of self-assembled gels
- In vitro mammalian and bacterial cell culture studies
- In silico docking study
- Well versed with the structural characterization techniques like NMR and Mass spectrometry
- Hands on experience on handling several instruments like HPLC, GPC, FTIR, Fluorescence, UV-Vis spectroscopy, Rheometer, PXRD, Dynamic Light Scattering (DLS) and Zeta Sizer
- Well acquainted with cell imaging and RTPCR techniques
- Well versed with computational software like Microsoft Office, Chem Draw Ultra, PowerPoint, and Auto Dock

Industrial Training

Worked as an intern for 1 month in Albert David Limited, Kolkata (**January 2015**) and Gluconate Health Limited, Kolkata (**September 2014**). The training includes exposure to their manufacturing units of pharmaceuticals (oral and parenteral dosage forms), analytical departments and quality control unit.

Research Interests

- Synthesis of peptide based biomimetic molecules
- Synthesis of organic molecules for biological applications

- Nanomaterial fabrication
- Tissue engineering

Publications

- **Halder, M.**; Singh, A.; and Singh, Y.; Investigating the Role of Amino Acids in Ultrashort Peptide Based Biomaterials for Hydroxyapatite Binding and Osteogenic Differentiation of Mesenchymal Stem Cells to Aid Bone Tissue Regeneration (Manuscript submitted)
- **Halder, M.**; Narula, M.; and Singh, Y.; Supramolecular naproxen and indomethacin conjugated peptide gels with antioxidant, antibiofilm, and anti-inflammatory properties for chronic wounds. *Bioconjug. Chem.* **2023**, 34, 4, 645-663
- Roy, S.; **Halder, M.**; Ramprasad, P.; Dasgupta, S.; Singh, Y.; and Pal, D.; Oxidized pullulan exhibits potent antibacterial activity against *S. aureus* by disrupting its membrane integrity. *Int. J. Biol. Macromol.* **2023**, 249, 126049
- **Halder, M.**; Bhatia, Y.; and Singh, Y.; Self-assembled di- and tripeptide gels for the passive entrapment and pH-responsive, sustained release of an antidiabetic drug, glimepiride. *Biomater. Sci.* **2022**, 10, 2248-2262
- Saini, S. K[#]; **Halder, M[#]**; Singh, Y.; Nair, R. V. Bactericidal Characteristics of Bioinspired Nontoxic and Chemically Stable Disordered Silicon Nanopyramids. *ACS Biomater. Sci. Eng.* **2020**, 6(5), 2778–2786
- Sharma, P. K.; **Halder, M.**; Srivastava, U.; Singh, Y. Antibacterial PEG-Chitosan Hydrogels for Controlled Antibiotic/Protein Delivery. *ACS Appl. Bio Mater.* **2019**, 2 (12), 5313–5322.
- Jain, M., Reddy, C. V. R., **Halder, M.**, Singh, S., Kumar, R., Wasudeo, S., Singh, P. P., Khan, S., Melissa R. J., Tekwani, B.L., Jain, R., Synthesis and Biological Evaluation of 8-Quinolinamines and Their Amino Acid Conjugates as Broad- Spectrum Anti-infectives, *ACS Omega* **2018**, 3, 3060–3075

Conference Attended

- **32nd Annual Conference of the European Society for Biomaterials (ESB 2022)** held at Bordeaux, France during 4-8th September, 2022
Activity: Poster presentation on the topic of “Naproxen and indomethacin-conjugated antioxidant and antimicrobial peptide gels for chronic wounds”
- **ACS Spring 2022** held on online mode during 5-16th April, 2021
Activity: Poster presentation on the topic of “Sustained release of an antidiabetic drug, glimepiride, from self-assembled peptide gels”
- **International virtual conference on biomedical materials innovation-2020 (ICBMI-2020)** during 6-9th December, 2020
Activity: Poster presentation on the topic of “Dipeptide gels for the sustained release of an antidiabetic drug, glimepiride”
- **International conference on biomaterial based therapeutic engineering and regenerative medicine, Bioterm 2019**, held at IIT Kanpur, during 28th Nov-1st Dec, 2019

Academic Achievements and Awards

- Received International Travel Support Grant from DST to attend ESB 2022 at Bordeaux, France
- Won Prof. S. Rajeswari Award for the best poster presentation at the SBAOI-STERMI International Virtual Conference on Biomedical Materials Innovation (ICBMI-2020), 6-9 December 2020
- Received scholarship from Ministry of Chemical and Fertilizer during M.S. (Pharm)
- Selected for merit scholarship by West Bengal Council of Secondary Education (WBCHSE), 2012
- Selected for merit scholarship by Indian Pharmaceutical Association (IPA), Bengal Branch, 2014
- Secured 2nd position in B. Pharm and received Silver Medal from

university, 2016

- Qualified GPAT in 2016 with AIR 219